MATERIALS AND INTERFACE ENGINEERING FOR SOLUTION-PROCESSED UV LIGHT RESPONSIVE ORGANIC PHOTOTRANSISTORS

MATERIALS AND INTERFACE ENGINEERING FOR SOLUTION-PROCESSED UV LIGHT RESPONSIVE ORGANIC PHOTOTRANSISTORS

By DARKO LJUBIC, B.Eng., M.Sc.Eng., M.S.

A Thesis Submitted to the School of Graduate Studies

in Partial Fulfilment of the Requirements for

the Degree Doctor of Philosophy

DOCTOR OF PHILOSOPHY (2017) McMaster University

(Chemical Engineering) Hamilton, Ontario

TITLE: Materials and Interface Engineering for solution-processed UV light responsive organic phototransistors

AUTHOR: Darko Ljubic

B.Eng. (Faculty of Technology in Novi Sad, Serbia)

M.Sc. Eng. (Faculty of Technology in Novi Sad, Serbia)

M.S. (Pittsburg State University, Kansas, USA)

SUPERVISOR: Dr. Shiping Zhu

INDUSTRIAL SUPERVISOR: Dr. Yiliang Wu

NUMBER OF PAGES: xxxii, 298

Lay abstract

Organic electronics have become a part of our daily life since they are integrated into cell phones, computers, TVs, displays, etc. Their advantage is their versatility due to a variety of organic compounds that can be used as semiconductors for the specific applications, low-cost processing methods (solution, printing, and melt) and large-area flexible substrates that can be used for their fabrication. For the same reasons, organic phototransistors are very attractive for modern optoelectronics. Generally, in this study, we developed and demonstrated new strategies of developing an organic phototransistor and enhancing/optimizing its performance. Firstly, we developed semiconducting blends that are responsive to UV-A light when integrated into an organic phototransistor. Secondly, by channel/gate dielectric interface manipulation we demonstrated control over photoelectrical properties of the organic phototransistor and discovered mechanisms of the enhancement. Thirdly, we optimized and developed reliable, high-performance, and highly UV responsive organic phototransistors with potential application as a photo memory element.

Abstract

Organic electronics have reached the level of commercialization and are important parts of our daily life. They are integrated into portable computers, cell phones, identification cards, television, cars, etc. The organic thin film transistors (OTFTs) are the most attractive organic electronic elements that have applications as electronic flexible paper, sensors, smart cards, erasable memory devices, RF-ID tags, and in backplanes for OLED displays. Their performance has already exceeded the performance of transistors based on the amorphous silicon (α-Si).

Organic thin film phototransistors (OPTs) have attracted significant research attention as functional OTFTs due to the unique structure of OTFTs (three-terminal device) complemented with the light (fourth terminal). The OTFTs structure enables modulation and amplification of the output signal (the drain current) while light gives the functionality and enhances the performance. Compared to organic photodiodes, OPTs have higher sensitivity and lower noise due to the OTFT structure. Additionally, the advantage of OPTs over inorganic PTs lays in a variety of light responsive organic materials that can be used as active channel materials. Accordingly, use of organic compounds enabled OPTs fabrication from solution, melt, and printing, over large areas of plastic substrates with which they are compatible. So far, many researchers have reported high-performance OPTs. Typically, synthesis of the new light receiving/emitting semiconducting materials is the common approach for the OPT development. Another way is to engineer the

device structure by introducing new layers with different functionalities. Often, synthesis is costly, complex, lengthy, and not industrially feasible.

This thesis focuses on the development of new methods and materials for OPT performance enhancement to avoid lengthy synthesis and fabrication processes. According to the layers in a typical OPT, that is, from the top to the bottom: active channel, channel/gate dielectric interface, and the gate dielectric layer, the thesis has three major focuses: engineering of the active channel for high-performance OPTs using existing small molecule and existing or new dielectric polymeric materials (Chapters 3-5), interface engineering (Chapter 6), and engineering of the gate dielectric layer (Chapter 7). Utilizing blends of a UV-A responsive 2,7-dipentyl[1]benzothieno[3,2-b][1]benzothiophene (C5-BTBT) small molecule semiconductor and various dielectric polymers (polyesters, PMMA, PVAc, PS, and PC) we developed highly photoresponsive and photosensitive OPTs. Furthermore, we designed and synthesized a new polyimide that is soluble, thermally stable, with reduced deep coloration and more importantly with the strong electron withdrawing groups. High-performance and highly photosensitive OPTs were achieved with capabilities of the application as photo memory elements characteristic of fast switching and long retention times of the persistent photocurrent. We demonstrated that by simple channel/dielectric interface modification using organosilanes with different end groups, the drain photocurrent, and hole mobility could be modulated and enhanced under the UV light illumination. In the final part, we demonstrated that both active channel and

dielectric layer engineering could synergistically enhance the performance of OPTs for potential fabrication as photo memory elements. This thesis contributed significantly to fundamental knowledge of photoresponsive organic electronic devices and application of OPTs in the area of printed and flexible electronics.

Acknowledgements

This has been such an interesting journey. After almost sixteen years of formal education, my dream came true. On that journey, I met and dealt with many people, many helped shape my future, most significantly the one who had the greatest impact from the moment I met him was my supervisor, Dr. Shiping Zhu.

There are no words to describe how grateful I am to Dr. Zhu for giving me the opportunity to be his student. It is an honour to know him and to have studied under his supervision. I am so thankful for his great mentoring, teaching, guidance, patience, and for all the help and support throughout my doctorate. I often call him my academic father and a life-coach. His bright and sharp mind always offered solutions when I was struggling. The things that he told me at the beginning of my studies, paved the way for my success: "Turn your fears and worries into driving force," and "Take a risk, be in the dark and don't be perfectionist." Thank you, Dr. Zhu.

I will always remember my first discovery with Dr. Yiliang Wu, about spiropyran behaviour in the polymer matrix. It made me jump around in front of his office at XRCC shouting that we would get the Nobel prize. The reality came fast like a cold shower. It was already a well-known property. This was the part of my learning curve. I am grateful for your endless patience and support throughout my time learning organic electronics, materials, research, and experiment design. I am thankful for all the support, advice and revisions that you provided even after moving forward in your career.

Most of my experiments were carried out at Xerox Research Centre of Canada in Mississauga, Ontario. I am truly grateful to the management of XRCC, Dr. Paul Smith and Dr. Patricia Burns, and all the amazing people at XRCC for unconditional support during my time there. It is no wonder why Xerox is recognized as one of the best employers when their facilities and working conditions support any research needs. In particular, I would like to thank Dr. Nan-Xing Hu for being a great support in the last two years of my research at XRCC, Sandra Gardner for x-ray measurements and microscopy training, Dr. Chad Smithson for valuable advice and support of my research, Dr. Sara Vela, Dr. Adela Goredema, and Sonja Hadzidedic, for support while caring out the experiments. I would also like to thank Dr. Marko Saban and XRCC librarian Gordana Pavlovic for support and encouragement while I was working at XRCC.

I am also thankful to my Supervisory Committee members, Dr. Robert Pelton and Dr. Qiyin Feng for their valuable input and guidance. Their advice, support, and research expertise from the beginning of my studies were always encouraging and useful. I would also like to express my gratitude to Dr. Carlos Filipe, Kristina Trollip, Linda Ellis, and Michelle Whalen, who are my shiny stars at the department and unconditional supporters. I cannot imagine not joking and sharing smiles with you daily. Special gratitude goes to current and former staff members of the Chemical Engineering Department at McMaster University: Justyna Derkach, Doug Keller, Paul Gatt, Dan Wright, Lynn Falkiner, Cathie Roberts, Kathy Goodram, Mark Clarke, and Tim Stephens for all the support and help.

My gratitude also goes to some incredible faculty members of the Chemical Engineering Department at McMaster University for conducting some amazing research and creating a welcoming environment at the department. I am thankful to Dr. Emily Cranston and her former and current group members for AFM facilities. I would like to extend my gratitude to Victoria Jarvis and Dr. James Britten from MAX facilities for valuable help in x-ray analysis, and Cristina E. González-Espinoza, a Ph.D. candidate in the Department of Chemistry and Chemical Biology of McMaster University for wonderful research collaboration and help in computational chemistry. I would like to thank Doris Stevanovic from the Centre for Emerging Device Technology in Engineering Physics department at McMaster University for valuable help in device fabrication.

I am grateful to current and former members of PolyMac Zhu research group who made memorable working and leaving experience during my studies. I apologize for being strict and sometimes annoying about lab safety and cleanness, but I always preferred us to go for dinner rather than to an emergency room. I am grateful to Dr. Weifeng Liu and Dr. Erlita Mastan for all the help and support with my research. They went above and beyond as my friends and colleagues. My heartfelt thanks go to Dr. Wen-Jun Wang and his research group, with Dr. Zhu, for enabling a memorable two months at Zhejiang University, in China. Also, I would like to thank the Chinese Scholarship Council and Consulate General of People's Republic of China in Toronto, for the financial support for my visit to China.

I would like to thank all the staff at McMaster research finance and accounts payable for help with Mosaic. Additionally, I would like to thank to a local office of

Canadian Union of Public Employees-CUPE 3906 at McMaster University for valuable two-year collaboration while I was an International Officer. During my four years at McMaster University, I made a lot of new friends and colleagues. I would like to thank them all for all the fun times and the enhanced international experience. They helped me to learn about different cultures, customs, and lifestyles.

While balancing between social life and school (aka partying and studying), I made many friends outside of University as well. I would like to thank you all for an amazing four years and making life-long friendships. Lis, Ilinka, Federico, Glenn, Fei, Carla, and Mai thank you for all the support and love. The special place in my heart and gratitude have my Canadian family Barb and Joe, Kipling, and Faith. You are a part of my success. Thank you.

Last, but not least, I would like to express my deepest gratitude to the two biggest heroes in my life, my parents Mirko and Milica. I sincerely thank you for all your love, support, and hope in me. I bow deeply in front of you. It was a terribly difficult task to raise and guide two children who would become doctors of philosophy. You succeeded. Thank you. I am also grateful to my older sister Dr. Maja Nujkic and her family for all the love and support on my journey. I am looking forward to our reunion and great achievements as researchers.

My success would not be complete without the emotional support of my beloved Dejan. You made my success greater and I hope to have you beside me forever. Thank you.

Table of contents

List of figures

List of tables

Declaration of academic achievement

This thesis is organized based on a “sandwich” style consisting of three published journal articles, one submitted manuscript, and two prepared manuscripts. The contributions from the authors of these articles are summarized below:

- Darko Ljubic is the primary author of all the articles and manuscripts reproduced in this thesis (Chapters 2-7).
- Dr. Shiping Zhu is the supervisor in all the works, providing ideas, guidance, and brainstorming, as well as revising paper drafts.
- Dr. Yiliang Wu is an industrial supervisor in all the works, providing ideas, guidance, brainstorming, and revision of the papers.
- Dr. Nan-Xing Hu is an advisor at Xerox Research Centre of Canada (Mississauga, Ontario), where I spent much time doing experiments. He also provided guidance and revision to the manuscripts, and co-authored two papers reproduced in Chapter 5 and 7.
- Dr. Chad S. Smithson is the co-author of three articles reproduced in Chapter 3, 4 and 6. He provided the necessary inputs and revisions to these manuscript drafts.
- Dr. Weifeng Liu is the co-author of two research papers reproduced in Chapter 5 and 7. He designed the polyimide polymer used in these two papers and provided necessary revisions to the manuscript drafts.

- Victoria Jarvis is the co-author of the paper reproduced in Chapter 6. She performed the 2D XRD analysis and provided a necessary knowledge base in understanding the results.
- Cristina González-Espinoza is the co-author of a paper reproduced in Chapter 5. She performed density functional theory calculations of the polyimide structure and energy levels and provided an understanding of the calculations results.

List of publications

1. Ljubic D., Liu W., González-Espinoza C.E., Hu N-Z., Wu Y., Zhu S., Binary Blends of Polyimide and Benzothienobenzothiophene for High-Performance Solution-Processed Organic Phototransistors, *Adv. Electron. Mater.*, **2017**, In progress.
2. Ljubic D., Jarvis V., Smithson C. S., Hu, N-X., Wu Y., Zhu S., Effects of gate dielectric surface modification on phototransistors with polymer-blended benzothieno [2, 3-b] benzothiophene semiconductor thin films, *Organic Electronics*, **2017**, 44, 253-262.
3. Ljubic D., Smithson C. S., Wu Y., Zhu S., Effect of Polymer Binders on UV-Responsive Organic Thin-Film Phototransistors with Benzothienobenzothiophene Semiconductor, *ACS App. Mater. Interfaces*, **2016**, 8 (6), 3744–3754.
4. Ljubic D., Smithson C. S., Wu Y., Zhu S., Highly UV-Sensitive and Responsive Benzothiophene/Dielectric Polymer Blend-Based Organic Thin-Film Phototransistor, *Adv. Electron. Mater.*, **2015**, 1, 1500119.

1 INTRODUCTION

This chapter gives an overview of the research objectives, the organization of the thesis and other works completed during this Ph.D. study but not included in the thesis.

§ 1.1 Research objectives

The research objectives of this thesis are summarized below, with the summary of specific contributions from each chapter in the following section.

- To develop new and engineer existing materials (i.e. blends) used for the active channel to enhance and control the performance of UV light responsive phototransistors (OPTs) as memory devices and sensors.
- To fundamentally study the effects of those materials on control and modulation of photoelectrical properties of OPTs.

- To fundamentally study the effects of channel/dielectric interface engineering on photoelectrical properties of OPTs, and
- To engineer the gate dielectric layer of an OPT device to develop a reliable and high-performance OPT with potential for flexible, low-voltage and printable OPTs.

§ 1.2 Thesis organization

The outline of this “sandwich style” thesis, includes eight chapters. Each chapter, except Chapters 1 and 8, represents either draft of the manuscripts prepared for peer-review journals (Chapters 2, 5 and 7) or articles published in peer-review journals (Chapters 3, 4 and 6). The published articles and associated supporting information were copied into the thesis with copyright permits placed at the beginning of each chapter. The figure and table numbers of the copied articles were adjusted for the consistency throughout the thesis. After Chapter 1 (Introduction) and Chapter 2 (Theoretical background and literature review), the thesis structure (chapters flow) follows the configuration of a typical top-contact bottom-gate OPT, and not the chronology of the works published/written, as follows:

- Chapters 3-5: Active channel
- Chapter 6: Channel/dielectric interface
- Chapter 7: Gate dielectric
- Chapter 8 Conclusions and recommendations for the future

research directions.

In **Chapter 3** and **4**, the effects of various dielectric polymer binders on photo electrical characteristics of a small molecule organic semiconductor, C5-BTBT, are investigated in detail. The effects of the polymer electronic nature on OPTs performance are also investigated. Various characterization techniques and measurements are employed to evaluate the OPTs. The general procedure for OPTs fabrication is provided. This approach enables development of the high-performance OPTs for UV sensing and photo memory elements (optical writing/electrical erasing of an information). **Chapter 5** focuses on the design and synthesis of a new polyimide with a strong electron withdrawing properties. By careful selection of the monomers, a highly soluble, amorphous, and thermally stable, with reduced deep coloration polyimide, was prepared. Characterization of polyimide properties and measurement protocol of OPT photo electrical characteristics are provided. The polyimide is blended with C5-BTBT and integrated into an OPT as the active channel material. The strong electron withdrawing polyimide remarkably enhanced the photoelectrical characteristic of OPTs. **Chapter 6** focuses on the channel/dielectric interface modification using organosilane-based self-assembly monolayers (SAM). The specific procedure for the interface modification and OPTs fabrication is provided. The channel/dielectric modification demonstrates that by controlling electrostatic nature of the interface, the photoelectrical and dynamic characteristics of OPT as sensors and photo memory can be controlled. The two fundamental findings from this study can be drawn: 1) the hole mobility in dark is governed by the structure-SAM interactions

affecting alignments of crystallites in the crystal structure of a semiconductor, and 2) the dynamic and photoelectrical characteristics including the mobility are driven by the electron accepting/donating nature of SAM. **Chapter 7** presents the dielectric layer engineering using the double gate dielectric approach to eliminate hysteresis under UV light, to increase the mobility, lower the operating voltage, and to modulate the photoelectrical and dynamic characteristics of OPTs. Lastly, **Chapter 8** concludes the thesis and summarizes all the contributions with recommendations as future research guidelines.

§ 1.3 Other works

The list of other contributions completed during the Ph.D. study that are not included in the thesis is as follows:

- Co-authored an article “The effect of azobenzene derivatives on UV-responsive organic thin-film transistors with a 2,7-dipentylbenzo[b]benzo[4,5]thieno[2,3-d]thiophene semiconductor” published in *Journal of Materials Chemistry C*, **2015**, 3, 31, 8090-8096, DOI: 10.1016/j.orgel.2016.06.022 (primary author Chad S. Smithson).
- Co-authored an article “Rapid UV-A photodetection using a BTBT organic thin-film transistor enhanced by a 1,5-dichloro-9,10-dintiro-anthracene acceptor” published in Organic Electronics. 2016, 37, 42-46, DOI: 10.1016/j.orgel.2016.06.022 (primary author Chad S. Smithson).

2 THEORETICAL BACKGROUND AND LITERATURE REVIEW

This chapter of the thesis presents a literature review on organic phototransistors with a brief theoretical background necessary for comprehensive understanding of the organic phototransistor. The literature review represents a recent progress in this field. It is structured to summarize all the strategies to develop an organic phototransistor. This chapter is a newly prepared manuscript draft for submission to a peer-reviewed journal.

§ 2.1 Abstract

Organic phototransistors (OPTs) are emerging devices for organic optoelectronics. In this progress report, the recent achievements in organic phototransistors are reviewed. Over the last few years, a remarkable progress has been made in OPTs owing to smart design and synthesis of new organic semiconductors, molecular engineering, and device and interface engineering. OPTs have been demonstrated to operate as photo sensors, photo switches, photodetectors, and memory, on both rigid and flexible substrates, printed or solution processed. A brief overview of OPTs structures, parameters that characterize an OPT performance, and operation mechanisms is given, followed by the recent advances in OPTs. The recent advances are discussed based on the channel materials that can be utilized for OPTs and interface engineering. Lastly, summary and outlook are briefly addressed.

§ 2.2 Introduction

Physicist J. E. Lilienfeld [1] was the first who patented the concept of FETs in 1925 but without evidence of the constructed device. After the invention of the transistors by Bell Laboratories scientists, the first commercial FET (metal–oxide–semiconductor field-effect transistor, MOSFET) was constructed by D. Kahng and M. Atalla in 1960. [2] Following the commercialization of the first MOSFETs, the transistors became an integrated part of all electronic devices. Furthermore, the

concept of the thin-film transistors (TFT) proposed by Paul Weimer in 1962 paved a way for OFETs development. [3]

The organic thin-film transistors (OTFTs), based on electrochemically polymerized polythiophene as semiconductor channel, were firstly reported in 1986 by Tsumara et al. [4] Soon after, OTFTs attracted significant research attention and performance of OTFTs was constantly improved. The reported high charge carrier mobilities support the previous statement. Vacuum deposited small molecule organic semiconductor (OSC) based on asymmetric tridecyl (C_{13}) substituted [1]benzothieno[3,2-b][1]benzothiophene (C13-BTBT) was 17.2 $cm^2V^{-1}s^{-1}$,[5] even higher mobility of solution processed symmetric C8-BTBT of 31.3 $cm^2V^{-1}s^{-1}$ was reported.[6] Using C8-BTBT/PS blends and off-center spin-coating, a remarkable mobility of 43 $cm^2V^{-1}s^{-1}$ was reported.[7] Finally, for solution processed conjugated polymer OSC, a high mobility of 10.5 $cm^2V^{-1}s^{-1}$ was achieved.[8] All the devices showed a high On/Off ratio of more than 10^6. These results unambiguously demonstrate that OPTs have largely exceeded the performance of α-Si-based FETs (a mobility of ~ 1 cm^2/Vs and On/Off ratio of 10^6 - 10^8) required commercialization of OFETs. [9]

Organic semiconductors for OTFTs, classified as small molecules and polymers, have been intensively researched in the last 50 years.[10] Among the small molecule SCs, pentacene is the most studied with the highest reported carrier mobility of 3-6 cm^2/Vs on polymer-based gate dielectrics.[10,11] The OFETs fabricated with single crystal layer and other nano-/micro- structures are also attractive since they can offer high ordered layer structures without grain

boundaries and low impurity content. Rubrene is the most promising small molecule single crystal for OFETs with carrier mobility higher than 10 cm^2/Vs. [12] OSCs are very appealing for optoelectronics. [13] Utilizing organic synthesis tools, a various OSCs for light harvesting and detection were made.[14] Properties of OSCs can be tuned for the broad absorbance of the light spectrum from deep UV to NIR. The advantage of light sensing OSCs over Si-based optoelectronics is in their low-temperature processability and compatibility with various plastic substrates for fabrication of high-performance large-area optoelectronics. The most attractive optoelectronic elements are organic phototransistors (OPTs) that are applied for photo sensing, as photo memory elements and photo-transducers. [15–18] The most general classification of OPTs is in respect of the type of OSCs used as channel materials. Therefore, OPTs based on OSCs of single crystals, [19–21] small molecules [22–24], polymers [25–27], and blends [28–33] were reported. Additionally, the use of organic-inorganic composites as channel materials, [34][35] and interface engineering [22] is sought as a promising strategy to enhance OPT performance. A high photoresponsivity and photosensitivity of ~10^4 AW^{-1} and 10^5 were reported for benzo[1,2-b:4,5- b′]dithiophene dimers, respectively.[36] For the solution processed 2,7-dioctyl[1]benzothieno[3,2-b][1]benzothiophene (C8-BTBT) single crystal ribbons, Wu et al[37] reported a photoresponsivity as high as 1200 AW^{-1} and photosensitivity of 10^4. If we compare these results with Si-based PTs and their photoresponsivity of 300 AW^{-1}, [38] it is clear that OPTs are feasible building blocks of modern optoelectronics.

In this survey, we attempt to summarize the very recent advances in OPTs according to the above classification. In Section 2.3., we briefly give an overview of the OPTs structure, basic characteristics, and parameters that are commonly used for evaluation of OPT performance (2.3.1-2). Section 2.3.3 explains the operation modes of OPTs. Section 2.4 summarizes the recent advances in the field. It is structured into a single crystal, small molecule, polymer, blend, and hybrid-based OPTs sections. More specifically, Section 2.4.1-2.4.3 reports OPTs based on single component channels made of OSC, while Section 2.4.4 and 2.4.5 on the blend- and hybrid (organic-inorganic composite)-based OPTs. The blend-based Section 2.4.4 summarizes work on bulk heterojunctions and small molecules/dielectric polymer blends for OPT active channel. The last Section 2.4.6 is dedicated to distinct works of the interface engineering in OPTs that is also a promising strategy for OPTs development.

§ 2.3 Theory and background

In the following section, we summarize the important aspects of OPTs necessary to understand their operation and performance.

2.3.1 The OPT structure

OPTs are unique devices utilizing the structure of OTFT, i.e. three-terminal device. Accordingly, the main parts of a typical OPT are source (S), drain (D), and gate (G) electrodes, active channel or organic semiconductor (AC), and the gate

dielectric (GD). OTFTs are often called three-terminal devices due to S-D-G electrodes and the main difference with OPTs is the presence of the fourth terminal, which is light, also called “a fourth electrode”. Therefore, in respect to the position of S-D-G electrodes, a typical OPT can adopt four structures: top-contact/bottom-gate (TCBG), bottom-contact/bottom-gate (BCBG), top-contact/top-gate (TCTG), and bottom-contact/top-gate (BCTG). In respect to the position of light illumination, all the above structures can be top-light (TL) and bottom-light (BL) as displayed in Fig. 2.1(a-f). When light illuminates from the bottom, a highly transparent gate and substrate materials are required to ensure efficient illumination of the active channel.

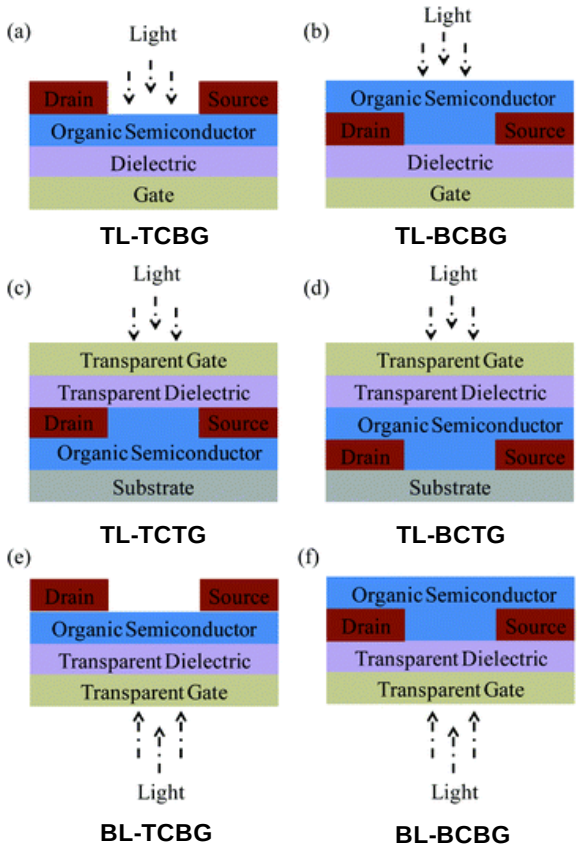

Fig. 2.1. Typical OPT structures in respect to the relative position of the active channel, gate dielectric, and S-D-G electrodes (a-d) and the incident light illumination (e-f). *Reprinted from* [84] *with permission. Copyright 2015 Royal Society of Chemistry*.

2.3.2 Photoelectrical characteristics and figure of merits

Since OPTs utilize the structure of OTFTs, for the purpose of comprehensive understanding, we summarize first the characteristics and parameters that are overlapped followed by OPTs specific figures of merit. The two typical characteristics of OTFTs and, therefore, OPTs measured in the dark and under

light illumination, are output (drain current, I_D, vs source-drain voltage, V_{DS}) and transfer (I_D vs gate voltage, V_G). Fig. 2.2 represent output characteristics of [2,3-b:2',3'-f]-thieno[3,2-b] thiophene (DNTT)/polystyrene based OPTs [39] in darkness and with the gate voltage variation (Fig. 2.2a), under constant light intensity of 80 $mWcm^{-2}$ but variable gate voltage (Fig. 2.2b), and variable light intensity at zero gate voltage (Fig. 2.2c).(V_G is changing in steps of -10 V). Compared to output characteristics in the dark, an obvious increase of the source-drain current can be observed due to the contribution of the photocurrent. As mentioned before, light represents the fourth electrode and it can be used as an axillary gate electrode to tune the level of I_D generated in the channel at zero gate voltage. Fig. 2.2d displays transfer characteristics of 2,7-dipenty[1]benzothieno[2,3-b][1]benzothiophene (C5-BTBT)/polyester blend based OPTs [29] in darkness (black curve) and under UV-A light with intensity of 3 $mWcm^{-2}$ (blue curve). Lastly, Fig. 2.2e represent transfer curves of DNTT/polystyrene OPTs [39] under variable light intensity.

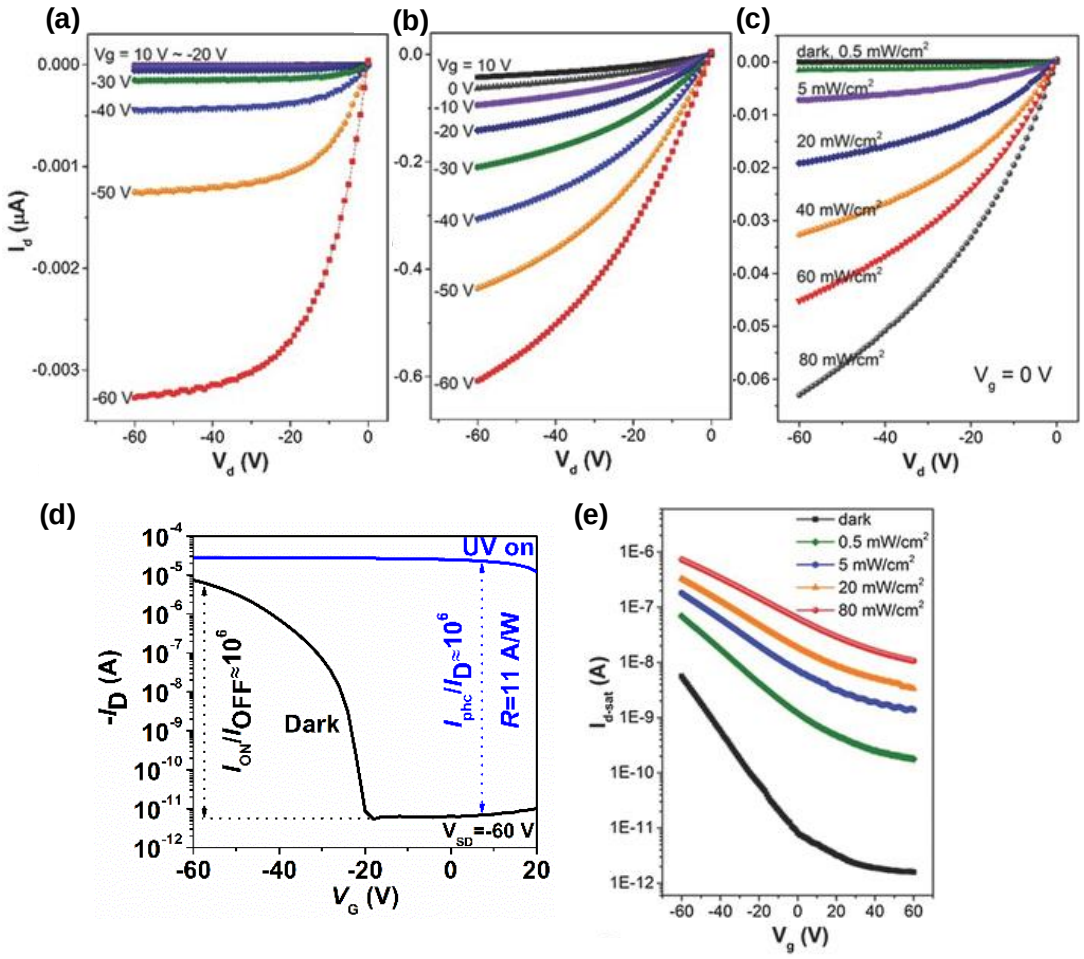

Fig. 2.2. Photoelectrical characteristics of OPTs. Output characteristics of DNTT/polystyrene OPTs in (a) darkness, (b) at constant light intensity and VG variation in steps of -10 V, (c) at variable light intensity and zero gate voltage; Transfer characteristics of (d) C5-BTBT/polyester OPTs in darkness (black line) and under UV-A light (3 $mWcm^{-2}$, blue line) at V_{DS}=-60 V, and (e) DNTT/polystyrene OPTs under variable light intensity at V_{DS}=-60 V. Panels a-c and e are reprinted with permission from [39]. *Copyright 2016, Wiley*. The panel in (d) is reprinted from [29]. *Copyright 2015, Wiley.*

From the transfer curves in the dark and UV light (Fig. 2.2d and e), the important parameters can be extracted to quantify the photoelectrical performance of OPTs. In the dark, the field-effect mobility (μ with units $cm^2V^{-1}s^{-1}$) in the saturation (Eqn. 2.1) and linear regime (Eqn. 2.2) can be estimated using the following equations: [2]

$$I_{DS} = \frac{W}{L}\mu C(V_G - V_{Th})V_{DS} \qquad V_{DS} < (V_G - V_{Th}) \qquad (2.1)$$

$$I_{DS} = \frac{W}{2L}\mu C(V_G - V_{Th})^2 \qquad V_{DS} > (V_G - V_{Th}) \qquad (2.2)$$

where *L* and W are the channel length and width (μm), respectively, *C* is the capacitance per unit area of the dielectric ($nFcm^{-2}$). The device electrical characteristics (*I* vs. *V*) can be quantified using the above-mentioned models (Eq. 2.1 and 2.2) developed for MOSFETs and modified for the OFETs. [40] The threshold voltage (V_{Th}, extrapolated from the slope of $I_D^{½}$ vs. V_G curves to I_D=0 A), turn-on voltage (V_{ON}) and dark current ratio when an OPT is on and off state (On/Off ratio) calculated from the transfer characteristics are other important parameters for evaluation of OPTs performance (Fig. 2.2d).

The operation of an OPT under light illumination or its efficiency is characterized by the basic parameters, namely, photoresponsivity, *R*, (AW^{-1}) and photosensitivity (*P*). The *R* can be defined as how much photocurrent (I_{phc}) is

generated per power of the incident light while photosensitivity is the I_{phc} to I_D ratio. Both parameters can be calculated using Eqn. 2.3 and Eqn. 2.4 as follows: [26]

$$R = \frac{I_{phc} - I_D}{P_{il} \cdot Z} \quad (2.3)$$

$$P = I_{phc}/I_D = \frac{I_{phc} - I_D}{I_D} \quad (2.4)$$

where P is the intensity of the incident ($mWcm^{-2}$) and Z (LxW) is the effective area illuminated by light. The other quantities were defined previously.

2.3.3 Operation modes

OPTs compared to photodiodes have higher signal and lower noise, which is enabled by the structure of OTFT and the light as the fourth electrode. Both light and electric field induced by gate electrode can amplify the signal, i.e. drain current at the same time. Under light illumination, OPTs can operate in photoconductive and photovoltaic mode. [41]

The photovoltaic mode (accumulation regime, $V_G < V_{DS}$ or on-state) is the most reported in the literature. [42] The indication of the photovoltaic effect in the channel of an OPT is a shift of V_{Th} (for p-type OSC positive and for n-type negative shift) as seen in Fig. 2.2d. The light illumination generates excitons (electron-hole pairs) that dissociate into free photo charge carriers. The photo-generated electrons and

holes accumulate below the source and drain electrodes, respectively. The accumulation of the negative charge carriers lowers the potential barrier between source and channel for holes to be further injected into the channel. [43,44] Consequently, lowering the injection potential barrier decreases the contact resistance, which results in a positive (negative) shift of V_{Th}.[13] At the drain electrode, a large increase of I_D can be recorded. The I_{phc} generated by photovoltaic effect ($I_{phc,pv}$) can be mathematically expressed as:[45]

$$I_{phc,pv} = g_m \Delta V_{Th} = \frac{BkT}{q} ln\left(\frac{\eta q \lambda P_{il}}{I_D hc} + 1\right) \qquad (2.5)$$

where g_m is the transconductance, ΔV_{Th} is the threshold voltage shift, B is the fitting parameter, η is the photogeneration quantum efficiency, I_D is the dark current, and hc/λ is the photon energy. The typical curve representing a photovoltaic induced photocurrent is displayed in Fig. 2.6e.

The photoconductive mode (depletion regime, $V_G > V_{DS}$ or off-state) occurs when I_D increases linearly with the intensity of incident light, P_{il}, (Fig. 2.2e). In addition to the light, the electric-field-induced by V_G (source-gate voltage) contributes to the enhancement of the photogenerated charge carriers. The I_{phc} caused by the photoconductive effect ($I_{phc,pc}$) can be mathematically expressed by Eqn 2.6:[46]

$$I_{phc,pc} = (nq\mu E)WD = BP_{il} \qquad (2.6)$$

where n is the carrier density, q is the elementary charge, μ is the field-effect mobility of dominant carriers, E is the electric field, W and D are the gate width and thickness of the active channel, respectively, B is a proportionality factor, and P_{il} the intensity of incident light.

§ 2.4 Literature review on the recent progress in OPTs

Based on the recent research achievements in the field of OPTs, the main directions (strategies) of turning OTFT into OPT can be classified as utilization of 1) the single component small molecule OSCs (including single crystals), 2) the single component conjugated polymers, and 3) blends of conjugated OSCs, OSCs, and dielectric polymers, and organic-inorganic composites (hybrid approach), as active channel light responsive materials, as well as 4) interface modification. According to this classification, in the following sections, after acknowledging the early works, we will summarize the most recent and distinct works using the above-mentioned strategies to develop OPTs. For the chemical structures cited in this report, please refer to Appendix (Section 2.7) for the summery of small molecule and for conjugated polymers OSCs chemical structures.

2.4.1 Single crystal OPTs

Organic small molecule single crystal OPTs (SC-OPTs) have been the research focus in the past decade. Likewise, in OTFTs, single crystal semiconducting layer-based OPTs enabled fundamental understanding of the mechanisms of photo charge carrier generation and the intrinsic properties of light responsive OSC molecules. SC-OPTs have high-performance with desired high mobility due to a lack of intrinsic and morphological defects. The story of high-performance SC-OPTs started in 2005 with the fabrication of rubrene-based OPT deposited on perylene dielectric via vapor deposition. [47] This work by Podzorov et al. offered a fundamental understanding of OPT photophysics and opened the venue for further research in the field of SC-OPTs. Soon after, Mas-Torrent et al. developed a new class of organic single crystals, namely, dithiophene-tetrathiafulvalene (DT-TTF, μ_{max}=1.4 cm^2V^{-1} s^{-1})[48] and dibenzo-tetrathiafulvalene (DB-TTF, μ_{max}=1 cm^2V^{-1} s^{-1}),[49] which were integrated into OPTs with P of ~10^4.[19] For more detailed achievements in the past 20 years on SC-OPTs, readers are encouraged to check two excellent reviews.[13][50] In the following section, we focus on the very recent advances.

As described in the theory section, in addition to field-effect mobility, P (photosensitivity or I_{phc}/I_D ratio) and R (photoresponsivity) are the important parameters, which are the indicators for the efficiency of an OPT and which are constantly improving over the last decade. Kim et al. developed solution processed SC-OPTs based on anthracene single crystal derivatives with high mobility 0.2-1.4

$cm^2V^{-1}s^{-1}$. [51] Anthracene served as the core for the two conjugated substituents on each of its 9,10-positions, namely, (4-hexylphenyl)ethynyl and 2-ethynyl-5-hexyldithieno[3,2-*b*:2',3'-*d*]thiophene (DTT). SC-OPTs showed high *R* of 10^4 AW^{-1} and *P* of $1.4x10^5$ under very weak light (1.4 μWcm^{-2}), which largely exceeded those of Si single crystalline PTs. Reaching such remarkable values was explained by J-type packing in the crystal structure of derivatives leading to a high degree of ordering and π-π interactions resulted in the high *R* and *P*. Very recently, using the same core material anthracene but different substituent (2,6-bis(4-methoxyphenyl) BOPAnt, Li et al. reported SC-OPTs fabricated via physical vapor transport (PVT) method in a bottom gate top contact SC-OPT structure. They systematically studied these UV light responsive SC-OPTs by comparison with TFTs based on the same single-crystal. SC-OPTs exhibited high *R* and *P* of $3.1x10^3$ AW^{-1} and ~10^6, respectively. An ultra-high external quantum efficiency (EQE) of 9.25×10^5% was achieved at a light intensity of 0.11 mW cm^{-2} due to lack of defects in the crystal structure and longer diffusion of an exciton in the channel.

Further advances in SC-OPTs are reflected through the development of the various single crystalline nano-/macro- structures for high-performance SC-OPTs. [52] Those structures include one and two-dimensional shapes such as ribbons, wires, and plates. One of the first works of OPTs based on air-stable, n-type F16CuPc sub-micro/nanometer ribbons was reported by Tang et al. [53] The single crystal OPTs were fabricated by PVT in TCBG configuration. SC-OPTs were used as photo-switches and were characterized by fast switching (on/off) speeds of 10-20 ms without V_G applied. Therefore, this work demonstrated the use of light as an

auxiliary electrode that can substitute the conventional gate electrode. When connected to the gate electrode, however, SC-OPTs had 2-3 orders of magnitude higher P (4.5×10^4) than photo-switches without V_G owing to efficient exciton separation by the electric field induced by V_G. Potentially, these SC-OTPs can be applied as optical switches with high sensitivity, optoisolators, and in the integrated circuits. As a less expensive alternative to PVT, solution-fabricated single crystal nano- and micrometer structure-based OPTs were developed. Ai et al. [54] fabricated a high-performance photodetector based on self-assembled sub-micrometer ribbons from condensed benzothiophene. By optimizing the type of gate dielectric, the high R and P of 4372 AW^{-1} and 1.3×10^4, respectively, were achieved. Thus, surface engineering also represents a simple and efficient method to achieve high-performance SC-OPTs.

Furthermore, the single crystal growth and intermolecular interactions of single crystal molecules play a crucial role in achieving the high-performance SC-OPTs. Hoang et al. [55] reported single-crystalline nanoneedles of π-extended porphyrin derivatives H_2TP and ZnTP. Both derivatives contained a porphyrin core with four 2-ethynyl-5-hexylthiophene peripheral arms that extended the π-conjugation and made SC-OPT sensitive to a wide spectrum of wavelengths (365-850 nm). Such molecular design of the channel material resulted in the highest R of 2.2×10^4 AW^{-1} reported so far and a hole mobility of 2.9 $cm^2V^{-1}s^{-1}$ for ZnTP. The high performance was attributed to the J- and H-type aggregation of porphyrin dimeric pairs via π-π interactions. However, the drawback of these SC-OPTs is very high V_{DS} that should be applied to reach the saturation I_D. Another example,

demonstrating the importance of the crystal structure alignment in single crystals is the work by Yu et al. [56] This group reported a single crystal OPT based on n-type N,N′-bis(2-phenylethyl)-perylene-3,4:9,10-tetracarboxylic diimide (BPE-PTCDI) nanowires fabricated via drop-casting on the top-contact bottom gate Si-substrates. The work demonstrated that the crystal growth along the *a*-axes (a shortest π-planar distance of 3.34 Å) facilitated the well-ordered molecular alignment where the charge transport occurs along the long axis of the nanowire. Consequently, SC-OPTs indicated the high *R* and *P* of $1.4x10^3$ AW^{-1} and $4.93x10^3$, respectively, to the light having a wavelength of 532 nm. The n-type mobility of 1.13 $cm^2V^{-1}s^{-1}$ was achieved in these air-stable SC-OPTs.

Nanowires have many advantages: 1) high aspect ratio (surface-to-volume) making them highly exposed to the photon of incident light, resulting in high conversion to the photo-charge carriers; 2) their dimensions (one dimension is elongated) making them highly compatible with flexible substrates, and 3) high mobility due to their single crystal structure. On the other hand, the challenge for the further development of nanowire-based SC-OPTs will be to develop a “top-down” approach to their alignment to produce highly aligned nanowires on a large scale.[57] A possible solution would be nanoimprinting lithography due to its capability of producing arrays with precisely ordered nanowires.[58,59] Moreover, using a direct printing method such as liquid-bridge-mediated nano transfer molding (LB-nTM) of molecular solutions (inks), Park et al. [60] developed a single crystal arrays-based OPTs based on TIPS-PEN, C60, and P3HT. This method enabled synthesis, alignment, and controlled orientation of single crystal nanowires

at once from molecular inks on pre-patterned molds. The desired orientation of the nanowires and thus the ability of the printing method to produce arrays of highly aligned nanowires were unambiguously confirmed with SEM analysis various x-ray techniques. Fig. 2.3 illustrates the fabrication procedure to prepare the single crystal nanowire arrays of TIP-PEN by LB-nTM with SEM images demonstrating highly aligned TIPS-PEN nanowires.

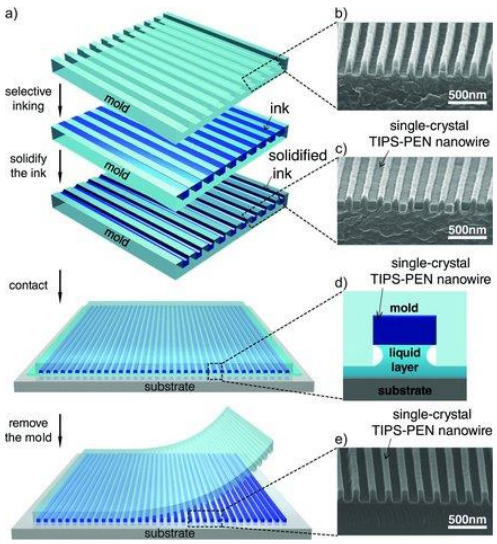

Fig. 2.3. Illustration of the single crystal TIPS-PEN nanowire arrays; a) fabrication steps using LB-nTM technique, (b) SEM image of the polyacrylate mold on the Si-wafer, c) SEM image of TIPS-PEN single crystal nanowires after solidification of the ink in the mold, d) schematic of the polar liquid formed between the nanowire and the substrate, e) SEM image of the nanowire arrays on the Si-wafer upon the mold removal. *Reprinted from* [60] *with permission, Copyright 2013, Wiley.*

Very recently, in achieving high *R* and *P* SC-OPTs using solution-grown nano- and micrometer single crystal structures, Liu et al. fabricated a low-voltage SC-OPTs based on naphthyl end-capped oligothiophene (5,5-bis(naphthyl)-2,20-bithiophene, NaT_2) nanofibers. [61] The OPTs were sensitive to monochromatic illumination with various intensities reaching an *R* of 0.91 AW^{-1} at V_G=−20 V and V_{DS} = −5 V. Rekab et al.[62] developed SC-OPTs from single- and multifiber assemblies. Fiber assemblies were formed by solvent-induced precipitation of air-stable N,N′-1H,1H-perfluorobutyl-dicyano perylene diimide (PDIF-CN_2) on Si-substrate. Both TCBG and BCBG SC-OPTs were fabricated on Si substrates with SiO_2 dielectric. The photoelectrical performance of SC-OPTs was measured under the white light illumination. A high mobility (>2 $cm^2V^{-1}s^{-1}$), *R* (2x10^3 AW^{-1}) and *P* (5x10^3) were achieved with the single fiber assembly due to low structural defects in the single crystal structure and closely packed PDIF-CN_2 molecules allowing for strong intermolecular coupling. Another example of the solution processed single crystal OPTs based on nanoribbons was reported by Wu et al. [37] This is the first example on single crystalline nanoribbons for deep UV light sensing. The nanoribbons were solution-grown via droplet-pinned crystallization (DPC) method from 2,7-dioctyl[1]benzothieno[3,2-b][1]benzothiophene (C8-BTBT) solutions in *m*-xylene. At very weak UV light illumination of 0.2 $mWcm^{-2}$, ultrahigh *R* and *P* of 1200 AW^{-1} and 3x10^4, respectively, were achieved at V_G=-23 V and V_{DS}=-30 V. At the light intensity of 1 $mWcm^{-2}$ (deep UV light, 280 nm) those values were 44 AW^{-1} and 8300, respectively. The use of C8-BTBT-based SC-OPTs is advantageous since they are blind to any wavelength beyond 365 nm and, and are good

candidates for the light selective photodetectors. Finally, an interesting work on single crystal microplate phototransistors was reported by Zhao et al. [63] The simple optimization of the gate dielectric by poly(methyl methacrylate) (i.e., PMMA) enabled high photosensitivity and high photocurrent of dinaphtho[3,4-d:3',4'-d']benzo[1,2-b:4,5-b']dithiophene (Ph5T2) single crystal microplate-based OPTs. These findings were supported by high photocurrent gain of 6.8×10^5 and p-type mobility of 0.018-0.43 $cm^2V^{-1}s^{-1}$ suitable for application in photo-switches.

2.4.2 Small molecule OPTs

Compared to SC-OPTs, OPTs based on a small molecule OSC have been widely studied mainly because of easier formation of the active channel and low-cost equipment needed for fabrication. Generally, small molecule OPTs can be fabricated by thermal evaporation and solution deposition of an OSC, typically in TCBG and BCBG configurations. The latter is, however, more dominant due to its low-cost and ease of fabrication. So far, great results in terms of *R*, *P*, and mobility have been reported for both thermally evaporated and solution processed OPTs based on phthalocyanines, acenes, oligoacenes, oligothiophenes, spiro-type and the star-shaped small molecule OSCs. [64–71] The applications of OPTs were for the light sensing/detection, and optical memory. While there were a number of reports published on small molecule OPTs in the past decade, in the following section we will focus on the very recent achievements. The interested reader can refer to the reviews. [14][42]

Yang et al. [72] developed photodetectors for circularly polarized light based on a helically shaped chiral semiconductor helicene. Helicene is known for its handedness that enabled the circularly polarized light detection (UV light). The enantiomerically pure 1-aza[6]helicene based photo-FETs showed good quality p-type performance with *P* and mobility of ~10^4 and 0.0004 $cm^2V^{-1}s^{-1}$. It was stated that the findings in this work represent the use of helicene-based OPTs as a new photonic technology that can be applied to quantum optical computing. Qi et al. [73] reported a high-performance OPTs based on n-type pi-conjugated NDI(2OD)(4tBuPh)-DTYM2 OSC. The core of this molecule is naphthalene diimide with expanded planar conjugation. Importantly, the deposition of the n-type OCS was performed from its solutions under ambient conditions, which is very important for the broader use of n-type OSCs since many of them are not air-stable. Under UV light illumination (0.107 $mWcm^{-2}$), OPTs reached large *R* and *P* of 2.7x10^4 AW^{-1} and 1.1x10^7, respectively. These two figures of merit were modulated by different intensities of the light and variation of V_G. The n-type OPTs developed in this work showed excellent persistent photoconductivity (PPC) suitable for optically writable/electrically erasable memory for multifunctional OPTs.

A further progress in OPTs for photo sensing applications was made almost simultaneously by two research groups that utilized anthradithiophene derivatives. OPTs were solution processed and highly sensitive to UV light with different intensities. Similar to the previous example, these OPTs showed optical memory due to electron trapping by light and slow trapping of electrons, i.e. slow decay of the persistent photocurrent. The recombination of charge carrier was accelerated

by a large negative bias voltage applied to the channel. The first derivative 2,8-difluoro-5,11-bis(triethyl silylethynyl) anthradithiophene (diF-TESADT)[69] as a channel material showed *R* and *P* of >10^3 AW^{-1} and 10^6, respectively, at the light intensity of 0.17 $mWcm^{-2}$. More importantly, the fast response times of <0.5 s were achieved under the light illumination. The second derivative triethyl germyl ethynyl substituted anthradithiophene (diF-TEG ADT) [74] as a channel material enabled not an only fabrication of the light responsive OPTs but moisture sensors at the same time when potassium alumina was used as the gate dielectric. Most likely, the use of potassium alumina lowered *R* and *P*. However, this concept demonstrated realization of OPTs that can operate in high humidity environments while sensing the light. Zhao et al. [75] synthesized new and soluble benzo[1,2-b:4,5- b']dithiophene dimers for OPT photosensors. Dimers were linked with unsaturated ethene and ethyne bonds. OPTs showed a high *R* (9336 AW^{-1}) to the UV light (37 μWcm^{-2}, 380 nm) and *P* of 4429. Moreover, OPTs fabricated using single crystals of dimers showed significantly higher *P* of 10^5.

Moving upscale in the electromagnetic spectrum, a new group of derivatives based on dithienyltetrathiafulvalene derivatives (TTF), previously reported for SC-OPTs,[19] have been utilized to fabricate solution processed thin film OPTs.[76] Thienyl- and t-butyl substituted tetrathiafulvalene derivatives were utilized as channel materials for sensing of the light with a broad range of wavelengths. OPTs were subjected to green, yellow, and red LED light illumination. Under the green light, the highest *P* of OPTs based on both TTF-derivatives was 10^2-10^3. These OPTs showed photo memory effects and low *R*. Despite the high photosensitivity

and broad wavelength sensing range, TTF-based OPTs exhibited a large hysteresis under the green light illumination and low mobility. Another set of OPTs for green, red, and yellow light sensing was very recently developed by Bharti et al. [77] As the light sensing material, TIPS-pentacene was deposited on ITO/PET substrates pre-treaded with HfO_2/PVP double layer dielectric. The TCBG flexible and transparent OPTs showed a moderate operating voltage of -10 V, max mobility of 0.23 $cm^2V^{-1}s^{-1}$, and high On/Off current ratio in dark of 10^5. Under the visible light of 460, 520, and 620 nm OPTs operated in the photovoltaic mode inducing a V_{Th} shift that was dependent on the light intensity, illumination time, and bias voltage during the illumination. Under the periodic light pulses, OPTs showed a fast response without persistent photocurrent (PPC) observed. The highest *R* (35 AW^{-1}) was achieved under the green light (0.4 $mWcm^{-2}$) while the highest *P* ($4x10^4$) under the blue light (1.7 $mWcm^{-2}$) at V_{DS}=-5 V for both parameters. Due to the fast response and reset, these OPTs have the potential for photo-controlled switches. For sensing of the blue light, Yu at al. [78] proposed an OPT based on dinaphtho[2,3-b:2',3'-f]thieno[3,2-b]thiophene (DNTT). To construct OPTs, DNNT was deposited by thermal evaporation on the stripped, flexible aluminum foil (AlO_x), previously treated with phosphoric acid to form self-assembled monolayers. Devices were TCBG configured to achieve a low operating voltage (-5 V), high mobility (0.53 $cm^2V^{-1}s^{-1}$) and high On/Off ratio ($1.7x10^5$) when OPTs were operated in the dark. Under the blue light illumination (450 nm), OPTs showed good photoelectrical properties with *R* and *R* of 50 AW^{-1} and 5 at the weak light intensity of 5 μWcm^{-2}.

OPTs had a fast response when the light was turned on and a fast reset (light-off) necessary for the fast sensing.

The low-voltage and flexible devices were also developed and reported. Chou et al. [79] developed an n-type OPT for the 532 nm monochromatic light sensing. OPT was solution processed using n-type OSC N,N'-ditridecyl-3,4,9,10-perylenetetracarboxylic diimide (PTCDI-$C_{13}H_{27}$) and crosslinked PVP (C-PVP) as a dielectric layer on flexible and transparent polyethersulfone (PES) substrates. The low-voltage device operated at -3 V indicating a low-power consumption. The two photoelectrical characterization states of flexible OPTs were applied, compression and tensile state. It was found that under compression and tensile states, the I_D under light switching conditions increased and decreased, respectively, relative to the flat state. This indicates the importance of the intermolecular distance of OSC in the channel. Furthermore, *R* and *P* of 0.41 AW^{-1} and $4x10^4$ were achieved.

For the absorption range of the near-infrared light spectrum, Li et al. [80] developed an OPT based on n-type 4,4-difluoro-4-bora-3a,4a-diaza-s-indacene (BODIPY-BF2). The OSC was solution processed under ambient conditions and spin-coated onto Si substrates. Owing to the strong absorbance around 850 nm due to its chemical structure, BODIPY-BF2 showed excellent photoelectrical properties as a channel material for OPTs. It was demonstrated that BODIPY-BF2 OPTs upon annealing exhibited high performance with 0.0113 $cm^2V^{-1}s^{-1}$ electron mobility, high On/Off ratio up to 10^6, and ambient stability. Furthermore, at the low-NIR light intensity of 0.5 $mWcm^{-2}$, OPTs exhibited high *R* and *P* of $1.14x10^4$ AW^{-1}

and $1.04x10^4$. This work clearly indicates that organic materials, especially organic small molecules, enter the field of application for IR and NIR light sensing that is still strongly occupied by inorganic compound-based PT for photodetectors. NIR and IR photodetectors are emerging devices for health care, border security, gas-leak detections, rail safety, soldiers night visions and space observation applications. [81]

The times of OPTs used as light sensors and optical switches, in response to the incident light, should be fast including their reset to the initial set without an external bias. When it comes to the optical memory, responses should also be fast when the light is turned on while very slow in reset. It was previously mentioned that some of the UV responsive OSCs have high persistent photocurrents (PPC), i.e. slow decay, which is a useful characteristic for optical memory development. Ren and Chan, [82] developed an OPT with a combination of the sensing and the non-volatile memory properties using DNTT OSC and polystyrene electret. OPTs were subjected to the blue light illumination combined with a programming bias where the threshold shift of more than 100 V (memory) was achieved. The *R* of these OPTs was 420 AW^{-1} with up to 23-bit dynamic range and high PPC. It was stated that these optically programmed OPTs can be used for multi-level data storage and a high-resolution optical sensing. Moreover, for OPT-based nonvolatile memory, it is not always required to design and synthesized a new OSC.

Besides, an OPT-based memory was integrated into imaging devices. Zhang et al. [83] developed a light-charge organic memory (LCOM) based on the new charge storage molecule. The LCOM was used to construct large-area flexible

imaging arrays with 20000 s retention time of 92% of the light stored charges. A single device was fabricated in TCBG configuration on a Si-wafer (Fig. 2.4a). Between the gate dielectric and a pentacene OSC, a layer of compound M-C10 was deposited. The role of pentacene was to facilitate photoexcited electrons while M-C10 was the trapping layer for those electrons, thus, generating the memory effect. Generally, the operational principle can be divided into two parts: 1) programming with positive bias and light illumination, and 2) sensing/erasing (Fig. 2.4b-e). While biased with the positive gate voltage (Fig. 2.4b) OPTs were programmed in the dark where electrons injection from gold electrode was blocked since pentacene is a p-type OSC. Upon light illumination at the fixed positive gate voltage, photo-generated electrons were generated in the pentacene layer (Fig. 2.4c). Governed by the positive gate voltage, photoelectrons were trapped at the pentacene/M-C10 layer and eventually into the M-C10 layer. Simultaneously, the photo holes were generated in the pentacene layer. The analog signal stored in M-C10 was sensed and measured by LCOM in TFT mode, while the device was reset by applying the negative bias voltage (Fig. 2.4d and e). The performance of LCOM was largely dependent on molecular organization of M-C10 molecules being significantly enhanced upon its annealing. The mobility, On/Off ratio and V_{Th} of pentacene on annealed M-C10 were 2.74 $cm^2V^{-1}s^{-1}$, $5x10^6$ and -1.95 V, respectively. This simple and smart design was applied into flexible imaging arrays constructed from LCOM where nice pictures of a letter A and a Chinese “taiji” were recorded by the programmed illumination and sensing working principle of LCOM arrays (Fig. 2.4f).

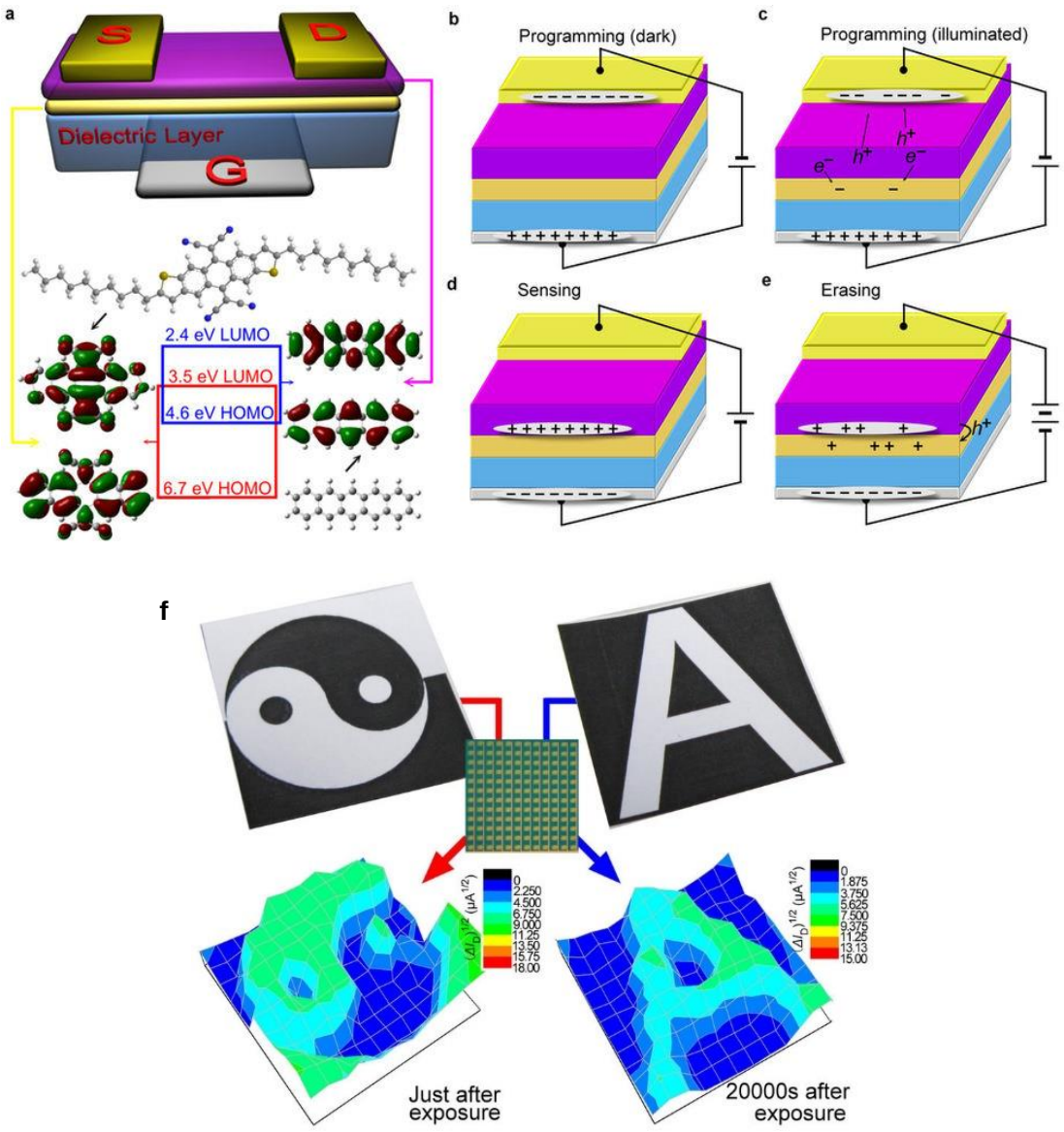

Fig. 2.4. (a) Illustration of LCOM structure that similar to an OTFT structure and structures of organic semiconductors including their HOMO/LUMO energy levels; (a-e) operational principle of the LCOM, and (f) illustration of the imaging using the LCOM. *Reprinted from* [83] *with permission, Copyright © 2013, Macmillan Publishers Limited.*

2.4.3 Polymer OPTs

Integration of the light responsive organic polymer semiconductors (pOSCs) into optoelectronic devices attracted significant research attention since they can be fabricated by low-cost solution deposition and printing methods over large areas of substrates. On the physical side, pOSCs have many advantages compared to small molecule OSC. They are mechanically flexible, have better processability in solution, and excellent compatibility with plastic flexible substrates. On the chemical side, pOSC have much longer conjugation path due to a long polymer chain and broader optical absorption. [84] Furthermore, polymers are less prone to crystallization and formation of highly ordered structures. As a result, mobility in polymer based OPTs is lower than that of small molecule based OPTs. [85] Besides, some challenges still need to be overcome such as efficient photo charge generation, transport, and their collection. [14]

Since the pioneering work of Narayan et al. in 2001, [25] who reported poly(3-octylthiophene-2,5-diyl) (P3OT) based OPTs with polymer dielectric PVA, many efforts have been made to overcome the aforementioned challenges due to the development of both organic semiconductors [86] and fabrication methods. [87] The distinct works were summarized in some excellent reviews. [14][84] Meanwhile we will focus on the very recent progress in the area of polymer OPTs. As observed, in the past few years, the main focus became donor-acceptor type conjugated (co)polymers. After a summary of the distinct works based on PDA polymer, we

summarized the recent progress in the development of D-A (co)polymers and the device engineering.

Nam et al.[88] developed a new mussel-inspired polydopamine (PDA) based OPT (Fig. 2.5a). It is well-known that mussels use a protein that is composed of dopamine to stick onto incompatible surfaces such are rock and stones. [89] A new synthetic route was developed for oxidative polymerization of dopamine and PDA was deposited onto SiO_2 dielectric (Fig. 2.5a and b). PDA semiconducting layer was characterized by dense and conformal surface by purging with oxygen instead of a conventional air stream while polymerized/deposited onto SiO_2. PDA had good adhesion on the substrate. The p-type OPTs had good electrical properties in the dark V_{Th} of -6 V, On/Off ratio $1.2x10^5$, and the high field-effect mobility of 0.96 $cm^2V^{-1}s^{-1}$ (Hall mobility was 16 $cm^2V^{-1}s^{-1}$). Under the white light illumination with an intensity of 193 $mWcm^{-2}$ at V_G=-12 V, OPTs exhibited high *R* and *P* of 9 AW^{-1} and $6.9x10^4$. When operated as a light sensor, OPTs showed a fast response time (0.5 s) and fast reset (1.2 s) when the light was turned off (no bias voltage applied) with excellent reproducibility (Fig. 2.5c). This concept indicates a bright future of the bio-inspired photoswitches.

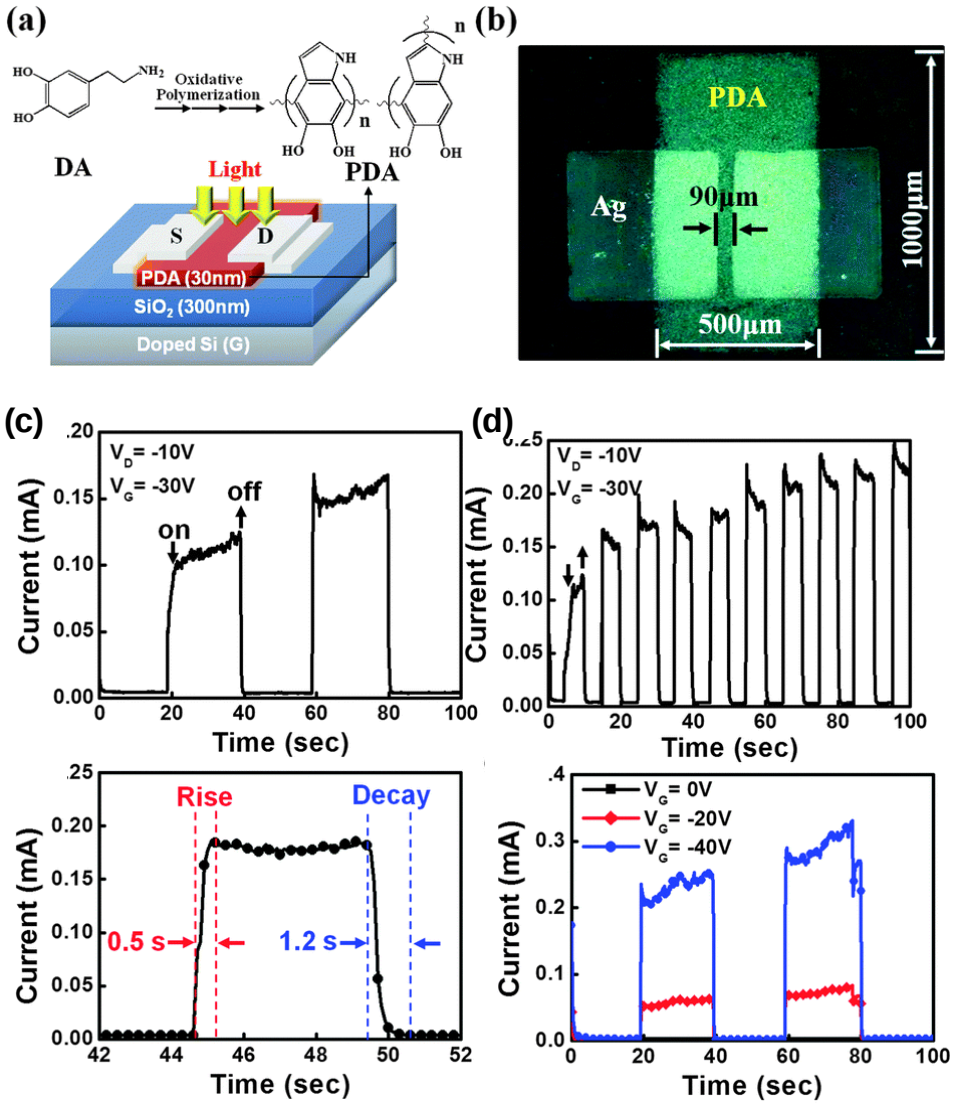

Fig. 2.5. (a) Schematic of the oxidative polymerization of DA and TCBG configuration of PDA-based OPT, (b) Optical micrograph image of the PDA-based channel of an OPT with Ag electrodes on the top and channel dimensions, (c and d) Dynamic characteristics of PDA OPTs under the white light (193 mWcm-2). *Reprinted from* [88] *with permission, Copyright 2013, Royal Society of Chemistry.*

Likewise, in solar cells, the donor-acceptor (D-A) strategy for developing high-performance polymer OPTs was applied in the field of OPTs. The D-A copolymers have broad absorption wavelengths, [90,91] and high charge carrier mobilities that can be tuned by the polymer chain microstructures. [92–94] OPTs based on copolymers as a single component in the channel were pioneered by Hamilton et al. in 2004. [27] A poly(9,9-dioctylfluorene-co-bithiophene) (F8T2) copolymer was integrated into an OPT for photodetection of the monochromatic light. It was found that under light illumination, I_{phc} increased significantly in the subthreshold region of OPT. Additionally, I_{phc} level was dependent on the light wavelength. With different wavelengths, the energy of light varies and the density of charge carriers generated by the light is different, resulting in different levels of I_{phc}. [26] The follow-up work using the F8T2 copolymer as a channel material enhanced R (18.5 AW^{-1}) by increasing the gate voltage. [95] These works opened the field for further progress in copolymer OPTs, especially D-A copolymers.

The new D-A copolymers synthesized having a planar benzo[1,2-*b*:4,5-*b*']-dithiophene (BDT) donor unit were integrated into OPTs with high-performance. [96,97] The BDT and similar units such as benzo[1,2-*b*:3,4-*b*']-difuran (BDF) appeared to be a good building block for D-A polymers. Recently, several works reported various D-A polymers containing BDT and BDF units. Liu et al. [98] tailored a series of conjugated copolymers containing BDT and bithiazole units for OPT white light photosensors. By optimization of the polymer backbone and side chains, it was demonstrated that OPT performance could be tuned by means of solubility behavior, molecular ordering, film morphology, field-effect mobility, and

photosensitivity. A copolymer with optimized structure (long and branched alkyl chains on BDT unit), used as a channel material, enabled OPTs with the best performance having the mobility of 0.194 $cm^2V^{-1}s^{-1}$, On/Off ratio of 10^6, and V_{Th} of -6 V. Photoelectrical characteristics were *R* of 132 AW^{-1} and *P* of $2x10^5$. It was claimed that OPTs based on this derivative exhibited long-time operational stability in ambient conditions. Using BDF containing copolymers, Huang et al. [99] fabricated an OPT photosensor based on poly{4,8-bis(2'-ethyl hexylthiophene)benzo[1,2-b;3,4-b']difuran-alt-5,5-(4',7'-di-2-thienyl-5',6'-dioctyloxy-2',1',3'-benzothiadiazole)} (PBDFTDTBT) on a Si-wafer substrate in a TCBG configuration. Under the white light illumination with various intensities, the highest *P* and *P* were 0.36 AW^{-1} and $1.2x10^5$, respectively. When operated in dark, OPTs had the mobility of 0.05 $cm^2V^{-1}s^{-1}$ and On/Off ratio of $4.6x10^5$. As an alternative to PBDFTDTBT polymer thin films, benzodifuran-based nanowires were proposed for high-photosensitive OPTs. Zhu et al. [100] prepared bis(2-oxoindolin-3-ylidene)-benzodifuran-dione (PBIBDF-TT) D-A conjugated polymer nanowires (NW) and fabricated high-performance OPT photosensors. The new NW ambipolar OPTs were responsive to NIR light (47.1 $mWcm^{-2}$), exhibiting higher *R* and *P* than thin film counterpart due to a high aspect ratio of NW. The *R* and *P* were 440 mAW^{-1} and $1.3x10^4$ for the p-type regime, respectively, and 70 mAW^{-1} and $3.3x10^4$ and for the n-type regime, respectively.

The trend of making new derivatives with the structure like BDT kept active and some other brilliant achievements were made. In contrast to mainly amorphous conjugated polymers, Li et al. [101] fabricated OPT photosensors for white light

utilizing a self-assembled ultrathin crystalline copolymer PQBOC8. The photoelectrical properties were greatly improved compared to previous examples, as indicated by very high *R* and *P* of 970 AW^{-1} and $1.36x10^4$, respectively, under the very low light intensity of 43 $mWcm^{-2}$. However, no sensing dynamics were reported. Wang et al. [102] developed an OPT based on D-A conjugated ambipolar polymer PBIBDF-BT with a high response speed to the red light. With both hole and electron transports, OPTs had very fast speeds below 14 ms. The *R* and *P* for the p-type channel were 108.43 mAW^{-1} and 4552, respectively, while for the n-type channel the same parameters were 38.72 mAW^{-1} and 1044, respectively. The I_{phc} in ambipolar OPTs showed a gradual increase in the illumination intensity. Moreover, planar D-A conjugated polymers for high performance OPTs photosensors were developed by Kang et al. [103] A series of novel conjugated polymers comprising of carbazole and benzo oxadiazole (CZ-BO) or benzothiadiazole (CZ-BT), as the donor and acceptor units, respectively, were synthesized and used for fabrication of OPTs for photo sensing of white light. All the devices exhibited a p-type operation mode with high mobilities in the range of 0.02-1 $cm^2V^{-1}s^{-1}$ and On/Off ratio of 10^6. Noteworthy, no post-treatment was required for these OPTs. The best characteristic of OPTs was their response times to the light. OPTs based on BO containing polymer responded to the light (rise times) within 1 s, while BT based OPTs had much longer rise times (12.7-17.1 s). When the light was turned off, no PPC was observed and devices were spontaneously reset (4.9-10.9s for BO based OPTs and 19.7-23.9 s for BT OPTs). This characteristic makes them good candidates for photosensors. Interestingly,

BO polymers showed faster response than BT polymers, which was explained by the more crystalline structure of BO polymers and the larger grains observed in the film morphology. For photo sensing of the light of broader wavelengths, Li et al. [104] developed OPTs based on ambipolar phenanthrene condensed thiadiazole quinoxaline D-A copolymer (PPhTQ). The ambipolar polymer-based OPTs with a very low optical bandgap of 0.80 eV showed high *R* of 400 AW^{-1}, and fast response times, when the light was turned on and fast reset times when the light was off. The balanced mobilities were 0.09 $cm^2V^{-1}s^{-1}$ and 0.06 $cm^2V^{-1}s^{-1}$ for the p- and n-type regimes.

Another group of OSC copolymers based on diketopyrrolopyrrole (DPP) unit represents a promising building block for OPTs due to their easily tailored polymer chain structure, solubility, and high crystallinity. [93,105] Since Yang et al. [106] reported two copolymers based on the DPP building blocks P(DTDPP-*alt*(1,6)PY) and P(DTDPP-*alt*(2,7)PY) with good hole mobility (0.23 $cm^2V^{-1}s^{-1}$) and excellent photoelectrical properties (*R*=0.36 WA^{-1} and P=1.2x10^5). DPP-based polymers attracted significant research attention. Besides the high mobility and the high *R* and *P*, which are required for high-performance OPTs, the operational voltage is one more parameter that should be kept low for their commercialization. The goal for high-end application, flexible devices are desired. While developing a low voltage, flexible, and the high-performance OPT, Liu et al. [107] went a step further and fabricated “2-in-1 OTFTs”, namely phototransistors and thermal detectors. PDQT and PDVT-10 copolymers were utilized individually for fabrication of the low-voltage OPT with PVA polymer dielectric on a PET substrate. Lowering the V_{DS} in

PDQT and PDVT-10 based OTFTs is very important for commercial application since they typically required a voltage above -60 V as demonstrated. [105,108] PDVT-10 based OPTs exhibited high hole mobility, On/Off ratio, and low threshold voltage of 11.0 $cm^2V^{-1}s^{-1}$, $1.2x10^4$, and -1.66 V, respectively. On the other hand, PDQT had lower mobility (1.7 $cm^2V^{-1}s^{-1}$), On/Off ratio ($8.0x10^3$), and similar V_{Th} (-1.30 V). The flexible PDVT-10 OPTs had *R* of 433 mAW^{-1} and *P* of 173 under a white light illumination (0.85 μWcm^{-2}). The only drawback of these OPTs was high leakage currents.

Low-cost fabrication techniques are the advantage of organic electronics compared to Si-based devices, among which printing is sought as an emerging technique for large-area devices. Wang et al. [109] constructed an OPT with another DPP-based copolymer that facilitated ultrahigh light responsive and high-performance photosensors. PDPPTzBT copolymer was utilized as a channel material to fabricate short channel geometry on TCBG configuration. The short channels were organized in a series of arrays via “coffee ring lithography” inkjet printing through a 50 µm orifice nozzle. Consequently, the channel lengths were 1 µm to 700 nm. At the channel length of 700 nm, the *R*, *P,* and max mobility were 106 AW^{-1}, $2x10^5$ and 1.80 $cm^2V^{-1}s^{-1}$ respectively, at an illumination of 40 μWcm^{-2}. As seen in Fig. 2.6a, the onset gate voltage was strongly dependent on the channel length and illumination intensity. At V_{DS} and V_G of -20 V and 20 V, respectively, the transient characteristics of OPTs showed fast responses upon LED light (650 nm) was turned on. The amount of photocurrent was strongly dependent on the light intensity, reaching the highest at the highest light intensity (40 μWcm^{-2}) (Fig. 2.6b).

Interestingly, PDPPTzBT showed memory characteristics since PPC was observed after the light was off, enabling application of these devices as light-triggered memory elements for optoelectronic devices.

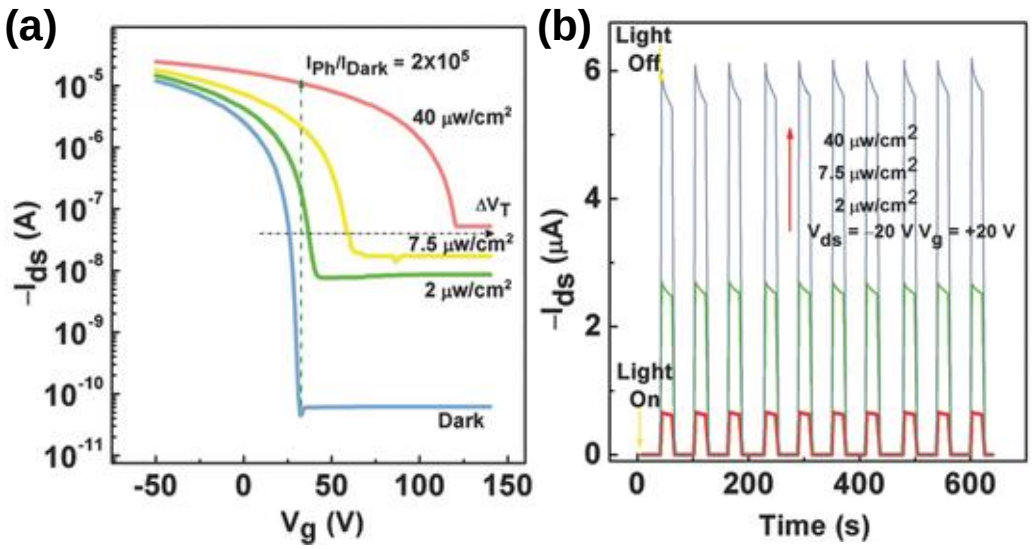

Fig. 2.6. (a) Transfer and (b) transient characteristics of a short-channel OPT (700 nm) under light illumination with different intensities compared to darkness. *Reprinted from* [109] *with permission, Copyright 2014, Wiley*.

Similarly, Ma et al. [110] reported OPT photosensors based on a new DPP-BDT copolymer (P(DPP4T-*co*-BDT). Thermally annealed thin film OPTs based on this copolymer exhibited hole mobility of 0.047 $cm^2V^{-1}s^{-1}$, high *R* of $4x10^3$ AW^{-1} and *P* of $6.5x10^5$ under the white light intensity of 9.7 μWcm^{-2}. Another example about OPTs was the very recent work (2017) based on very attractive DPP containing copolymers. It was focused on the investigation of the effects of polymer chain

design on the performance of OPTs. Kim et al. [111] proposed a DPP-BT copolymer, abbreviated as pTTDPP-BT, containing two acceptor units (DPP and BT) and one donating unit (TT). The specific polymer structure was chosen upon DFT calculations to lower LUMO level for better charge separation and electron transport. The mobility in OPTs based on this ambipolar polymer was strongly dependent on thermal annealing. The hole and electron mobilities after thermal annealing at 200°C were 0.066 $cm^2V^{-1}s^{-1}$ (before 0.007 $cm^2V^{-1}s^{-1}$) and 0.115 $cm^2V^{-1}s^{-1}$ (0.005 $cm^2V^{-1}s^{-1}$). The OPTs exhibited a broad spectral light absorption, high switching speeds and *P* of 150 at 1 $mWcm^{-2}$ and V_G=30 V.

To achieve the high mobility and highly light responsive characteristics of OPTs based on conjugated polymers containing DPP-unit, nanowire OPTs for the monochromatic light sensing (632 nm) were reported. Um et al. [112] synthesized highly crystalline conjugated polymer nanowires based on DPP and 1,2-bis(5-(thiophen-2-yl)-selenophen-2-yl)ethene (DPPBTSPE) in the repeating unit. The DPPBTSPE showed p-type operation regime when integrated into OPT as the channel material. The combination of a planar and rigid electron donating selenophene unit with DPP facilitated a high mobility of 24 $cm^2V^{-1}s^{-1}$. The R_{max} and *P* were 1920 AW^{-1} and 10^3-10^4, respectively. Another example for high-performance OPTs based on NW networks was recently reported by Lei et al. [113] A narrow bandgap diketopyrrolopyrrole-dithienylthieno[3,2-b] thiophene (DPP-DTT) polymer (D-A type) was solution processed to prepare NW networks on a SiO_2 coated Si wafer substrate. 2D NWs were prepared via polymer matrix-assisted molecular self-assembly method using polystyrene (PS). The photoelectrical

properties of NW-OPTs indicated high-performance with *R*, *P* and EQE of ~246 AW-1, 1180 and $3.5x10^4$% obtained. The high molecular ordering and low-density structural defects were used to explain the enhancement and high-performance of the NW networks based OPTs.

2.4.4 Blend-based OPTs

In the recent years, semiconducting blends as active channel materials for OPTs become very attractive due to the possibility of employing the best property of each component to synergistically generate a new or enhanced existing property. By blending of two or more components, a large interface can be generated. In turn, control of morphology and, thus, enhancement of OPTs properties are expected. Up to date, two major groups of blends as channel materials can be observed 1) bulk heterojunctions (BHJ) and 2) OSC/dielectric polymer blends. In the former, both components are semiconductors while in the latter at least one component is dielectric. The main advantage of BHJ is that it allows the combination of D-A types of OSC by simple solution blending, thus eliminating complex synthetic routes often required to produce a conjugated D-A polymer. In terms of the mechanism, a special attention should be paid to the generation of the interface to produce a high-performance BHJ OPT. Thus, BHJ is the interface governed channel materials, facilitating a long-range and fast charge separation at the donor-acceptor interface. [33,114–116] The BHJ materials are widely used in organic photovoltaic devices for the above reasons and they have paved the way

into OPTs for fast optical sensing. In the following paragraphs, we summarize the most recent achievements in the field of BHJ OPTs.

Bulk heterojunctions. Very recently, Peng et al. [117] developed the board spectral response OPTs for light sensing, based on three-component planar-bulk heterojunction. The utilized small molecules were 3,4,9,10-perylene tetracarboxylic dianhydride (PTCDA), chloroaluminum phthalocyanine (AlClPc) and C60, with complementary optical absorption. The layered blend thin films were used for OPTs fabrication via a thermal evaporation process. All the devices showed a response to the light with broad wavelength range 300-850 nm. Under light illumination of 70 μWcm^{-2}, the average *R* was 0.40 AW^{-1}. When SiO_2 dielectric was replaced with crosslinked PVA, the OPT performance was further improved and reached the average *R* of 2.44 AW^{-1}.

BHJ OPT based on conjugated polymer or small molecule D-A materials has been reported. Yasin et al. [118] developed BCTG BHJ OPTs based on P3HT and PCBM blends with *R* of 3 AW^{-1}, at V_{DS} of -3 V and UV-vis illumination of 100 $mWcm^{-2}$. Similarly, to polymer OPTs (single component in the channel), DPP-based polymers are also attractive for BHJ OPT, as demonstrated by Xu et al. [119] An NIR BHJ OPT was constructed based on poly(N-alkyl diketopyrrolo-pyrrole dithienylthieno[3,2-b]thiophene) (DPP-DTT), and $PC_{61}BM$ small molecule. The OPTs showed high *R* of 105 AW^{-1} and a wide tunability of the photoconductive gain (>$1x10^4$). By applying the optically tunable gate voltage, the photocurrent gain was further modulated, suppressing the noise currents. The high-sensitivity of OPTs enabled the use of the low-power light source and it reduced the overall power consumption of

sensors. OPTs had fast response and relatively fast reset. With the ultra high responsivity and predominant hole charge transport (0.3 $cm^2V^{-1}s^{-1}$), these devices are promising for application as photoplethysmographic (PPG) sensor (Fig. 2.7a), that detects light emitted from skin (Fig. 2.7b and c), to measure the heart rate, blood pressure (Fig. 2.7d) and other health parameter. PPG can also be integrated into the wearable accessories.

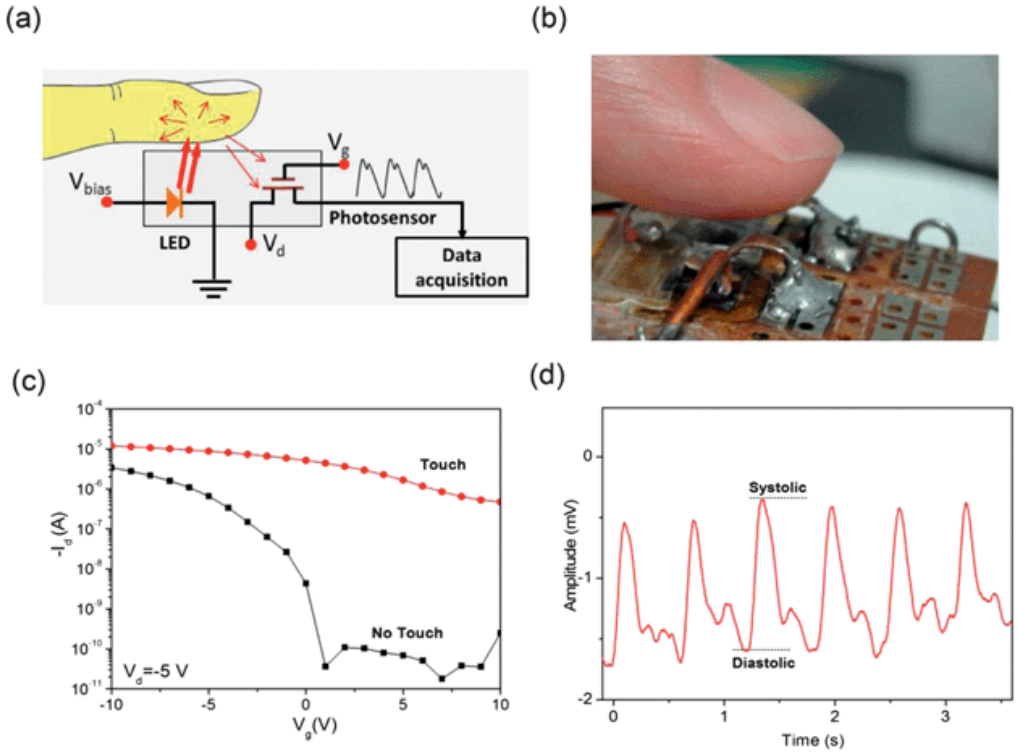

Fig. 2.7. (a) Illustration of photoplethysmography (PPG), (b) Digital image of the PPG sensor. (c) Transfer curves of the phototransistor sensing “touch” and “no touch” and (d) Amplitude vs time measurement of the systolic and diastolic process (output waveform of the pulse) (V_{DS} = −20 V, V_G = 10 V). *Reprinted from* [119] *with permission, Copyright 2013, Royal Society of Chemistry*.

Another example of BHJ OPTs to utilize DPP-type polymer and PCBM was reported in 2015. Rim et al. [120] fabricated a transparent BHJ OPT, based on PBDTT-DPP/$PC_{61}BM$ blends on In-Ga-Zn-O (IGSO)/glass substrates. OPT photodetectors exhibited ultra-high *P* and broad spectral photoresponses (UV to NIR light). Very broad responsivity was achieved by selection of the channel materials and a transparent substrate (73% transmittance under visible light). Use of an IGZO electrode suppressed the electron-hole recombination and affected positively the performance of OPTs. OPTs on rigid substrates, operated in the dark, are characterized by high mobility of 7.02 $cm^2V^{-1}s^{-1}$ and high On/Off ratio of 10^6. Under visible light (400-780 nm, 1 $mWcm^{-2}$), the photo again was more than 10^5 at V_G=-5 V, while detectivity of $1.7x10^{12}$ Jones and 168% of external quantum efficiency (EQE, at 588 nm incident light) were achieved. The high *P* remained relatively unchanged in the fabrication of flexible devices using the same BHJ material on polyimide substrates.

Recently, it was demonstrated that the channel materials and the gate modification can be beneficial for the development of BHJ OPTs for biomedical applications. [121] Since the construction of the aqueous electrolyte gated OTFT, [122] the research interest was placed on the use of organic solution gated transistors (OWGTs). The electrolytes can form a double-electric layer with relatively high capacitances and lower potentials at the interface. [123,124] This enabled their application in solution-gated PTs with semiconductor/solution interface. [125,126] Xu et al. [127] reported a new concept in OPTs, the ambipolar BHJ-based OPT based on OWGT (Fig. 2.8a). The capacitance of the OWGT dielectric was ~3 μFcm^{-2}. Devices showed tunable photodetection in the n-type regime (Fig. 2.8b) and stable operational stability (both carrier types, Fig. 2.8c). OWGT

OPTs exhibited an *R* of 0.87 AW^{-1}. The photocurrent gain and responsivity were dependent on the light intensity while OPTs showed a stable and fast response to light.

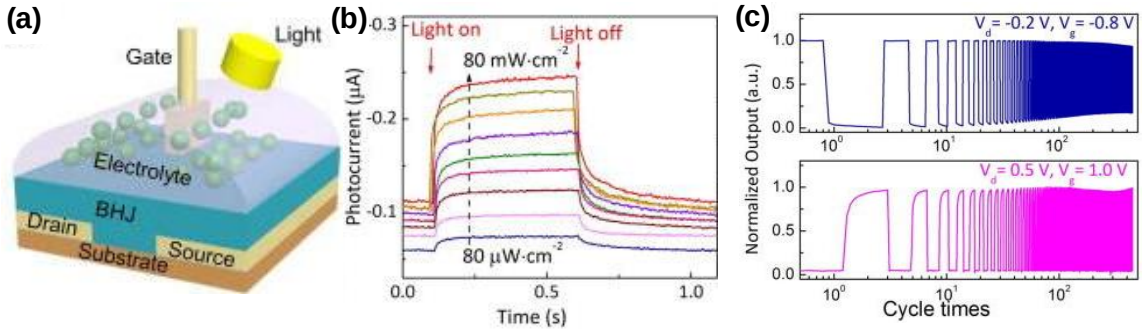

Fig. 2.8. (a) Illustration of the bottom-contact, bottom organic-solution gate phototransistor, (b) transient characteristics of OPTs showing the light tunable response of the photocurrent, and (c) operation stability measurements in n- and p-type regime. *Reprinted from* **[127]** *with permission, Copyright 2016, AIP Publishing LLC.*

The field of all conjugate polymer heterojunctions has attracted much research attention since Hwang et al. [128] reported the OPTs with nanoscale phase-separated ambipolar polymer/polymer BHJ. Using P3HT and F8T2, they fabricated OPTs on ITO/glass substrates with polymer gate dielectric (PMDA-ODA polyimide). With optimized P3HT/F8T2 composition of 60:40, the OPTs showed the highest quantum efficiency and photoresponsivity of 4.3 AW^{-1} at light intensity of 1 μWcm^{-2} (470 nm), indicating their potential application for conventional cooled charge coupled devices (CCD) for detection of the low light intensity in space industries

and biomedicine. For the realization of the broadband polymer-polymer BHJ OPTs, Han et al. [129] employed BHJ of the newly synthesized poly[{2,5-bis-(2-ethylhexyl)-3,6-bis-(thien-2-yl)-pyrrolo[3,4-c]pyrrole-1,4-diyl}-co-{2,2'-(2,1,3-benzothiadiazole)}-5,5'-diyl}] (PEHTPPD-BT) as n-type copolymer with the p-type P3HT blend (1:1) for NIR (PEHTPPD-BT) and visible light (P3HT) sensing. The BHJ layers were nanostructured upon deposition with randomly distributed domains of one component into another. The high interface that polymers generated was the main reason of high-performance where charge separation process occurred from D-polymer HOMO (P3HT) to A-component LUMO. The OPTs were fabricated on rigid and flexible substrates, with *R* reaching 450 mAW^{-1} (visible light) and 250 mAW^{-1} (NIR). Devices on flexible substrates were operated at low voltages -1 to -5 V and could detect the visible and NIR lights even in the bent state. Another work on all-polymer BHJ OPT with P3HT as a donor component was reported by Nam et al. [130] Similarly to the previous approach, these authors used P3HT:PBDTTPD blends in a different ratio to fabricated the OPTs on rigid substrates. It was found that 80:20 P3HT:PBDTTPD exhibited the best performance with *R* reaching 33.3 AW^{-1} under illumination of the green light (555 nm, intensity 0.16 μWcm^{-2}) at V_G and V_{DS} of -60 V. Furthermore, the same group used P3HT:PBDTTPD blends to fabricate one more type of the visible-NIR BHJ OPT sensor. [114] Using this composition of the n-/p-type conjugated polymer blends, BCTG OPTs were constructed on a glass substrate, allowing an incident light of various intensities and wavelengths to efficiently illuminate the channel. As gate dielectrics, the double gate layer constructed from PMMA and PVA were used.

Ambipolar OPTs had hole and electron saturation mobilities of 0.16 and 0.06 $cm^2V^{-1}s^{-1}$ at V_G=±60. Under light illumination (450, 555, and 795 nm), it was found that I_D increased in both n- and p-type modes. The highest *R* was obtained under the light wavelength of 450 nm with an intensity of 5.32 μWcm^{-2} for both n- and p-type modes and were higher of those for pristine BHJ components.

Further, progress in the field of all-polymer BHJ OPTs for light sensing/detection still involved a traditional conjugated polymer P3HT, but it was expanded by the design of a new type of n-type polymers for BHJ blends. Kim's group reported three more excellent all-polymer BHJ OPTs. In 2016, they reported a new THBT-ht n-type polymer (poly(3-hexylthiopehe-co-benzothiadiazole) end-capped with hexylthiophene) for BHJ with P3HT. [131] OPTs were fabricated on ITO/glass substrates with PVP-MMF polymer dielectric at THBT-ht: P3HT blending ratio of 30:70. All the OPTs showed a remarkable increase of the drain current at all the wavelengths (470, 550 and 665 nm) and intensities of the light illumination. The OPTs on flexible PET substrates were also fabricated. The corrected responsivity was ~4 AW^{-1} at 470 nm and ~2 AW^{-1} at 550 nm, which was much higher than on ITO/glass substrates. In a similar work of this group reported this year, a new end-capped 4-hexylthiophene (THBT-4ht) poly(3-hexylthiopehe-co-benzothiadiazole) was proposed for BHJ blends with P3HT. [132] It was found that the composition effect strongly affected the performance of OPTs. The best charge transport characteristics of OPT were obtained at 10 wt.% of THBt-4ht, while the highest *R* and charge separation were determined for OPTs at THBT-4ht contents of 20 and 30 wt.%, respectively. To develop an efficient BHJ OPT for deep red-

light sensing, Nam et al.[133] prepared blends of p-type PTB7 (poly[4,8-bis[(2-ethylhexyl)-oxy] benzo [1,2-b:4,5-b']dithiophene-2,6-diyl] [3-fluoro-2-[(2-ethylhexyl) carbonyl] thieno[3,4-b]-thiophenediyl]) and n-type P(NDI2OD-T2) (poly-[[N,N'-bis(2-octyldodecyl)-naphthalene-1,4,5,8-bis(dicarboximide)-2,6-diyl]-alt-5,5'-(2,2'-bithiophene)]). Devices were fabricated in BCTG configuration using glass as a substrate. By variation of the red-light intensity, the highest R ~14 AW^{-1} was obtained owing to a nanostructured/crystalline morphology of the blend.

Small molecule/dielectric polymer blends. In the last five years, blending of small molecule OSCs and dielectric polymers became a promising strategy to enhance, control and modulate photoelectrical properties of small molecule OSCs that are responsive to light. The advantage of this strategy is that a large interface can be generated enabling interaction of functional groups of the polymer and OSC molecule on a quantum level. The mechanism of OSC/polymer interaction could be similar to BHJ but blends are not mixed on the nanoscale level and one of the components is not conjugated. The most utilized OSCs for UV light responsive blends are p-type 2,7-dialkyl[1]benzothieno[3,2-b][1]benzothiophene derivatives (C*n*-BTBT). Since the first demonstration of channel materials for OTFTs by Ebata et al. [134] C*n*-BTBT derivatives were widely used for solution processed and high-performance OTFTs. The mobilities as high as 43 $cm^2V^{-1}s^{-1}$ were reported for C8-BTBT/PS blends deposited by the off-center spin-coating method. [7] Smithson et al. [28] were first to report C5-BTBT responsivity to UV-A light (365 nm) and its modulation of photoelectrical characteristics by a dielectric polymer containing dye molecules. In an attempt to modulate C5-BTBT photoelectrical properties with aid

of functional groups in the dielectric polymer, an azobenzene derivative (DR1) functionalized PMMA was prepared (Fig. 2.9a). DR1 represents an azobenzene-based small molecule dye containing strong electron withdrawing nitro groups. A binary blend (1:1 by weight) comprising of C5-BTBT and a small molecule dye functionalized PMMA (*p*-DR1) was solution mixed and used as a channel material in TCBG OPTs (Fig. 2.9b). C5-BTBT:PMMA blend-based OPTs were used as control devices. Compared to C5-BTBT:PMMA devices, OPTs to contain a *p*-DR1 highly enhanced photoelectrical properties. OPTs in the dark exhibited a typical p-type behavior while I_D increased more than six orders of magnitude in the subthreshold region under the UV light illumination. A significant increase of the photocurrent was attributed to strong interface trapping in the blend due to the strong electron accepting nitro groups. OPTs operated in the photovoltaic mode as indicated by a large shift of the threshold voltage of 90 V. Transient characteristics of OPTs with p-DR1 revealed the fast response to UV light with the high PPC upon light was off (Fig. 7c). This report represents a smart design for the light selective OPTs with photo memory since C5-BTBT is blind to visible (Fig. 2.9).

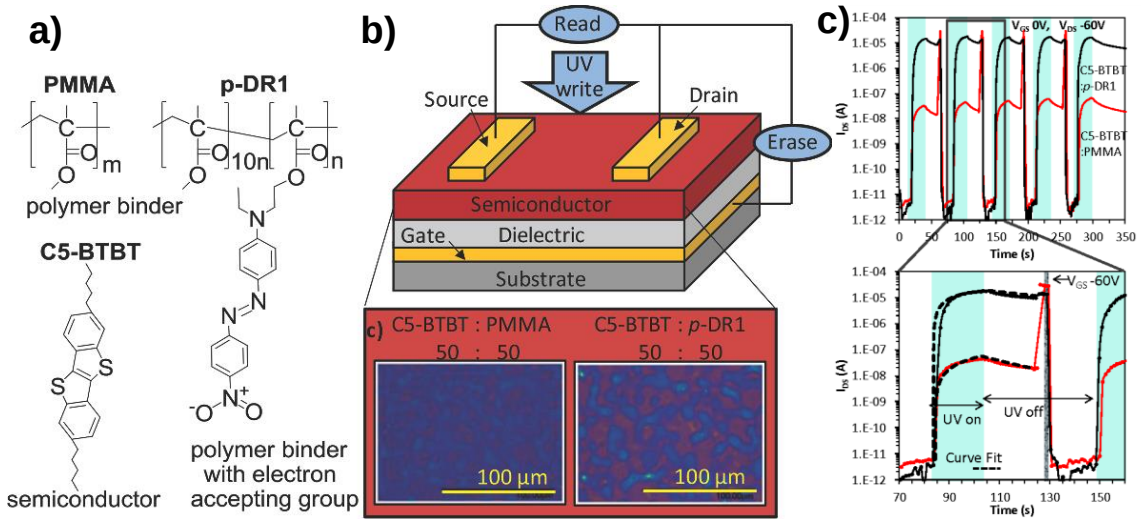

Fig. 2.9. (a) Chemical structures of the channel materials, (b) TCBG configuration of the OPT with operation step while working as photo memory and optical micrographs of the thin film morphologies, and (c) transient characteristics of C5-BTBT/p-DR1 based OPTs. *Reprinted from* [134] *with permission, Copyright 2015, Wiley*.

To further investigate the effects of D-A groups on OPTs performance, Smithson et al. fabricated OPTs using three-component blends, namely C5-BTBT/PMMA/azobenzene derivatives. [135] Various azobenzene derivatives were employed as additives (5 mol% with respect to C5-BTBT) and their main difference was functional D-A groups attached (or none) on the azobenzene moiety. The subthreshold characteristics of OPTs were strongly dependent on D-A nature of the azobenzene derivatives. The *P* of OPTs was similar for all devices with azobenzene additives (10^5-10^6) compared to control C5-BTBT/PMMA OPT (10^3). The main conclusions from this work were: 1) blends that contained more electron

accepting azobenzene derivatives generated higher amount of the photocurrent (the higher *P*), and 2) transient characteristics of OPTs were highly affected by D-A nature of the azobenzene derivative i.e. the fastest response and the longest decay of PPC were with electron accepting additives in blend (photo memory effect). The mechanistic study of these systems using DFT calculations and experimental data revealed that, if it is to generate memory devices with OPT structure, the HOMO and LUMO energy levels of the chosen material should be lower than that of C5-BTBT to facilitate an efficient generation/separation of photogenerated charge carriers under light illumination, strong trapping and thus slow recombination. Moreover, this concept was utilized by the same group to fabricate rapid UV-A photodetectors based on C5-BTBT/PMMA blends with 1,5-dichloro-9,10-dintiro-anthracene (2Cl-2NO2-Anth) additive (5 mol% of total mol of C5-BTBT).[136] The 2Cl-2NO_2-Anth is a very strong electron accepting molecule due to two nitro groups and chlorine atoms attached to the anthracene molecule. The effect of light intensity on OPTs performance was investigated and it was found that subthreshold current largely depended on the intensity of incident light. OPTs based on C5-BTBT/PMMA/2Cl-2NO2-Anth blends showed *P* of 10^5 under very weak UV light of 0.0427 $mWcm^{-2}$ and *R* of 40 AW^{-1} at V_G=-60 V. The devices operated as light write/electrical erase memory with fast responses to UV-A (1.6 s), fast saturation and slow decay of the persistent photocurrents of more than 2 h. It is interesting to note that azobenzene undergoes cis-trans isomerization under light and some concepts rely on the property. Here, the authors solely relied on the

concept of interface charge trapping by D-A functional groups and not on the azobenzene isomerization.

Since dielectric polymers may contain different D-A functional groups or their structure can be tailored with proper functionalized monomers, the modulation of the photoelectrical properties using dielectric polymers only was reported. Ljubic et al. [30] were the first to report OPTs based on C5-BTBT/dielectric polymer blends (no additives) with highly enhanced photoelectrical properties. The TCBG OPTs utilized C5-BTBT/linear polyester blend (1:1 by weight) exhibited a large photoresponse under UV-A light (3 $mWcm^{-2}$ at V_{DS}=-60 V) in the subthreshold region. The significant increase of drain photocurrent was attributed to an efficient trapping of the photo charge carriers at the interface by polyester functional groups and a thin film morphology (lateral phase separation). The *R* and *P* values at VG=0 V were 11 AW^{-1} and $3.9x10^6$ with fast responses to UV light of 1.80 s and slow relaxation of PPC. These findings were compared with C5-BTBT/PMMA blend based OPTs (*R* and *P* of 0.04 AW^{-1} and $4.4x10^4$) and it was clear that polyester had a strong effect on photoelectrical properties of OPTs. In a follow-up work, Ljubic et al. [30] utilized C5-BTBT/branched polyester blend-based OPTs and compared them with the blends containing poly(vinyl acetate), PVAc, polystyrene, PS, and polycarbonate, PC in 1:1 ratio by weight. A large shift of V_{Th} (86 V) was observed under the UV-A light illumination in polyester blend based OPTs due to photovoltaic effect. This was an indication for excess charge carriers generated under light illumination that increased the drain photocurrent of more than five orders of magnitude than other polymers (Fig. 2.10a). Both *R* and *P* were

dependent on the type of polymer in the blend (Fig. 2.10b) The transient characteristics of OPTs were also affected by the type of polymer, as displayed in Fig. 2.10c. These two examples unambiguously confirmed that blending of OSCs and dielectric polymers is a good strategy for the development of high-performance OPTs.

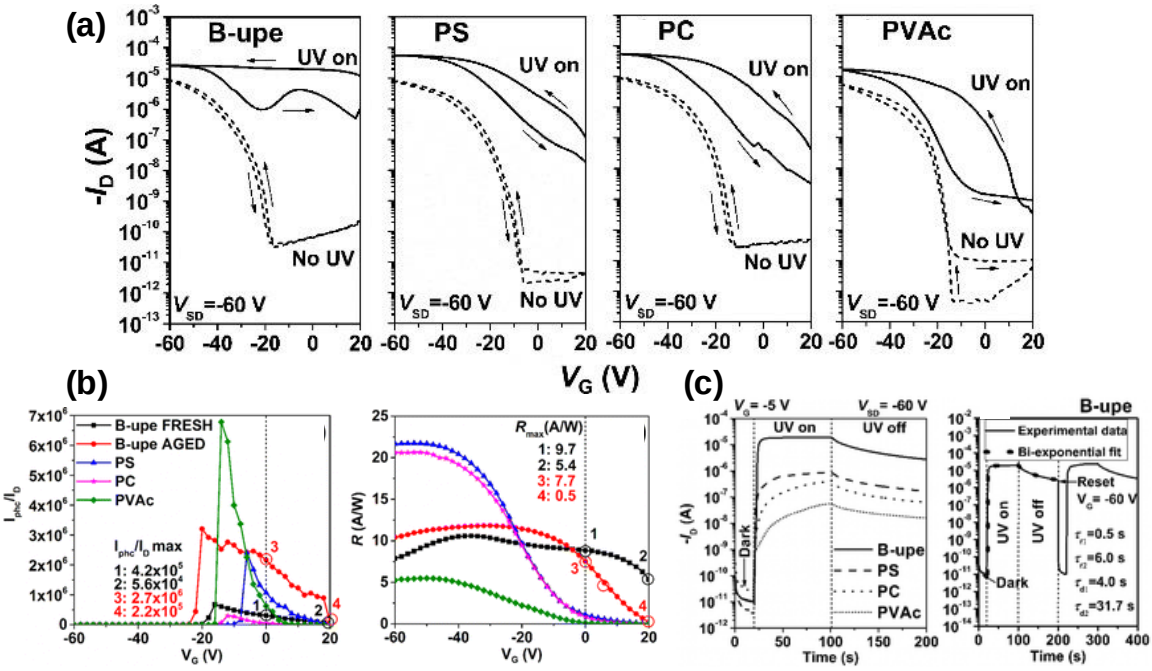

Fig. 2.10. (a) Transfer characteristics, (b) photoresponsivity and photosensitivity as a function of the gate voltage, and (c) transient characteristics of C5-BTBT/polymer bland-based OPTs. *Reprinted from* [30] *with permission, Copyright 2016, American Chemical Society*.

Using the same concept of interface charge trapping of electrons by the dielectric polymer, Huang et al. [31] developed flexible and printable OPTs based on

C8-BTBT/PLA blends (Fig. 2.11a and b). OPTs were evaluated in TCBG configuration on rigid and flexible substrates. OPTs based on layered and blended channels were fabricated for comparison. The drain photocurrent in the subthreshold region was strongly dependent on the light intensity, structure of active channel (layered or blended) and blend composition. The blended OPTs (9 wt% of C8-BTBT in the blend) had high *P* (10^5) due to larger interface in the blend, facilitating strong charge trapping at the interface. The layered OPTs showed much higher photoresponsivity (393 vs 56 (blended) AW^{-1}), due to better alignment of C5-BTBT molecules in the thin film. Flexible devices were fabricated by inkjet printing of a blend solution of C8-BTBT/PLA blend (10:1 by weight). The transient characteristics of printed OPTs were characterized by fast responses to UV light and reset to dark state with decent *P* (10^2 at V_G=-40 V). Flexible OPTs showed reproducible characteristics, both in a flat and a bent state (300 um radius), as shown in Fig. 2.11c and d).

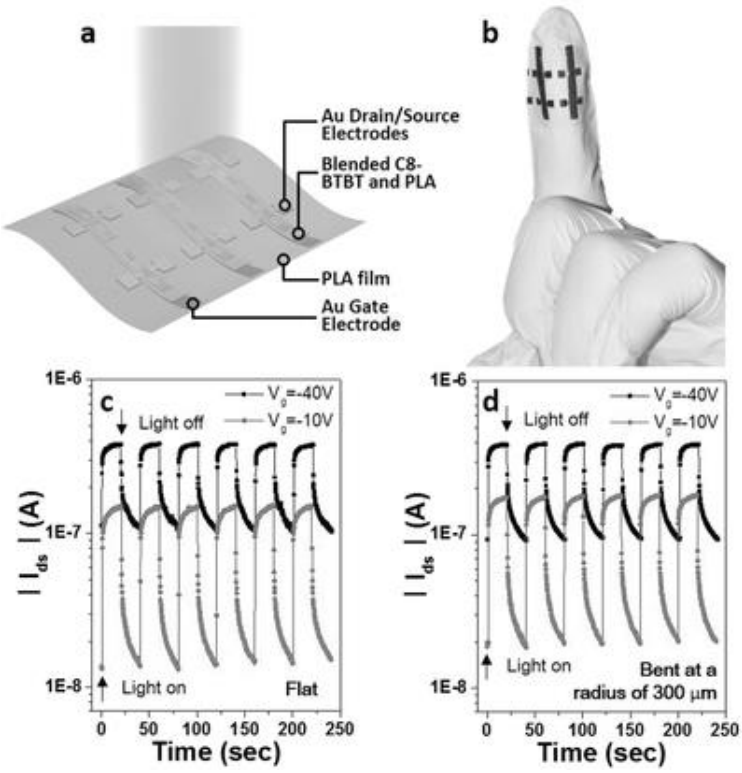

Fig. 2.11. Illustration of inkjet printed and flexible OPT on PLA substrate and the dielectric at the same time, (b) photograph of OPTs, and transient characteristics of OPT in (c) flat and (b) bent state (radius 300 μm) under a light intensity of 1.0 $mWcm^{-2}$. *Reprinted from* [31] *with permission, Copyright 2017, Wiley*.

2.4.5 Hybrid OPTs

Apart from using all organic components for an OPT channel formation, organic-inorganic composites were also employed for enhancement of the photoelectrical characteristics. The blends of P3HT/CdSe quantum dots [137] and P3HT/TiO_2 nanoparticles [34] were incorporated into an OPT as channel materials. In both works, the presence of inorganic quantum dots or nanoparticles increased

the drain photocurrent and enhanced the separation of the light generated excitons. The P3HT/CdSe QD OPT showed memory characteristics for several hours after the light was turned off due to a strong electron trapping in CdSe. In contrast, P3HT/TiO_2 composites showed fast response and reset (good for sensors). Moreover, It was observed that the photoresponse was dependent on TiO_2 content, the wavelength of the incident light and V_{DS}.

Another way of producing BHJ for OPTs is blending of p-type conjugated polymer P3HT with n-type inorganic semiconductor ZnO nanoparticles. Nam et al. [138] used P3HT:ZnO blends to fabricate PTs on ITO/glass substrates with crosslinked PVP as a gate dielectric. The effects of ZnO on PTs performance were investigated by means of the blend composition (ZnO content up to 50 wt.%), light intensity and wavelengths. The best performance OPTs were obtained with 1:1 blends at any intensity of the incident light. Reported apparent and corrected photoresponsivity were 4.7 and 2.07 AW^{-1}, respectively, under 0.27 μWcm^{-2} green light intensity (555 nm). The reported OPT operated in the typical p-type regime, even though the n-type material was present in the channel at the higher content. More recently, a comparative work on incorporating quantum dots and conjugated polymers were reported by Song at al. [139] The poly [2-methoxy-5-(2'-ethylhexyloxy-p-phenylenevinylene)] (MEH-PPV) and PbS QD were used to fabricate the layered (LHJ) and bulk heterojunction OPTs. Both OPTs were ambipolar with R of 10 AW^{-1} for LHJ OPT due to the better ordering of the material in the channel. The BHJ OPTs had two orders of magnitude lower R and showed

lower electron and hole mobility of ~3.7 cm2$V^{-1}s^{-1}$ than LHJ (electron and hole mobility of 52 and 37 $cm^2V^{-1}s^{-1}$, respectively).

Another example of hybrid OPTs was reported by Jung et al in 2016. [140] OPTs were based on small molecule n-type N,N'-bis(2-phenylethyl)-perylene-3,4:9,10-tetracarboxylic diimide (BPE-PTCDI) nanowires decorated with gold nanorods. The hybrid OPTs exhibited high-performance for a very broad spectral responsivity (UV-vis-NIR light detection). The OPTs had remarkable optoelectronic properties due to ultra-high R of $7.70x10^5$ AW^{-1}, EQE of $1.42x10^8$%, and P of 10^6 under weak light illumination of 2.5 μWcm^{-2}. Both light scattering plasmon resonance (LSPR) and scattering effect of gold nanorods enabled detection in the NIR region (R=10.7 AW^{-1} and EQE=$1.35x10^3$% at 980 nm). The OPTs showed reproducible fast detection and reset at different wavelengths of the light. It is noteworthy that this work represents a unique example for high-performance solution-processed hybrid OPTs with very broad spectral responsivity.

2.4.6 Interface engineering in OPTs

Interface engineering in OPTs is as important as the choice of metals for source-drain electrodes, materials for active channel and the gate dielectric. Interface engineering enables alignment of the energy levels for better charge carrier injection and transport. Interfaces in OPTs are metal/channel, air/channel (top-contact bottom-gate and bottom-contact bottom-gate), channel/channel (in blends), channel/gate dielectric, and gate dielectric/gate. However, the most

studied is the channel/gate interface. In the following paragraphs, we summarize the recent progress in the interface engineering of OPTs.

Metal/channel interface. Yao et al. [141] reported a photoresponsivity enhancement of pentacene TCBG OPTs by introducing a C60 buffer layer at S-D electrodes or channel interface (metal channel interface). The buffer layer increased the mobility and lowered the threshold voltage. The *R* and *P* of 4.27 AW^{-1} and $5x10^4$ at V_G= 0 V and the red-light intensity of 0.2 $mWcm^{-2}$ were the highest reported for single layer pentacene OPTs.

Channel/dielectric interface. Moving down toward channel/dielectric interface, more examples were reported for OPTs with enhanced performance. Using 2D materials such as fluorographene nanosheets, as an interface modification layer, Wang et al. [142] investigated their effects on the OPT's performance based on pentacene and bitriisopropylsilylethynyltetraceno[2,3-b]thiophenes (TIPSEthiotet) OSCs. TCBG OPTs on Si-substrates showed highly enhanced photoelectrical characteristics under the white light illumination (25 μWcm^{-2}). The field-effect mobility, *R* and *P* for pentacene based OPTs were 0.085 $cm^2V^{-1}s^{-1}$ (0.025 $cm^2V^{-1}s^{-1}$ no fluorographene layer), 21.83 AW^{-1} (11.30 AW^{-1} no fluorographene layer), and $4.27x10^4$ ($1.85x10^6$ no fluorographene layer). The same parameters for the pentacene-based OPTs were 0.35 $cm^2V^{-1}s^{-1}$ (0.16 $cm^2V^{-1}s^{-1}$ no fluorographene layer), 144.00 AW^{-1} (106.30 AW^{-1} no fluorographene layer), and $3.17x10^6$ ($4.60x10^5$ no fluorographene layer). According to the authors, these OPTs have potential use as photodetectors. Recently, Liu et al. [143] reported the high-efficiency OPTs with epitaxially grown C8-BTBT crystals on graphene at the

channel/dielectric interface were reported. The graphene layer was 1.3 nm thick, while the number of C8-BTBT crystal layers was varied from 1.03 to 6.6. The sequential epitaxial growth of C8-BTBT enabled understanding of the OPT's performance evolution. Under the light of 355 nm wavelength (100 μWcm^{-2} intensity), an OPT with C8-BTBT monolayer (less than 3 nm) showed remarkable *R* of $1.57x10^4$, photocurrent gain $>10^8$, and very fast response time of 25 ms. Furthermore, with the few layers of C8-BTBT, OPTs showed EQE of $1.84x10^9$ and interfacial charge transfer efficiency of 41%. One more important finding was that with the increased number of C8-BTBT layers, EQE linearly increased up to ~7 layers, but decay time of the photocurrent was slower due to slower recombination. More layers increased the energy barrier for the charge carriers hoping to recombine. According to the authors, these values were among the highest reported for graphene-based photodetectors.

The modification of gate dielectric surface is sought as a promising strategy to enhance the photoelectrical performance of OPTs while avoiding often complex and lengthy synthetic routes. Liu et al. [144] fabricated multifunctional OPT-based non-volatile memory devices by simple UV/O_3 treatment of the Ta_2O_5 gate dielectric on ITO/glass substrates. The channel was formed through thermal evaporation of pentacene with photo sensing of a blue OLED light. Non-volatile memories were operated as optical writing/electrical erasing devices. With adjustment of Ta_2O_5 gate dielectric properties, OPT-based memory could operate in two memory regimes, as a flash memory or as a write-once-read-many-times memory. As suggested by XPS and C-V measurements, UV/O_3 treatment affected the density of oxygen vacancies and traps in the 1.8 nm

surface layer. Accordingly, the device properties were affected. This work demonstrated for the first time a unique combination of photo sensing and optical memory characteristics in one device for an optical feedback system to tune the brightness of an OLED.

Very recently, Ljubic et al. [145] demonstrated that photoelectrical characteristics of OPTs based on a small molecule OSC/dielectric polymer blend could be modulated by simple surface modification of the gate dielectric using organosilanes. Commercially available organosilanes were used to form a self-assembly monolayer onto the SiO_2 dielectric surface. SAMs were characterized by different end-groups oriented toward the channel (electron neutral, accepting and donating). The active channel was formed by spin-coating of C5-BTBT/polyester (dielectric) blend solution to form UV responsive TCBG OPTs. From this work, two important conclusions were drawn: 1) the amount of photocurrent generated in the subthreshold region depended on the electron accepting strength of SAM. With the sulfonyl chloride group and chlorine atom at the end of SAM, the highest *R*, *P,* and mobility were achieved under UV light. Those effects were attributed to more efficient excitons dissociation and consequently higher concentration of the mobile photo holes than other SAMs; 2) In the dark, the hole mobility was governed by the chemical structure of SAM and its intermolecular interactions with C5-BTBT crystallites forcing better edge-on alignment, as confirmed by 2d XRD analysis. Thus, the highest mobility in the dark was achieved by SAM having -SH end-groups that are more likely to interact with S and benzene rings of a C5-BTBT molecule.

This work represents a straightforward way of performance control of OPTs for photo sensing applications.

§ 2.5 Summary and outlook

In this progress report, we summarized the recent advances in OPTs for various potential applications. In half a decade, significant work has been done to achieve high-performance OPTs. The main focus was on the molecular design and synthesis of new organic semiconductors and their molecular engineering. In addition, there is a clear trend of the device and interface engineering to enhance the performance of OPTs for a broad range of wavelengths. The recent advances in single-crystal OPT including nano- and macro-structures (wires, ribbons, plates) demonstrated the potential of their application in high-end organic electronics (high mobility, photoresponsivity and photosensitivity), while the fabrication methods should still be improved to produce a highly aligned structure for the large-area devices. On the other hand, less aligned small molecules and polymers offered a cost-effective processing for the price of lower performance. Nevertheless, donor-acceptor (co)polymers are rapidly emerging and pushing the traditional conjugated oligothiophene-based polymers to the history. Not only small molecule and polymer OSCs but their blends opened a whole new field of layered bulk heterojunctions that sense up to NIR light wavelengths. However, for the wavelength selective photosensors, the blends of small molecule organic semiconductors and dielectric polymers have been integrated into the channel, showing a high-performance

OPTs. Similarly, to OTFTs, OPTs are very sensitive to changes in the interface and it is demonstrated that by its simple modification, photoelectrical properties can be significantly enhanced. All the strategies were integrated into arrays, flexible, and printable devices for photo switching, photodetection, optical memory, and imaging. Therefore, based on all the above observations, OPTs have a bright future, but there still exist many aspects to be improved (polymer chain structure, crystallinity, stability, reliability, theoretical modeling, device structure, and application). Together, chemists and engineers have a thought assignment but with less uncertainty compared with the previous decades.

§ 2.6 References

[1] J. E. Lilienfeld, Method and apparatus for controlling electric current **1930**.

[2] G. Horowitz, *Adv. Mater.* **1998**, *10*, 365.

[3] P. Weimer, *Proc. IRE* **1962**, *50*, 1462.

[4] A. Tsumura, H. Koezuka, T. Ando, *Appl. Phys. Lett.* **1986**, *49*, 1210.

[5] A. Y. Amin, A. Khassanov, K. Reuter, T. Meyer-Friedrichsen, M. Halik, *J. Am. Chem. Soc.* **2012**, *134*, 16548.

[6] H. Minemawari, T. Yamada, H. Matsui, J. Tsutsumi, S. Haas, R. Chiba, R. Kumai, T. Hasegawa, *Nature* **2011**, *475*, 364.

[7] Y. Yuan, G. Giri, A. L. Ayzner, A. P. Zoombelt, S. C. B. Mannsfeld, J. Chen, D. Nordlund, M. F. Toney, J. Huang, Z. Bao, *Nat. Commun.* **2014**, *5*, 3005.

[8] J. Li, Y. Zhao, H. S. Tan, Y. Guo, C.-A. Di, G. Yu, Y. Liu, M. Lin, S. H. Lim,

Y. Zhou, H. Su, B. S. Ong, *Sci. Rep.* **2012**, *2*, 1.

[9] H. Sirringhaus, *Adv. Mater.* **2014**, *26*, 1319.

[10] A. Facchetti, *Mater. Today* **2007**, *10*, 28.

[11] J. Mei, Y. Diao, A. L. Appleton, L. Fang, Z. Bao, *J. Am. Chem. Soc.* **2013**, *135*, 6724.

[12] J. Takeya, M. Yamagishi, Y. Tominari, R. Hirahara, Y. Nakazawa, T. Nishikawa, T. Kawase, T. Shimoda, S. Ogawa, *Appl. Phys. Lett.* **2007**, *90*, 102.

[13] K.-J. Baeg, M. Binda, D. Natali, M. Caironi, Y.-Y. Noh, *Adv. Mater.* **2013**, *25*, 4267.

[14] H. Dong, H. Zhu, Q. Meng, X. Gong, W. Hu, *Chem. Soc. Rev.* **2012**, *41*, 1754.

[15] Y. Zang, F. Zhang, D. Huang, C. Di, Q. Meng, X. Gao, D. Zhu, *Adv. Mater.* **2014**, *26*, 2862.

[16] T.-D. Tsai, J.-W. Chang, T.-C. Wen, T.-F. Guo, *Adv. Funct. Mater.* **2013**, *23*, 4206.

[17] M. Debucquoy, S. Verlaak, S. Steudel, K. Myny, J. Genoe, P. Heremans, *Appl. Phys. Lett.* **2007**, *91*, 103508.

[18] Y. Y. Noh, D. Y. Kim, K. Yase, *J. Appl. Phys.* **2005**, *98*, 7450.

[19] M. Mas-Torrent, P. Hadley, N. Crivillers, J. Veciana, C. Rovira, *ChemPhysChem* **2006**, *7*, 86.

[20] Y. Wu, Z. Yin, J. Xiao, Y. Liu, F. Wei, K. J. Tan, C. Kloc, L. Huang, Q. Yan, F. Hu, H. Zhang, Q. Zhang, *ACS Appl. Mater. Interfaces* **2012**, *4*, 1883.

[21] J. H. Jung, M. J. Yoon, J. W. Lim, Y. H. Lee, K. E. Lee, D. H. Kim, J. H. Oh, *Adv. Funct. Mater.* **2017**, *27*, 1604528.

[22] X. Liu, G. Dong, L. Duan, L. Wang, Y. Qiu, *J. Mater. Chem.* **2012**, *22*, 11836.

[23] B. Yao, W. Lv, D. Chen, G. Fan, M. Zhou, Y. Peng, *Appl. Phys. Lett.* **2012**, *101*, 163301.

[24] B. Gunduz, F. Yakuphanoglu, *Sensors Actuators, A Phys.* **2012**, *178*, 141.

[25] K. S. Narayan, N. Kumar, *Appl. Phys. Lett.* **2001**, *79*, 1891.

[26] M. C. Hamilton, J. Kanicki, *IEEE J. Sel. Top. Quantum Electron.* **2004**, *10*, 840.

[27] M. C. Hamilton, S. Martin, J. Kanicki, *IEEE Trans. Electron Devices* **2004**, *51*, 877.

[28] C. S. Smithson, Y. Wu, T. Wigglesworth, S. Zhu, *Adv. Mater.* **2015**, *27*, 228.

[29] D. Ljubic, C. S. Smithson, Y. Wu, S. Zhu, *Adv. Electron. Mater.* **2015**, *1*, 1500119.

[30] D. Ljubic, C. S. Smithson, Y. Wu, S. Zhu, *ACS Appl. Mater. Interfaces* **2016**, *8*, 3744.

[31] J. Huang, J. Du, Z. Cevher, Y. Ren, X. Wu, Y. Chu, *Adv. Funct. Mater.* **2017**, *27*, 1604163.

[32] H. Hwang, H. Kim, S. Nam, D. D. C. Bradley, C.-S. Ha, Y. Kim, *Nanoscale* **2011**, *3*, 2275.

[33] A. K. Pandey, M. Aljada, A. Pivrikas, M. Velusamy, P. L. Burn, P. Meredith, E. B. Namdas, *ACS Photonics* **2014**, *1*, 114.

[34] S. M. Mok, F. Yan, H. L. W. Chan, *Appl. Phys. Lett.* **2008**, *93*, 2006.

[35] C. Raimondo, N. Crivillers, F. Reinders, F. Sander, M. Mayor, P. Samori, *Proc. Natl. Acad. Sci.* **2012**, *109*, 12375.

[36] G. Zhao, J. Liu, Q. Meng, D. Ji, X. Zhang, Y. Zou, Y. Zhen, H. Dong, W. Hu, *Adv. Electron. Mater.* **2015**, *1*, 1500071.

[37] G. Wu, C. Chen, S. Liu, C. Fan, H. Li, H. Chen, *Adv. Electron. Mater.* **2015**, *1*, 1500136.

[38] K.-J. Baeg, M. Binda, D. Natali, M. Caironi, Y.-Y. Noh, *Adv. Mater.* **2013**, *25*, 4267.

[39] Y. Chu, X. Wu, J. Lu, D. Liu, J. Du, G. Zhang, J. Huang, *Adv. Sci.* **2016**, *3*, 1.

[40] C. D. Dimitrakopoulos, D. J. Mascaro, **2001**, *45*, 11.

[41] B. Lucas, T. Trigaud, C. Videlot-Ackermann, *Polym. Int.* **2012**, *61*, 374.

[42] C. Di, F. Zhang, D. Zhu, *Adv. Mater.* **2013**, *25*, 313.

[43] H.-S. Kang, C.-S. Choi, W.-Y. Choi, D.-H. Kim, K.-S. Seo, *Appl. Phys. Lett.* **2004**, *84*, 3780.

[44] T. P. I. Saragi, J. Londenberg, J. Salbeck, *J. Appl. Phys.* **2007**, *102*, 46104.

[45] C. Y. Chen, *Appl. Phys. Lett.* **1981**, *39*, 979.

[46] M. S. Sze, *Physics of semiconductor devices*; 2nd ed.; Wiley: New York, 1982.

[47] V. Podzorov, M. E. Gershenson, *Phys. Rev. Lett.* **2005**, *95*, 2.

[48] M. Mas-Torrent, P. Hadley, S. T. Bromley, X. Ribas, J. Tarr?s, M. Mas, E. Molins, J. Veciana, C. Rovira, *J. Am. Chem. Soc.* **2004**, *126*, 8546.

[49] M. Mas-Torrent, P. Hadley, S. T. Bromley, N. Crivillers, J. Veciana, C. Rovira,

Appl. Phys. Lett. **2005**, *86*, 12110.

[50] Y. Guo, C. Du, C. Yu, C. A. Di, S. Jiang, H. Xi, J. Zheng, S. Yan, C. Yu, W. Hu, Y. Liu, *Adv. Funct. Mater.* **2010**, *20*, 1019.

[51] K. H. Kim, S. Y. Bae, Y. S. Kim, J. A. Hur, M. H. Hoang, T. W. Lee, M. J. Cho, Y. Kim, M. Kim, J. Il Jin, S. J. Kim, K. Lee, S. J. Lee, D. H. Choi, *Adv. Mater.* **2011**, *23*, 3095.

[52] R. Li, W. Hu, Y. Liu, D. Zhu, *Acc. Chem. Res.* **2010**, *43*, 529.

[53] Q. Tang, L. Li, Y. Song, Y. Liu, H. Li, W. Xu, Y. Liu, W. Hu, D. Zhu, *Adv. Mater.* **2007**, *19*, 2624.

[54] N. Ai, Y. Zhou, Y. Zheng, H. Chen, J. Wang, J. Pei, Y. Cao, *Org. Electron. physics, Mater. Appl.* **2013**, *14*, 1103.

[55] M. H. Hoang, Y. Kim, M. Kim, K. H. Kim, T. W. Lee, D. N. Nguyen, S.-J. Kim, K. Lee, S. J. Lee, D. H. Choi, *Adv. Mater.* **2012**, *24*, 5363.

[56] H. Yu, Z. Bao, J. H. Oh, *Adv. Funct. Mater.* **2013**, *23*, 629.

[57] Y. Wakayama, R. Hayakawa, H.-S. Seo, *Sci. Technol. Adv. Mater.* **2014**, *15*, 24202.

[58] Y. Chen, Y. Luo, *Adv. Mater.* **2009**, *21*, 2040.

[59] C. Huang, B. Dong, N. Lu, B. Yang, L. Gao, L. Tian, D. Qi, Q. Wu, L. Chi, *Small* **2009**, *5*, 583.

[60] K. S. Park, B. Cho, J. Baek, J. K. Hwang, H. Lee, M. M. Sung, *Adv. Funct. Mater.* **2013**, *23*, 4776.

[61] X. Liu, L. Tavares, A. Osadnik, J. L. Lausen, J. Kongsted, A. Lützen, H.-G. Rubahn, J. Kjelstrup-Hansen, *Org. Electron.* **2014**, *15*, 1273.

[62] W. Rekab, M. A. Stoeckel, M. El Gemayel, M. Gobbi, E. Orgiu, P. Samorì, *ACS Appl. Mater. Interfaces* **2016**, *8*, 9829.

[63] X. Zhao, Q. Tang, H. Tian, Y. Tong, Y. Liu, *Org. Electron. physics, Mater. Appl.* **2015**, *16*, 171.

[64] T. P. I. Saragi, R. Pudzich, T. Fuhrmann, J. Salbeck, *Appl. Phys. Lett.* **2004**, *84*, 2334.

[65] Y.-Y. Noh, D.-Y. Kim, K. Yase, *J. Appl. Phys.* **2005**, *98*, 74505.

[66] T. P. I. Saragi, R. Pudzich, T. Fuhrmann-Lieker, J. Salbeck, *Appl. Phys. Lett.* **2007**, *90*, 2005.

[67] Y.-Y. Noh, J. Ghim, S.-J. Kang, K.-J. Baeg, D.-Y. Kim, K. Yase, *J. Appl. Phys.* **2006**, *100*, 94501.

[68] J.-M. Choi, J. Lee, D. K. Hwang, J. H. Kim, S. Im, E. Kim, *Appl. Phys. Lett.* **2006**, *88*, 43508.

[69] J. Kim, S. Cho, Y. H. Kim, S. K. Park, *Org. Electron. physics, Mater. Appl.* **2014**, *15*, 2099.

[70] B. Mukherjee, M. Mukherjee, Y. Choi, S. Pyo, *J. Phys. Chem. C* **2009**, *113*, 18870.

[71] B. Mukherjee, M. Mukherjee, Y. Choi, S. Pyo, *ACS Appl. Mater. Interfaces* **2010**, *2*, 1614.

[72] Y. Yang, R. C. da Costa, M. J. Fuchter, A. J. Campbell, *Nat. Photonics* **2013**, *7*, 634.

[73] Z. Qi, X. Liao, J. Zheng, C. A. Di, X. Gao, J. Wang, *Appl. Phys. Lett.* **2013**, *103*, 1.

[74] W. Guo, Y. Liu, W. Huang, M. M. Payne, J. Anthony, H. E. Katz, *Org. Electron. physics, Mater. Appl.* **2014**, *15*, 3061.

[75] G. Zhao, J. Liu, Q. Meng, D. Ji, X. Zhang, Y. Zou, Y. Zhen, H. Dong, W. Hu, *Adv. Electron. Mater.* **2015**, *1*, 1.

[76] T. Kakinuma, H. Kojima, T. Kawamoto, T. Mori, *J. Mater. Chem. C* **2013**, *1*, 2900.

[77] D. Bharti, V. Raghuwanshi, I. Varun, A. Mahato, S. P. Tiwari, *IEEE Sens. J.* **2017**, *11*, 1.

[78] F. Yu, S. Wu, X. Wang, G. Zhang, H. Lu, L. Qiu, *RSC Adv.* **2017**, *7*, 11572.

[79] W.-Y. Chou, Y.-S. Lin, L.-L. Kuo, S.-J. Liu, H.-L. Cheng, F.-C. Tang, *J. Mater. Chem. C* **2014**, *2*, 626.

[80] F. Li, Y. Chen, C. Ma, U. Buttner, K. Leo, T. Wu, *Adv. Electron. Mater.* **2017**, *3*, 1600430.

[81] A. Rogalski, *Acta Phys. Pol. A* **2009**, *116*, 389.

[82] X. Ren, P. K. L. Chan, *Appl. Phys. Lett.* **2014**, *104*, 113302.

[83] L. Zhang, T. Wu, Y. Guo, Y. Zhao, X. Sun, Y. Wen, G. Yu, Y. Liu, *Sci. Rep.* **2013**, *3*, 1.

[84] P. Gu, Y. Yao, L. Feng, S. Niu, H. Dong, *Polym. Chem.* **2015**, *6*, 7933.

[85] V. et al. Coropceanu, *Chem. Rev.* **2007**, *107*, 926.

[86] C. Wang, H. Dong, W. Hu, Y. Liu, D. Zhu, *Chem. Rev.* **2012**, *112*, 2208.

[87] H. Dong, X. Fu, J. Liu, Z. Wang, W. Hu, *Adv. Mater.* **2013**, *25*, 6158.

[88] H. J. Nam, J. Cha, S. H. Lee, W. J. Yoo, D.-Y. Jung, *Chem. Commun.* **2014**, *50*, 1458.

[89] H. Lee, S. M. Dellatore, W. M. Miller, P. B. Messersmith, *Science* **2007**, *318*, 426.

[90] L.-M. Chen, Z. Hong, G. Li, Y. Yang, *Adv. Mater.* **2009**, *21*, 1434.

[91] L. Dou, J. You, Z. Hong, Z. Xu, G. Li, R. A. Street, Y. Yang, *Adv. Mater.* **2013**, *25*, 6642.

[92] L. Feng, P. Gu, Y. Yao, H. Dong, W. Hu, *Chinese Sci. Bull. (Chinese Version)* **2015**, *60*, 2169.

[93] Y. Li, P. Sonar, L. Murphy, W. Hong, *Energy Environ. Sci.* **2013**, *6*, 1684.

[94] C. B. Nielsen, M. Turbiez, I. McCulloch, *Adv. Mater.* **2013**, *25*, 1859.

[95] X. Wang, K. Wasapinyokul, W. De Tan, R. Rawcliffe, A. J. Campbell, D. D. C. Bradley, *J. Appl. Phys.* **2010**, *107*.

[96] R. Qin, W. Li, C. Li, C. Du, C. Veit, H.-F. Schleiermacher, M. Andersson, Z. Bo, Z. Liu, O. Inganäs, U. Wuerfel, F. Zhang, *J. Am. Chem. Soc.* **2009**, *131*, 14612.

[97] H. Dong, Z. Bo, W. Hu, *Macromol. Rapid Commun.* **2011**, *32*, 649.

[98] Y. Liu, Q. Shi, L. Ma, H. Dong, J. Tan, W. Hu, X. Zhan, *J. Mater. Chem. C* **2014**, *2*, 9505.

[99] W. Huang, B. Yang, J. Sun, B. Liu, J. Yang, Y. Zou, J. Xiong, C. Zhou, Y. Gao, *Org. Electron.* **2014**, *15*, 1050.

[100] M. Zhu, S. Lv, Q. Wang, G. Zhang, H. Lu, L. Qiu, *Nanoscale* **2016**, *8*, 7738.

[101] H. Li, Y. Wu, X. Wang, Q. Kong, H. Fu, *Chem. Commun.* **2014**, *50*, 11000.

[102] Q. Wang, M. Zhu, D. Wu, G. Zhang, X. Wang, H. Lu, X. Wang, L. Qiu, *J. Mater. Chem. C* **2015**, *3*, 10734.

[103] C. Kang, J. Zhang, H. Dong, W. Hu, Z. Bo, *J. Mater. Chem. C* **2015**, *3*, 12083.

[104] M. Li, C. An, T. Marszalek, X. Guo, Y. Z. Long, H. Yin, C. Gu, M. Baumgarten, W. Pisula, K. Müllen, *Chem. Mater.* **2015**, *27*, 2218.

[105] Y. Li, P. Sonar, S. P. Singh, M. S. Soh, M. van Meurs, J. Tan, *J. Am. Chem. Soc.* **2011**, *133*, 2198.

[106] D. S. Yang, K. H. Kim, M. J. Cho, J.-I. Jin, D. H. Choi, *J. Polym. Sci. Part A Polym. Chem.* **2013**, *51*, 1457.

[107] X. Liu, Y. Guo, Y. Ma, H. Chen, Z. Mao, H. Wang, G. Yu, Y. Liu, *Adv. Mater.* **2014**, *26*, 3631.

[108] H. Chen, Y. Guo, G. Yu, Y. Zhao, J. Zhang, D. Gao, H. Liu, Y. Liu, *Adv. Mater.* **2012**, *24*, 4618.

[109] H. Wang, C. Cheng, L. Zhang, H. Liu, Y. Zhao, Y. Guo, W. Hu, G. Yu, Y. Liu, *Adv. Mater.* **2014**, *26*, 4683.

[110] L. Ma, Z. Yi, S. Wang, Y. Liu, X. Zhan, *J. Mater. Chem. C* **2015**, *3*, 1942.

[111] M. J. Kim, S. Choi, M. Lee, H. Heo, Y. Lee, J. H. Cho, B. Kim, *ACS Appl. Mater. Interfaces* **2017**, *9*, 19011.

[112] H. A. Um, D. H. Lee, D. U. Heo, D. S. Yang, J. Shin, H. Baik, M. J. Cho, D. H. Choi, *ACS Nano* **2015**, *9*, 5264.

[113] Y. Lei, N. Li, W.-K. E. Chan, B. S. Ong, F. Zhu, *Org. Electron.* **2017**, *48*, 12.

[114] S. Nam, H. Han, J. Seo, M. Song, H. Kim, T. D. Anthopoulos, I. McCulloch, D. D. C. Bradley, Y. Kim, *Adv. Electron. Mater.* **2016**, *2*, 1600264.

[115] B. Luszczynska, M. Z. Szymanski, J. M. Verilhac, P. Reiss, D. Djurado, *Org. Electron.* **2013**, *14*, 3206.

[116] J. D. Zimmerman, V. V. Diev, K. Hanson, R. R. Lunt, E. K. Yu, M. E. Thompson, S. R. Forrest, *Adv. Mater.* **2010**, *22*, 2780.

[117] Y. Peng, F. Huang, J. Zhang, X. Luo, K. Xu, W. Lv, S. Xu, Y. Wang, Y. Tang, Y. Wei, Z. Xu, Y. Yang, F. Lu, *Org. Electron. physics, Mater. Appl.* **2017**, *43*, 27.

[118] M. Yasin, T. Tauqeer, K. S. Karimov, S. E. San, A. Kösemen, Y. Yerli, A. V. Tunc, *Microelectron. Eng.* **2014**, *130*, 13.

[119] H. Xu, J. Li, B. H. K. Leung, C. C. Y. Poon, B. S. Ong, Y. Zhang, N. Zhao, *Nanoscale* **2013**, *5*, 11850.

[120] Y. S. Rim, Y. Yang, S. H. Bae, H. Chen, C. Li, M. S. Goorsky, Y. Yang, *Adv. Mater.* **2015**, *27*, 6885.

[121] T. Cramer, A. Kyndiah, M. Murgia, F. Leonardi, S. Casalini, F. Biscarini, *Appl. Phys. Lett.* **2012**, *100*, 143302.

[122] L. Kergoat, L. Herlogsson, D. Braga, B. Piro, M.-C. Pham, X. Crispin, M. Berggren, G. Horowitz, *Adv. Mater.* **2010**, *22*, 2565.

[123] J. Kofler, K. Schmoltner, A. Klug, E. J. W. List-Kratochvil, *Appl. Phys. Lett.* **2014**, *104*, 193305.

[124] S. Inal, J. Rivnay, P. Leleux, M. Ferro, M. Ramuz, J. C. Brendel, M. M. Schmidt, M. Thelakkat, G. G. Malliaras, *Adv. Mater.* **2014**, *26*, 7450.

[125] T. Cramer, T. Steinbrecher, T. Koslowski, D. A. Case, F. Biscarini, F. Zerbetto, *Phys. Rev. B* **2009**, *79*, 155316.

[126] W. Xie, S. Wang, X. Zhang, C. Leighton, C. D. Frisbie, *Phys. Rev. Lett.* **2014**, *113*, 246602.

[127] H. Xu, Q. Zhu, T. Wu, W. Chen, G. Zhou, J. Li, H. Zhang, N. Zhao, *Appl. Phys. Lett.* **2016**, *109*, 213301.

[128] W. E. Moerner, D. P. Fromm, *Rev. Sci. Instrum.* **2003**, *74*, 3597.

[129] H. Han, S. Nam, J. Seo, C. Lee, H. Kim, D. D. C. Bradley, C.-S. Ha, Y. Kim, *Sci. Rep.* **2015**, *5*, 16457.

[130] S. Nam, H. Kim, D. D. C. Bradley, Y. Kim, *Org. Electron. physics, Mater. Appl.* **2016**, *39*, 199.

[131] H. Han, S. Nam, J. Seo, J. Jeong, H. Kim, D. D. C. Bradley, Y. Kim, *IEEE J. Sel. Top. Quantum Electron.* **2016**, *22*, 147.

[132] H. Han, C. Lee, H. Kim, J. Seo, M. Song, S. Nam, Y. Kim, *ACS Appl. Mater. Interfaces* **2017**, *9*, 628.

[133] S. Nam, J. Seo, H. Han, H. Kim, D. D. C. Bradley, Y. Kim, *ACS Appl. Mater. Interfaces* **2017**, *9*, 14983.

[134] H. Ebata, T. Izawa, E. Miyazaki, K. Takimiya, M. Ikeda, H. Kuwabara, T. Yui, *J. Am. Chem. Soc.* **2007**, *129*, 15732.

[135] C. S. Smithson, D. Ljubic, Y. Wu, S. Zhu, *J. Mater. Chem. C* **2015**, *3*, 8090.

[136] C. S. Smithson, D. Ljubic, Y. Wu, S. Zhu, *Org. Electron.* **2016**, *37*, 42.

[137] C.-C. Chen, M.-Y. Chiu, J.-T. Sheu, K.-H. Wei, *Appl. Phys. Lett.* **2008**, *92*, 143105.

[138] S. Nam, J. Seo, S. Park, S. Lee, J. Jeong, H. Lee, H. Kim, Y. Kim, *ACS Appl. Mater. Interfaces* **2013**, *5*, 1385.

[139] X. Song, Y. Zhang, R. Wang, M. Cao, Y. Che, J. Wang, H. Wang, L. Jin, H. Dai, X. Ding, G. Zhang, J. Yao, *Appl. Phys. Lett.* **2015**, *106*, 253501.

[140] J. H. Jung, M. J. Yoon, J. W. Lim, Y. H. Lee, K. E. Lee, D. H. Kim, J. H. Oh, *Adv. Funct. Mater.* **2017**, *27*, 1604528.

[141] B. Yao, W. Lv, D. Chen, G. Fan, M. Zhou, Y. Peng, *Appl. Phys. Lett.* **2012**, *101*, 163301.

[142] L. Wang, X. Xie, W. Zhang, J. Zhang, M. Zhu, Y. Guo, P. Chen, M. Liu, G. Yu, *J. Mater. Chem. C* **2014**, *2*, 6484.

[143] X. Liu, X. Luo, H. Nan, H. Guo, P. Wang, L. Zhang, M. Zhou, Z. Yang, Y. Shi, W. Hu, Z. Ni, T. Qiu, Z. Yu, J. Bin Xu, X. Wang, *Adv. Mater.* **2016**, *28*, 5200.

[144] X. Liu, H. Zhao, G. Dong, L. Duan, D. Li, L. Wang, Y. Qiu, *ACS Appl. Mater. Interfaces* **2014**, *6*, 8337.

[145] D. Ljubic, V. Jarvis, C. S. Smithson, N.-X. Hu, Y. Wu, S. Zhu, *Org. Electron.* **2017**, *44*, 253.

§ 2.7 Appendix

Small molecule organic semiconductors referred in the literature review

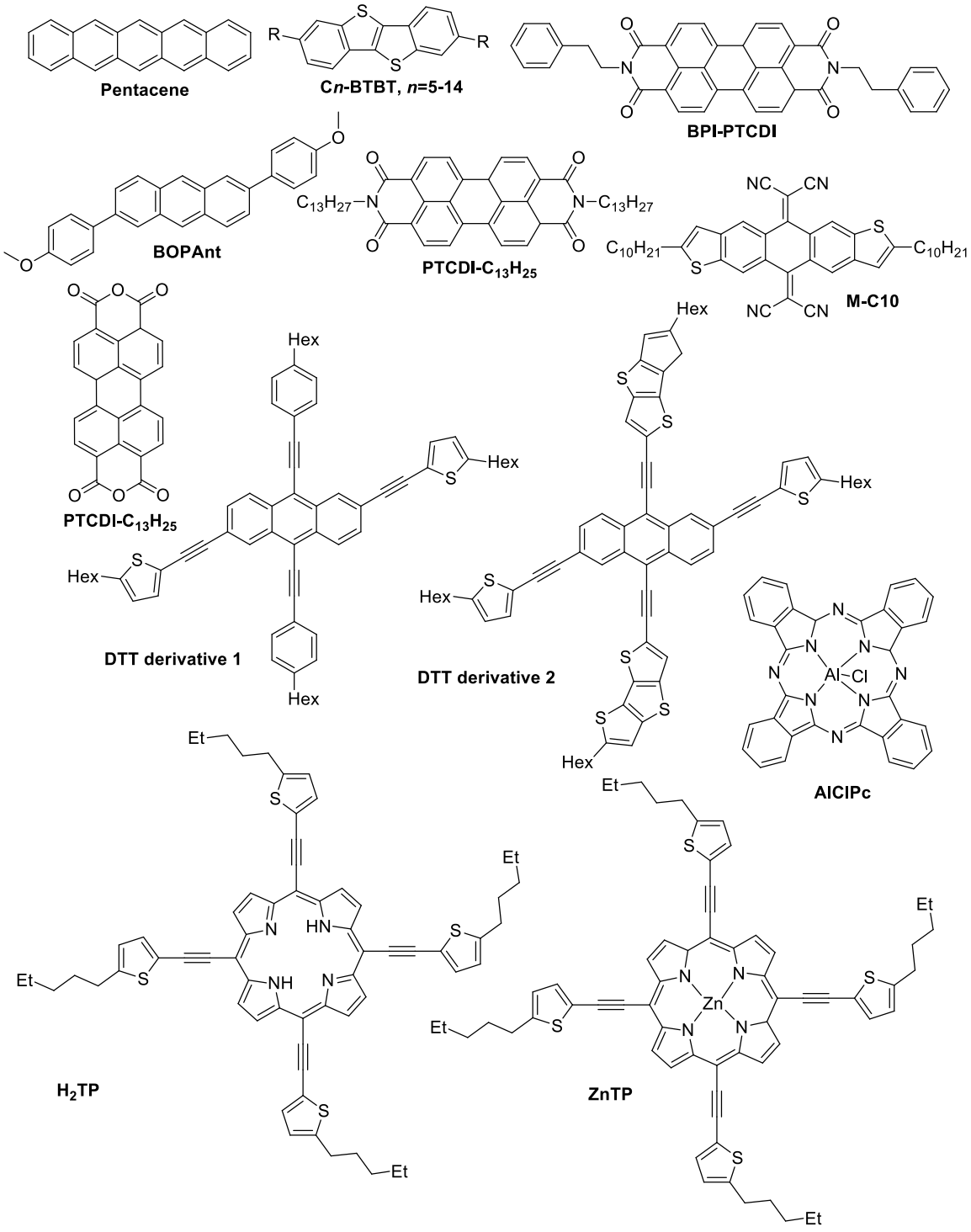

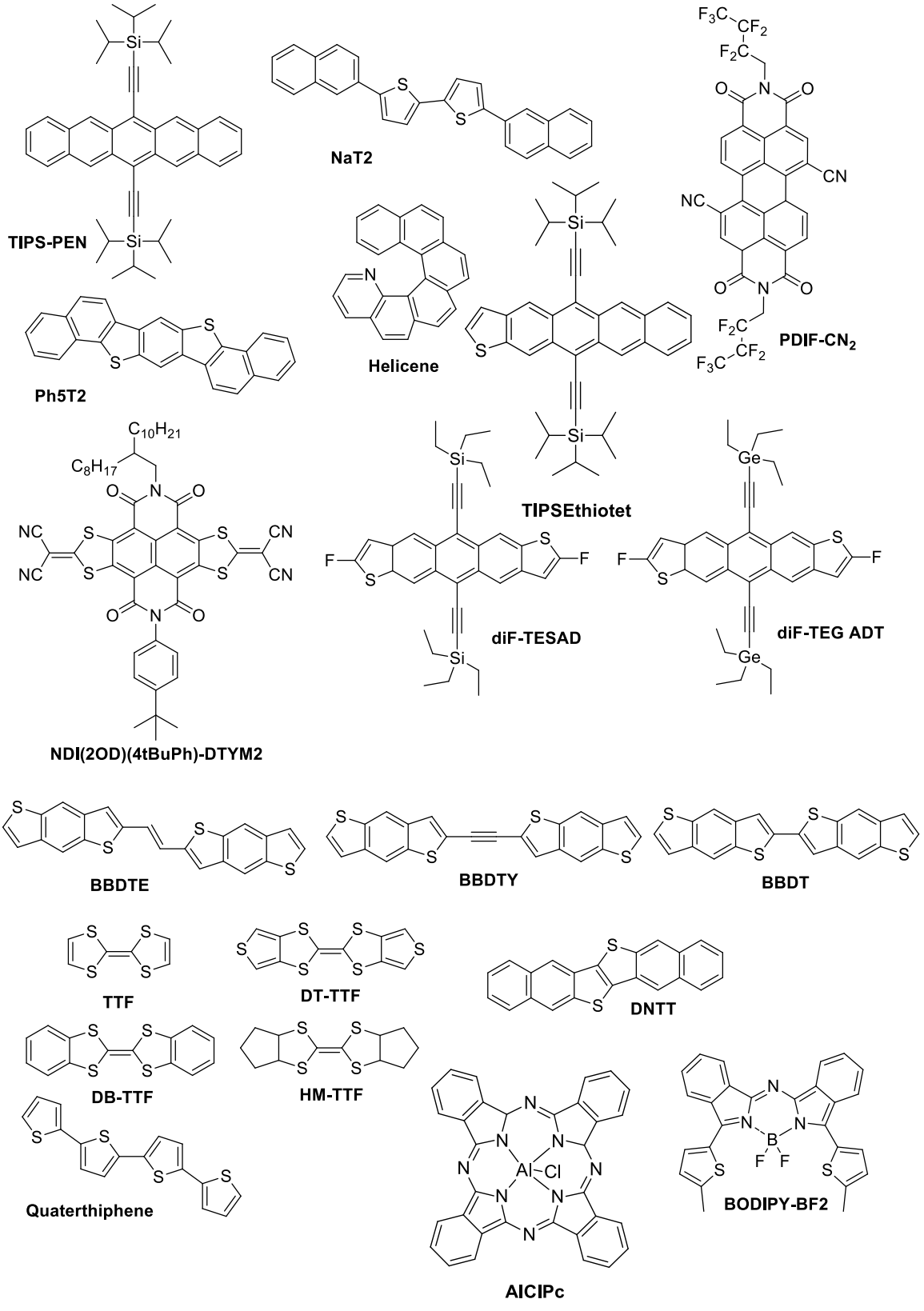
TIPS-PEN
NaT2
Ph5T2
Helicene
PDIF-CN2
TIPSEthiotet
diF-TESAD
diF-TEG ADT
NDI(2OD)(4tBuPh)-DTYM2
BBDTE
BBDTY
BBDT
TTF
DT-TTF
DNTT
DB-TTF
HM-TTF
Quaterthiphene
AlClPc
BODIPY-BF2

Conjugated polymers referred in the literature review

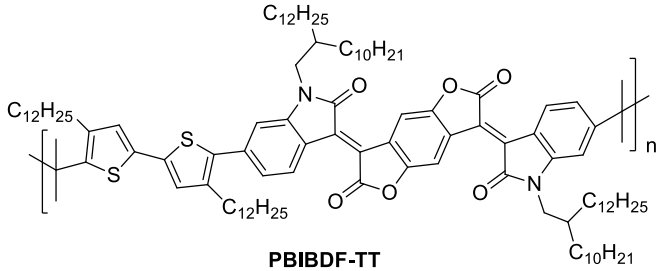

PBIBDF-TT

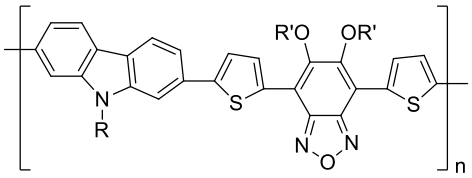

CZ-BT8: R=2-hexyldecyl; R'= n-octyl
CZ-BT12: R=2-hexyldecyl; R'= n-dodecyl

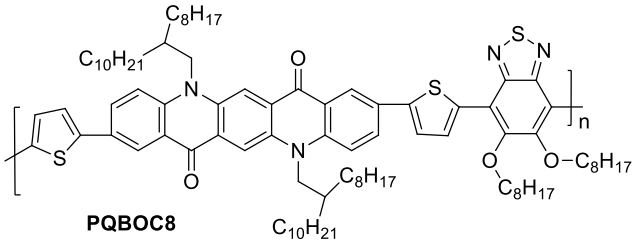

PQBOC8

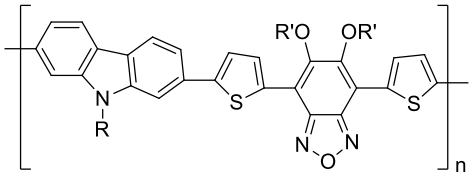

CZ-BO8: R=2-hexyldecyl; R'= n-octyl
CZ-BO12: R=2-hexyldecyl; R'= n-dodecyl

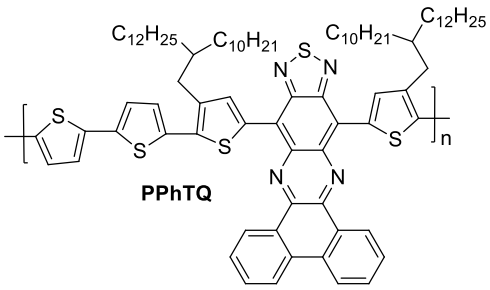

PPhTQ

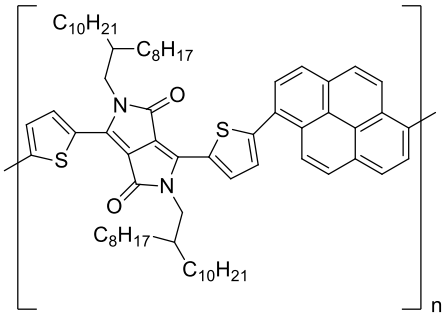

P(DTDPP-alt(1,6)PY

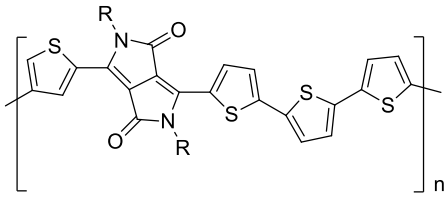

PDQT, R=2-octyl-1-1dodecyl

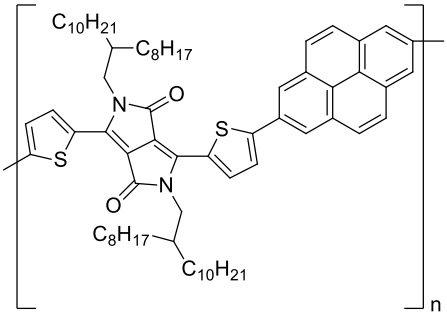

P(DTDPP-alt(2,7)PY

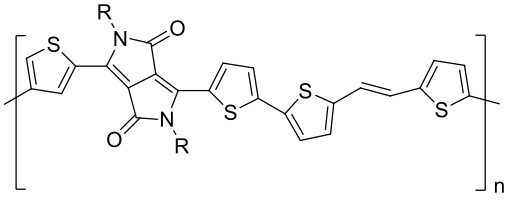

PDVT-10, R=2-decyltetradecyl

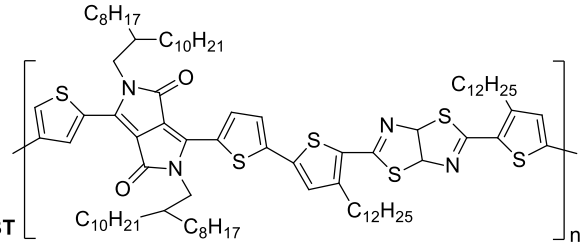

PDPPTzBT

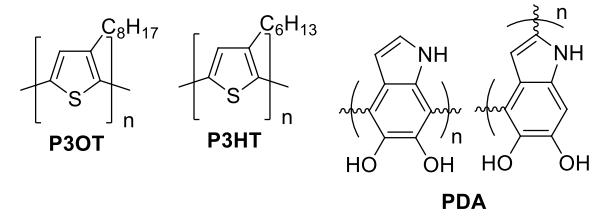

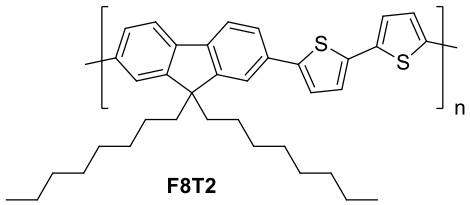

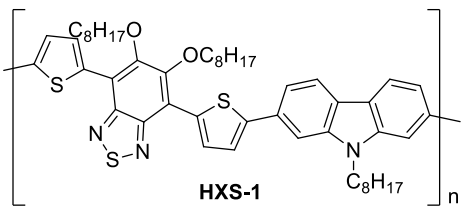

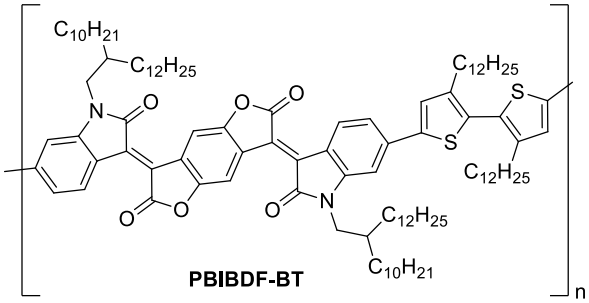

BDT and Bithiazole derivatives

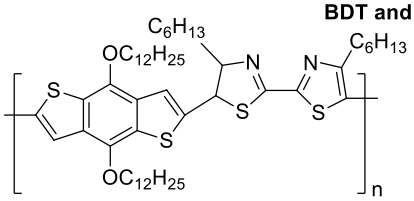

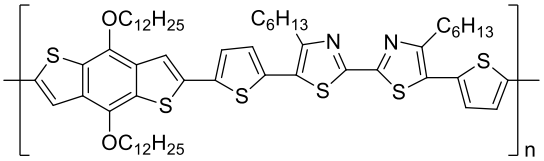

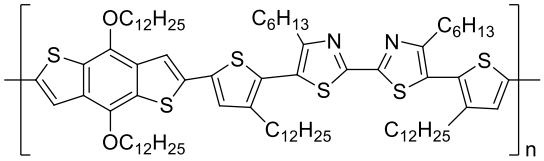

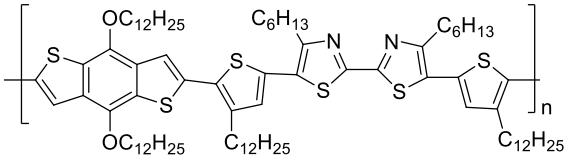

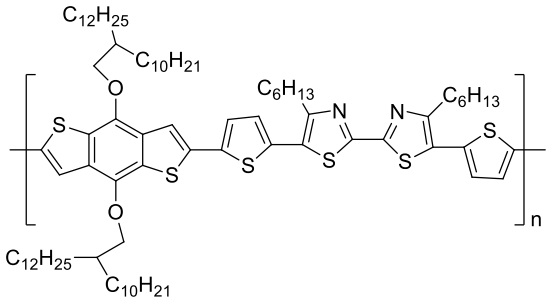

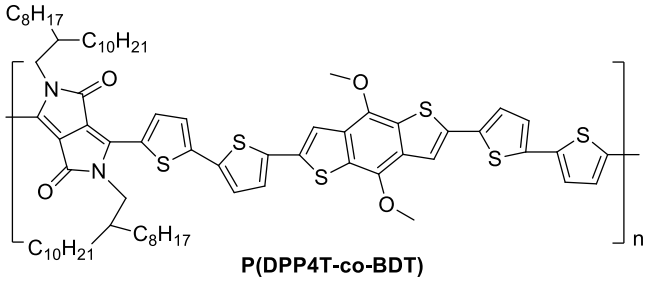

P(DPP4T-co-BDT)

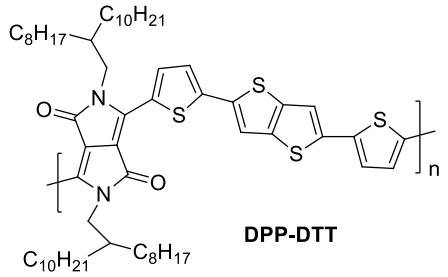

DPP-DTT

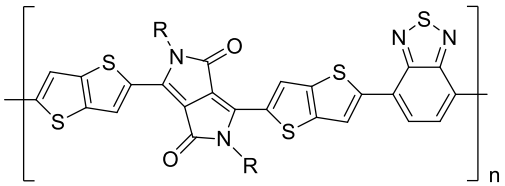

pTTDPP-BT

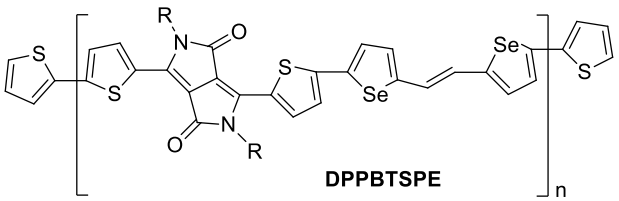

DPPBTSPE

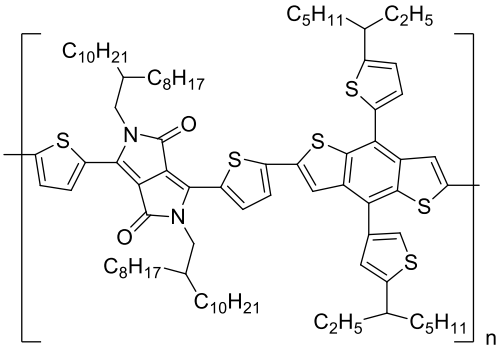

PBDTT-DPP

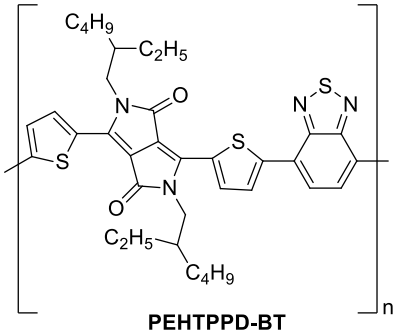

PEHTPPD-BT

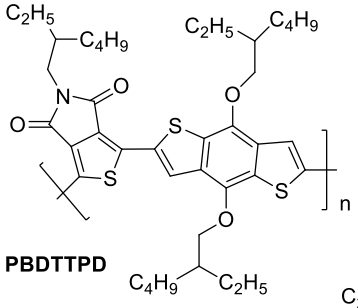

PBDTTPD

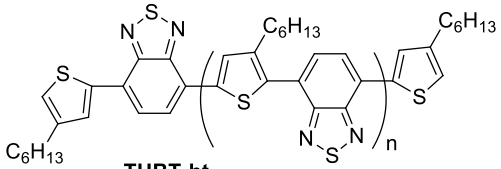

THBT-ht

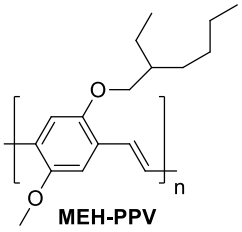

MEH-PPV

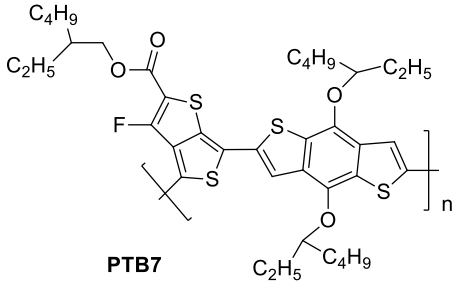

PTB7

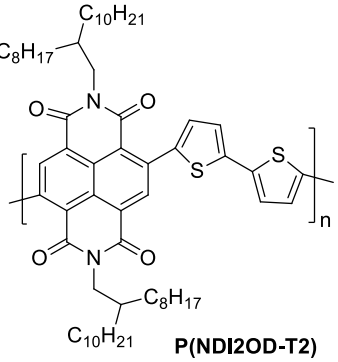

P(NDI2OD-T2)

3 HIGHLY UV SENSITIVE AND RESPONSIVE BENZOTHIOPHENE/DIELECTRIC POLYMER BLEND-BASED ORGANIC THIN-FILM PHOTOTRANSISTOR

In this chapter, the modulation of photoelectrical characteristics of a solution-processed UV responsive organic phototransistors using polyester polymer/2,7-dipentyl[1]benzothieno[3,2-b][1]benzothiophene blend as the active channel material is presented. This chapter is based on the paper published in the peer-

reviewed journal, as follows: “Ljubic D., Smithson C. S., Wu Y., Zhu S., Highly UV-Sensitive and Responsive Benzothiophene/Dielectric Polymer Blend-Based Organic Thin-Film Phototransistor, *Adv. Electron. Mater*., **2015**, 1, 1500119 (DOI: 10.1002/aelm.201500119). Reprinted with permission from *Adv. Electron. Mater*., **2015**, 1, 1500119. Copyright © 2015, Wiley.

Author contributions

Darko Ljubic conducted the experiments and wrote the first draft of the manuscript under the guidance of Dr. Shiping and Dr. Yiliang Wu. Dr. Chad S. Smithson provided the first revision of the manuscript. The final revision was provided by Dr. Wu and Dr. Zhu.

§ 3.1 Abstract

We report on drain current modulation by UV light, in an organic thin-film phototransistor, based on a small molecule semiconductor 2,7-dipentyl[1]benzothieno[3,2-b][1]benzothiophene (C5-BTBT) blended with a linear unsaturated polyester (L-upe) to form the active channel material. The electrical properties of the phototransistor (L-upe+C5-BTBT) and physical properties of thin-films were evaluated by means of two- and three-terminal current-voltage characteristics (in the dark and under UV light) and structure-morphology analysis, respectively. Upon illumination with UV light, a dramatic change in the electrical properties of the L-upe+C5-BTBT transistors was observed, compared to low

responsive control transistors based on a blend of poly(methyl methacrylate) and C5-BTBT. Drain current was increased by more than six orders of magnitude with maximum photosensitivity and responsivity of $4.0x10^6$ and 11.1 AW^{-1}, respectively, using a V_G=0 V. Modulated photoelectrical properties were explained by structure-morphology characteristics and efficient charge trapping at the polymer/semiconductor interface due to the presence of electron withdrawing groups in the polymer. The fast rise time of 1.80 s and slow relaxation time of 24.27 s, estimated using bi-exponential fitting models, confirmed a charge trapping/releasing mechanism and revealed sensing-memory properties of the devices.

§ 3.2 Introduction

Research in organic thin-film transistors (OTFTs) has been a dynamic field over the last two decades. Development of OTFTs is justified by organic materials compatibility used as building components and low-cost fabrication such as printing, solution deposition and melt processing. This development reached the point where OTFTs are applied for electronic flexible paper, OLED flexible displays, sensors, re-writable memory devices, radio frequency identification tags, etc.[1][2] Performance of OTFTs has been significantly improved in the last decade through engineering of the materials, interfaces, and architecture of devices.[3][4][5] Reported maximum charge carrier mobilities reached 17.2 $cm^2V^{-1}s^{-1}$ for vacuum deposited asymmetric tridecyl (C13) substituted [1]benzothieno[3,2-b][1]benzothiophene

(C13-BTBT),[6] 31.3 $cm^2V^{-1}s^{-1}$ [7] and 43 $cm^2V^{-1}s^{-1}$ [8] for solution processed OTFTs based on symmetric C8-BTBT, and 10.5 $cm^2V^{-1}s^{-1}$ for solution processed conductive polymers.[9] Compared to the FETs made from the amorphous silicon (α-Si) that have a mobility of ~ 1 $cm^2V^{-1}s^{-1}$ these results are very promising for the massive commercialization of OTFTs. Moreover, an understanding of device physics has been achieved through simultaneous experimental and modeling analysis. [10][11][12][13]

Finding new and specific functionalities and thus widening the applications of OTFTs is in the main research focus. One of the specific functionalities is optical control over OTFT electrical characteristics to attain air-stable photo-controlled transistors, i.e. organic thin-film phototransistors (OTF-PT), with sensing and/or memory properties. [14][15] OTF-PTs are four-terminal devices, namely, *gate-source-drain-light* electrodes where adjustment of the incident light intensity amplifies the drain current. As a result, OTF-PTs have a higher signal-to-noise ratio (higher sensitivity-lower noise), compared to photodiodes [14] and they are also suitable for application in optical transducers. [16] OTF-PTs have an advantage over their inorganic counterparts due to the ability to choose from a variety of organic materials to tune the sensing properties within the ultraviolet (UV) and visible light spectrum. However, response times are slower compared with inorganic UV sensors recently reported. [17] Therefore, the current challenge in the fabrication of OTF-PT with high photocurrent gain is to design and engineer organic sensors and memory devices with properties comparable to common inorganic devices. Important parameters for the fabrication of high-quality OTF-PT are operational

stability (electrical and light), photosensitivity, and retention times (long for memory and short for sensors).

So far, photo-control of OTFTs electrical properties has been achieved through the incorporation of photochromic organic molecules capable of undergoing a photo-isomerization, electrons exchange (redox reactions), dissociation, and intramolecular group transfer upon illumination with UV light and reversely by visible light or heat.[3][18] Major methods to achieve optically controlled OTFT's include doping the active channel material,[19] modifying the interface of the dielectric/semiconductor[20] or semiconductor/source-drain,[21] and blending a photochromic material into the dielectric.[22] Changes in the molecular dipole moment associated with photoisomerization upon light irradiation result in the generation of an additional electric field that modulated a drain current and threshold voltage. However, conversion of one isomer to another can be a slow process requiring long irradiation time. Prolonged irradiation can induce degradation of the semiconductor material or scatter charge carriers and lower the mobility due to the strong dipoles generated in the photochromic molecule.[19] Other approaches include phototransistors using small molecular photo-responsive semiconductors such as TIPS-pentacene[23] and pentacene.[24][25] These materials achieve optical control by photogeneration of charge carriers in the active channel increasing the drain current within the subthreshold region of the devices. These OTFTs have acceptable responsivities and photosensitivities but slow response times and often show poor air stability.

The presence of the charge trapping/releasing moieties (i.e., electron withdrawing (EW) and electron donating (ED) groups) in the active channel materials has been shown to result in a successful optical modulation of electrical properties of the OTFTs for memory and sensing applications.[26,27] In both cases, photoactive channel materials were completely or partially composed of the photochromic molecules, namely, oligomeric stilbenes containing EW/ED groups[26] and a polyester functionalized with pendant azobenzene moieties having EW/ED groups.[27] The authors attributed the drain current modulation not only to the cis-trans isomerization of the photochromic moieties but also to the charge trapping of the photo-generated charge carriers by the EW/ED groups. The work recently published by our group, [28] demonstrated a successful engineering of such systems, utilizing a 2,7-dipentyl[1]benzothieno[3,2-b][1]benzothiophene (C5-BTBT) and Disperse Red 1 functionalized poly(methyl methacrylate) (p-DR1). As a result, a highly UV responsive OTFT was obtained. The enhanced UV response was attributed to the efficient separation of photogenerated charge carriers and their slow recombination due to the existence of the strong EW groups (trapping sites) in DR1 (nitro-group). Our results showed that the mechanism responsible for photocurrent modulation does not involve the cis-trans isomerization of the DR1 moieties since no response was observed upon irradiation with visible light which causes isomerization of DR1.

The mechanisms that affect OTFT properties based on isomerization of photochromic moieties having EW and ED groups are not fully understood yet. [29] Here we engineered a UV responsive blend for the active channel of an OTF-PT

by choosing UV responsive C5-BTBT semiconductor and a dielectric polymer without photochromic moieties (insert in the UV-Vis spectrum, i.e. 300-800 nm). With appropriate EW groups acting as the charge trapping sites, we hope to achieve high responsivity and high photosensitivity through enhanced separation of the photo-generated charge carriers at the polymer/semiconductor interface to increase the charge carrier density. A blending approach was expected to increase the interface area due to phase separation of the semiconductor thin-film.

We chose a linear unsaturated polyester polymer, designated as L-upe (Fig. 3.1a), composed of isopropoxylated bisphenol A (source of ED groups) and fumaric acid (source of ester EW groups and weak ED double bonds) monomers for blending with C5-BTBT (Fig. 3.1a) in 1,1,2,2-tetrachloroethane solution (blend designated as L-upe+C5-BTBT). For the control device, we prepared a PMMA+C5-BTBT blend as the active channel material, which was previously reported by our group and exhibited a lower response to UV light. PMMA is considered as a source of EW groups (free ester groups) beside neutral aliphatic moieties. Solutions of the semiconductor/polymer blends were used for the top-contact-bottom-gate structured OTFTs fabrication (Fig. 3.1b) by spin-coating onto surface modified Si wafers followed by the evaporation of gold as an electrode material. Various electrical characteristics measurements evaluated properties of the devices both in the dark and under UV illumination, as well as characterization of the thin-film structure and morphology.

Fabricated L-upe+C5-BTBT transistors exhibit an excellent UV response quantified by photosensitivity ratios, where the drain current increased more than six orders of magnitude, with a maximum photosensitivity and responsivity at V_G=0 V of 4.0×10^6 and 11.1 AW^{-1}, respectively. On the other hand, the PMMA+C5-BTBT transistors exhibited a significantly lower UV response ($I_{phc}/I_{d,\,max} = 4.4 \times 10^4$ and max responsivity of 0.040 AW^{-1}). These results revealed that enhanced charge trapping of the photogenerated electrons increased the charge carrier (hole) density and the photocurrent in the subthreshold region. Computed response/retention times of the time-dependent drain current measurements under UV light and in the dark, respectively, suggested fast sensing and slow relaxation memory properties of the L-upe+C5-BTBT transistor. Structure and morphology analysis revealed that the polymer affects the size and degree of dispersion of C5-BTBT crystallites, thus, affecting the UV response and mobility. Smaller crystals of C5-BTBT highly dispersed in the L-upe polymer contributed to the high UV response due to a large interface and surface area exposed to the UV light.

§ 3.3 Results and discussion

The UV response of the L-upe+C5-BTBT transistor was first investigated by two-terminal I-V measurements without an external electrical field applied, using a bias voltage sweeping from 1 to -1 V. I-V characteristics of the devices under two light conditions (i.e. in the dark and under UV light) are displayed in Fig. 3.1c. Four I-V measurements were performed under continuous UV illumination until the

maximum current was reached. Only the initial and final measurements are displayed in Fig. 3.1c, to show how fast the system responses to irradiation. The final measurement at 3 min UV illumination showed complete current saturation of the channel. In the dark, fabricated OTF-PTs generated a small current, measured at $<10^{-12}$ A (insets). Illuminated with UV light, L-upe+C5-BTBT transistors exhibited a large current jump of more than five orders of magnitude within the applied voltage range (Fig. 3.1c, left plot). Little difference was observed between the first and the last measurements. The current of L-upe+C5-BTBT devices (solid line) was linearly dependent on the bias voltage with symmetric response to UV light. On the other hand, PMMA+C5-BTBT transistors had a much lower current upon UV illumination and a slower response as seen from the large current difference between the first and the last measurements. The I-V curves slightly deviated from the linearity and symmetry (i.e., rectifying properties) (Fig. 3.1c, right plot, solid line). The current increase from 1 to 0.75 V (dash line) is due to the slowly increasing charge carrier density. Both OTFTs indicated an ohmic contact at the gold electrode/active channel interface.

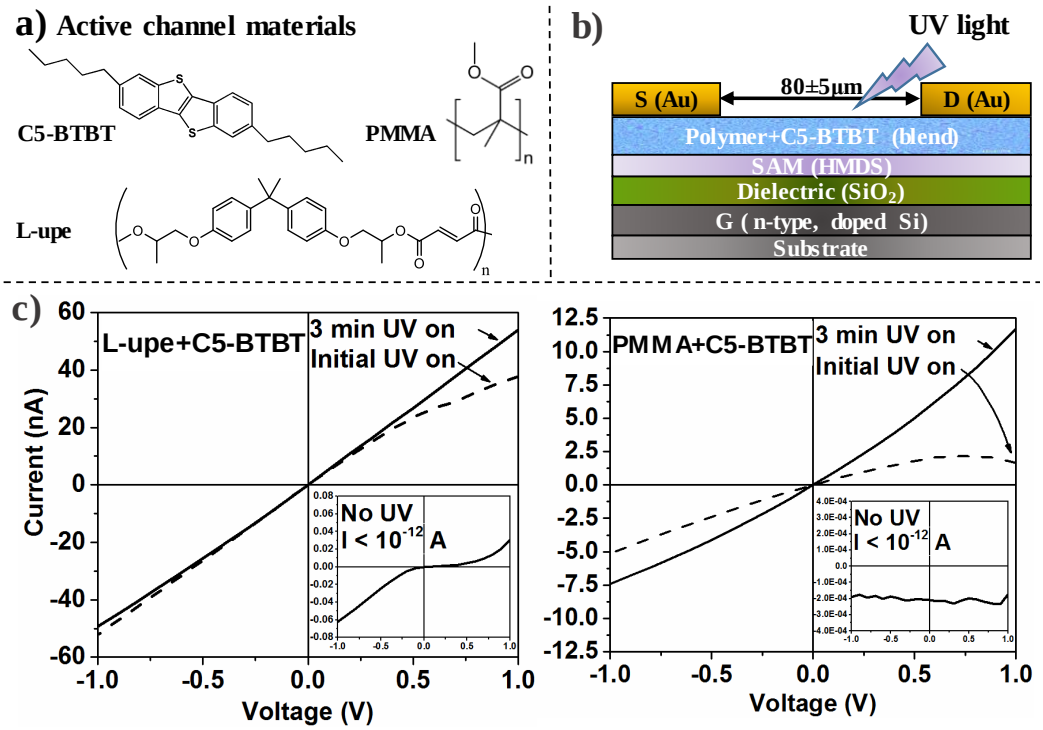

Fig. 3.1. Small molecule organic semiconductor (C5-BTBT) and polymers (L-upe and PMMA) used for the blend preparation as channel materials in OTFTs (a); schematic of top-contact-bottom-gate architecture of OTFTs where S, D, and G are source, drain and gate electrodes, respectively (b); and two-terminal I-V characteristics of L-upe (left) and PMMA (right) based devices measured in the dark (inset) and under UV illumination (c).

To identify the UV response of each component in the blends, UV-Vis spectroscopy of the Polymer+C5-BTBT thin-films was performed on glass substrates. Fig. 3.2 displays UV-Vis absorption spectra recorded for thin-films of pure C5-BTBT and Polymer+C5-BTBT blends. C5-BTBT exhibited a characteristic absorption peak only in the UV-A region at 356 nm. The peak at 356 nm remained

in all Polymer+C5-BTBT thin films and no other peaks are observed reflecting the optical transparency of pure L-upe and PMMA polymers to visible and UV light in the measured range. Different absorption peak intensities originate from the different thickness of the thin films while a slight blue shift of the peak at 356 nm (C5-BTBT) for the spectra of Polymer-C5-BTBT devices is ascribed to the polar effect of the functional groups present in the binding polymer (Fig. 3.2, inset).

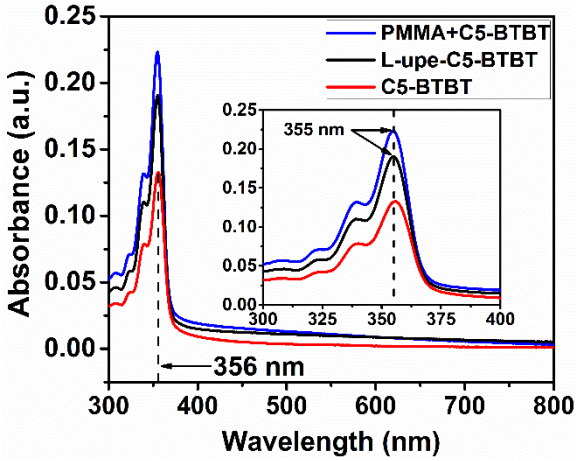

Fig. 3.2. UV-Vis spectra of Polymer+C5-BTBT and C5-BTBT thin-films on glass substrate showing characteristic UV absorbance of C5-BTBT at 356 nm in all thin-films (inset plot represents a zoom-in of the observed blue shift (300-400 nm region) of the characteristic C5-BTBT absorbance at 356 nm when blended with polymers).

Based on UV-Vis analysis (Fig. 3.2), the UV response can be assigned to the C5-BTBT molecule. The magnitude of the UV response and mechanism were evaluated by three-terminal I-V measurements (i.e., source-drain-gate electrodes).

Fig. 3.3(a,b) and 3.2(e,f-dashed curves) display a typical p-type output (drain current, I_D, vs. source-drain voltage, V_{SD}) and transfer (I_D vs. gate voltage, V_G) characteristics, respectively, for the fabricated transistors measured in the dark. The linear part of the output curves for both devices indicates an ohmic contact at the gold electrode-active channel interface, which is already observed by the two-terminal measurements in Fig. 3.1c. Both transistors reached a complete I_D saturation after a high negative V_{SD} was applied (Fig. 3.3a and b).

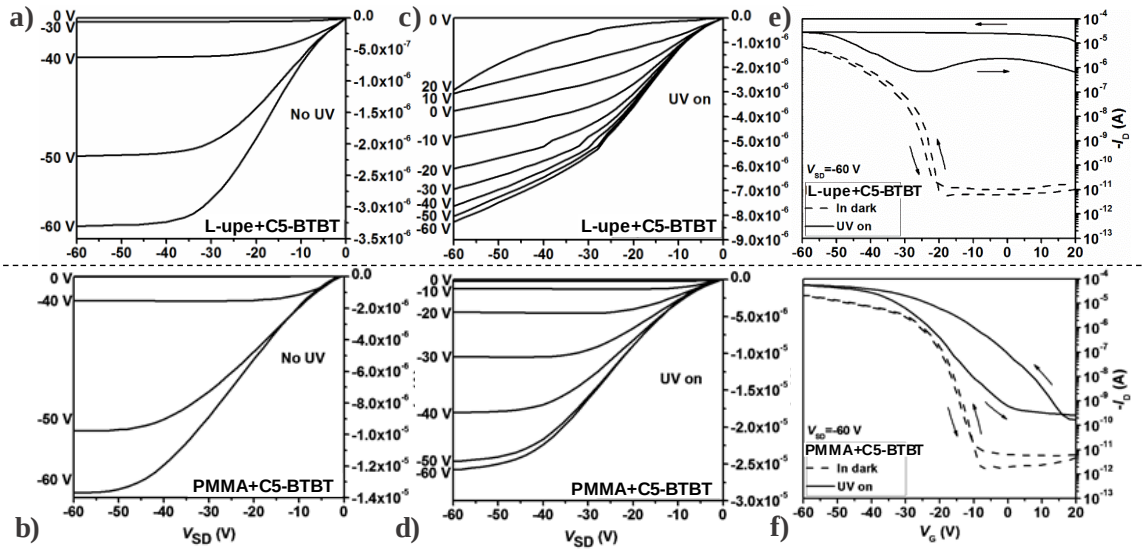

Fig. 3.3. Output characteristics of the fabricated transistors measured (a,b)-in the dark and (c,d)-under UV illumination in V_G sweep from 20 to -60 V; and transfer characteristics with hysteresis investigation for (e)-L-upe+C5-BTBT and (f)-PMMA+C5-BTBT OTFTs in the dark (dashed curves) and under UV illumination (solid curves), at V_{SD}= - 60 V.

During transfer characteristics measurements, a V_{SD}= -60 V was applied corresponding to the saturation region in the output characteristics of the devices and an electric field of 7.5×10^3 V/cm (L=80 µm) (Fig. 3.3e and f, dashed curves). The applied electric field in our devices is comparable with the electric fields of 6×10^3-1.0×10^4 V/cm and 1.6×10^3 V/cm used for TIPS-pentacene[30] and pentacene/Ta_2O_5[24] based phototransistors, respectively, as well as the recently reported 2.4×10^3-1.2×10^4 V/cm for inorganic phototransistors based on interpenetrated ZnO nano tetrapods networks.[17] Threshold voltage (V_{Th}, extracted

from the slope of $I_D^{½}$ vs. V_G curves), onset voltage (V_{SO} or turn ON voltage), field-effect hole mobility (μ_{FE}), On/Off ratio in dark, and charge trap density in dark ($N_{trap,dark}$) were determined from the transfer curves for each device and given in Table 3.1. A total of five devices for each type of transistor was characterized and electrical parameters displayed in Table 3.1 are given as mean values with standard deviations. The field-effect hole mobility, $\mu_{FE,}$ was determined using equation $\mu_{FE} = (2L/W) \cdot I_D / (C_{ox}(V_G - V_{Th})^2)$,[31] in the saturation regime of the transfer characteristic curves, where L (cm) and W (cm) are the active channel length (electrode gap) and width (electrode length), respectively, and C_{ox} is the capacitance per unit area of the dielectric (SiO_2, 15 nFcm^{-2}). Trap density for the devices in the dark ($N_{trap,dark}$) was determined using equation $N_{trap}=(|V_{Th}|C_{ox})/q$,[32] where q is an elementary charge.

Table 3.1 Determined parameters of electronic properties for fabricated devices in dark and under UV illumination (λ=365 nm and 3 mWcm^{-2}) extracted from I_D/V_G curves at V_{SD}= -60 V.

Parameter/Device	L-upe+C5-BTBT		PMMA+C5-BTBT	
	No UV	UV on	No UV	UV on
μ_{FE} (cm^2 V^{-1}s^{-1})	0.10±9.2x10^{-3}	0.13±1.8x10^{-2}	0.22±5.4 x10^{-3}	0.44±6.4 x10^{-2}
On/Off ratio, dark	1.3x10^6±1.9x10^4	n/a	1.3x10^7±7.9x10^6	n/a
V_{Th} (V)	-29.8±2.3	54.0±3.8	-16.7±0.8	-8.3±1.0
V_{SO} (V)	-17.3±1.2	>20	-7.3±1.2	14.7±4.2
$N_{trap,dark}$ (cm^{-2})	2.8x10^{12}	n/a	1.6x10^{12}	n/a

In the dark, observed differences in V_{SO} and V_{Th} between the studied transistors can be explained by different $N_{trap,dark}$. $N_{trap,dark}$ for L-upe based device ($2.8x10^{12}$) is higher than for PMMA based device ($1.6x10^{12}$), suggesting that a more negative gate voltage is required for L-upe device to generate enough electrons and holes to fill the traps and form the conductive channel (i.e., reach the threshold). More importantly, the presence of certain types of functional groups (EW and ED groups) in the active channel material is well-known to affect the shift in V_{Th} towards more negative values and lower the hole mobility for p-type semiconductors. [26] The L-upe polymer chain is composed of both EW and ED groups while PMMA is composed only of pending EW groups and neutral aliphatic moieties.

Once illuminated with UV light, OTF-PTs exhibited significantly different behavior. In output characteristics, the L-upe+C5-BTBT transistor showed a large increase of I_D without a complete saturation at all V_G (Fig. 3.3c). In contrast, the PMMA+C5-BTBT transistor had a lower UV response, reaching current saturation at all negative V_G (Fig. 3.3d). In transfer characteristics, a large and positive V_{Th} shift of ~84 V due to UV illumination was observed in L-upe+C5-BTBT OTF-PT compared to an 8.4 V positive shift for PMMA+C5-BTBT OTF-PT. However, UV illumination induced a lower back sweep current hysteresis [33] (Fig. 3.3e and f, solid curves) when compared to the virtually hysteresis-free behavior of both devices in the dark (Fig. 3.3e and f, dashed curves). Likewise, in output characteristics, a large increase of drain current in the subthreshold region of I_D-V_G characteristics, was observed for the L-upe+C5-BTBT transistor under UV illumination and is assigned to the contribution of the photocurrent (I_{phc}) generated

by UV light (Fig. 3.3e). This is supported by estimated values of I_{phc}/I_D ratio and R for transistors.

Photosensitivity values are defined as I_{phc} to I_D ratio (I_{phc}/I_D at V_G=20 V and 0 V). I_{phc}/I_D ratio at V_G= 0 V was chosen to avoid electrical contribution to the charge carrier generation. Higher I_{phc}/I_D ratios at gate voltage 20 V ($I_{phc}/I_{D,max}$=1.2x10^6) and 0 V ($I_{phc}/I_{D,max}$=3.9x10^6) than at -60 V (2.8±0.4), reflect that electrical carrier generation (injection and thermal) have lesser effects on the carrier photogeneration in the subthreshold region under UV light, where L-upe+C5-BTBT device is in the OFF-state in the dark. Therefore, photogenerated charge carriers are the main contributors to the largely increased I_{phc} and photosensitivity of the L-upe+C5-BTBT transistor. Photosensitivity ratios observed for PMMA+C5-BTBT OTF-PT are significantly lower ($I_{phc}/I_{D,max}$ of 34, 4.4x10^4 and 1.6 at V_G of 20 V, 0 V and -60 V, respectively) suggesting a superior UV response of the L-upe based device. Another important figure of merit that quantifies a photoresponse of OTF-PTs is responsivity (R) and it is estimated using equation $R=(I_{phc}-I_D)/(PLW)$[34], where P is an incident UV light intensity (3 mW/cm^2) and LxW effective area of the transistor illuminated by UV light. R_{max} values for L-upe based devices of 5.4 AW^{-1} (4.8±0.5) and 11.1 AW^{-1} (10.8±0.4) for a V_G 20 V and 0 V, respectively, are remarkably higher than those in PMMA based devices (R_{max} of 7.3x10^{-5} AW^{-1} and 4.0x10^{-2} AW^{-1} at V_G 20 V and 0 V, respectively). Compared to the R for a-Si device (300 AW^{-1}), our values for L-upe based devices are much lower but comparable or even higher than those reported for organic phototransistors based on TIPS-pentacene (~40 mAW^{-1})[30] and pentacene (761 mAW^{-1} [24], 4.24 AW^{-1} [25], and ~1

AW^{-1} [35]). Additionally, the maximum photosensitivity value for L-upe based device is significantly higher than those reported for the TIPS-pentacene ($26.1x10^3$) [30] and pentacene ($7.3x10^4$ [24], $5x10^4$ [25] and $9x10^3$ [35]) devices.

We have attempted to explain the mechanisms that govern this remarkably increased UV response of the L-upe+C5-BTBT device when compared with the PMMA+C5-BTBT device. UV illumination increased the charge carrier density by the photogeneration of excitons in the channel that dissociated into free electrons and holes. The rate and amount of dissociation of photogenerated excitons depend on the charge trapping sites [25] and applied an electric field. Since transistors were characterized under the same conditions, only the influence of charge trapping sites on the photogeneration of free charge carriers will be considered. Moderately strong EW groups in the L-upe polymer chain enhanced the amount and rate of electron-pair dissociation (i.e., charge separation), thus increasing the hole density by efficient trapping of photogenerated free electrons at the polymer/C5-BTBT interface. Simultaneously, photogenerated electrons, driven by the applied V_G, are additionally trapped under the source electrode while mobile holes can diffuse towards the drain electrode due to an applied V_{SD}. As a result, a large and positive shift of the V_{Th} for the L-upe+C5-BTBT OTFT under UV illumination is observed due to the photovoltaic effect caused by trapped photogenerated electrons that lowered the energy barrier for effective carrier injection from the electrode. [34]

The number of trapped photogenerated carriers that caused a shift of the V_{Th} is quantified by trap density determined using the equation $\Delta N_{trap}=\Delta V_{Th}C_{ox}/q$ [24] where q, C_{ox}, and ΔV_{Th} are an elementary charge, the capacitance of the dielectric

layer and threshold voltage shift, respectively. In other words, the magnitude of the V_{Th} shift is proportional to the photogenerated charge density that can be trapped per unit area at the dielectric/semiconductor interface.[36] The estimated number of trapping sites or photogenerated carriers per unit area is one order of magnitude higher for the L-upe+C5-BTBT device ($7.8x10^{12}$ cm^{-2}) than for the PMMA+C5-BTBT device ($7.8x10^{11}$ cm^{-2}), indicating a higher number of photogenerated carriers and more efficient charge trapping in the L-upe based device results in a larger UV response. Thus, EW groups present in the L-upe polymer chain provide deeper charge traps that suppress charge recombination resulting in an increased I_{phc} of more than six orders of magnitude.

On the other hand, the existence of the deeper traps in the channel of the L-upe+C5-BTBT device induced a large hysteresis upon UV illumination (Fig. 3e and f, solid curves), due to a slower recombination of trapped electrons and holes. [33] Hysteresis in L-upe based transistors is larger than in PMMA based transistors where the back sweep curve did not reach the initial drain current value causing a change in V_{Th}. This represents a memory property of an L-upe based transistor because of the memory window induced upon UV illumination ($\Delta V_{Th,hysteresis}$). Slower recombination of electrons and holes can be evaluated by measuring I_D vs. time or switching characteristics of fabricated OTF-PTs, immediately after UV illumination was removed.

The influence of UV illumination on time-dependent I_D (i.e., switching properties) for transistors at V_{SD}= -60 V and V_G= -5 V is given in Fig. 3.4. Like the previous measurements, the L-upe+C5-BTBT transistor had a sharp and more

than six orders of magnitude of I_{phc} jump followed by a saturation plateau (Fig. 3.4, solid curve). The PMMA+C5-BTBT transistor had a significantly lower response without achieving complete saturation within the measured timeframe (Fig. 3.4, dotted curve). At 100 s the UV light was removed and both devices exhibited a slow decay maintaining the higher drain current state. By applying a high negative V_G pulse of -60 V, that accelerated charge carrier recombination, we could reset the devices and returned them to the original low current state. This demonstrates both optical and electrical control over the working operation of OTFTs. After the reset pulse, OTF-PTs were subjected to the second cycle indicating a reproducible behavior.

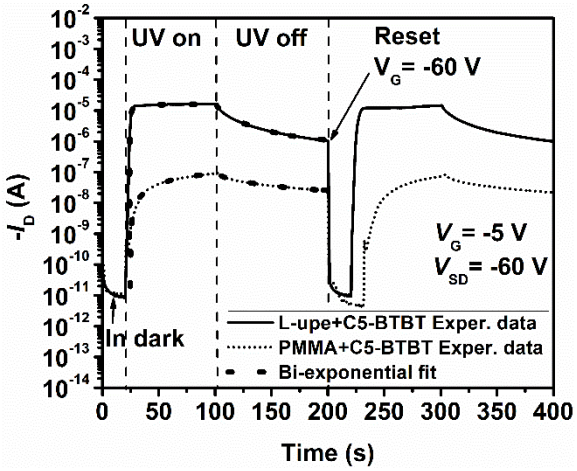

Fig. 3.4. Switching characteristics of studied OTF-PTs with (UV turned on at 20 s) and without UV illumination (UV light was turned off at ~100 s), at V_{SD}= -60 V and V_G= -5; the reset gate voltage of -60 V at 200 s, demonstrates a successful device reset in the low current state, in dark; bold dotted curves represent a bi-exponential curve fitting of the first switching cycle.

I_{phc} rise (UV on) and drain current decay (UV off) for both devices followed the time-dependent bi-exponential responses comprised of the fast/slow rise and fast/slow decay (Fig. 3.4, bold dotted curves-first cycle). Response times (τ) of a time-dependent photocurrent for the Polymer+C5-BTBT devices were estimated and compared. The first cycles of photocurrent rise and decay of devices were fitted using bi-exponential equations 1 and 2, respectively: [17]

$$I_{phc}(t) = I_{D,0} + A_1[1-\exp(-t/\tau_{r1})] + A_2[1-\exp(-t/\tau_{r2})] \quad (3.1)$$

$$I_D(t) = I_{D,0} + A_3\exp(-t/\tau_{d1}) + A_4\exp(-t/\tau_{d2}) \quad (3.2)$$

where I_{phc}, I_D and $I_{D,0}$ are photocurrents at time t, current (when UV was turned off) and initial drain current at the beginning of a measurement, respectively; $A_{1\text{-}4}$ are positive constants while τ_{r1}, τ_{r2}, and τ_{d1}, τ_{d2} are response times of the fast/slower rise, and fast/slow decay, respectively. Both bi-exponential models (equations 3.1 and 3.2) fit the experimental data very well as indicated by the coefficients of determination for the bi-exponential fit (R^2) for the rise/decay times 0.9630-0.9902/0.9918-0.9995 and 0.9868-0.9987/0.9792-0.9996 for L-upe+C5-BTBT and PMMA+C5-BTBT devices, respectively.

Rise times for the L-upe+C5-BTBT device under UV illumination are significantly shorter ($\tau_{r1,fastest}$=1.80 s or 1.86±0.08 s on average, and $\tau_{r2,\ fastest}$=11.72 s or 22.98±11.36 s on average) compared with the PMMA based device

($\tau_{r1,fastest}$=49.02 s or 71.18±26.14 s on average, and $\tau_{r2,fastest}$ =813 s or 2852.77±2182.65 s on average), suggesting faster carrier generation results in a sharp I_{phc} jump. Rise times for the L-upe based transistor are faster compared with previously reported OTFT photo-sensors (τ_{r1}=13 s and τ_{r2}=112 s [28], and τ_{r1}=10 s and τ_{r2}=73 s [37]) and some specifically engineered inorganic semiconductors (τ_{r1}=τ_{r2}=27 s),[17] which means that our device has a potential as a photo-sensor. The faster decay time for L-upe based transistor ($\tau_{d1,fastest}$=3.01 s or 4.11±1.35 on average) is similar to the faster decay time for PMMA based device ($\tau_{d1,fastest}$=5.03 s or 12.19±7.05 on average) while the slower decay times are different being $\tau_{d2,fastest}$=24.27 s (38.54±15.26 s on average) and $\tau_{d2,fastest}$=41.67 s (187.10±146.40 s on average) for L-upe and PMMA based transistor, respectively. The later can be explained by the existence of ED groups in L-upe as shallow traps that release trapped carriers faster than the deeper traps in the bulk, resulting in a faster recombination, thus, faster decay. Overall, obtained slow decay times in addition to the hysteresis generated under UV light makes L-upe+C5-BTBT transistor suitable for non-volatile memory devices fabrication. The L-upe device can be fully optically and electrically controlled, namely, UV light can act as a fourth terminal or switch due to a high photosensitivity and responsivity observed for this device.

Digital optical micrographs of thin-films of Polymer(s)+C5-BTBT blends revealed two distinct morphologies features: wrinkling and phase separation (Fig. 3.5a). We assumed that wrinkles did not affect the UV response for both devices. To confirm our assumption, we compared the results recently published by our group, [28] where wrinkle-free morphology was obtained from a PMMA+C5-BTBT

blend processed using chlorobenzene as a solvent (TCE was used in this report) with the similar order of magnitude of the UV response was reported. Under an optical microscope, a laterally segregated morphology was observed for the L-upe+C5-BTBT thin-film blend (Fig. 3.5, left) while the PMMA+C5-BTBT blend formed a vertically segregated morphology indicating a continuous polymer phase with unevenly distributed C5-BTBT crystals (“islands or clusters”) (Fig. 3.5, right). C5-BTBT “clusters” were not observed in L-upe+C5-BTBT thin-films indicating highly dispersed C5-BTBT crystals within the L-upe binder.

The lateral phase separation is desirable for a strong influence of the charge trapping sites at the interface on the photogenerated charge separation. On the other hand, it lowers the mobility due to the disturbed crystal growth (numerous small crystals without contact necessary for the charge hopping) and increased grain boundaries as physical charge traps. Vertical phase separation is desirable for the high mobility OTFTs and encapsulation of the air-sensitive small molecule semiconductor. In our case, fresh PMMA+C5-BTBT devices with vertically segregated phases have overall higher mobilities and significantly lower UV response, while fresh L-upe based devices (lateral phase separation) have overall lower mobilities and high UV response.

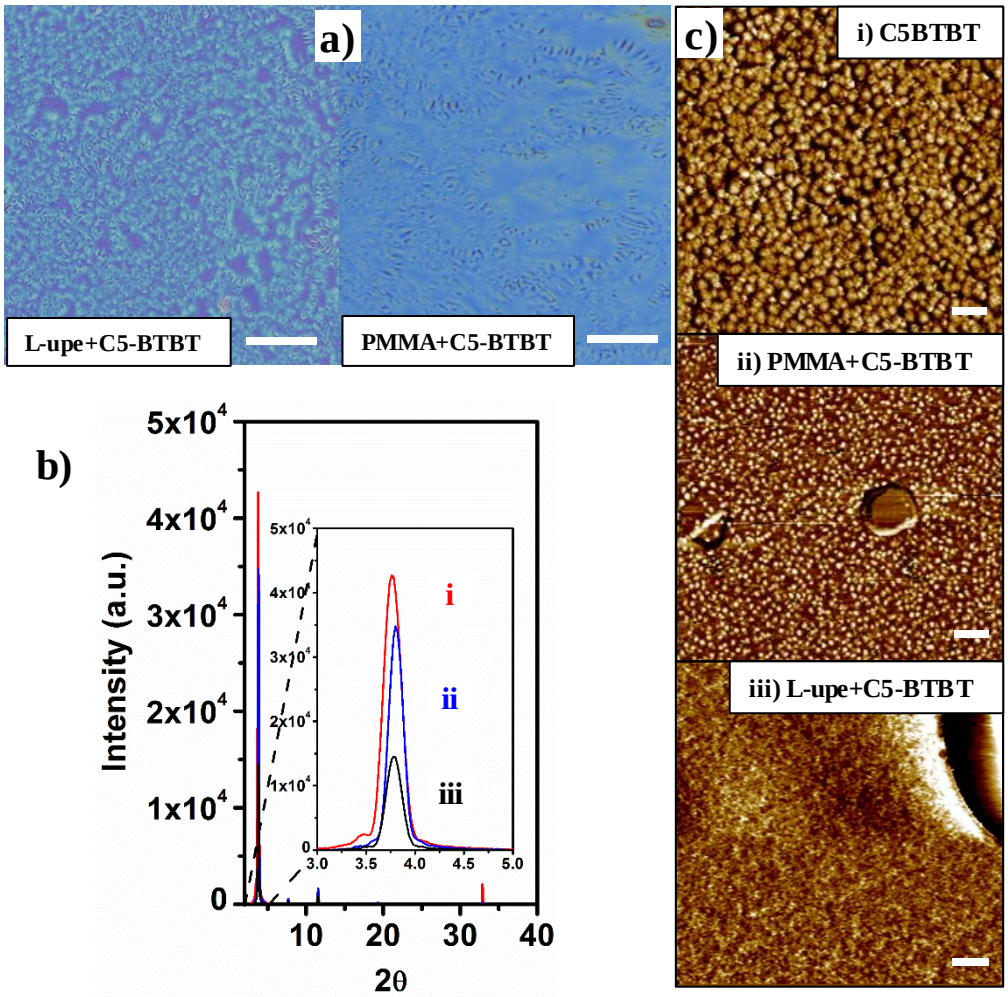

Fig. 3.5. Digital optical micrographs for Polymer+C5-BTBT thin-film blend morphologies (scale bars represent 100 μm) (a); powder X-ray diffractograms for Polymer(s)+C5-BTBT thin-film blends and pristine C5-BTBT (inset plot represents a magnification of 2θ range from 3° to 5°) (b); and AFM phase images of (i) C5-BTBT thin-film and (ii-iii) Polymer(s)+C5-BTBT thin-film blends, obtained in non-contact mode in ambient conditions (scale bar 100 nm) (c); C5-BTBT thin-film was fabricated under the same conditions as OTFTs.

X-ray diffractograms for the C5-BTBT thin film (Fig. 5b, red curve), displayed a characteristic peak of C5-BTBT crystal structure at $2\theta = 3.77°$ [38] that remained in all Polymer+C5-BTBT thin-film blends, but was slightly shifted likely due to internal stresses and crystal lattice strain induced by the X-ray beam (Fig. 5b inset, black and blue curves). The intensity of the peaks suggests that once immersed in a polymer binder, C5-BTBT crystal formation is hindered by a polymer, reflecting changes in crystallite size. Peak intensities (XRD patterns) and C5-BTBT crystallite sizes observed in AFM images (Fig. 3.5c) correlate each other very well. The L-upe binder has the lowest content of undisturbed C5-BTBT crystals (lowest intensity in XRD) and very small crystallites formed (Fig. 3.5c, iii), while bigger crystallites are observed in the PMMA continuous film (Fig. 3.5c, ii) with a higher content of undisturbed C5-BTBT crystals (higher peak intensity in XRD) relative to C5-BTBT XRD peak intensity (Fig. 3.5b, red line) and crystallite size (Fig. 3.5c, i). Therefore, C5-BTBT is highly dispersed and immersed in L-upe binder which generated a large semiconductor/polymer interface and facilitated a strong influence of EW groups on efficient charge separation of photogenerated excitons, resulting in the increased hole density and highly increased drain current, i.e. high UV responsivity, in the subthreshold region.

Air stability of OTFTs is a very important parameter for the application in commercial products such as flexible electronics. We investigated the ambient stability of the L-upe+C5-BTBT phototransistors after six months being stored at room temperature and atmospheric pressure, in the dark. Corresponding I_D-V_G characteristics for the aged L-upe+C5-BTBT devices, measured in the dark and

under UV light at V_{DS}=-60 V, are given in Fig. 3.6a. Characteristic electrical parameters, extracted from the I_D-V_G curves, photosensitivities, responsivities, and rise/decay times estimated from the Equations 3.1 and 3.2, are summarized in Table 3.2.

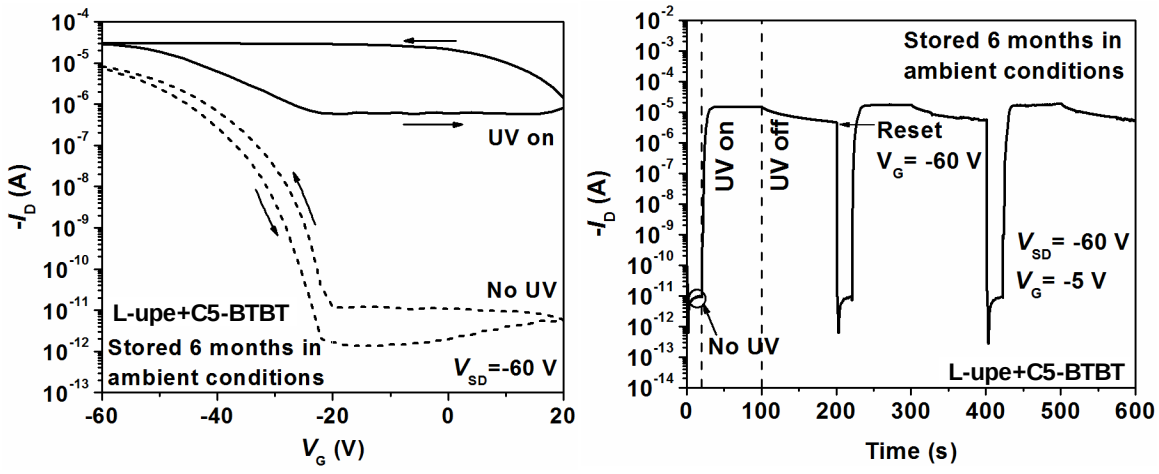

Fig. 3.6. Stability investigation of the 6-month aged L-upe+C5-BTBT phototransistors stored under ambient conditions (room temperature and atmospheric pressure): (a) transfer characteristics with hysteresis at V_{SD}= - 60 V; (b) switching characteristics (three cycles, UV light was turned on at 20 s, 220 s, and 420 s; turned off at 100 s and 400s, at V_{SD}= -60 V and V_G= -5); the reset gate voltages of -60 V at 200 s and 400 s, demonstrate a successful device reset to the low current state.

After six months, L-upe+C5-BTBT transistors exhibited stable transfer characteristics and typical p-type behavior both in the dark and under UV illumination (Fig. 3.6a). Transfer curves in the dark and under UV illumination for

L-upe based phototransistors indicate a slightly increased hysteresis most likely due to OH groups (trapping sites) from absorbed moisture. In the dark, all changes in the electrical parameters are negligible within statistical error (Table 3.2, No UV). The threshold voltage shift under UV illumination (Table 3.2, V_{Th}, UV on) is ~30 V lower than that of the fresh device (Table 3.1, V_{Th}=54 V), indicated by a lower photovoltaic effect due to a lower photogenerated charge carrier density (ΔN_{trap}= $5.3x10^{12}$ cm^{-2}) compared to $7.8x10^{12}$ cm^{-2} for the fresh device. However, the L-upe+C5-BTBT devices still exhibited a strong UV response of more than six orders of magnitude with a similar R_{max} value at V_G=0 V (9.7 AW^{-1} for the aged device vs 11.1 AW^{-1} for the fresh device). Interestingly, the field-effect mobilities under UV light are significantly higher for the aged devices ($\mu_{FE,max}$=0.53 cm^2 $V^{-1}s^{-1}$), comparing to the fresh transistors ($\mu_{FE,max}$=0.15 cm^2 $V^{-1}s^{-1}$). The reason for such an increase of the mobility can be probably attributed to a potential morphology change, i.e. ambient annealing over the period of six months and the absorbed moisture from the air.

Table 3.2 Estimated electrical parameters for the six months old L-upe+C5-BTBT phototransistors in the dark and under UV illumination (λ=365 nm and 3 mWcm^{-2}); R^2-coefficient of determination for the bi-exponential fit.

L-upe+C5-BTBT (aged devices)		
Parameter/Condition	UV off	UV on
μ_{FE} (cm^2 V^{-1}s^{-1})	0.14±1.9x10^{-2}	0.45±4.9x10^{-2}
On/Off ratio, dark	6.5x10^5±3.4x10^4	n/a
V_{Th} (V)	-32.5±1.9	23.9±2.5
V_{SO} (V)	-21.3±2.1	>20
$N_{trap,dark}$ (cm^{-2})	3.0x10^{12}	n/a
	V_G (V)	
	20	0
$I_{phc}/I_{D,max}$ (average)	2.2x10^5 (2.0x10^5±2.4x10^4)	2.0x10^6 (1.9x10^6±9.8x10^4)
R_{max} (AW^{-1}) (average)	0.7 (0.6±0.1)	9.7 (9.4±0.3)
Rise times (s), τ_{r1}/τ_{r2}; R^2 (fitting)	fastest 3.90/17.90 (5.40±1.41/46.98±32.3); 0.9716-0.9979	
Decay times (s), τ_{d1}/τ_{d2}; R^2 (fitting)	fastest 9.71/144.3 (5.99±6.62/189.77±65.71); 0.9716-0.9979	

The time-dependent I_{phc} UV-switching characteristics of the aged L-upe+C5-BTBT devices was re-evaluated. As seen in Fig. 6b we subjected L-upe based transistors to three “UV ON/OFF-RESET” cycles to observe any possible instabilities in aged devices and estimated the corresponding rise/decay times. In all three cycles, the device exhibited repeatable characteristics without visible signs of deteriorated properties. Therefore, after six months a successful optical (UV light)-electrical (reset voltage) control over the device performance was achievable

and devices retained their sensing and memory properties. Furthermore, calculated rise/decay times correlate with the observed changes of parameters in Table 3.2. The shortest τ_{r1}=3.90 s is twice of the fresh transistor (1.80 s) but still in line with the times reported in the previous studies. [28][37] Fast and slow decay times for the aged devices are largely increased (longer decay times), compared to those of the fresh devices, possibly due to the increased content of OH groups from absorbed moisture. OH-groups are known to be deep charge traps that lower the charge carrier recombination rates.

§ 3.4 Conclusions

We have demonstrated a modulation of a UV response of OTFT-PT by utilizing a dielectric polymer binder rich in EWGs. L-upe+C5-BTBT transistors were characterized by I-V electrical measurements in dark and under UV light followed by structure-morphology analysis of an L-upe+C5-BTBT thin-film blend. Under UV illumination, an excellent maximum photosensitivity and responsivity of 4.0×10^6 and 11.1 AW^{-1} was obtained, respectively for the L-upe+C5-BTBT transistor compared with a significantly lower response of the PMMA-based control. The enhanced photoelectronic properties were most likely due to the strong influence of the EWGs as deep traps at the polymer/C5-BTBT interface that enhanced the charge separation by trapping the photogenerated electrons and preventing fast charge recombination. The fast rise time of 1.80 s under UV light for L-upe+C5-BTBT suggests fast charge trapping, results in a large drain current increase. A

slow relaxation, when the UV light was removed, reflected a slow charge recombination. Moreover, structure and morphology analysis revealed a morphological contribution to the enhanced UV response. Small and highly dispersed crystallites in the L-upe+C5-BTBT thin film blend increased the polymer/C5-BTBT interface enabling many more contacts between the EWGs and C5-BTBT allowing efficient charge trapping at the interface. After six months of storage in ambient air, L-upe+C5-BTBT retained the high UV response of more than six orders of magnitude, and good sensing and memory properties estimated by corresponding response times.

Overall, the results presented herein reflected the simple fabrication of an OTF-PT with highly improved photoelectronic properties for sensing and memory applications. On-going research in our group aims to systematically investigate this phenomenon by careful design of the active channel materials utilizing different polymer binders and detailed analysis of the electronic structure influence of blend components on OTF-PT UV response.

§ 3.5 Experimental

Materials. Small molecule semiconductor 2,7-dipentyl[1]benzothieno[3,2-b][1]benzothiophene (C5-BTBT), was synthesized following procedures in references [38] and [39]. Linear unsaturated polyester polymer (L-upe, MW=50000), based on propoxylated bisphenol A and fumaric acid, was generously provided by Xerox Research Center of Canada. Poly(methyl methacrylate) (PMMA,

MW=140000) was purchased from Sigma Aldrich (CA). 2-propanol (Caledon, CA), methanol (Caledon, CA) toluene (Sigma Aldrich, CA), 1,1,2,2-tetrachloroethane (TCE, Sigma Aldrich, CA) and hexamethyldisilazane (HMDS, Sigma Aldrich, CA) were used as received. The highly n-doped Si wafers, used as substrates and a gate electrode, with 200 nm thick thermally grown SiO_2 dielectric layer, were purchased from Silicon Quest International (San Jose, CA, USA).

Preparation of Polymer+C5-BTBT blends. Linear unsaturated polyester was dissolved in toluene, precipitated in methanol and dried in a vacuum oven at 80°C for 48 h to eliminate any low molar mass compounds. Polymer+C5-BTBT blends (i.e. L-upe+C5-BTBT and PMMA+C5-BTBT) were prepared through solution mixing. Equal amounts of C5-BTBT and polymer were dissolved in TCE to obtain 1 wt% of C5-BTBT and polymer in solution. All solutions were filtered through an acrodisc PTFE syringe filter (Milipore 0.45 μm) and used for the spin coating onto Si wafers. Solutions and, later, OTFT devices were designated as L-pe+C5-BTBT and PMMA+C5-BTBT. The 1 wt% solution of C5-BTBT in TCE without polymer binder was prepared for the fabrication of the control OTFT.

OTFT fabrication. The OTFT fabrication was performed in ambient conditions under yellow light unless noted. The top-contact-bottom-gate architecture was adopted for OTFT fabrication. Si wafers were thoroughly washed with 2-propanol, air dried, and plasma cleaned for 2 min in a PDC-32G plasma cleaner (Harrick Plasma, USA). Clean Si wafers were soaked in deionized water for 5 min, rinsed with 2-propanol, air dried, followed by immersion in an HMDS/toluene solution at 60°C for 30 min. HDMS formed a self-assembled monolayer on the SiO_2 dielectric

surface of the wafer helping ensure adhesion of an active layer. Surface modified Si wafers were rinsed successively with toluene and isopropanol and dried by air and in a vacuum oven at room temperature for 30 min. Prepared Polymer+C5-BTBT solutions were then spin-coated (spin coater SCS P-6700, Sitek Process Solutions, Inc., CA, USA; conditions: 2000 rpm, ramp time 2 s and total spin time 120 s) onto the surface modified Si wafers yielding 260 nm (L-upe+C5-BTBT) and 350 nm (PMMA+C5-BTBT) thick films. Spin-coated substrates were placed in a vacuum oven at room temperature for 30 min to remove residual solvent. The electron beam evaporation (Edwards A306 Belljar Evaporator, Boc Edwards, West Sussex, UK) using a shadow mask was employed for the 60 nm thick Au source-drain electrodes deposition. Electrode length (an active channel width) and electrodes gap (an active channel length) were 930±10 μm and 80±5 μm, respectively.

Characterization. The thickness of the Polymer+C5-BTBT and C5-BTBT thin films spin-coated on the glass plates was measured using surface profiler DektakXT (Bruker, USA). UV-Vis absorption spectra were recorded from 300-800 nm in Nicolete UV-Vis-NIR spectrophotometer (Cary 5000, Varian, USA) on the same thin films on the glass used for the thickness measurements in the range 300-800 nm. Thin-film morphologies of the devices were examined using digital optical microscope Keyence VHX-2000 (Keyence, Canada) and MFP-3D atomic force microscope (Asylum Research and Oxford Instrument Company, Santa Barbara, CA, USA) in non-contact mode using a silicone tip (OMCL- AC240TS, Olympus Corp., Japan) with nominal spring constant 1.8 N/m and frequency 70

Hz), under ambient conditions. AFM data was collected and analyzed using the Asylum Research AFM software build on Igor Pro (Wavemetrics, Portland, OR, USA). C5-BTBT structure in polymer binders was studied by powder out-of-plane X-ray diffraction (XRD) using Rigaku Miniflex X-Ray diffractometer (TX, USA) fitted with a Cu X-ray tube operated at 30kV. Electrical characteristics of all devices were measured in ambient conditions (humidity 30% RH and 23°C), under the yellow light on a 4200-SCS Parameter Analyzer (Keithley Instruments, USA). UV lamp (Black-Ray, UVP B 100 AP, long wave UV lamp, 100 W, λ=365 nm, Entela, USA), UV-A light intensity of 3 mW/cm^2 at ~25 cm distance from the sample was used for the irradiation of devices during electrical characteristics measurements, illuminating the entire surface of OTFTs.

§ 3.6 References

[1] H. Sirringhaus, *Adv. Mater.* **2014**, *26*, 1319.

[2] P. S. K. Amegadze, Y.-Y. Noh, *J. Inf. Disp.* **2014**, *15*, 213.

[3] P. Lutsyk, K. Janus, J. Sworakowski, G. Generali, R. Capelli, M. Muccini, *J. Phys. Chem. C* **2011**, *115*, 3106.

[4] J. Mei, Y. Diao, A. L. Appleton, L. Fang, Z. Bao, *J. Am. Chem. Soc.* **2013**, *135*, 6724.

[5] C. Di, Y. Liu, G. Yu, D. Zhu, *Acc. Chem. Res.* **2009**, *42*, 1573.

[6] A. Y. Amin, A. Khassanov, K. Reuter, T. Meyer-Friedrichsen, M. Halik, *J. Am. Chem. Soc.* **2012**, *134*, 16548.

[7] H. Minemawari, T. Yamada, H. Matsui, J. Tsutsumi, S. Haas, R. Chiba, R. Kumai, T. Hasegawa, *Nature* **2011**, *475*, 364.

[8] Y. Yuan, G. Giri, A. L. Ayzner, A. P. Zoombelt, S. C. B. Mannsfeld, J. Chen, D. Nordlund, M. F. Toney, J. Huang, Z. Bao, *Nat. Commun.* **2014**, *5*, 3005.

[9] J. Li, Y. Zhao, H. S. Tan, Y. Guo, C.-A. Di, G. Yu, Y. Liu, M. Lin, S. H. Lim, Y. Zhou, H. Su, B. S. Ong, *Sci. Rep.* **2012**, *2*, 1.

[10] G. Horowitz, *Adv. Mater.* **1998**, *10*, 365.

[11] A. J. Kronemeijer, V. Pecunia, D. Venkateshvaran, M. Nikolka, A. Sadhanala, J. Moriarty, M. Szumilo, H. Sirringhaus, *Adv. Mater.* **2014**, *26*, 728.

[12] W. Ou-Yang, M. Weis, D. Taguchi, X. Chen, T. Manaka, M. Iwamoto, *J. Appl. Phys.* **2010**, *107*, DOI 10.1063/1.3449078.

[13] T. Li, J. W. Balk, P. P. Ruden, I. H. Campbell, D. L. Smith, *J. Appl. Phys.* **2002**, *91*, 4312.

[14] H. Yu, Z. Bao, J. H. Oh, *Adv. Funct. Mater.* **2013**, *23*, 629.

[15] M. Debucquoy, S. Verlaak, S. Steudel, K. Myny, J. Genoe, P. Heremans, *Appl. Phys. Lett.* **2007**, *91*, 103508.

[16] Y. Y. Noh, D. Y. Kim, K. Yase, *J. Appl. Phys.* **2005**, *98*, DOI 10.1063/1.2061892.

[17] D. Gedamu, I. Paulowicz, S. Kaps, O. Lupan, S. Wille, G. Haidarschin, Y. K. Mishra, R. Adelung, *Adv. Mater.* **2014**, *26*, 1541.

[18] F. Ercole, T. P. Davis, R. A. Evans, *Polym. Chem.* **2010**, *1*, 37.

[19] Y. Ishiguro, R. Hayakawa, T. Chikyow, Y. Wakayama, *J. Mater. Chem. C* **2013**, *1*, 3012.

[20] H. Zhang, X. Guo, J. Hui, S. Hu, W. Xu, D. Zhu, *Nano Lett.* **2011**, *11*, 4939.

[21] N. Crivillers, E. Orgiu, F. Reinders, M. Mayor, P. Samorì, *Adv. Mater.* **2011**, *23*, 1447.

[22] Q. Shen, L. Wang, S. Liu, Y. Cao, L. Gan, X. Guo, M. L. Steigerwald, Z. Shuai, Z. Liu, C. Nuckolls, *Adv. Mater.* **2010**, *22*, 3282.

[23] B. Gunduz, F. Yakuphanoglu, *Sensors Actuators, A Phys.* **2012**, *178*, 141.

[24] X. Liu, G. Dong, L. Duan, L. Wang, Y. Qiu, *J. Mater. Chem.* **2012**, *22*, 11836.

[25] B. Yao, W. Lv, D. Chen, G. Fan, M. Zhou, Y. Peng, *Appl. Phys. Lett.* **2012**, *101*, 163301.

[26] H. Karimi-Alavijeh, F. Panahi, A. Gharavi, *J. Appl. Phys.* **2014**, *115*, 093706.

[27] S. L. Lim, N. J. Li, J. M. Lu, Q. D. Ling, C. X. Zhu, E. T. Kang, K. G. Neoh, *ACS Appl. Mater. Interfaces* **2009**, *1*, 60.

[28] C. S. Smithson, Y. Wu, T. Wigglesworth, S. Zhu, *Adv. Mater.* **2015**, *27*, 228.

[29] C. W. Tseng, D. C. Huang, Y. T. Tao, *ACS Appl. Mater. Interfaces* **2012**, *4*, 5483.

[30] F. Yakuphanoglu, B. Gunduz, *Synth. Met.* **2012**, *162*, 1210.

[31] C. D. Dimitrakopoulos, P. R. L. Malenfant, *Adv. Mater.* **2002**, *14*, 99.

[32] J. Smith, R. Hamilton, Y. Qi, A. Kahn, D. D. C. Bradley, M. Heeney, I. McCulloch, T. D. Anthopoulos, *Adv. Funct. Mater.* **2010**, *20*, 2330.

[33] M. Egginger, S. Bauer, R. Schwödiauer, H. Neugebauer, N. S. Sariciftci, *Monatshefte für Chemie - Chem. Mon.* **2009**, *140*, 735.

[34] K.-J. Baeg, M. Binda, D. Natali, M. Caironi, Y.-Y. Noh, *Adv. Mater.* **2013**, *25*, 4267.

[35] Y.-Y. Noh, D.-Y. Kim, *Solid. State. Electron.* **2007**, *51*, 1052.

[36] P. Heremans, G. H. Gelinck, R. Müller, K.-J. Baeg, D.-Y. Kim, Y.-Y. Noh, *Chem. Mater.* **2011**, *23*, 341.

[37] T. P. I. Saragi, R. Pudzich, T. Fuhrmann-Lieker, J. Salbeck, *Appl. Phys. Lett.* **2007**, *90*, 143514.

[38] H. Ebata, T. Izawa, E. Miyazaki, K. Takimiya, M. Ikeda, H. Kuwabara, T. Yui, *J. Am. Chem. Soc.* **2007**, *129*, 15732.

[39] M. Saito, I. Osaka, E. Miyazaki, K. Takimiya, H. Kuwabara, M. Ikeda, *Tetrahedron Lett.* **2011**, *52*, 285.

4 EFFECT OF POLYMER BINDERS ON UV-RESPONSIVE ORGANIC THIN-FILM PHOTOTRANSISTORS WITH 2,7-DIPENTYL[1]BENZOTHIENO[3,2-B][1]BENZOTHIOPHENE SEMICONDUCTOR

In this chapter, the effect of different polymer dielectrics on photoelectrical characteristics of a solution-processed UV responsive organic phototransistors based on polymer/2,7-dipentyl[1]benzothieno[3,2-b][1]benzothiophene blend as the active channel material is presented. This chapter is based on the paper published in the peer-reviewed journal, as follows: “D. Ljubic, C.S. Smithson, Y.

Wu, S. Zhu, Effect of Polymer Binders on UV-Responsive Organic Thin-Film Phototransistors with Benzothienobenzothiophene Semiconductor, *ACS Appl. Mater. Interfaces*, **2016**, 8 (6), 3744-3754 (DOI: 10.1021/acsami.5b09001). Reprinted with permission from *Appl. Mater. Interfaces*, **2016**, 8 (6), 3744-3754.

Author contributions

Darko Ljubic conducted the experiments and wrote the first draft of the manuscript under the guidance of Dr. Shiping and Dr. Yiliang Wu. Dr. Chad S. Smithson provided the first revision of the manuscript. The final revision was provided by Dr. Wu and Dr. Zhu.

§ 4.1 Abstract

The influence of polymer binders on the UV response of organic thin-film phototransistors (OTF-PTs) is reported. The active channel of the OTF-PTs was fabricated by blending a UV responsive 2,7-dipenty[1]benzothieno[2,3-b][1]benzothiophene (C5-BTBT) as small molecule semiconductor and a branched unsaturated polyester (B-upe) as a dielectric binder (ratio 1:1). To understand the influence of the polymer composition on the photo-electrical properties and UV response of C5-BTBT, control blends were prepared using common dielectric polymers, namely, poly(vinyl acetate) (PVAc), polycarbonate (PC), and

polystyrene (PS), for comparison. Thin-film morphology and nanostructure of the C5-BTBT/polymer blends were investigated by means of optical and atomic force microscopy, and powder X-ray diffraction, respectively. Electrical and photoelectrical characteristics of the studied OTF-PTs were evaluated in the dark and under UV illumination with a constant light intensity (P=3 mW cm^{-2}, λ=365 nm), respectively, using two- and three-terminal *I-V* measurements. Results revealed that the purposely chosen B-upe polymer binder strongly affected the UV response of OTF-PTs. A photocurrent increase of more than five orders of magnitude in the subthreshold region was observed with a responsivity as high as 9.7 AW^{-1}, at V_G= 0 V. The photocurrent increase and dramatic shift of $V_{Th,\ average}$ (~86 V) were justified by the high number of photogenerated charge carriers upon the high trap density in bulk 8.0 $x10^{12}$ cm^{-2} eV^{-1} generated by highly dispersed C5-BTBT in B-upe binder. Compared with other devices, the B-upe OTF-PTs had the fastest UV response times (τ_{r1}/τ_{r2}=0.5/6.0) reaching the highest saturated photocurrent (>10^6), at V_G=-5 V and V_{SD}=-60. The enhanced UV sensing properties of B-upe based OTF-PTs were attributed to a self-induced thin-film morphology. The enlarged interface facilitated the electron withdrawing/donating functional groups in the polymer chains in influencing the photo-charge separation, trapping, and recombination.

§ 4.2 Introduction

The organic thin-film transistors (OTFTs), based on electrochemically polymerized polythiophenes, were first reported in 1986 by Tsumara et al.[1] Immediately after, OTFTs attracted significant research attention and their performance and design were constantly improved, providing advantages over the performance level of amorphous silicon based field-effect transistors.[2],[3] The reasons for this development are that organic materials are compatible with many plastic substrates, are flexible and can be used in low-cost printing processes including solution-processed deposition and melt processing.[4] The maximum charge carrier mobilities, reported for solution-processed OTFTs are as high as ~11 $cm^2V^{-1}s^{-1}$ for donor-acceptor conjugated polymers,[5] and 31.3-43.0 $cm^2V^{-1}s^{-1}$ for a symmetric small molecule C8-BTBT semiconductor (dioctyl substituted [1]benzothieno[3,2-b][1]benzothiophene),[6-7] with On/Off ratios of more than 10^6 for all the devices. OTFTs already have many applications such as electronic flexible paper, sensors, smart cards, erasable memory devices, flexible displays, and radio frequency identification tags (RFID).[8-9] OTFTs are the most versatile platform for the development of phototransistors (PTs), which can have an advantageous performance over photodiodes, i.e. high signal (sensitivity) to noise (low noise) ratio.[10] The drain current (I_D) gain in organic thin-film phototransistors (OTF-PTs) is fully controllable by four terminals, namely, gate, source/drain electrodes, and light,[11],[12] offering their applications as memory and/or sensing devices,[10],[13] and photo-transducers.[14]

The most common approach to optically controlling electrical properties of OTF-PTs is to incorporate a photochromic molecule (azobenzenes, spiropyrans, spirooxazines, diarylethenes, and fulgides) at the OTF-PTs interfaces and/or directly into the semiconducting (SC) layer.[15-18] Operational mechanisms in these OTF-PTs rely on the physical (photo-isomerization: cis-trans and structural or ring opening) or electronic (dissociation, redox reactions) changes in the SC molecule induced by heat or light (UV or visible).[19],[20] Alternatively, the photosensitive SC layer in OTF-PTs without photochromic molecules can also be formed from light-responsive SC small molecules and polymers, or by mixing a small molecule SC and dielectric polymer, as it is done in the work presented here. This can be achieved through solution processing of the chosen compounds spin-coated onto a substrate. Solution blending of a polymer with a small molecule or another polymer has advantages such as the formation of a smooth, uniformly deposited and flexible SC layer, allowing for improved photo-electrical properties of the OTF-PTs. Additionally, blending can induce different thin-film morphologies that may affect predominant photo-control mechanisms and increase environmental stability of the small molecule SC by encapsulation in the polymer binder. [21] In OTF-PTs without a photochromic moiety, the enhanced response under light is governed by photogeneration of charge carriers in the channel that results in the increased photocurrent in the subthreshold region where the device would otherwise be in an OFF state.

In designing an OTF-PT, the major parameters to be considered are photosensitivity (I_{phc}/I_D) and responsivity (R), operational and environmental

stability, and fast sensing times with long retention of the high current state for memory devices. To achieve high photosensitivity and responsivity without the aid of a photochromic moiety, the various organic small molecules and polymers can be utilized by choosing those with the light response in a specific region of the spectrum (UV and/or visible part of the spectrum). So far, many devices are reported to reach high photo-electrical properties comparable with inorganic PTs.[22] However, these devices have still not reached a fast response required for light sensors or photodetector applications.[23] The most studied p-type OTF-PTs are based on pentacene,[24,25] and TIPS-pentacene.[26] Less attention has been paid to 2,7-dipenty[1]benzothieno[2,3-b][1]benzothiophene (C5-BTBT), which is blind to the visible and sensitive to the UV light. It should be pointed out that with the traditional use of photochromic moieties, the transition between isomers is a slow process requiring long exposure to the light illumination, which can induce channel degradation, lowering the device performance.

Although not yet fully understood, the influence of electron withdrawing (EW) and electron donating (ED) groups, present in the photochromic molecule that undergoes photoisomerization, is necessary for the design of OTF-PTs to achieve a high subthreshold current gain and to avoid long exposure to the light.[27],[28], It has been reported by our group that dramatically enhanced UV responses of OTF-PTs could be realized by the use of an EW/ED containing photochromic molecule (azobenzene) attached to a polymer chain or in a three-component blend.[29,30] A proposed mechanism used to explain such a behavior is based on the HOMO-LUMO difference between C5-BTBT semiconductor and azobenzene derivative,

which acts as trapping/detrapping levels for photo-excited electrons, rather than the cis-trans photoisomerization of the azobenzene chromophores. This mechanism was further confirmed by using a dielectric polymer binder rich in EW/ED groups in absence of photochromic moiety, in a binary blend with the UV sensitive C5-BTBT. [31]

Following these findings, herein we report on the further investigation of the UV response enhancement (UV sensing and memory properties) of the small molecule semiconductor C5-BTBT in various polymer binders. Chemical structures of the used semiconductor and polymers are displayed in Fig. 4.1a. We first utilized a novel branched unsaturated polyester (B-upe), as the dielectric polymer, to prepare a binary blend with the highly UV sensitive C5-BTBT. The blend was used as an active channel material and the electrical properties in dark and under UV light were investigated. To have a clear picture of the influence of the polymer binder on the UV response of a semiconductor, we prepared control blends based on poly(vinyl acetate) (PVAc), polycarbonate (PC), and polystyrene (PS). PVAc has a similar structure to the previously investigated PMMA/C5-BTBT blend based OTF-PTs that was proven to have low UV sensing properties, while PC has the bisphenol A unit in the backbone in addition to the carbonate EWGs and it is similar in structure to the B-upe polymer. Lastly, PS is considered as a neutral polymer binder because it is composed of the neutral aliphatic backbone and dangling benzene rings. All the thin-film blends were subjected to the UV-Vis spectroscopy investigation in the UV-A range. The spectra recorded for the polymer+C5-BTBT blends, displayed in Fig. 4.1b, clearly show that the UV response originates only

from the C5-BTBT SC (with the characteristic peak at 356 nm for the pristine C5-BTBT thin-film as a reference). Thin-film morphology analysis and electrical measurements under UV illumination and in dark, contrasted with the control OTF-PTs, reveal that the strong enhancement of the UV response of the B-upe based device can be attributed to the strong interface trapping in the bulk of the photo-generated charge carriers by EW/ED groups enabled by the lateral phase separation. In addition, the measurements of electrical properties of the 8 months aged B-upe based devices reveal its excellent environmental stability and retained excellent UV sensing and memory properties.

§ 4.1 Experimental

Materials. The symmetric small molecule organic semiconductor 2,7-dipentyl[1]benzothieno[3,2-b][1]benzothiophene (C5-BTBT) was synthesized following the previously reported procedures.[32,33] The branched unsaturated polyester polymer (B-upe, MW=60800), based on dipropoxylated bisphenol A and fumaric acid, was synthesized using proprietary procedures at Xerox Research Center of Canada. Poly(vinyl acetate) (PVAc, MW=10000) polystyrene (PS, MW=100000,), and polycarbonate (PC, MW=60000-70000) were purchased from Scientific Polymer Products, Inc. (Ontario, NY, USA), Sigma Aldrich, CA and Mitsubishi Gas Chemical Company Inc., respectively. Solvents: 2-propanol (Caledon, CA), methanol (Caledon, CA), toluene (Sigma Aldrich, CA), 1,1,2,2-tetrachloroethane (TCE, Sigma Aldrich, CA), and surface modifier

hexamethyldisilazane (HMDS, Sigma Aldrich, CA) were used as received. The highly n-doped Si wafers, used as a substrate and a gate electrode, with 200 nm thick thermally grown SiO_2 dielectric layer, were purchased from Silicon Quest International (San Jose, CA, USA).

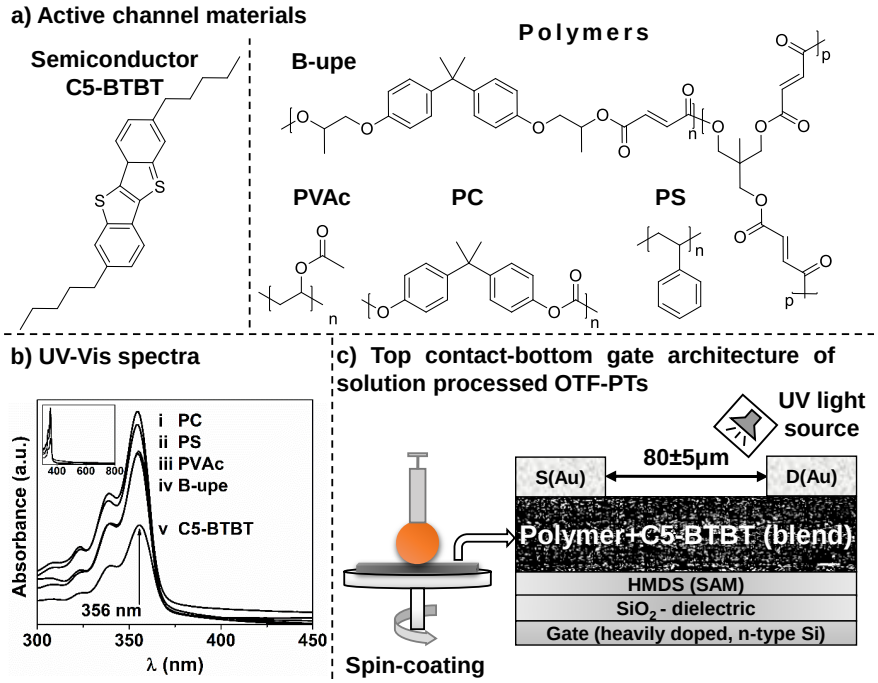

Fig. 4.1. Chemical structures of small molecule organic semiconductor (C5-BTBT) and polymers used for binary blends preparation as active channel materials in OTF-PTs (a); zoom-in (300-450 nm) of UV-Vis spectra (inset) of polymer+C5-BTBT thin-films on glass substrates showing characteristic UV absorbance of C5-BTBT at 355 nm in all thin-films (pure C5-BTBT thin-film is included as reference, λ=356 nm) (b); schematic of the spin-coating process that resulted in the top contact-bottom gate architecture adopted for OTF-PTs, where S and D are source and drain electrodes, respectively (c).

Preparation of polymer+C5-BTBT blends. Branched unsaturated polyester (B-upe) was dissolved in toluene, precipitated from methanol (to eliminate any low molar mass compounds), and it was dried in a vacuum oven at 80°C for 48 h to remove residual solvent. Polymer+C5-BTBT blends were prepared through solution mixing of polymer and C5-BTBT, in a ratio of 1:1, using TCE as the solvent. C5-BTBT and the polymer were dissolved in TCE to obtain 1 wt% of C5-BTBT and polymer in solution. All solutions were filtered through an acrodisc PTFE syringe filter (Milipore 0.45 µm) and used for the spin coating onto Si wafers (Fig. 4.1c). The 1 wt% solution of C5-BTBT in TCE without a polymer binder was prepared for fabrication of the control OTF-PT.

OTF-PTs Fabrication and Characterization. The OTF-PTs fabrication and characterization are performed according to the procedures reported in our previous work, [31] with details given in the supporting information. The top-contact-bottom-gate architecture was adopted for OTF-PTs fabrication (Fig. 4.1c). General notation for the devices is polymer+C5-BTBT OTF-PTs while in the further text a specific OTF-PT will be designated as B-upe, PS, PC and PVAc for B-upe+C5-BTBT, PS+C5-BTBT, PC+C5-BTBT, and PVAc+C5-BTBT blend based OTF-PTs.

§ 4.2 Results and discussion

4.2.1 Morphology and structure of the thin-film blends

The thin-film morphologies of 1:1 polymer+C5-BTBT blends, formed by spin-coating from TCE solution onto a SiO_2 dielectric layer of a Si-wafer, are investigated by means of optical and atomic force microscopy (Fig. 4.2, background images). The 1:1 ratio blends were chosen to study the effect of various polymers by considering several factors such as solubility of the polymers, uniformity of the semiconductor films, and the charge carrier mobility of the semiconductor blends. For example, when B-upe+C5-BTBT blends with different ratios were used, the uniform film was only obtained at the 1:1 ratio (Fig. S4.1). Although good films could be obtained for some of the polymer/C5-BTBT blends (e.g. PS/C5-BTBT) at different ratios. As shown in Fig. S4.2, the blend with 1:1 ratio provided the best electrical performance. This is in agreement with previous reports. [21],[34],[35] Therefore, we only used the semiconductor blends with 1:1 ratio to study the effect of various polymers.

There are two major morphological patterns observed under the optical microscope: wrinkling and phase separation. The B-upe based blends formed a continuous thin-film with predominant laterally segregated morphology and uniform dispersion of C5-BTBT in the binder, with no clear discernible difference between the two phases (Fig. 4.2a). In contrast, the phases in the thin-films of PS, PC and PVAc based blends (Fig. 4.2b-d) are predominantly vertically segregated, with

aggregated C5-BTBT phase formed as yellowish “islands” (see Fig. 4.2e, pristine C5-BTBT to identify the semiconductor phase).

AFM phase images for polymer+C5-BTBT blend thin-film morphologies (Fig. 4.2a-d, insets) were acquired in a non-contact mode and compared with the pristine C5-BTBT thin-film (Fig. 4.2e, inset). The observed morphologies in AFM images provide additional support that there is a more uniform dispersion of C5-BTBT in the polymer phase since the chosen polymer binder would affect the crystal growth and size of C5-BTBT. In PS, PC, and PVAc, C5-BTBT domains retained the characteristic ball-shaped growth as in the pristine C5-BTBT thin-film. In contrast, C5-BTBT domains in the B-upe polymer are very small and highly dispersed making them hard to be identified. Thus, a large polymer/semiconductor interface in B-upe+C5-BTBT blend is expected to facilitate an efficient trapping by EW/ED groups in the polymer chain of the UV generated excitons and their dissociation into free charge carriers.

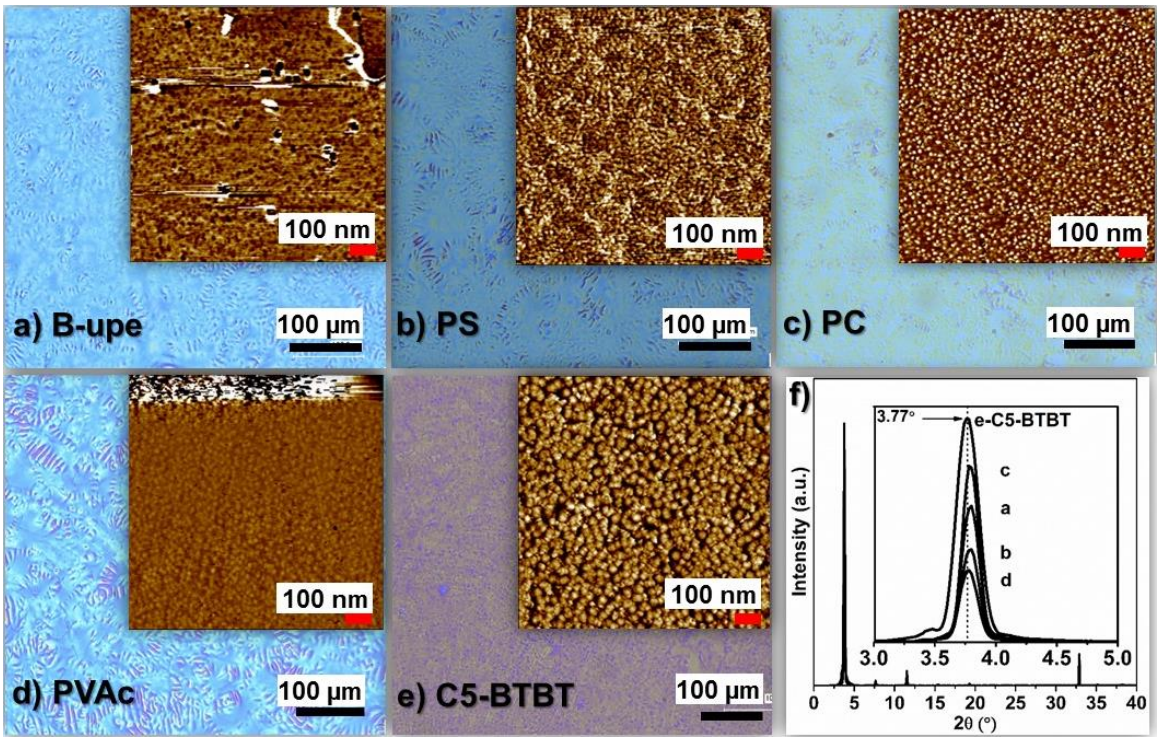

Fig. 4.2. Digital optical micrographs and AFM phase images for thin-film morphologies of polymer+C5-BTBT blends (a-d) and pristine C5-BTBT as a reference (e) (AFM images were acquired in a non-contact mode at room temperature and ambient pressure while thin-film of the pristine C5-BTBT was fabricated under the same conditions as the thin films of blends), and powder X-ray patterns (f) of the studied thin-films (inset plot represents a zoom-in of 2θ=3°-5°).

Although the AFM analysis showed that C5-BTBT domains and their dispersion were affected by the type of polymers, the X-ray diffraction (XRD) patterns confirmed the undisturbed intact crystal structure of C5-BTBT in the polymer binders. A characteristic d-spacing peak of C5-BTBT at 2θ = 3.77°remained in all

polymer+C5-BTBT thin-films (Fig. 4.2f, inset).[32] Furthermore, to better address the influence of morphology and structure of the thin-films on the performance of the studied OTF-PTs, we estimated an average crystallite size (XS) of C5-BTBT in each polymer binder using the well-known Scherrer's equation (Table 4.1). Compared with the XS of C5-BTBT in the pristine thin-film (no polymer binder) with those in the polymer binders, one can see that polymer binders affected the size of C5-BTBT crystallites, which could, in turn, affect the charge carrier mobility along with the phase separation. It should be noted that the domain size in the AFM images has no correlation to the crystallite size estimated from the XRD. AFM images only reveal the surface morphology. The C5-BTBT crystals are embedded in the amorphous polymer matrix for the semiconductor blends so that they cannot be visualized from the top surface.

Table 4.1 Characteristic parameters of the thin-film structures determined from XRD analysis (*Reference; d-interplanar (spacing) distance and XS- average crystallite size of C5-BTBT).

Thin-film blend (Polymer+ C5-BTBT)	Parameter		
	2θ (°)	d (Å)	XS (nm)
*C5-BTBT	3.77	2.34	62
B-upe	3.79	2.33	97
PS	3.78	2.33	99
PC	3.79	2.33	>100
PVAc	3.77	2.34	90

4.2.2 Electrical characteristics of polymer+C5-BTBT devices

Two-terminal measurements. The conductive nature or current-voltage (*I-V*) characteristics of polymer+C5-BTBT OTF-PTs, in dark and under continuous UV illumination, were investigated by the current versus bias voltage measurement. This measurement is characterized by no external electric field applied in the voltage range 1–(-1) V, showing a simple resistance of the active channel in the dark (Fig. 3a), after the initial UV illumination (Fig. 4.3b), and upon the current saturation (Fig. 3c). The current saturation was reached after the fourth measurement under continuous UV illumination, which corresponded to 3 min of elapsed time. For clarity, only the first and fourth measurements (curves) under UV light are presented since the intermediate curves show only a gradual rise of the current, until saturation in the positive and negative bias voltage ranges.

In the dark, all OTF-PTs acted as real resistors with their measured currents lower than 1 pA in the applied bias voltage range (Fig. 4.3a). Once illuminated by the UV light, the OTF-PTs exhibited a different current response. The highest response of more than five orders of magnitude was achieved in the B-upe based device (solid curve), compared with the increase of only two orders of magnitude in the lowest responsive device PVAc (dashed curve). This is a positive indication that the polymer binder composition affects the UV response (i.e. type and content of functional groups), along with the thin-film morphology observed for the B-upe based device (Fig. 4.2). The channel was highly sensitive even without an external electric field applied due to an obviously stronger interfacial polarization in the B-upe/C5-BTBT blend that generated an additional electric field in the channel, lowering the energy barrier for efficient charge injection from the source electrode. Considering the observations from our previously reported phototransistors based on the linear unsaturated polyester (L-upe)/C5-BTBT blend, we purposely designed a blend of C5-BTBT/branched unsaturated polyester (B-upe) that contains a higher number of ED and EW groups per chain. These groups are responsible for the charge trapping-releasing at the interface, thus affecting the current response. The B-upe polymer chain is essentially an L-upe extended by two branches, which are the source of the EW ester groups and weak ED double bonds.

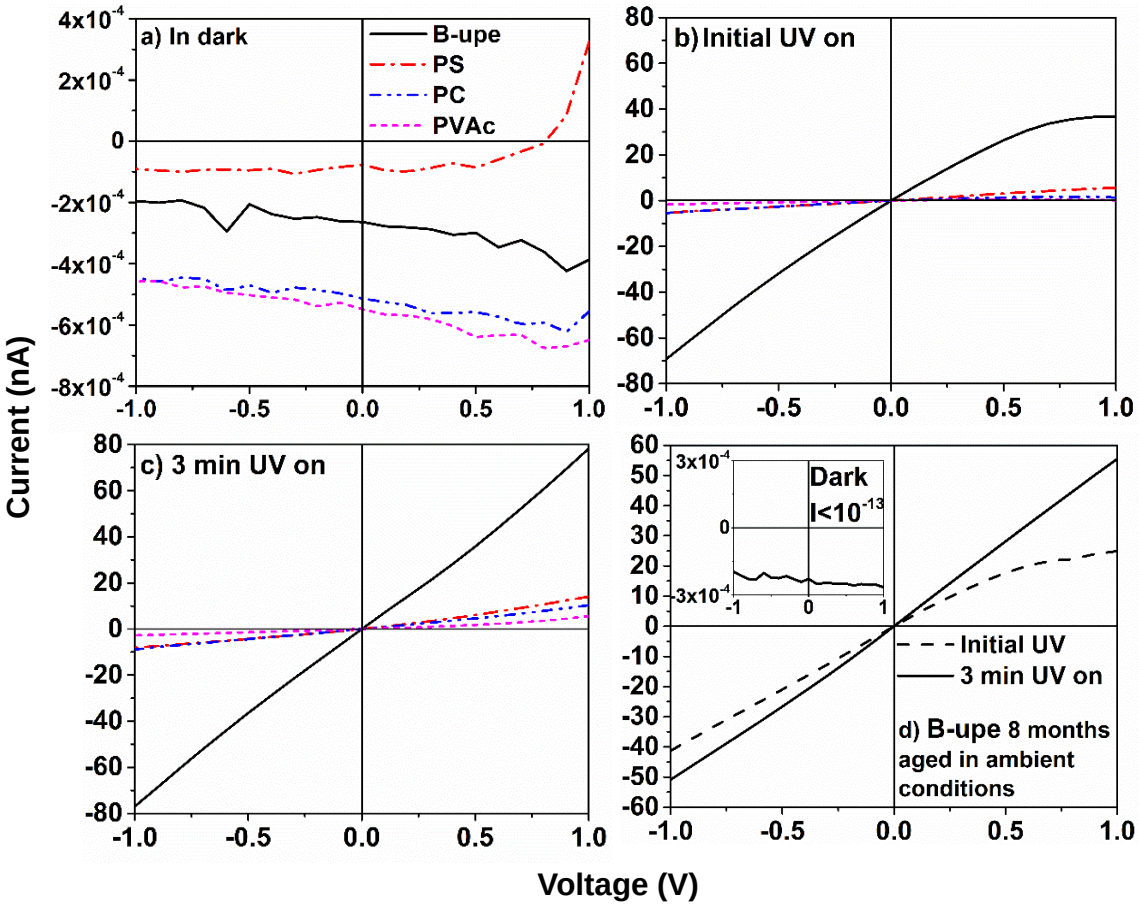

Fig. 4.3. *I-V* characteristics of the studied polymer+C5-BTBT OTF-PTs measured (a) in dark, (b) under initial and (c) saturation (3 min) continuous UV illumination (P=3 mW cm^{-2}, λ=365 nm), showing an immediate UV response (highest current increase or lowest resistance) in B-upe based OTF-PTs; plot in (d) represents *I-V* characteristics of the B-upe based phototransistor, in the dark (inset) and under the UV light, measured after 8 months ageing in the ambient conditions (standard laboratory temperature and humidity, and atmospheric pressure); legend for the devices notation in (a) applies for the plots in (b) and (c).

The large polymer/semiconductor interface and the higher content of EW/ED groups strongly affected the UV response in B-upe based devices, manifesting as a dramatic current increase, in the positive and negative voltage range. The highest current achieved at -1 and 1 V was ~80 nA, which is ~20 nA higher than our previously reported device based on an L-upe/C5-BTBT blend. The UV sensitivity of the B-upe based device is also evident when observing differences in the current rise after the initial UV illumination within the studied devices. The B-upe device had an instantaneous current response of ~3 orders of magnitude compared to virtually no responsive PVAc. However, the slow current increase in the range 1-0.50 V (Fig. 4.3b, solid line) may be related to a slow photogeneration of the charge carriers in the observed bias voltage range associated with the slow polarization of the ester groups without an external electric field applied, i.e. slow interfacial polarization. Linear and symmetric *I-V* curves, under the UV light, at the saturation currents of B-upe based OTF-PTs, indicate an ohmic contact at the electrode/channel interface. After 8-month storage under ambient conditions (23°C, RH=30%, and atmospheric pressure), the B-upe based devices retained the low resistance behavior and the high UV response of more than five orders of magnitude as displayed in Fig. 4.3d, reflecting its excellent ambient stability.

Three-terminal measurements. Dependence of the I_D on the source-drain voltage (V_{SD}) for polymer+C5-BTBT OTF-PTs, and gate voltage (V_G) sweep 20–(-60) V, in dark and under UV light, is displayed in Fig. 4.4. All devices showed a typical p-type field-effect behavior, in the dark (dashed curves) and under the UV illumination (solid lines). In the dark, the I_D-V_{SD} curves of all devices are

characterized by linear and saturation regimes. The linear regimes as a result of an ohmic contact at the electrode–channel interface, reflect an efficient charge carrier injection with some deviation from the linearity in the PS and PVAC based devices (Fig. S4.3). The cut-off V_G for all devices was -30 V, except for the B-upe based device (-40 V), reflecting a different number of the fast filling trapping sites at the SiO_2/active channel interface.

As observed in Fig. 4.4, the UV illumination increased the drain current and modulated the cut-off voltages in all devices. Likewise, in the dark, the I_D-V_{SD} curves are characterized by linear and saturation regimes. Considering the I_D response and its value, at the cut-off voltage (V_G=20 V), the B-upe based OTF-PTs were most affected by UV light. The cut-off at V_G=20 V and drain current of ~2 µA indicated a high UV sensitivity of this blend, confirming the observations discussed in the two-terminal measurements. Even after 8 months stored in ambient conditions, the B-upe devices did not show any severe signs of degradation since the measured output properties, i.e., cut-off voltage at V_G=20 V and high I_D of ~9 µA (fresh device I_D ~11 µA), at V_G and V_{SD} of -60 V, were retained at similar levels of the fresh devices (Fig. S4.4).

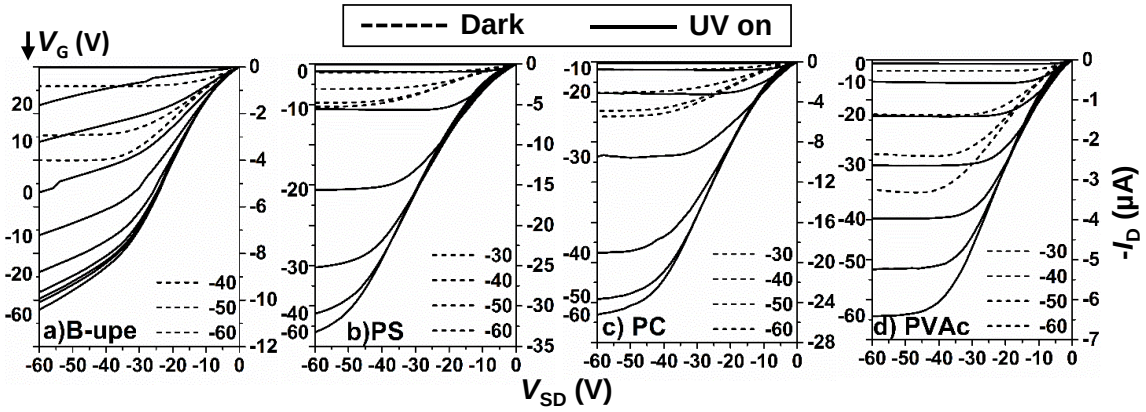

Fig. 4.4. I_D-V_{SD} characteristics for (a-d) polymer+C5-BTBT OTF-PTs acquired in dark (dashed curves) and under UV illumination (solid curves), in V_G range 20 to -60 V (steps of -10 V, scan rate 6 Vs^{-1}) showing I_D modulation upon UV light while retaining a p-type behavior and cut-off (turn-on) voltage already at V_G=20 V for B-upe based OTF-PTs (L=80 μm and W=930 μm)

To further analyze the influence of polymer composition on the UV response of C5-BTBT blended with a dielectric polymer, we evaluated transfer characteristics of polymer+C5-BTBT OTF-PTs, at V_{SD}= -60 V, in dark and under UV light. Fig. 4.5 represents typical p-channel I_D-V_G curves (forward and reverse) for the studied phototransistors, in the dark (dashed curves) and under the UV illumination (solid curves). The applied V_{SD} corresponds to the electric field of 7.5x10^3 Vcm^{-1} (L=80 μm) and it is comparable to the electric fields reported for TIPS-pentacene, [36] pentacene/Ta_2O_5,[24] and specifically engineered inorganic phototransistors of 6x10^3-1.0x10^4 Vcm^{-1}, 1.6x10^3 Vcm^{-1} and 2.4x10^3-1.2x10^4 Vcm^{-1}, [23] respectively.

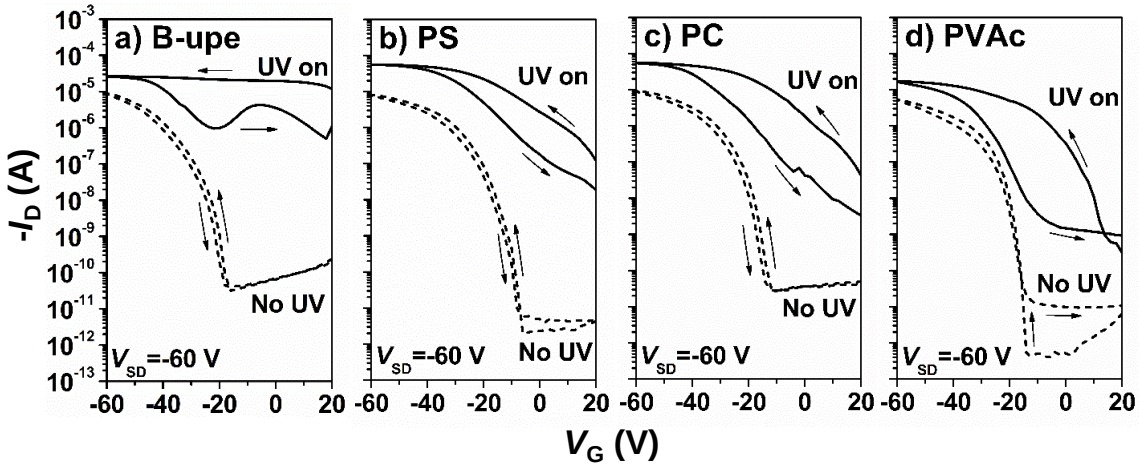

Fig. 4.5. I_D-V_G transfer-hysteresis curves for (a-d) polymer+C5-BTBT OTF-PTs acquired in dark (dashed curves) and under UV illumination (solid curves), at V_{SD}= - 60 V (L=80 μm and W=930 μm) and scan rate of 6 Vs^{-1}, showing different magnitudes of the I_D response (i.e. photocurrent-solid curves), where OTF-PTs are turned "ON" already at V_G=20 V, especially in the case of B-upe based device.

Data from the I_D-V_G curves were used to determine the threshold voltage, V_{Th} (slope of $I_D^{½}$ vs. V_G curves), turn ON voltage (V_{SO}), field-effect hole mobility (μ_{FE}), and On/Off ratio (dark) for polymer+C5-BTBT OTF-PTs. μ_{FE} in the saturation regime was calculated using the equation $\mu_{FE}=(2L/W)I_D/(C_{ox}(V_G-V_{Th})^2)$,[37] where L (cm) and W (cm) are the p-channel length and width, respectively, and C_{ox} is the capacitance per unit area of the SiO_2 dielectric layer (15 $nFcm^{-2}$). The quality of the interface in the used blends is investigated upon charge trap density ($N_{trap,dark}$), the inverse subthreshold slope (SS) and the density of deeper traps at the interface

(D_{it}). $N_{trap,dark}$ was estimated using the equation $N_{trap}=(|V_{Th}|C_{ox})/q$,[21] where q is elementary charge, while *SS* (the slope of the linear part of $\log I_D$-V_G curves at $V_G<V_{Th}$) was calculated using the equation $SS=(d\log I_D/dV_G)^{-1}$,[38] D_{it} values were calculated based on the inverse subthreshold slope and $D_{it}=[(qSS\log(e)/k_BT)-1]C_{ox}/q^2$, assuming that the density of deeper traps in a semiconductor and at polymer/semiconductor interface is independent of the energy under the same fabrication conditions and with the same semiconductor.[21,24] k_B and T are the Boltzmann constant and absolute temperature, respectively. All the above-mentioned parameters, which were estimated as the mean values from five devices of each type of OFT-PTs, are summarized in Table 4.2.

Table 4.2 Characteristic parameters quantifying the electrical properties of polymer+C5-BTBT OTF-PTs in the dark and under UV illumination, calculated from the I_D-V_G forward curves, at V_{SD}= -60 V (L=80 μm and W=930 μm).

Device	Parameter									
	μ_{FE} x10^{-2} (cm^2 V^{-1} s^{-1})		On/Off (dark) X10^5	V_{Th} (V)		V_{SO} (V)		$N_{trap,dark}$ x10^{12} (cm^{-2})	SS (V/dec) (dark)	D_{it} x10^{12} (cm^{-2} eV^{-1}) (dark)
	No UV	UV on		No UV	UV on	No UV	UV on			
B-upe	12.0±0.1	12.3±0.1	1.6±1.1	-26±2	60±13	-15±1	>20	2.4	3.4±0.1	5.3
PS	8.5±0.4	46±7	37±6	-16±2	-1±6	-5±1	>20	1.5	2.6	4.0
PC	9.1±0.3	39±3	2.6±0.6	-18±3	-2±8	-10±2	>20	1.7	2.6	4.0
PVAc	5.0±0.4	22±14	190±160	-19±3	-3±4	-13±2	17±1	1.8	1.3	2.0

In the dark, all the devices showed good characteristics for solution-processed OTFTs, i.e. negligible hysteresis, low gate (leakage) current (Fig. S4.5), high On/Off ratio, and mobility comparable with those reported for small

molecule/dielectric polymer blends used as active channel materials. [3,8] The threshold voltage strongly depends on the fabrication conditions, dielectric/polymer interface, and chemical nature of the active channel components. Since all the studied OTF-PTs were fabricated under the same conditions, we can consider only the influence of the polymer composition on $V_{Th.}$ As observed in Table 4.2, different V_{Th} and V_{SO} values of the devices could be attributed to the presence of functional groups in the polymer binders that acted as trapping sites. This can be justified by the following observations: in the tabulated array of OTF-PTs electrical properties, the lowest (more negative) V_{Th} and V_{SO} occur in the B-upe based device, which coincides with its "heterogeneous nature" in terms of EW/ED functional groups present in the main and side chains. In contrast, the PS based device has these values closers to 0 V due to its neutral chemical nature, comprised of a neutral aliphatic backbone and dangling benzene rings. Calculated $N_{trap,dark}$, which is the number of real traps at the dielectric/channel interface, indicates the higher number of fast filling traps at the SiO_2/active channel interface occurred for the B-upe device. This causes a more negative gate voltage to be applied before a conductive channel is formed (i.e., reached threshold), and vice versa, in the case of PS based device.

Moreover, the estimated inverse subthreshold slopes (*SS*) and density of the interface traps at the deeper energy levels (D_{it}) in the bulk of the channel can be used along with the morphology investigation to explain the mechanism behind the better UV sensing properties of the B-upe based devices compared with the other three studied systems. The thin-film morphology analysis of the B-upe+C5-BTBT

blend revealed a high dispersion of C5-BTBT in B-upe, which generated a large polymer-semiconductor interface. Also, the enlarged interface means more disorder in the bulk resulting in an increased D_{it}=5.3 x10^{12} (cm^2 eV^{-1}). It caused an increase in the deeper charge trapping sites at the interface (EWG are deeper traps) responsible for the increased dissociation of photo-excitons and the trapping of resulting photoelectrons. Trapped electrons give rise to mobile photo-holes and increase the photocurrent in the subthreshold region. This is easier to understand when we discuss the transfer characteristics under the UV illumination and estimate parameters that characterize phototransistors.

Like the output characteristics, UV light modulated the I_D, $V_{SO,}$ and V_{Th} (Table 4.2), in the subthreshold region where the devices would normally be in their OFF state in dark conditions. The UV light (or “photo-gate”) strongly affected V_{Th} and V_{SO}, making the phototransistors already in their ON state at a positive gate voltage of 20 V. V_{Th} and V_{SO} shifts, under the certain power of the UV light, shown in Table 4.2, are caused by the photovoltaic effect due to the photo-generated free electrons trapped in the bulk of the channel and under the source electrode, thus, lowering the energy barrier of the efficient charge carrier injection.

We estimated parameters that quantify the performance of phototransistors, using the data extracted from the transfer curves under UV light (Fig. 4.5, solid curves). The magnitude of the UV response and how much photocurrent (I_{phc}) is generated per power of the UV light, are evaluated in the subthreshold region (V_G at 20 V and 0 V) by photosensitivity (I_{phc}/I_D) and responsivity (R) values, respectively. Electrical contributions to the charge carrier generation are neglected

at V_G=0 V. *R* values are calculated using $R=(I_{phc}-I_D)/(PLW)$, [22] where P is the power of the incident UV light (3 mWcm^{-2}) and *L*x*W* is the effective area of the transistor under UV illumination. The charge carrier density generated by UV light, responsible for the increase in I_{phc} and the shift of V_{Th} is expressed as the trap density, ΔN_{trap}, using the equation $\Delta N_{trap}=\Delta V_{Th}C_{ox}/q$, [24] where q, C_{ox}, and ΔV_{Th} are ab elementary charge, capacitance of the dielectric layer and threshold voltage shift, respectively. All the parameters are summarized in Table 4.3, as the mean values based on five devices of each type of polymer+C5-BTBT OTF-PTs.

Table 4.3 Characteristic parameters for polymer+C5-BTBT phototransistors under UV light illumination (λ=365 nm and P=3 mWcm^{-2}) extracted from the I_D-V_G and I_D-time curves

Device	Parameter						
	ΔN_{trap} x10^{12} (cm^{-2})	I_{phc}/I_D at V_G (V)		R (AW^{-1}) at V_G (V)		Times (s)*	
		20	0 (x10^5)	20 V	0 V	Rise, τ_{r1}/τ_2 (s)	Decay, τ_{d1}/τ_{d2} (s)
B-up*	8.0	4.1±1.4x10^4	2.9±1.5	4.6±0.7	9.2±0.5	1.13±0.68/ 11.41±6.56	4.04±0.33/ 31.75±4.52
PS	1.4	1.4±1.3x10^4	6.2±4.5	0	0.7±0.4	17.7/3.3x10^3	3.8/35.1
PC	1.5	4.2±4.0x10^2	0.31±0.21	0	0.5±0.3	169/1.7x10^3	4.1/32.4
PVAc	2.0	49±44	2.7±2.5	0	0.1±0.1	217/5.41x10^3	5.0/41.9

*For B-upe+C5-BTBT PT reported are mean times with standard deviation (coefficients of estimation R^2 for the rise and decay times are 0.9700-0.9921 and 0.9921-0.9997, respectively) while for the other devices reported are the fastest rise and corresponding decay (relaxation) times.

Since the magnitude of the shift of V_{Th} is directly proportional to the density of photogenerated charge carriers that can be trapped per unit area of the dielectric/semiconductor interface, ΔN_{trap} represents a very useful parameter to explain the UV response in the studied devices. [39] The highest ΔN_{trap} among the

studied phototransistors is estimated for the B-upe based device (ΔN_{trap}=8.0x10^{12} cm^{-2} based on the mean value of the threshold voltage shift). This highest ΔN_{trap} corresponds to the highest shift of V_{Th} and the highest photocurrent rise at the initial 20 V and 0 V V_G, in the subthreshold region. In contrast, the existence of deeper traps associated with the density of interface traps in the bulk, determined for polymer+C5-BTBT devices, induced a large lower back sweep current hysteresis under the UV illumination (Fig. 4.5, solid-reverse curves). This is a consequence of slower recombination of photo-generated charge carriers (electrons trapped in deeper traps and mobile holes), in back gate voltage sweep (-60-20 V), i.e., charge carrier trapping near the active channel.

Although all the phototransistors showed UV sensing properties, different magnitudes of the drain current change expressed as I_{phc}/I_D ratios are observed (Table 4.3). At the highest positive V_G (20 V, beginning of the measurement), the B-upe and PS based devices had the highest photosensitivities. Photosensitivity of the PS based device is somewhat higher than in B-upe based device most likely due to the maintained low leakage (gate) currents (I_G) and lower dark I_D in the subthreshold region.

The photoresponsivity (R) values, estimated for the phototransistors, reflect a superior conversion of the UV light power into the photocurrent in the B-upe based OTF-PT, as compared with the other three devices. The R for the B-upe OTF-PT is driven by the light in the subthreshold region where electrical contributions to the charge carrier generation are negligible (Fig. 4.6b). It is clearly visible that R at V_G=0 (max 9.7 AW^{-1}) is higher than R at -60 V, which confirms the contribution of

photo-charge carriers to the increased photocurrent, in the subthreshold region. Additionally, the I_{phc}/I_D vs. V_G curves displayed in Fig. 4.6(a) confirms the photocurrent contribution to the increased drain current followed by a dramatic drop of the photosensitivity after the channel reached a threshold, which indicates that electrical contribution to the charge carrier generation is dominant after a threshold is reached. After then, the V_G no longer affects the photosensitivity. Hence, both I_{phc}/I_D and R are dependent on the V_G and the constant UV light power, in the subthreshold region. This is important to acknowledge as we want to use our device as a UV sensor or non-volatile memory that operates in the subthreshold region fully controlled by UV light at a constant V_G and V_{SD}. The following section is devoted to the UV sensing properties of the B-upe+C5-BTBT OTF-PT contrasted with the PS, PC, and PVAc based OTF-PTs.

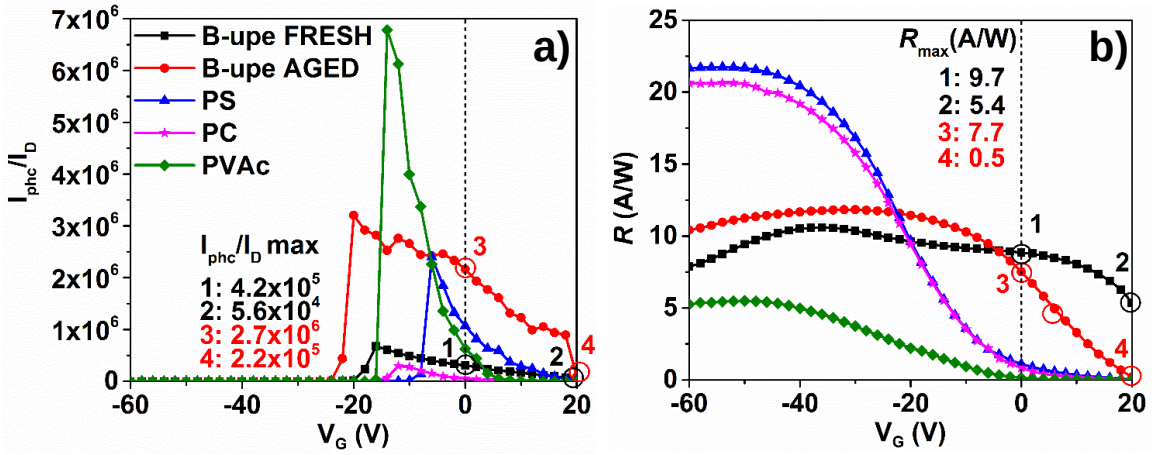

Fig. 4.6. I_{phc}/I_D (a) and R (b) dependence on the gate voltage for polymer+C5-BTBT devices under the constant UV illumination power (3 mW cm^{-2}, λ=365 nm), in the subthreshold region at V_{SD}=-60 V; the maximum values of both parameters at two characteristic V_G (20 V and 0 V) are depicted in the corresponding plot; legend in left applies to the right plot.

Switching properties. As we discussed in the section for transfer characteristics, blending two chemically incompatible materials would generate a large interface that facilitates an excessive charge trapping by functional groups in the polymer chain, resulting in an increased density of interface traps in the bulk. Therefore, the dissociation rate of the photo-excitons and the amount of the obtained free holes will be dependent on the charge trapping sites at the interface in the polymer/C5-BTBT blends characterized under the same conditions. This is most easily observed while measuring the time-dependent evolution of the mobile photo holes at the interface, responsible for the photocurrent increase at V_G=-5 V and V_{SD}=-60 V (i.e. immediate response or switching and I_{phc} saturation) (Fig. 4.7). The different

time-dependent photocurrent responses provide more insight into the interface charge trapping by functional groups on the UV response of C5-BTBT small molecule semiconductor and trapping/detrapping kinetics.

Likewise, the transfer characteristics for the polymer+C5-BTBT OTF-PTs under UV light and the different I_{phc} time responses can be directly related to the chemical composition of the used polymer binder and blend morphology, which enabled efficient charge trapping at the interface in the bulk. The B-upe based devices have a sharp, more than six orders of magnitude, UV response followed by a complete saturation within 75 s (solid line in Fig. 4.7a). The lowest UV response is observed for the PVAc based PT, that coincides with the UV response of the PMMA based devices reported previously.[29,31] In that light, the B-upe based device had the highest response among the studied OTF-PTs, similar to the L-upe based OTF-PT also reported by our group.[31] The systems can be grouped into PVAc and PMMA, and B-upe and L-upe OTF-PTs, with each group having similar polymer chain compositions, and thin-film morphologies, thus similar UV responses. Therefore, our approach, which relies on polymer chain composition and self-induced morphology to modulate UV response in a UV-responsive small molecule semiconductor such as C5-BTBT, is justified. In other words, the results confirmed that the UV response of C5-BTBT can be controlled and modulated by the simple use of a dielectric polymer binder with a high content of EWGs, in a two-component blend. Due to the absence of absorption in the visible range (Fig. 4.1c), the device is blind to the visible light. No response of the drain current was observed upon irradiation with different visible light (Fig. S4.6).

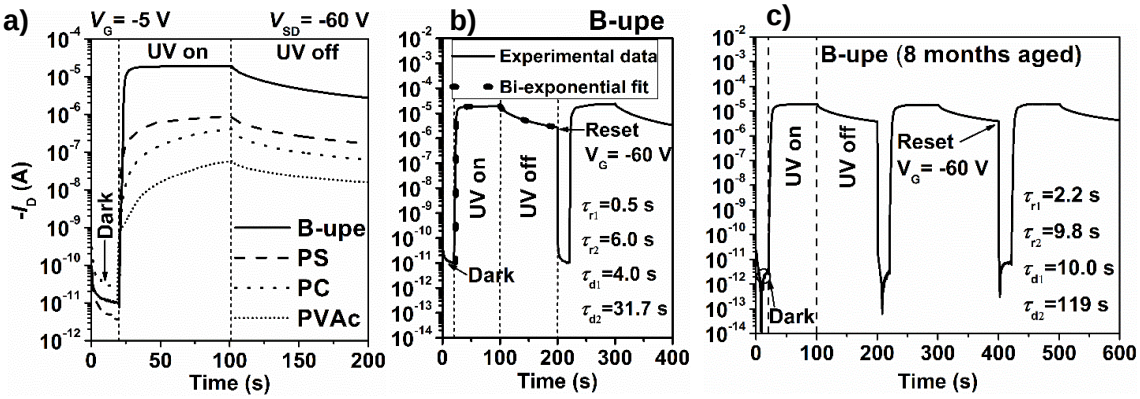

Fig. 4.7. (a) - Overlay of the UV responses for polymer+C5-BTBT OTF-PTs under UV illumination, showing different magnitudes of the I_{phc} rise and saturation, and relaxation (decay) when UV light is OFF; Switching characteristics of (b) B-upe based OTF-PTs upon two cycles and a short reset V_G= -60 V (~6 s), applied after the first cycle (at ~200 s) turned the device completely into a lower current state (OFF-state); dotted curve in the first cycle is bi-exponential fitting (the fastest initial rise and corresponding decay times are included in the plot); and (c) switching properties and UV response of the B-upe+C5-BTBT OTF-PT after 8 months of exposure to ambient conditions with the reported fastest initial response and decay times, showing its excellent stability in the environmental conditions; all the measurements were carried out at V_{SD}= -60 V and V_G= -5.

All the devices exhibited ability of returning to the low drain current state ("OFF-state") with reproducible properties (2nd cycle), upon a short gate voltage of -60 V. This enables a dual or "UV light-Gate voltage (optical-electrical)" control over the work operation of the best performing B-upe device, in the two displayed cycles

within the cycling sequences (1^{st}(2^{nd}) cycle): *DARK@0s(~206s)»UVon@25s(225s)» UVoff@100s(300s)-RESET@200s(400s)*. The cycling properties of the control OTF-PTs are given in Fig. S4.7. The mechanism behind the device reset to the low drain current state lies in the accelerated (forced) recombination of the excited holes and trapped electrons induced by the high polarization voltage (-60 V).

The I_D-time curves of the polymer+C5-BTBT OTF-PTs are characterized by two major parts: rise (fast and slow or saturation), and decay (fast and slow relaxation). Applying bi-exponential equations to fit the photocurrent rise and decay I_D vs time experimental data, we estimated fast/slow rise and fast/slow decay times of the UV responses. We used the equation $I_{phc}(t) = I_{D,0} + A_1\left(1 - e^{-t/\tau_{r1}}\right) + A_2\left(1 - e^{-t/\tau_{r2}}\right)$ for rise time and the equation $I_D(t) = I_{D,0} + A_3 e^{-t/t_{d1}} + A_4 e^{-t/t_{d2}}$ for decay time estimation,[23] where I_{phc}, I_D and $I_{D,0}$ are the photocurrent, at time t, current with UV off, and dark drain current at the beginning of measurements, and $A_{1\text{-}4}$ are the constants, while τ_{r1}, τ_{r2} and τ_{d1}, τ_{d2} are the times of the fast/slow I_{phc} rise, and the fast/slow decay of I_D, respectively. The fast components in both rise and decay photocurrent equations (τ_{r1} and τ_{d1}) could be ascribed to the instantaneous generation/recombination of the light induced charge carriers in the channel; the slow components (τ_{r2} and τ_{d2}) can be attributed to the polarization effects at the interface in the bulk of the channel that influence the generation/recombination of the light induced charge carriers due to the built-in electric field.

A representative bi-exponential fit for the B-upe device experimental data is presented with the fastest rise and corresponding decay times (Fig. 4.7b, dotted curve). The mean rise/decay times for the device responses, when exposed to the UV light, are based on the means of 5 devices and are summarized in Table 4.3. The estimated rise times indicate superior UV sensing properties of the B-upe based OTF-PTs (τ_{r1}/τ_{r2}=0.5/6.0 s; R^2= 0.9806), not only compared with the other devices studied in this work but also with the organic/inorganic UV sensors recently reported in literature. More interestingly, the devices based on B-upe polymer binder can be used as a non-volatile memory due to long relaxation times of the high drain current state when the UV light is turned off. The slowest relaxation times obtained for the B-upe based device are τ_{d1}/τ_{d2}=4.3/36.7 s (R^2= 0.9949), confirming the existence of the deep traps responsible for slow spontaneous recombination of the charge carriers. These times are similar to the decay times of the other studied OTF-PTs, reflecting the contribution of C5-BTBT itself to the carrier trapping/detrapping.

4.2.3 Environment stability of B-upe based phototransistor

The environment stability of active channel is a very important parameter that determines the performance of OTF-PTs. This is especially true in the case of polyesters used as binders, which are prone to hydrological decomposition. It is already indicated by the *I*-*V* and I_D-V_{SD} measurements that B-upe+C5-BTBT devices do not exhibit much deterioration. We re-evaluated I_D-time (switching) (Fig.

4.7c) and the transfer (Fig. 4.8) characteristics (Fig. 4.7c) of the B-upe based OTF-PTs after 8 months. The corresponding parameters extracted from the transfer and switching data are summarized in Table 4.4. After 8 months, the B-upe+C5-BTBT OTF-PT still operates as a typical p-type device with low leakage gate currents in the dark and under the UV light. Additionally, the devices retained hysteresis-free (dashed curve) operation in the dark and similar hysteretic behavior under the UV light. It is also noticeable that the hysteresis loop (solid curve) is smaller than that of the fresh device, with the same returning point (reverse curve) as the origin of the forward curve.

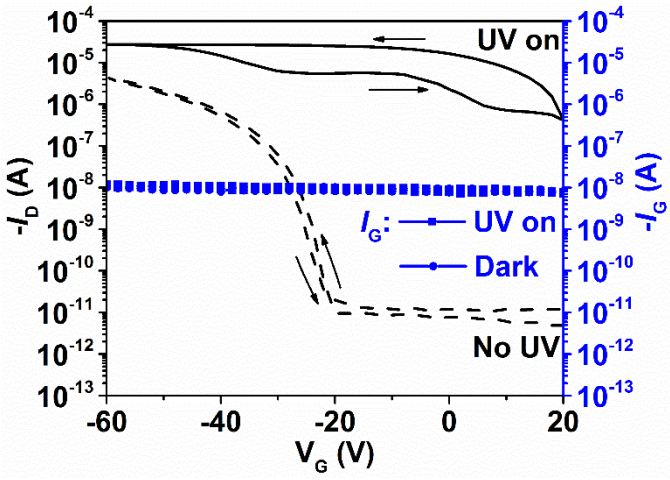

Fig. 4.8. Transfer characteristics of B-upe+C5-BTBT phototransistors with hysteretic properties and displayed gate leakage currents, in dark and under UV illumination, after 8 months of aging.

From the parameters given in Table 4.4, one can see that some electrical properties of the B-upe based OTF-PT in dark and under UV light were affected after 8 months of storage under ambient conditions. These changes are most obvious under the UV light, while those in the dark are within statistical errors. For instance, the change of V_{Th}, as the parameter indicating the channel instability and deterioration, in the dark for the aged device, is not observed compared with the fresh counterpart. Additionally, the estimated $N_{trap,dark}$ (cm^{-2}) remained the same, reflecting an unchanged amount of trap density at SiO_2/channel interface, also responsible for the stable V_{Th} under the same measurement and fabrication conditions, i.e. maintained the same quality of SiO_2 dielectric/active channel interface.

Although the V_{Th} under UV light is shifted toward less positive gate voltages (24 V for aged device vs 60 V for the fresh device), the B-upe+C5-BTBT OTF-PT showed self-induced improvements of the photo-electrical properties. Under the UV light, the increased field-effect mobility (saturation) reached the maximum of 0.508 $cm^2\ V^{-1}\ s^{-1}$ compared with 0.123 $cm^2\ V^{-1}\ s^{-1}$ of the fresh B-upe based OTF-PT. The I_{phc}/I_D ratio of the aged device is significantly increased (max $2.7x10^5$) at the V_G=0 V compared with the fresh one (max $2.7x10^5$), while the responsivity is somewhat reduced at the observed gate voltage (aged 7.7 AW^{-1} vs fresh 9.7 AW^{-1}).

Table 4.4 Electrical properties of B-upe+C5-BTBT extracted from I_D-V_G forward curves, at V_{SD}= -60 V (L=80 μm and W=930 μm), in the dark and under UV illumination, after 8 months of aging.

Parameter	Light condition		Parameter	UV ON at V_G (V)	
	UV off	UV on		20	0
μ_{FE} x10^{-2} (cm^2 V^{-1} s^{-1})	4.9±0.2	41.1±8.2	ΔN_{trap} (cm^{-2})	4.8 x10^{12}	
On/Off (dark)	4.8±0.3x10^5	n/a	$I_{phc}/I_{D,max}$	1.0x10^5±6.9x10^4	2.2x10^6±4.2x10^5
V_{Th} (V)	-27±2	24±0.1	R (AW^{-1})	0.2±0.2	7.5±0.1
V_{SO} (V)	-19±2	>20	Rise times (s), τ_{r1}/τ_{r2}	2.65±0.49/12.23±3.93	
$N_{trap,dark}$ (cm^{-2})	2.5x10^{12}	n/a	R^2 (fitting), (τ_{r1}/τ_{r2})	0.9778-0.9942	
SS (V/dec)	1.9±0.1	n/d	Decay times (s), τ_{d1}/τ_{d2}	10.99±0.85/128.86±13.28	
D_{it} x10^{12} (cm^{-2} eV^{-1})	2.9	n/d	R^2 (fitting), (τ_{d1}/τ_{d2})	0.9973-0.9986	

The re-evaluated switching characteristics of the B-upe based phototransistors indicate their excellent stability and reproducible characteristics under the UV light. We subjected the B-upe device to multiple cycles of the sequence *Dark-UV rise-Relaxation (UV off)-Reset,* which allowed estimation of the rise/decay times (I_D-time curves, Fig. 4.7c). Both sets of the response times given in Table 4.4 are longer compared with times for the freshly prepared devices but are still comparable to the response times of the reported devices (Table 4.5). Nonetheless, this increase of the decay times can be useful in terms of the memory properties, meaning that after 8 months the devices can retain the high current

state longer (Fig. 4.7c), in spite of the doubled mean fast rise time (τ_{r1}) or UV response (fastest response τ_{r1}=2.18 s).

Finally, we compared the performance of B-upe+C5-BTBT OTF-PT with the PTs recently reported in the literature (Table 4.5). Our device is comparable with the OTF-PTs and some inorganic PTs reported in the given references, demonstrating the feasibility of our approach for the simple fabrication of OTF-PTs with highly improved UV sensing/memory properties.

Table 4.5. Comparison of the B-upe based OTF-PT with the PTs recently reported in the literature.

Device [ref]	Method*	$\mu_{FE,\,max}$ ($cm^2V^{-1}s^{-1}$) Dark/Light	$I_{phc}/I_{D,\,max}$ (V_G=0 V)	$R_{,max}$ (AW^{-1})	τ_{r1}/τ_{r2} (s)	τ_{d1}/t_{d2} (s)	UV light density ($mW\ cm^{-2}$)
B-upe+C5-BTBT, fresh (this work)	SB	0.120/0.133	$>10^5$	9.7	0.5/6	4/32	3
B-upe+C5-BTBT, 8 m aged (this work)	SB	0.052/0.508	$>10^6$	7.7	2.2/10	10/119	3
L-upe+C5-BTBT [31]	SB	0.10/0.13	$>10^6$	11.1	1.8	49/813	3
p-DR1+C5-BTBT[29]	SB	0.129/0.778	nd	nd	13/112	110/1647	4
Spiro-DPO[40]	TE	$3.3x10^{-7}$	$<10^3$	6.5	7.6	10.1/73.2	~0.01
Pentacene [41]	TE	0.01	$<10^3$	0.015	0.1	nd	7
P3HT:TiO_2 [42]	SB	nd	$~10^3$	nd	~0.2	nd	1.5
ZnO nanorods/nanotetrapods [43]	TE	nd	$<10^3$	0.63	4.8	na	1.5
ZnO nanotetrapod networks [23]	TE	nd	$<10^3$	nd	0.068	0.032/0.2	45

*SB-solution blending, TE-thermal evaporation.

§ 4.3 Conclusions

This work investigated in detail the effects of polymer binders on the drain current modulation or UV response in the subthreshold region, of a UV-responsive

semiconductor, without the aid of commonly used photochromic molecules. We engineered an active channel material for OTF-PTs, utilizing a binary blend composed of a small molecule UV-A responsive semiconductor C5-BTBT and a branched unsaturated polyester dielectric polymer (B-upe). We contrasted the optoelectrical characteristics of B-upe based OTF-PTs with those based on commonly used dielectric polymers, namely, PS, PC, and PVAc. The results obtained confirmed that the type of polymer binder significantly affected the UV response of the small molecule semiconductor C5-BTBT due to different self-induced thin-film morphologies and chemical composition of the polymer chain, i.e. the existence of EW/ED groups. The enhancement is indicated as a sharp photocurrent increase of more than six orders of magnitude in the subthreshold region at V_G=-5 V and V_{SD}=-60 V. The fastest response (initial rise) obtained followed by a fast current saturation for the B-upe based OTF-PTs were 0.5 s and 6.0 s, respectively, while maintaining a high current state (decay) after removal of the UV light. We attributed this to a self-induced thin-film morphology, i.e. a lateral phase separation characterized by highly dispersed C5-BTBT phase into B-upe binder. This enabled a large C5-BTBT/polymer interface that facilitated a strong influence of the EW/ED groups, at the interface, on photo-excitons separation, trapping/recombination, and photocurrent generation in the subthreshold region. Therefore, this concept offers a simple and efficient fabrication of the highly UV-responsive OTF-PTs, i.e. UV sensors and non-volatile memory with reliable properties even after eight months of aging under the ambient conditions.

§ 4.4 References

[1] A. Tsumura, H. Koezuka, T. Ando, *Appl. Phys. Lett.* **1986**, *49*, 1210.

[2] K. Hagen, *Organic Electronics: Materials, Manufacturing, and Applications*; Hagen, K., Ed.; John Wiley & Sons, 2066.

[3] J. Mei, Y. Diao, A. L. Appleton, L. Fang, Z. Bao, *J. Am. Chem. Soc.* **2013**, *135*, 6724.

[4] B. D. Naab, S. Himmelberger, Y. Diao, K. Vandewal, P. Wei, B. Lussem, A. Salleo, Z. Bao, *Adv. Mater.* **2013**, *25*, 4663.

[5] J. Li, Y. Zhao, H. S. Tan, Y. Guo, C.-A. Di, G. Yu, Y. Liu, M. Lin, S. H. Lim, Y. Zhou, H. Su, B. S. Ong, *Sci. Rep.* **2012**, *2*, 1.

[6] H. Minemawari, T. Yamada, H. Matsui, J. Tsutsumi, S. Haas, R. Chiba, R. Kumai, T. Hasegawa, *Nature* **2011**, *475*, 364.

[7] Y. Yuan, G. Giri, A. L. Ayzner, A. P. Zoombelt, S. C. B. Mannsfeld, J. Chen, D. Nordlund, M. F. Toney, J. Huang, Z. Bao, *Nat. Commun.* **2014**, *5*, 3005.

[8] H. Sirringhaus, *Adv. Mater.* **2014**, *26*, 1319.

[9] P. S. K. Amegadze, Y.-Y. Noh, *J. Inf. Disp.* **2014**, *15*, 213.

[10] H. Yu, Z. Bao, J. H. Oh, *Adv. Funct. Mater.* **2013**, *23*, 629.

[11] S. Dutta, K. S. Narayan, *Adv. Mater.* **2004**, *16*, 2151.

[12] K. S. Narayan, N. Kumar, *Appl. Phys. Lett.* **2001**, *79*, 1891.

[13] M. Debucquoy, S. Verlaak, S. Steudel, K. Myny, J. Genoe, P. Heremans, *Appl. Phys. Lett.* **2007**, *91*, 103508.

[14] Y. Y. Noh, D. Y. Kim, K. Yase, *J. Appl. Phys.* **2005**, *98*, 7450.

[15] Y. Ishiguro, R. Hayakawa, T. Chikyow, Y. Wakayama, *J. Mater. Chem. C* **2013**, *1*, 3012.

[16] H. Zhang, X. Guo, J. Hui, S. Hu, W. Xu, D. Zhu, *Nano Lett.* **2011**, *11*, 4939.

[17] N. Crivillers, E. Orgiu, F. Reinders, M. Mayor, P. Samorì, *Adv. Mater.* **2011**, *23*, 1447.

[18] Q. Shen, L. Wang, S. Liu, Y. Cao, L. Gan, X. Guo, M. L. Steigerwald, Z. Shuai, Z. Liu, C. Nuckolls, *Adv. Mater.* **2010**, *22*, 3282.

[19] P. Lutsyk, K. Janus, J. Sworakowski, G. Generali, R. Capelli, M. Muccini, *J. Phys. Chem. C* **2011**, *115*, 3106.

[20] F. Ercole, T. P. Davis, R. A. Evans, *Polym. Chem.* **2010**, *1*, 37.

[21] J. Smith, R. Hamilton, Y. Qi, A. Kahn, D. D. C. Bradley, M. Heeney, I. McCulloch, T. D. Anthopoulos, *Adv. Funct. Mater.* **2010**, *20*, 2330.

[22] K.-J. Baeg, M. Binda, D. Natali, M. Caironi, Y.-Y. Noh, *Adv. Mater.* **2013**, *25*, 4267.

[23] D. Gedamu, I. Paulowicz, S. Kaps, O. Lupan, S. Wille, G. Haidarschin, Y. K. Mishra, R. Adelung, *Adv. Mater.* **2014**, *26*, 1541.

[24] X. Liu, G. Dong, L. Duan, L. Wang, Y. Qiu, *J. Mater. Chem.* **2012**, *22*, 11836.

[25] B. Yao, W. Lv, D. Chen, G. Fan, M. Zhou, Y. Peng, *Appl. Phys. Lett.* **2012**, *101*, 163301.

[26] B. Gunduz, F. Yakuphanoglu, *Sensors Actuators, A Phys.* **2012**, *178*, 141.

[27] C. W. Tseng, D. C. Huang, Y. T. Tao, *ACS Appl. Mater. Interfaces* **2012**, *4*, 5483.

[28] H. Karimi-Alavijeh, F. Panahi, A. Gharavi, *J. Appl. Phys.* **2014**, *115*, 93706.

[29] C. S. Smithson, Y. Wu, T. Wigglesworth, S. Zhu, *Adv. Mater.* **2014**.

[30] C. S. Smithson, D. Ljubic, Y. Wu, S. Zhu, *J. Mater. Chem. C* **2015**.

[31] D. Ljubic, C. S. Smithson, Y. Wu, S. Zhu, *Adv. Electron. Mater.* **2015**, *1*, 1500119.

[32] H. Ebata, T. Izawa, E. Miyazaki, K. Takimiya, M. Ikeda, H. Kuwabara, T. Yui, *J. Am. Chem. Soc.* **2007**, *129*, 15732.

[33] M. Saito, I. Osaka, E. Miyazaki, K. Takimiya, H. Kuwabara, M. Ikeda, *Tetrahedron Lett.* **2011**, *52*, 285.

[34] J. Smith, R. Hamilton, I. McCulloch, N. Stingelin-Stutzmann, M. Heeney, D. D. C. Bradley, T. D. Anthopoulos, *J. Mater. Chem.* **2010**, *20*, 2562.

[35] D. K. Hwang, C. Fuentes-Hernandez, J. Kim, W. J. Potscavage, S.-J. Kim, B. Kippelen, *Adv. Mater.* **2011**, *23*, 1293.

[36] F. Yakuphanoglu, B. Gunduz, *Synth. Met.* **2012**, *162*, 1210.

[37] C. D. Dimitrakopoulos, P. R. L. Malenfant, *Adv. Mater.* **2002**, *14*, 99.

[38] A. Takshi, J. D. Madden, *J. Comput. Electron.* **2010**, *10*, 154.

[39] P. Heremans, G. H. Gelinck, R. Müller, K.-J. Baeg, D.-Y. Kim, Y.-Y. Noh, *Chem. Mater.* **2011**, *23*, 341.

[40] T. P. I. Saragi, R. Pudzich, T. Fuhrmann-Lieker, J. Salbeck, *Appl. Phys. Lett.* **2007**, *90*, 143514.

[41] B. Lucas, a. El Amrani, M. Chakaroun, B. Ratier, R. Antony, a. Moliton, *Thin Solid Films* **2009**, *517*, 6280.

[42] S. M. Mok, F. Yan, H. L. W. Chan, *Appl. Phys. Lett.* **2008**, *93*, 23310.

[43] N. K. Hassan, M. R. Hashim, N. K. Allam, *Sensors Actuators A Phys.* **2013**,

192, 124.

§ 4.5 Supporting information

4.5.1 Experimental [1]

OTF-PTs fabrication. The OTF-PT fabrication was performed in ambient conditions under yellow light unless noted. Si wafers were thoroughly washed with 2-propanol, air dried, and plasma cleaned for 2 min in a PDC-32G plasma cleaner (Harrick Plasma, USA). Clean Si wafers were soaked in deionized water for 5 min, rinsed with 2-propanol, air dried, followed by immersion in an HMDS/toluene solution at 60°C for 30 min. HDMS formed a self-assembled monolayer on the the SiO_2 dielectric surface of the wafer helping ensure adhesion of an active layer. Surface modified Si wafers were rinsed successively with toluene and isopropanol and dried by air and in a vacuum oven at room temperature for 30 min. The prepared Polymer+C5-BTBT solutions were then spin-coated (spin coater SCS P-6700, Sitek Process Solutions, Inc., CA, USA; conditions: 2000 rpm, ramp time 2 s and total spin time 120 s) onto the surface modified Si wafers yielding 250-350 nm thick films. The spin-coated substrates were placed in a vacuum oven at room temperature for 30 min to remove residual solvent. The electron beam evaporation (Edwards A306 Belljar Evaporator, Boc Edwards, West Sussex, UK) using a shadow mask was employed for the 60 nm thick Au source-drain electrodes

deposition. Electrode length (an active channel width) and electrodes gap (an active channel length) were 930±10 μm and 80±5 μm, respectively.

***Characterization*.** The thicknesses of polymer+C5-BTBT and C5-BTBT thin films spin-coated on the glass plates were measured using surface profiler DektakXT (Bruker, USA). UV-Vis absorption spectra were recorded from 300-800 nm in Nicolete UV-Vis-NIR spectrophotometer (Cary 5000, Varian, USA) on the same thin films on the glass used for the thickness measurements in the range 300-800 nm. Thin-film morphologies of the devices were examined using digital optical microscope Keyence VHX-2000 (Keyence, Canada) and MFP-3D atomic force microscope (Asylum Research and Oxford Instrument Company, Santa Barbara, CA, USA) in a non-contact mode using a silicone tip (OMCL- AC240TS, Olympus Corp., Japan) with nominal spring constant 1.8 N/m and frequency 70 Hz), under ambient conditions. AFM data were collected and analyzed using the Asylum Research AFM software build on Igor Pro (Wavemetrics, Portland, OR, USA). C5-BTBT structure in polymer binders was investigated by powder out-of-plane X-ray diffraction (XRD) using Rigaku Miniflex X-Ray diffractometer (TX, USA) fitted with a Cu X-ray tube operated at 30kV. Electrical characteristics of all devices were measured in ambient conditions (humidity 30% RH and 23°C), under the yellow light on a 4200-SCS Parameter Analyzer (Keithley Instruments, USA). UV lamp (Black-Ray, UVP B 100 AP, long wave UV lamp, 100 W, λ=365 nm, Entela, USA), UV-A light intensity of 3 $mWcm^{-2}$ at ~25 cm distance from the sample was used for the irradiation of devices during electrical characteristics measurements, illuminating the entire surface of OTFTs.

4.5.2 Results and discussion

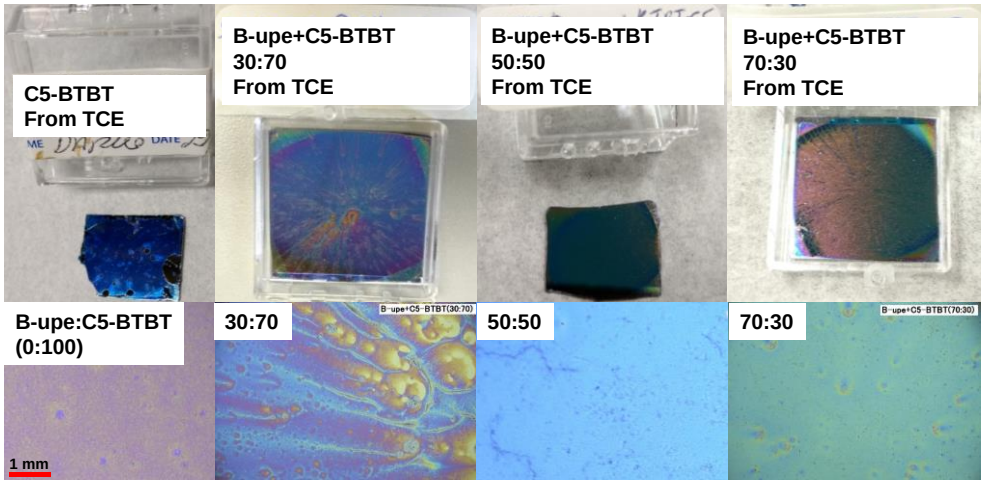

Fig. S4.1. Upper raw - Digital photography images and lower raw - optical micrographs of C5-BTBT thin-film (no polymer present, top and bottom left corner) and B-upe+C5-BTBT PTs on a silicon wafer with different B-upe:C5-BTBT ratios.

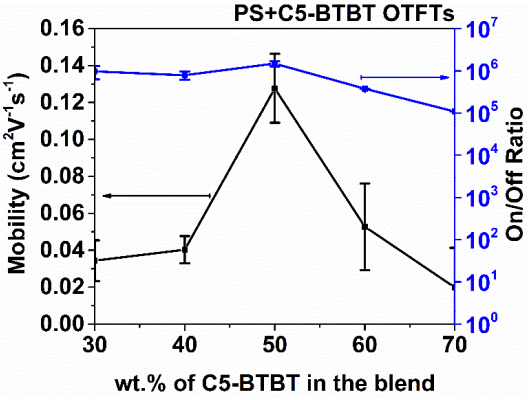

Fig. S4.2. Charge carrier mobility and on/off ratio dependence on C5-BTBT content (wt.%) in PS binder, including standard deviations as error bars; extracted from the transfer curves in the dark, V_G sweep 20-(-60) V and V_{SD}= -60 V (*L*=80 μm and W=930 μm).

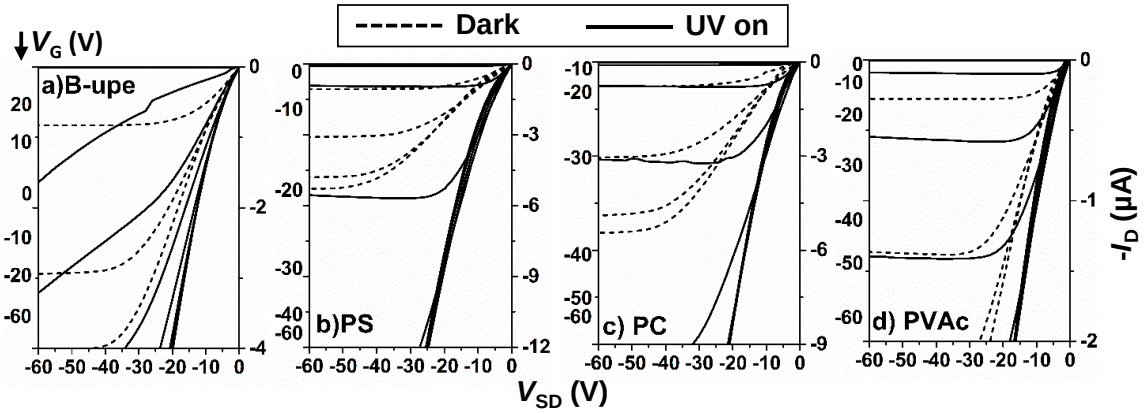

Fig. S4.3. Magnification of the initial part of the I_D vs. V_{SD} curves (output characteristics) displayed in Fig. 4, showing an ohmic contact at the gold electrode/active channel interface responsible for the efficient charge carrier injection in the studied Polymer+C5-BTBT devices under UC light and in dark; I_D scale is set to be approx. 1/3 of the full scale for the certain device in Fig. 4.4.

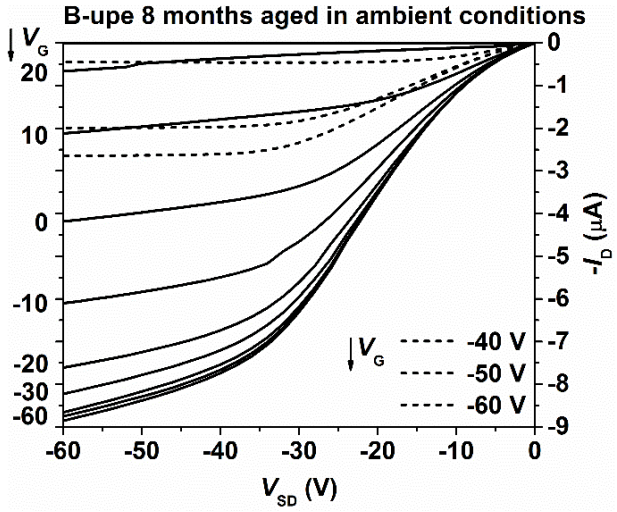

Fig. S4.4. Output characteristics of the B-upe device measured after 8 months of aging under ambient conditions.

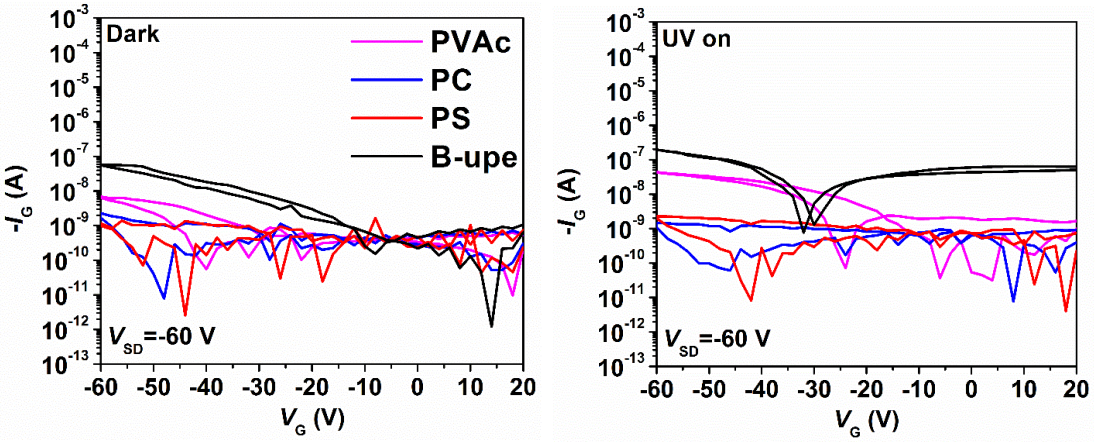

Fig. S4.5. Gate current (I_G) against V_G in dark (left) and under UV illumination (right) for polymer+C5-BTBT OTF-PTs; a legend in the left plot is identical for the right plot.

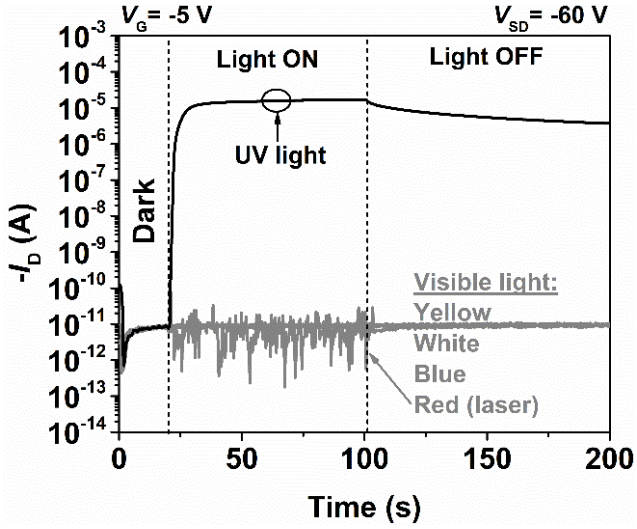

Fig. S4.6. The response to the drain current under the irradiation of different sources of visible light, compared with the response of the drain current to UV light used in this work (P=3 mWcm^{-2}), at V_G= -5 V and V_{SD}= -60 V.

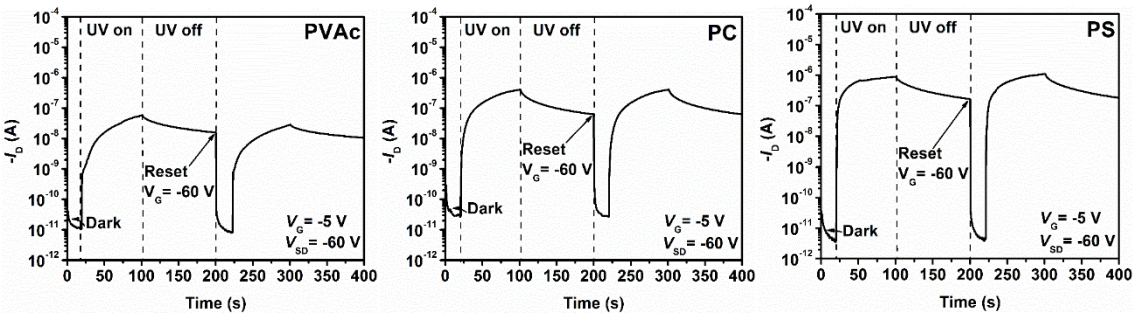

Fig. S4.7. Switching characteristics (I_D-Time) of PVAc, PC and PS based OTF-PTs under UV illumination upon two cycles at V_G= -5 V and V_{SD}= -60 V, showing their sensing properties and ability to be turned into a low current state after a reset gate voltage of -60 V is applied.

4.5.3 References

[1] D. Ljubic, C. S. Smithson, Y. Wu, S. Zhu, *Adv. Electron. Mater.* **2015**, *1*, 1500119.

5 Binary Blends of Polyimide and 2,7-dipentyl[1]benzothieno[3,2-b][1]benzothiophene for High-Performance Solution-Processed Organic Phototransistors

In this chapter, the design and synthesis of new polyimide are presented. The soluble a strong electron withdrawing polyimide was used in binary blends as channel materials to enhance the performance of organic phototransistors via strong electron trapping at the interface. A UV responsive small molecule semiconductor 2,7-dipentyl[1]benzothieno[3,2-b][1]benzothiophene was used as the second component. This chapter is based on the manuscript entitled “Binary Blends of Polyimide and Benzothienobenzothiophene for High-Performance

Solution-Processed Organic Phototransistors", D. Ljubic, W. Liu, C. E. González-Espinoza, N-X. Hu., Y. Wu, S. Zhu, submitted to Advanced Electronic Materials, Status: Under review).

Author contributions

Darko Ljubic designed and conducted the experiments on organic phototransistors, synthesized the polyimide, and wrote the first draft of the manuscript under the guidance of Dr. Shiping and Dr. Yiliang Wu. Dr. Weifeng Liu designed the polyimide, provided valuable inputs for the manuscript, and first revision of the manuscript, Cristina E. González-Espinoza performed the density functional theory calculations and knowledge base in quantum chemistry and revised the manuscript. Dr. Nan-Xing Hu provided valuable advice while writing the manuscript and revised the manuscript. The final revision was provided by Dr. Wu and Dr. Zhu.

§ 5.1 Abstract

We report on the design and synthesis of a strong electron withdrawing, soluble, and dielectric polyimide (PI) used in binary blends for UV responsive organic thin film phototransistors (OPTs). A new PI comprising electronegative and strong electron withdrawing monomer units, DAPS and 6FDA, was synthesized via a two-step method where lower (6400) and higher (14800) MWs were obtained. PI was solution blended with UV responsive small molecule organic semiconductor

2,7-dipentyl[1]benzothieno[3,2-b][1]benzothiophene (C5-BTBT). The effects of PI molecular weight and blend ratio on photoelectrical properties of OPTs were studied and compared with control C5-BTBT OPTs. All the effects were dependent on PI content in the blend but not on MW, which can be attributed to strong charge trapping at the interface due to the strong EW nature of PI. Only 10 wt.% of PI (PI1, MW=6400) in the blend was required to completely suppress the hysteresis under UV light and to increase the drain photocurrent of more than 6 orders of magnitude in the subthreshold region. All the blend-based OPTs showed excellent operational stability in air and high sensitivity to UV light at a low intensity of 0.12 $mWcm^{-2}$. I_{phc}/I_D and photosensitivity were 10^6 and 429 AW^{-1}, respectively, for 70:30 PI1:C5-BTBT blends. All the blend-based OPTs had fast response times of ~1 s at P_{UV} = 3 $mWcm^{-2}$ (λ=365 nm) and long decay times (UV off) of 149 s, which was 16 times faster and 2 times slower than the control C5-BTBT OPTs. Mechanisms of the decreased response time and increased retention time were explained by means of the density functional theory calculations. This work demonstrates that blending of the PI with C5-BTBT represents an excellent approach realizing high-performance OPTs for photo memory devices. This is the first report on this type of PI used to modulate the photoelectrical characteristics of solution processed OPTs.

§ 5.2 Introduction

Organic thin film transistors (OTFTs) have reached the level of commercialization for flexible electronics and stretchable devices, RF-ID tags, smart electronics and OLED displays after more than two decades of intensive research. [1,2] Their performance significantly exceeded that of a-Si:H based field-effect transistors (FETs). The progressive development of OTFTs was enabled by the wide spectrum of organic compounds that can be selected in design, synthesis, and engineering of materials for targeted performance and application of OTFTs. Additionally, OTFTs can be easily fabricated over large area substrates by inexpensive and low-temperature methods such as solution deposition, printing, and melt processing. Similarly, organic optoelectronic devices such as organic phototransistors (OPTs) have recently become a research focus due to their ease of fabrication and a variety of material choices to tune their light responsive properties for desired applications. [3] OPTs are employed in photo sensing, [4,5] as photo memory devices[6,7] and photo-transducers.[8]

A variety of light sensitive small molecule semiconductors, [9–11] polymers, [12] organic small molecule/ conjugated polymer[13] or organic semiconductor/dielectric polymer blends,[14–17] and single crystal/gold hybrid materials [18] have been employed to fabricate OPTs. Recently, photoresponsivity of ~10^4 AW^{-1} and photosensitivity of 10^5 were reported for benzo[1,2-b:4,5- b′]dithiophene dimers at UV light intensity of 37 μWcm^{-2}.[19] Furthermore, Wu et al. reported solution processed OPTs based on 2,7-dioctyl[1]benzothieno[3,2-b][1]benzothiophene

(C8-BTBT) single crystal ribbons with photoresponsivity as high as 1200 AW^{-1} and photosensitivity of 10^4.[20] These results indicate a successful realization of OPTs with a performance that has largely exceeded Si-based PTs (300 AW^{-1}).[21] However, such OPTs require long fabrication times and complex synthetic routes. In comparison, blending represents a much more efficient approach for fabrication of the high-performance OPTs with minimal processing times.

Blending of existing small molecule organic semiconductors (OSC) with existing or new dielectric polymers is an excellent method to enhance their stability and performance both in dark and under light illumination. [22] It simplifies fabrication and avoids complex synthesis of the channel materials. The most interesting small molecule OSCs for blending are 2,7-dialkyl[1]benzothieno[3,2-b][1]benzothiophene derivatives (C*n*-BTBT, where *n*=5-12). Typically, they are used for high-performance solution-processed OTFTs. [23,24] C5-BTBT is one of the derivatives that are blind to the visible light but responsive to UV-A light. Its UV light response has been demonstrated to be easily tuned by polymers and/or small molecule dyes, [16][17][25] via simple solution blending of the components. Polymer phase ensures better film quality, flexibility, thermal stability, lowers the exposure toward oxygen for operational stability and cuts the material cost. [26] The polymer electrostatic nature can modulate the drain photocurrent, I_{phc}, via charge trapping effects at the large interface introduced by blending. By adjusting the electron withdrawing (EW) or electron donating (ED) nature of the polymer, the density of photogenerated charge carriers in the OPT channel is dramatically affected upon light illumination. It enables not only modulation of the I_{phc} but also the device

response times, which is important for its application as a sensor or a photo memory. Nevertheless, the following properties of OPT devices still need to be improved: low saturation mobilities in the dark (typically below 1 cm^2Vs^{-1}), low photoresponsivity, and a large hysteresis of the I_{phc} observed under light illumination. Besides, for the high-performance photo memory, the response times (light on) should be short while decay times (light off) should be long to store an optically written information for a long time. Overall, the pursuit of high-performance OPTs with stable operation and reliable properties is a long-term goal for commercial applications.

In this work, we report a new soluble polyimide (PI) having strong EW groups and its blends with the UV responsive organic semiconductor C5-BTBT at different ratios, for high-performance OPTs. Aromatic polyimide is a widely-used polymer as a substrate and dielectric in the electronic industry due to its excellent thermal stability, mechanical and electrical properties, and chemical resistivity. [27][28][29] On the other hand, most of the PIs have deep coloration and are insoluble in common organic solvents, which limit their application. Transparent, colorless PIs with good solubility and thermal stability have great potential in the application for organic phototransistors. [30][31] For the synthesis of strong EW PI, 4,4′-diaminodiphenyl sulfone (DAPS) and 4,4′-(hexafluoro isopropylidene)diphthalic anhydride (6FDA) were chosen as monomers because they contain electronegative fluorine atoms and EW sulfonyl groups, respectively (Fig. 5.1a). Both monomers are aromatic, highly polar, and without flexible spacers (e.g. -S-, -O-, CH_3) endowing the PI with dramatically reduced deep coloration, [28] high thermal stability, and high glass

transition temperature (T_g). The bulky chemical structure of the monomers and asymmetric structure of the polymer chains prevented from close packing. [32] As a result, the PI has high solubility in common organic solvents, especially in the solvent used in this work for OPTs fabrication.

The blending of the new PI with C5-BTBT had a strong influence on the performance of OPTs. OPTs with different PI:C5-BTBT ratios were fabricated and photoelectrical properties were investigated. Effects of two different molecular weights of PI were also investigated. All effects were dependent on the content but not on the molecular weight of the PI. Those effects were investigated and discussed by means of the drain photocurrent hysteretic behavior under UV light, photosensitivity and photoresponsivity of OPTs, and saturation hole mobility. We anticipate that the strong electron withdrawing nature of the PI facilitated strong charge trapping effects at the interface enhancing the properties of OPTs relative to C5-BTBT OPT. It also affected the response times when the UV light was on and off, which is explained by the density functional theory calculations. This work demonstrates that the PI is an excellent material for the realization of the high-performance, solution processed OPTs for photo memory devices. To the best of our knowledge, this is the first report on this type of PI and the use of PI, in general, as a channel component to enhance the photoelectrical properties of OPTs.

§ 5.3 Experimental

5.3.1 Materials

C5-BTBT was synthesized according to the procedures reported in the references. [23][33] All chemicals were used as received. Solvents 2-propanol (Caledon, CA), methanol (Caledon, CA), ethanol (Commercial Alcohols, Brampton, ON, CA), acetone (Caledon, CA), toluene (Sigma-Aldrich, CA), 1,1,2,2-tetrachloroethane (TCE, Sigma-Aldrich, CA), tetrahydrofuran (THF, Caledon, CA) and N,N-dimethylacetamide (DMAc, Sigma-Aldrich, CA) were all reagent grade. Monomers 4,4′-Diaminodiphenyl sulfone (DAPS), 4,4′-(hexafluoro isopropylidene)diphthalic anhydride (6FDA) and phthalic anhydride (PA) were purchased from Sigma-Aldrich (CA) and Synquest Laboratories, respectively. Acetic anhydride and trimethylamine as a catalytic system were purchased from Sigma-Aldrich (CA). Hexamethyldisilazane (HMDS), was purchased from Sigma-Aldrich and used as the surface modifying agent. Si-wafers as substrates (highly n-doped with 200 nm thermally growth SiO_2 as dielectric) were supplied by Silicon Quest International (San Jose, CA, USA).

5.3.2 Polyimide synthesis

PI with two molecular weights was synthesized using the same recipe as follows (Fig. 5.1a). Lower MW PI (PI1) was synthesized without water removal. For the synthesis of a higher MW PI (PI2), water as a toluene/water azeotropic mixture

was constantly removed from the reactor using a Dean-Stark trap. In a 500 mL three-neck round-bottom flask, 19.988 g (80.5 mmol) of DAPS was dissolved in 100 g of DMAc as a solvent. The mixture was purged with nitrogen and stirred to obtain a homogeneous solution. All the following steps were carried out under an N_2 blanket. Additional 100 g of DMAc, 35.539 g (80.0 mmol) of 6FDA, and 0.148 g (1 mmol) of PA (end-capping agent) were added to a reactor where a dark yellow mixture was formed. The reaction mixture was stirred overnight (~12 h) at room temperature to yield a dark yellow viscous solution of poly(amic acid). To remove water from the reactor, 20 mL and 10 mL of toluene were added in a Dean-Stark trap and reactor, respectively, followed by addition of a catalytic mixture of acetic anhydride (2 mL)/trimethylamine (1 mL) into the reactor. The temperature was then increased to 180°C and imidization reaction was carried out for another 9 h. After cooling to room temperature, a dark orange mixture (polyimide) was observed in the reactor. Crude polyimide was poured into an excess of ethanol (~2 L) and vigorously stirred for at least 2 h. The polymer was left to precipitate overnight followed by additional washing with ethanol. Polyimide was collected by filtration, dried in air and *in vacuo* 12 h at 100°C, 2 h at 150°C, and 6 h at 180°C. Finally, purification was carried out by PI dissolution in THF followed by precipitation in methanol. NMR and FT-IR analyses confirmed the structure of the PI.

5.3.3 Preparation of PI:C5-BTBT blends and Phototransistors fabrication

PI (PI1 and PI2) and C5-BTBT were solution-blended in 10:90, 30:70, 50:50, 70:30 and 90:10 ratios in TCE solvent (Fig. 5.1b), with the total solute at 2 wt.% concentration. Although clear PI:C5-BTBT blend solutions (all ratios) were obtained within 30 min at room temperature using a small stirring bar, dissolution of solids was carried out overnight at 60°C to ensure complete dissolution of the polymer. Before spin-coating onto a substrate, solutions were filtered through an acrodisc PTFE syringe filter (Millipore 0.20 μm).

All OPTs were fabricated under ambient conditions (23°C and relative humidity 40%) using the top-contact, bottom-gate device configuration (Fig. 5.1c). Prior to spin-coating of the blend solutions, 1x1 inch Si-wafers (two for each blend and a control) were thoroughly cleaned using cold and warm 2-propanol, acetone and chloroform in a sonication bath, air dried, followed by cleaning in a plasma cleaner PDC-32G (Harrick Plasma, USA) for 2 min. After UV/plasma treatment, Si wafers were immersed in deionized water for 10 min, rinsed with 2-propanol, and air dried. HMDS/toluene solution at 60°C for 30 min was used to treat the SiO_2 surface of a Si wafer to ensure good adhesion of a channel material. Surface modified substrates were rinsed with toluene, air, and vacuum dried for 20 min at 70°C. Spin-coating of PI:C5-BTBT solutions was performed on a spin coater SCS P-6700, Sitek Process Solutions, Inc., CA, USA, under the following conditions: 2 min surface wetting, total spin-coating time 2 min at 2000 rpm, ramp time 2 s. Finally,

60-nm source and drain gold electrodes were deposited through a shadow mask using electron beam evaporator (Nano 36, FTM-2400, Kurt J. Lesker, UK). Channel length and width were 85 μm and 930 μm, respectively. Control OPTs based on pristine C5-BTBT were fabricated under the same conditions from a 2.0 wt% C5-BTBT solution in TCE.

5.3.4 Characterization and computational methodology

MW of PI was determined using a gel permeation chromatography system (GPC, Waters) relative to a polystyrene standard in THF at room temperature. Thermal characteristics of PI (DSC and TGA) were evaluated using TA Instruments (DE, USA). In DCS analysis, 5-7 mg of each PI was subjected to two heating/cooling cycles (10°C/min from room temperature to 400°C). The sample was placed in a hermetic aluminum pan. The glass transition temperature (T_g) was determined from the second heating cycle using TA Instruments TRIOS software (version 4.1.0.31739). TGA analysis of the PI samples (6-8 mg) was run in air and argon atmosphere at 10°C/min ramp from room temperature to 1000°C. For spectroscopic analysis of PIs, we employed Nicolete UV-Vis-NIR (Cary 5000, Varian, USA, thin films) and ThermoScientific (FT-IR, Nicolete 6700 on KBr disc) spectrophotometers, and a Bruker NMR spectrometer (400 MHz, DMSO-d6, room temperature).

UV-vis spectra of all thin films on glass slides (deposited under the same conditions as on Si-wafers) were recorded using aforementioned spectrometer

while surface profiler DektakXT (Bruker, USA) was used to determine the thin film thicknesses. The thin film morphology was examined using Keyence VHX-2000 (Keyence, Canada) digital optical microscope and MFP-3D atomic force microscope (Asylum Research and Oxford Instrument Company, Santa Barbara, CA, USA) in tapping mode (silicone tip FMR-20, Nano World, Switzerland, force constant 2.8 N/m, and a frequency of 75 Hz), under ambient conditions. AFM data were acquired and analyzed with aid of the Asylum Research AFM software build on Igor Pro (Wavemetrics, Portland, OR, USA). Crystal structure data of PI:C5-BTBT thin films and a C5-BTBT control, on HMDS modified Si wafers, were acquired in a two-dimensional X-ray diffractometer (XRD^2) equipped with a Bruker Smart6000 CCD area detector, Bruker 3-circle D8 goniometer, Rigaku RU200 Cu $K\bar{\alpha}$ rotating anode, and Göebel cross-coupled parallel focusing mirrors. Acquisition conditions were as follows: scan type Omega sweep (from 0.5°-13°), frame exposure: 300 s, 2θ = 2.5° - 35°, at the detector distance of 11.86 cm and power setting 90 mA and 50 kV. Photoelectrical characteristics of all the OPTs were measured under yellow (considered as dark in this report) and UV light on a 4200-SCS Parameter Analyzer (Keithley Instruments, USA). A hand operated UV lamp (Black-Ray, UVP B 100 AP, long wave UV lamp, 100 W, λ=365 nm, Entela, USA), UV-A light intensity (P_{UV}) 3 $mWcm^{-2}$ and 0.12 $mWcm^{-2}$ was used for illumination of the OPTs during photoelectrical characteristics measurements.

Theoretical calculations of the polyimide repeating unit were performed using Gaussian 09 program. We optimized the basic unit by means of the density functional theory (DFT), using the hybrid functional B3LYP (Becke, three-

parameter Lee-Yang-Parr) [34][35][36] and the Pople double-zeta polarized basis set 6-31G(d).[37][38] The isosurfaces of the molecular orbitals were constructed with the VMD[39] visualization software using a value of 0.02 Bohr.

§ 5.4 Results

5.4.1 PI synthesis and properties

PI having two different molecular weights (PI1, MW=6400, PDI=1.54; PI2, MW=14800, PDI=1.84) were synthesized via a two-step method described in the experimental section (Fig. 5.1a). Chemical structure of the repeating unit of PI1 and PI2 was confirmed by NMR and FT-IR analyses (Section 5.7, Fig. S5.1 and S5.2). From ^{1}H and ^{13}C NMR, no residual monomers were identified, but characteristic shifts originated from the benzene protons (8.25-7.75 ppm). FT-IR spectra clearly showed characteristic bands for proposed molecular structure of the PI repeating unit: a strong (symmetric) and a weak C=O (asymmetric) peaks around 1750 cm^{-1} and 1760 cm^{-1}, respectively, along with the peak around 1375 cm^{-1} (C-N stretch). The UV-vis spectra of PI1 thin films showed an absorbance onset around 350 nm with the appearance of the absorbance peak onset at 350 nm (Fig. S5.3).

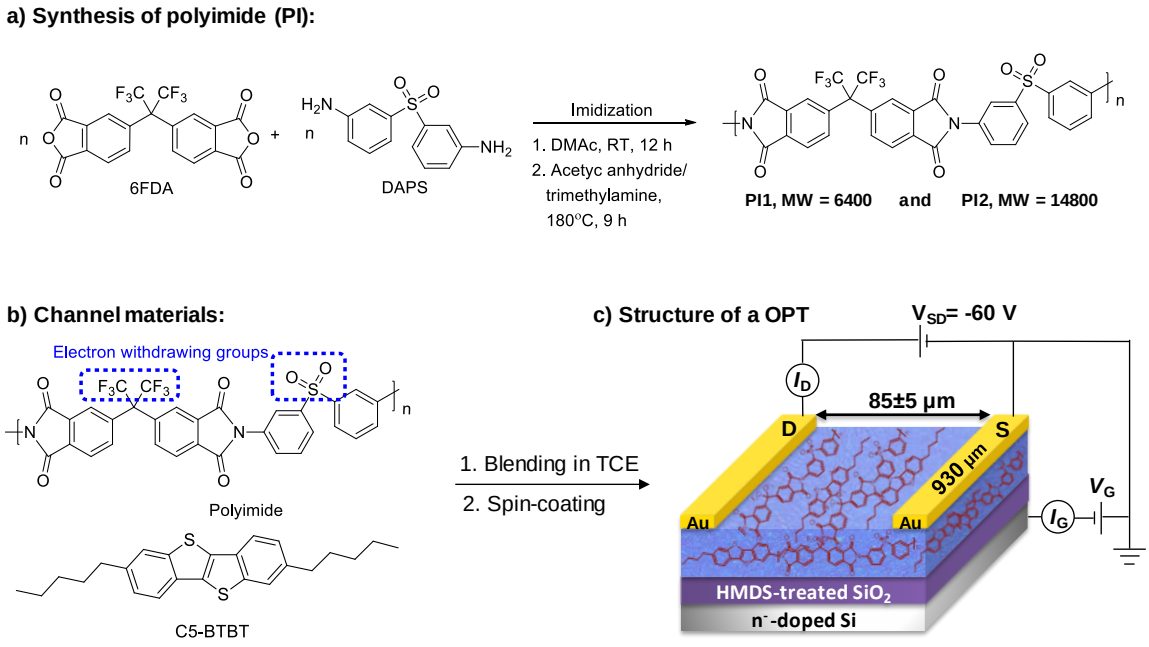

Fig. 5.1 (a) Synthesis scheme of the strong EW asymmetric polyimide, (b) molecular formulas of the channel materials (blued dotted rectangles denote the origin of the strong EW properties), and (c) the top-contact, the bottom-gate structure of OPTs (channel length L/W=85/930).

The solubility of PI was investigated in common organic solvents including those commonly used for solution processing OTFTs. Both the low and high molecular weight PIs exhibited excellent solubility (60 mg/mL) in THF, DMSO, DMF and TCE, and limited solubility in DMAc, NMP, and $CHCl_3$ at room temperature. PIs were insoluble in toluene, chlorobenzene, dichlorobenzene, and methanol, at any temperature. PI used in electronic industry has very high solvent resistance. Our design of the PI structure demonstrated altered solubility of PI via targeted selection of the monomers having polar and bulky functional groups. This enabled

successful incorporation of the PI in solution processed OPT and allowed investigation of the effect of its electronic nature on OPTs characteristics. Furthermore, both MW PIs exhibited excellent thermal stability up to 550°C in inert (argon) and oxidative (air) environments examined by TGA (Fig. S5.4a and b), which is comparable with the thermal stability of PI reported in the literature [40]. An only characteristic glass transition was detected when heated up to 400°C in the DSC analysis for both PIs indicating its amorphous structure. The T_g value of 253°C and 267°C for PI1 and PI2, respectively, were determined from the second heating cycle (Fig. S5.4c). DSC results strongly correlated with the solubility properties of PI. The asymmetrical structure of PI chains containing bulky -CF_3 groups, prevented the formation of crystalline domains, therefore, enabling good solubility in common organic solvents.

5.4.2 Thin film morphology and structure

The optical microscopy images of the blend- and C5-BTBT-based thin films are displayed in Fig. S5.5. The thin film quality was improving with the increasing content of PI in the blend (better film formation and fewer defects). The 90:10 PI:C5-BTBT blends formed mirror-like thin films. The thickness of the thin films was in the range of 210-320 nm (Table S5.1), being higher for the higher content of PI in the blend. AFM analysis of the blend-based thin film morphologies showed that blends with the same ratio had similar morphologies regardless of the molecular weight (Fig. 5.2 and S5.6). Similarly, to the optical images, AFM images showed

better film quality for the higher PI content in the blend, compared to the thin film of C5-BTBT. Consequently, incorporation of PI influenced surface roughness (R_{RMS}, RMS-root means square) of the thin films as reported in Fig.5. 2 and S5.6. The higher the content of the PI, the lower the R_{RMS} of thin film where C5-BTBT grains were merging with the PI phase.

The crystal structure of the thin films was investigated by XRD[2] (Fig. S5.7). The C5-BTBT molecule has a preferred orientation in (00*1*) crystal plane (strong, sharp peak at $2\theta = 3.8°$, *d*-spacing of 2.3 nm). For all thin films, only the preferred (00*1*) crystal plane orientation was observed showing that PI did not influence the C5-BTBT crystal structure. The peak intensity varied with the film thickness and the content of C5-BTBT in the blend. This is the most evident in the case of 90:10 ratio, regardless of the PI MW, where C5-BTBT (00*1*) peak was not detected due to small content of C5-BTBT dispersed in the polymer matrix.

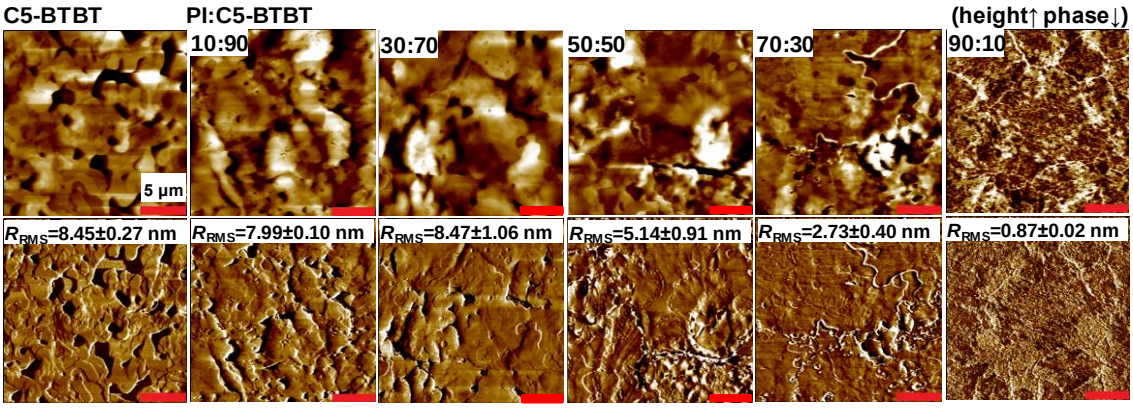

Fig. 5.2. AFM height (upper row) and phase images (lower row) of PI1:C5-BTBT thin films on HMDS modified Si-wafer with reported R_{RMS} values estimated from the 20x20 µm height images; a thin film of C5-BTBT was included for comparison.

5.4.3 Photoelectrical characteristics of OPTs

Photoelectrical characteristics of the solution processed, top-contact bottom-gate OPTs (Fig. 5.1c), revealed the effects of PI on C5-BTBT. Those effects were independent on MW of PI and for clarity, only plots showing photoelectrical curves of PI1-based OPTs were represented here. The performance of PI1:C5-BTBT OPTs was compared with that of C5-BTBT-based OPTs. All the OPTs showed a typical p-type operation regime in dark and under UV light (P_{UV}= 3 mWcm^{-2}, λ=365 nm). The output characteristics represented by I_D-V_{SD} curves in Fig. 5.3 and S5.8, indicated the strong influence of PI on photoelectrical properties of OPTs with UV responsive C5-BTBT. OPTs in the dark operated in the linear (ohmic contact) and saturation regimes. The cut-off gate voltage (V_G) for all OPTs ranged from -40 to -

50 V at the source-drain voltage (V_{SD}) sweep between 0 and -60 V. Compared to C5-BTBT OPTs, the drain current (I_D) at V_G and V_{SD} of -60 V decreased once PI1 was incorporated up to 50 wt.%. Surprisingly, when C5-BTBT was blended with 70 wt.% of PI1, the I_D at V_G and V_{SD} of -60 V exceeded the I_D of C5-BTBT OPTs. OPTs with 90 wt.% of PI1 were nonconductive both in the dark and under UV light due to a lack of "the threshold content" of C5-BTBT necessary to form a continuous semiconducting path in the channel. The absence of crystalline C5-BTBT phase was also confirmed by XRD[2] where no preferred C5-BTBT orientation (00*l*) was observed due to its low content.

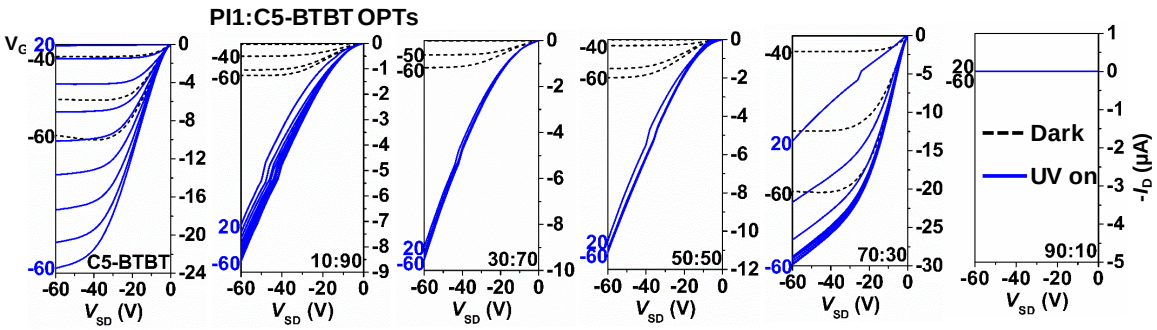

Fig. 5.3. Output characteristics in dark (dashed line) and under UV light (solid line, P_{UV}=3 mW cm^{-2}, λ=365 nm) of PI1:C5-BTBT OPTs with different ratios; the output characteristics plot for C5-BTBT OPTs is included for comparison; V_G was varied from 20 to -60 V (step of -10 V) during V_{SD} sweep from 0 to -60 V (scan rate 6 Vs^{-1}, L/W=85/930 μm).

Under UV light illumination, even a small amount of PI1 in the blend (10 wt.%) strongly affected I_D of OPTs. C5-BTBT and 70:30 OPTs showed good ohmic contacts compared to other OPTs where *s*-shape I_D-V_{SD} curves were observed even though the channel length was large. All the blend-based OPTs under UV light showed no or weak (70:30) saturation regime. PI1 significantly increased the I_D at lower V_G (especially at 20 V), thus, giving a rise to the drain photocurrent (I_{phc}) in the subthreshold region (an off-state region in the dark). As soon as UV light was turned on, the OPTs were immediately on, with I_{phc} being instantaneously saturated and independent on a further increase of V_G. All the blends except 70:30, had a lower max I_{phc} at V_G= -60 V relative to C5-BTBT OPTs due to morphology effects. However, the I_{phc} of a 70:30 blend, likewise in the dark, exceeded the I_{phc} of C5-BTBT OPTs at all V_G. At 70:30 ratio, saturation of the I_{phc} seemed to be initially slower but upon V_G = 10 V it became independent on a further increase of the V_G, similarly to OPTs with the lower PI content. These effects were further investigated by means of the transfer characteristics in the dark and under UV light illumination.

The transfer characteristics of PI:C5-BTBT OPTs in the dark and under UV light strongly correlated with the output characteristics as seen in Fig. 5.4. The electric field of $7.1x10^3$-$8.0x10^3$ Vcm^{-1} was generated while measuring the transfer characteristics in the dark coinciding with the values reported for pentacene and P3HT-based OPTs (10^3-10^4 Vcm^{-1}) [41][42] and amorphous metal-oxide solution processed TFTs with polymer dielectrics (10^6 Vcm^{-1}).[43] The transfer characteristic plots of PI2:C5-BTBT OPTs were identical to PI1-based OPTs and are omitted here. In the dark, the 70:30 blending ratio increased the drain current above the

level of C5-BTBT OPTs, while other blending ratios lowered the max I_D. All the blend-based OPTs were hysteresis-free in the dark, exhibiting high on/off ratios, typically 10^5-10^6. The threshold (V_{Th}) and turn-on (V_{SO}) voltages of PI:C5-BTBT OPTs estimated from the transfer characteristics in the dark are displayed in Fig. 5.4b and c, respectively. Incorporation of PI did not significantly affect these two parameters relative to C5-BTBT OPTs. Other electrical parameters estimated for all OPTs in the dark are given in Table S5.1. Equations used to estimate all figures of merit are given in Supp. Info, Section 5.7.

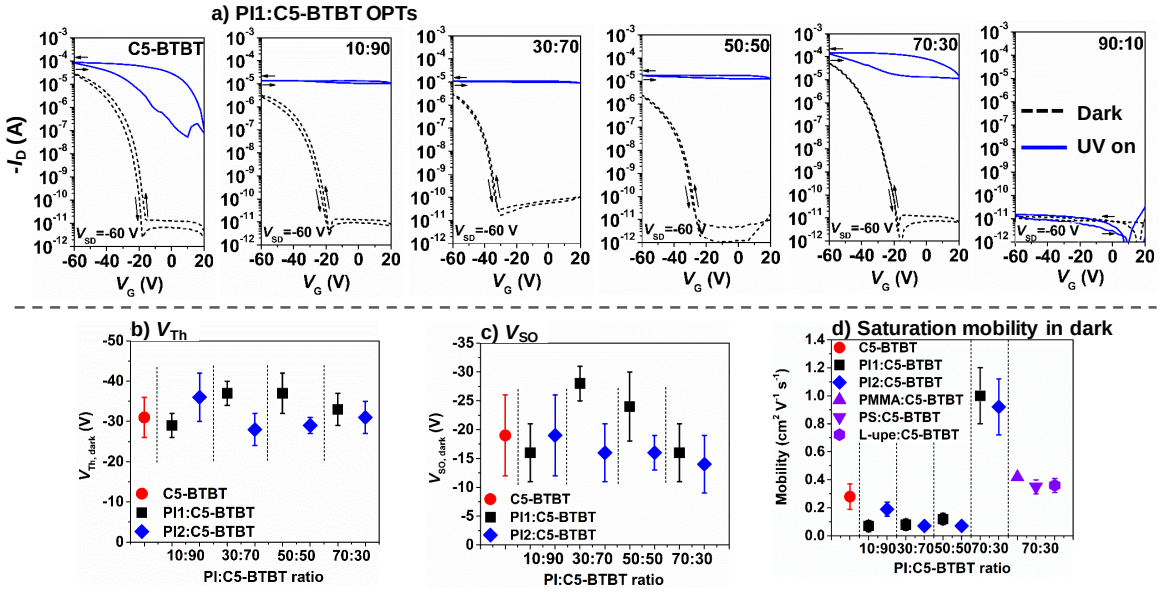

Fig.5. 4. Transfer characteristics in the dark (dashed line) and under UV light (solid line, P_{UV}=3 mW cm^{-2}, λ=365 nm) of (a) PI1:C5-BTBT OPTs at V_{SD}= -60 V (scan rate 6 Vs^{-1}); the transfer characteristics plot for C5-BTBT OPTs was included for comparison in (a); (b) variation of $V_{Th,dark}$, (c) $V_{SO,dark}$, and (d) saturation mobility in dark of OPTs with different PI content; the mobiltiy of 70:30 model blends-based OPTs was included in (d) (L/W=85/930 μm).

On the other hand, Fig. 5.4d shows that blending PI with C5-BTBT had a strong influence on the filed-effect hole mobility in saturation regime (μ_{FE}) estimated from the transfer curves. The μ_{FE} of blend-based OPTs decreased with the increasing content of PI up to 70:30 blending ratio due to morphology effects, i.e. incorporation of the polymer generated more physical traps for the mobile holes in the channel. To our surprise, the μ_{FE} value jumped three-fold higher relative to C5-BTBT OPTs

when the PI content reached 70 wt.%, despite the fact of the physical traps introduced by blending. To investigate the reason for the increased mobility in 70:30 blends, we estimated μ_{FE} of OPTs fabricated with 70:30 model blends in the channel (Fig. 5.4d), namely, PMMA:C5-BTBT, PS:C5-BTBT, and L-upe:C5-BTBT. PMMA and PS are polymers commonly used for OTFT fabrication as dielectric layers or for blending with the semiconductors. L-upe represents a linear unsaturated polyester with strong effects on OPT photoelectrical properties. [14] The thin film morphology images, transfer characteristics plots, and electrical parameters of the model blend-based OPTs are given in Fig. S5.8 and S5.9, and Table S5.2, respectively. OPTs with the model blends also showed a slightly higher mobility relative to C5-BTBT OPT but significantly lower than 70:30 PI:C5-BTBT OPTs. These results revealed that both the film structure (phase separation) and the PI electronic nature dominated over the mobility.

Under the UV light illumination, incorporation of the PI strongly affected the subthreshold behavior of the I_D, where OPTs were normally in off-state in the dark. With the low content of PI1 in the blend (10 wt.%), the generated I_{phc} in the subthreshold region was immediately in its maximum (saturated) at V_{SD}= -60 V and P_{UV}=3 mWcm^{-2}. The fast and more than five orders of magnitude generation of I_{phc} in the subthreshold region was a result of the strong interface trapping by PI in the bulk of the channel and resulting photovoltaic effect (voltage drop in the channel due to the high concentration of the excess photo charge carriers). The V_{Th} and V_{SO} were dramatically shifted toward the positive values of the gate voltage being out of the measuring span. Strong EW nature of the PI enhanced the charge

separation and trapping of the photoinduced charge carriers, meaning that channel was formed faster due to a fast filling of the trapping sites at the channel/SiO_2 interface. Unfortunately, no values for the charge carrier density generated by light could be estimated since we could not estimate the V_{Th} and V_{SO} of OPTs under UV light illumination using equations reported previously. [44] More importantly, the presence of the PI in the blend eliminated (10:90, 30:70 and 50:50 blends) or significantly suppressed (70:30 blends) hysteresis under UV light, as compared to C5-BTBT OPTs. Slow trapping and detrapping of the charge carriers are known to generate the lower back current hysteresis in OTFTs. [45] Therefore, PI as a polar and strong EW dielectric enabled fast trapping/detrapping of the charge carriers at the PI/C5-BTBT and channel/SiO_2 interfaces. This is the first time that we observed no or little hysteresis of OPTs under UV light illumination compared to our previous works. [15][14][46] Unfortunately, no other works reported in the literature investigated the I_D - V_G hysteretic behavior of OPTs under light illumination.

5.4.4 Photosensitivity and photoresponsivity of OPTs

The UV light sensitivity of C5-BTBT enhanced by PI was quantified by photosensitivity (I_{phc}/I_D) and photoresponsivity (R, AW^{-1}) (Table S5.3, for equations, see Supporting Info, Section 1.3). The strong effect of PI on C5-BTBT UV response was clearly observed from the I_{phc}/I_D ratio at V_G=20 V, i.e. start of the measurement. At this V_G, only 10 wt.% of PI1 increased the I_{phc}/I_D ratio by two orders of magnitude (10^6) compared to C5-BTBT OPTs. The I_{phc}/I_D ratio at V_G=0 V reached as high as

10^7 (70:30 blends in PI1:C5-BTBT OPTs). Furthermore, Fig. 5.5a gives the dependence of I_{phc}/I_D ratio on V_G of PI:C5-BTBT OPTs. The I_{phc}/I_D ratio increased with V_G, reached its maximum right before the OPT turn-on, followed by the sharp decrease due to electrical contribution (electric field) to the I_D generation.

To evaluate R of OPTs, we chose $V_G = 0$ V so that there would be no electrical contributions to the charge carrier generation. This was based on R vs V_G curves included in Fig. 5.5a, from which it became clear that R value was at its maximum, except for C5-BTBT and 70:30 OPTs. In 70:30 OPTs, R was independent on V_G until OPT reached the V_{Th}. Compared to C5-BBTBT OPTs at $V_G = 0$ V (R=10.6±2.5 AW^{-1}), R values for PI1:C5-BTBT OPTs were lower (4.6±0.8 – 6.4±0.8 AW^{-1}) up to 70:30 blending ratio. They were tripled when 70:30 blends were used compared to C5-BTBT OPTs (Table S5.1), which could be explained by the better alignment of C5-BTBT crystallites in the blend.

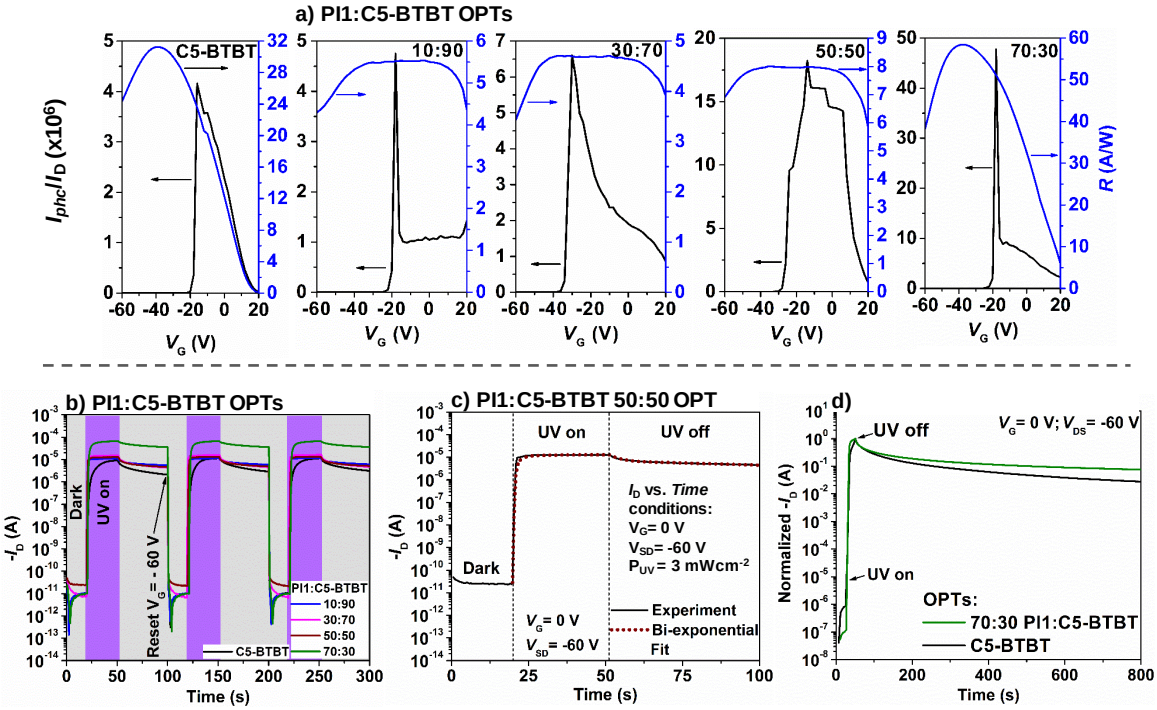

Fig. 5.5. Representation of (a) photosensitivity and photoresponsivity as a function of V_G for PI1:C5-BTBT OPTs (C5-BTBT OPTs characteristics were included for comparison), (b) switching characteristics of PI1:C5-BTBT OPTs, and (c) bi-exponential curve fitting for a representative OPT.

5.4.5 Dynamic properties of OPTs

EW nature of the PI had a strong influence on the I_{phc} evolution in time. This was investigated by I_D vs. time measurements. These measurements enabled determination of two important parameters: how fast OPT responded to the UV light and how much I_{phc} was developed in time (Fig. 5.5b). It also demonstrated how long OPT could store the information written by the UV light (optically writeable photo memory). The I_D vs. time curve of all OPTs was generated at V_G = 0 V and

V_{SD} = -60 V. Each OPT was subjected to a three-cycle measurement to investigate the reproducibility of its response. The typical cycling sequence was *Dark @ 0 s ≫ UV on @ 20 s ≫ UV off @ 50 s ≫ Reset @ 100 s.* From Fig. 5.5b (black curve), one can see that I_D vs time curves for C5-BTBT OPTs are characterized by the slow increase of the I_{phc} without saturation in the measuring range. In contrast, incorporation of the PI dramatically affected the I_{phc} evolution in time. UV light illumination generated the I_{phc} time response with two distinct regimes: a fast rise to the maximum and fast saturation (horizontal part of the curve). The I_{phc} raise was as high as ~7 decades (70:30 blends). Furthermore, the persistent I_{phc} decayed noticeable slower compared to C5-BTBT OPTs upon UV illumination was turned off. This indicated the enhanced photo memory properties of blend-based OPTs (longer retention of the stored information). Therefore, the strong EW nature of PI affected the kinetics of the charge carrier generation under UV light illumination and their recombination in the dark via interface charge trapping. All the blend based OPTs were easily reset upon applying a short (~4 s) pulse of V_G= - 60 V, indicating that PI did not affect the reset voltage as compared to C5-BTBT OPTs. In our previous work, we demonstrated that different states at the channel/dielectric interface could significantly affect the reset voltage of a blend-based PTs.[44]

The dynamic response of OPTs under UV light was fitted using bi-exponential equations: $I_{phc}(t) = I_D + R_1\left(1 - e^{-t/\tau_{r1}}\right) + R_2\left(1 - e^{-t/\tau_{r2}}\right)$ for rise times and $I_{phc}(t) = I_D + D_1 e^{-t/t_{d1}} + D_2 e^{-t/t_{d2}}$ for decay time.[47] R_1, R_2, D_1 and D_2 are constants, while τ_{r1}, τ_{r2} and τ_{d1}, τ_{d2} are times of the fast/slow I_{phc} rise, and the

fast/slow I_{phc} decay, respectively. The response times were calculated based on at least five OPTs and the three cycles per device. The bi-exponential fitting of the representative OPT (PI1:C5-BTBT 50:50) is displayed in Fig. 5.5c, while detailed response times for all OPTs are summarized in Table S5.3. Using PI as a strong EW polymer we altered dynamics of the OPT response to UV light. Only 10 wt.% of the PI1 in a blend made the τ_{r1} 16 times faster (0.95±0.24 s) compared to C5-BTBT OPTs (16.2±8.0). Besides, τ_{r2} of the blend-based OPTs indicated that the time for I_{phc} to saturation was decreased, enabling illumination even shorter than 30 s to reach the max I_{phc}. This is important for the device operation speed and off-on-off switch.

The τ_d for OPTs with blends confirmed the strong EW nature of the PI. The τ_{d1} or fast photo charge carrier recombination indicated that EW PI accumulated excessive photoelectrons (electron withdrawing) from the bulk at the channel/SiO_2 interface. Their fast recombination with the photo holes at the interface decreased the τ_{d1} in the blend-based OPTs. In contrast, photoelectrons trapped in the bulk of the channel and at deeper energy levels due to PI EW nature were diffusion dependent, thus, slowing down the recombination with photo holes. This is indicated by significantly increased τ_{d2} compared to C5-BTBT OPT (76.4±21.5). The slowest decay was observed for OPTs with 70:30 PI1:C5-BTBT blends (149.3±9.5). It is noteworthy that response times (τ_{r1}/τ_{d2}) of PI1:C5-BTBT OPTs are comparable with those reported for spiro-DPO OPTs (7.6/73.2 s), [48] P3HT:TiO_2 (~0.2/nd s) [49] OPTs, and fullerene-based (0.50/0.62 s) PTs. [50]

5.4.6 DFT calculations and mechanism

To further understand the mechanism for the decreased response and increased photo memory times of PI1:C5-BTBT OPTs, DFT calculations were performed using Gaussian 09 software to estimate the HOMO/LUMO of the PI repeating unit and to compare it with C5-BTBT molecule. Fig. 5.6 represents a summary of the charge density isosurfaces of the PI repeating unit, energetically preferred molecular geometry, HOMO/LUMO energy levels for C5-BTBT and PI repeating unit, and the proposed mechanism of the photo-charge carrier generation/recombination under UV light illumination. From the molecular calculations of the PI repeating unit (Fig. 5.6a), one can see how polarized is the electron distribution along the different energy levels, proving a strong EW nature. For instance, we observed that both EW groups (6FDA and DAPS units) are electron deficient at the LUMO energy level, contrary to the occupied orbitals where the electronic density is located mostly on any or both groups, meaning that it requires more energy to take off electrons from them.

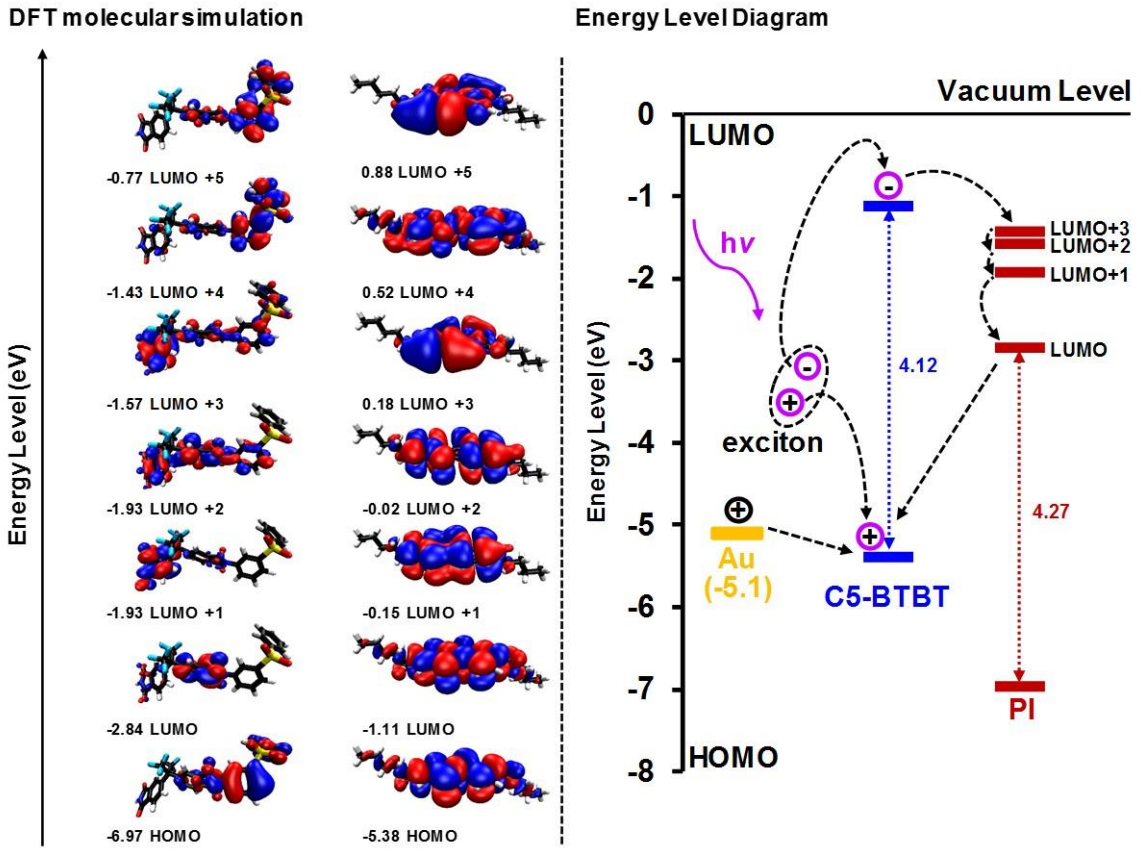

Fig. 5.6. Schematic representation of (a) DFT isosurfaces of the PI repeating unit and C5-BTBT molecule, and (b) proposed mechanism of the charge carrier generation and recombination related to the switching mechanism of PI:C5-BTBT OPTs.

The energy levels diagram in Fig. 5.6b revealed the mechanism of the shorter rise times (faster response) and longer decay times in the blend-based OPTs compared to C5-BTBT OPTs. Both HOMO and LUMO levels of PI are lower than HOMO/LUMO levels of C5-BTBT. More interestingly, up to LUMO+3 level is lower than LUMO level of C5-BTBT. When the channel is illuminated with UV light, the

generated excitons diffuse to the C5-BTBT/PI interface where the charge separation occurs. The driving force for the effective charge separation is the difference between HOMO of C5-BTBT and LUMO of PI. The high difference of 2.54 eV enabled an effective and fast charge separation into the free photo charge carriers. Thus, a large I_{phc} is generated in the subthreshold region of a blend-based OPT compared to C5-BTBT OPT due to a fast charge carrier generation. In contrast, for the I_{phc} to come back to the off I_D, all the photoelectrons need to recombine with the photo holes. The HOMO level of C5-BTBT conducts holes while electrons are moving through LUMO levels while PI does not participate in conductivity. For recombination to occur, an excited electron from LUMO of C5-BTBT falls first onto LUMO+3 of PI followed by successive transitions through LUMO+2, LUMO+1, and LUMO down to HOMO level of C5-BTBT. At each LUMO level of PI, attracted by the EW nature of PI, electrons reside for some period of time, which slows down the electron/hole recombination. In this manner, the decay time is increased, i.e. the stored information is retained longer than in C5-BTBT OPT. The bias voltage of -60 V forces electrons to recombine and OPT to reset enabling optical and electrical control of OPTs for photo memory devices. The black line circle with the + sign in it, represents a hole injected from the gold electrode to the channel to generate the dark I_D. I_D contributes together with the I_{phc} to the overall output current of OPTs.

5.4.7 UV sensitivity and operational stability of OPTs

The UV sensitivity of PI1:C5-BTBT OPTs was investigated by comparison of I_{phc}/I_D ratios at V_G 20 V and 0 V under P_{UV} of 3 mWcm^{-2} and 0.12 mWcm^{-2}, at V_{SD}= -60 V. I_{phc}/I_D and R max values for all OPTs are given in Table S5.4. Fig. 5.7 displays transfer curves of the representative PI1:C5-BTBT 70:30 OPTs under UV light with two intensities, compared with C5-BTBT OPT. Fig. 5.7 supported by values in Table S5.3, shows that even under weak UV light intensity of 0.12 mWcm^{-2}, PI1:C5-BTBT OPTs exhibited high I_{phc}/I_D of 10^4-10^5 at V_G = 20 V and 10^5-10^6 at V_G = 0 V. Lowering the UV light intensity to 0.12 mWcm^{-2}, significantly increased the R that reached as high as 429 AW^{-1} (70:30 PI1:C5-BTBT OPTs).

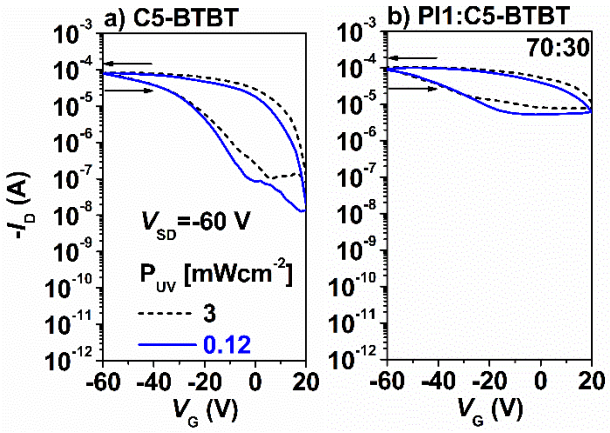

Fig. 5.7. I_D-V_G transfer curves under UV light of (a) C5-BTBT OPT as a reference and (b) a representative PI1:C5-BTBT 70:30 OPT; transfer curves were generated at V_{SD}= -60 V and under P_{UV} of 3 mWcm^{-2} and 0.12 mWcm^{-2} (L/D=85/930 μm and a scan rate 6 Vs^{-1}).

The operational stability of PI:C5-BTBT OPTs in the air was investigated by 50 cycles of a V_G forward/reverse sweep, in the dark and under high-intensity UV light illumination (3 mWcm^{-2}). Stability of blend-based OPTs was compared with stability of C5-BTBT OPTs. Fig. 5.8 displays transfer characteristics of a representative OPT (70:30 PI1:C5-BTBT) in comparison with C5-BTBT OPT. Values for μ_{FE}, V_{SO}, and V_{Th} in the dark for the first and fiftieth cycle of all OPTs are summarized in Table S5.5. PI slightly suppressed bias stress instability of the channel compared with C5-BTBT OPTs. It decreased shifting of the V_{SO} toward more negative values. Additionally, decreasing of the max I_D at V_G = -60 V with number of cycles was suppressed when C5-BTBT was blended with the PI. Under the UV light, PI:C5-BTBT OPTs did not show any evidence of the channel instability compared to C5-

BTBT OPT where we observed changes in the forward and reverse characteristics of the I_D under UV light. Therefore, the operation stability of PI:C5-BTBT OPTs under the high-power UV light was superior to C5-BTBT OPTs.

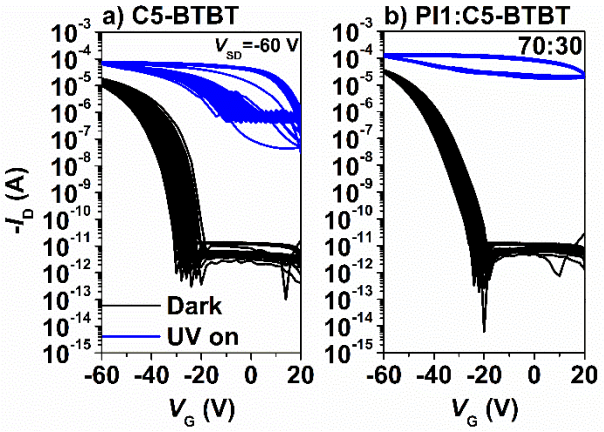

Fig. 5.8. Transfer curves in the dark and under UV light illumination (3 mWcm^{-2}) showing operation stability of PI1:C5-BTBT OPTs up to 50 cycles (forward-reverse sweep V_G) compared to C5-BTBT OPTs (L/W 85/930 μm; scan rate 6 Vs^{-1}).

§ 5.5 Conclusions

This study demonstrated that blending of a strong electron withdrawing and soluble polyimide and C5-BTBT at different ratios enabled fabrication of the stable, hysteresis-free, highly UV responsive (429 AW^{-1}), and UV sensitive (10^6) organic phototransistors. Results presented in this work showed that PI:C5-BTBT blends are potential candidates for fabrication of the photo memory devices where the fast response (fast optical writing of the information, <1 s) and long retention times (149

s) of the stored information are required. The density functional theory calculations proved our concept and enabled understanding of the mechanism of the decreased/increased response times. Tailoring the polyimide chain structure and its electronic nature by careful selection of the monomers was demonstrated to be an effective approach to modulate the photoelectrical characteristics of solution processed organic phototransistors based on a UV light responsive small molecule organic semiconductor. This work was first to report this type of polyimide and its integration as a channel material component for enhancing the photoelectrical properties of organic phototransistors for potential use as photo memory deices.

§ 5.6 References

[1] H. Sirringhaus, *Adv. Mater.* **2014**, *26*, 1319.

[2] Z. Bao, X. Chen, *Adv. Mater.* **2016**, *28*, 4177.

[3] Y. Guo, G. Yu, Y. Liu, Functional organic field-effect transistors. *Adv. Mater.* **2010**, *22*, 4427–4447.

[4] Y. Zang, F. Zhang, D. Huang, C. Di, Q. Meng, X. Gao, D. Zhu, *Adv. Mater.* **2014**, *26*, 2862.

[5] T.-D. Tsai, J.-W. Chang, T.-C. Wen, T.-F. Guo, *Adv. Funct. Mater.* **2013**, *23*, 4206.

[6] M. Debucquoy, S. Verlaak, S. Steudel, K. Myny, J. Genoe, P. Heremans, *Appl. Phys. Lett.* **2007**, *91*, 103508.

[7] Y. Y. Noh, D. Y. Kim, K. Yase, *J. Appl. Phys.* **2005**, *98*.

[8] X. Liu, G. Dong, L. Duan, L. Wang, Y. Qiu, *J. Mater. Chem.* **2012**, *22*, 11836.

[9] B. Yao, W. Lv, D. Chen, G. Fan, M. Zhou, Y. Peng, *Appl. Phys. Lett.* **2012**, *101*, 163301.

[10] B. Gunduz, F. Yakuphanoglu, *Sensors Actuators, A Phys.* **2012**, *178*, 141.

[11] Z. Qi, J. Cao, H. Li, L. Ding, J. Wang, *Adv. Funct. Mater.* **2015**, *25*, 3138.

[12] D. Ljubic, C. S. Smithson, Y. Wu, S. Zhu, *Adv. Electron. Mater.* **2015**, *1*, 1500119.

[13] D. Ljubic, C. S. Smithson, Y. Wu, S. Zhu, *ACS Appl. Mater. Interfaces* **2016**, *8*, 3744.

[14] C. S. Smithson, Y. Wu, T. Wigglesworth, S. Zhu, *Adv. Mater.* **2014**.

[15] J. Huang, J. Du, Z. Cevher, Y. Ren, X. Wu, Y. Chu, **2017**, 1.

[16] J. H. Jung, M. J. Yoon, J. W. Lim, Y. H. Lee, K. E. Lee, D. H. Kim, J. H. Oh, *Adv. Funct. Mater.* **2017**, *27*, 1604528.

[17] G. Zhao, J. Liu, Q. Meng, D. Ji, X. Zhang, Y. Zou, Y. Zhen, H. Dong, W. Hu, *Adv. Electron. Mater.* **2015**, *1*, 1500071.

[18] G. Wu, C. Chen, S. Liu, C. Fan, H. Li, H. Chen, *Adv. Electron. Mater.* **2015**, *1*, 1500136.

[19] K.-J. Baeg, M. Binda, D. Natali, M. Caironi, Y.-Y. Noh, *Adv. Mater.* **2013**, *25*, 4267.

[20] S. H. Kim, W. M. Yoon, M. Jang, H. Yang, J.-J. Park, C. E. Park, *J. Mater. Chem.* **2012**, *22*, 7731.

[21] H. Ebata, T. Izawa, E. Miyazaki, K. Takimiya, M. Ikeda, H. Kuwabara, T. Yui, *J. Am. Chem. Soc.* **2007**, *129*, 15732.

[22] M. E. Cinar, T. Ozturk, *Chem. Rev.* **2015**, *115*, 3036.

[23] C. S. Smithson, D. Ljubic, Y. Wu, S. Zhu, *J. Mater. Chem. C* **2015**, *3*.

[24] C. Pitsalidis, A. M. Pappa, S. Hunter, A. Laskarakis, T. Kaimakamis, M. M. Payne, J. E. Anthony, T. D. Anthopoulos, S. Logothetidis, *J. Mater. Chem. C* **2016**, *4*, 3499.

[25] C. D. Sheraw, D. J. Gundlach, T. N. Jackson, *MRS Proc.* **1999**, *558*, 403.

[26] H. jiang Ni, J. gang Liu, Z. he Wang, S. yong Yang, *J. Ind. Eng. Chem.* **2015**, *28*, 16.

[27] S. Pyo, H. Son, K. Y. Choi, M. H. Yi, S. K. Hong, *Appl. Phys. Lett.* **2005**, *86*, 1.

[28] C.-L. Tsai, C.-J. Chen, P.-H. Wang, J.-J. Lin, G.-S. Liou, *Polym. Chem.* **2013**, *4*, 4570.

[29] S. U. Tzy-Hsiang, S. H. Hsiao, C. S. Liou, *J. Polym. Sci. Part A Polym. Chem.* **2005**, *43*, 2085.

[30] T. Kurosawa, T. Higashihara, M. Ueda, *Polym. Chem.* **2013**, *4*, 16.

[31] M. Saito, I. Osaka, E. Miyazaki, K. Takimiya, H. Kuwabara, M. Ikeda, *Tetrahedron Lett.* **2011**, *52*, 285.

[32] C. Lee, W. Yang, R. G. Parr, *Phys. Rev. B* **1988**, *37*, 785.

[33] A. D. Becke, *J. Chem. Phys.* **1993**, *98*, 5648.

[34] J. P. Perdew, K. Burke, M. Ernzerhof, *Phys. Rev. Lett.* **1996**, *77*, 3865.

[35] W. J. Hehre, R. Ditchfield, J. A. Pople, *J. Chem. Phys.* **1972**, *56*, 2257.

[36] M. M. Francl, W. J. Pietro, W. J. Hehre, J. S. Binkley, M. S. Gordon, D. J. DeFrees, J. A. Pople, *J. Chem. Phys.* **1982**, *77*, 3654.

[37] W. Humphrey, A. Dalke, K. Schulten, *J. Mol. Graph.* **1996**, *14*, 33.

[38] M. Ghosh, *Polyimides: Fundamentals and Applications*; Taylor & Francis, 1996.

[39] K. P. Pernstich, S. Haas, D. Oberhoff, C. Goldmann, D. J. Gundlach, B. Batlogg, A. N. Rashid, G. Schitter, *J. Appl. Phys.* **2004**, *96*, 6431.

[40] F. Yakuphanoglu, B. Gunduz, *Synth. Met.* **2012**, *162*, 1210.

[41] V. Pecunia, K. Banger, H. Sirringhaus, *Adv. Electron. Mater.* **2015**, *1*, 1400024.

[42] D. Ljubic, V. Jarvis, C. S. Smithson, N.-X. Hu, Y. Wu, S. Zhu, *Org. Electron.* **2017**, *44*, 253.

[43] M. Egginger, S. Bauer, R. Schwödiauer, H. Neugebauer, N. S. Sariciftci, *Monatshefte für Chemie - Chem. Mon.* **2009**, *140*, 735.

[44] C. S. Smithson, D. Ljubic, Y. Wu, S. Zhu, *Org. Electron. physics, Mater. Appl.* **2016**, *37*.

[45] D. Gedamu, I. Paulowicz, S. Kaps, O. Lupan, S. Wille, G. Haidarschin, Y. K. Mishra, R. Adelung, *Adv. Mater.* **2014**, *26*, 1541.

[46] T. P. I. Saragi, R. Pudzich, T. Fuhrmann-Lieker, J. Salbeck, *Appl. Phys. Lett.* **2007**, *90*, 143514.

[47] S. M. Mok, F. Yan, H. L. W. Chan, *Appl. Phys. Lett.* **2008**, *93*, 23310.

[48] L. Du, X. Luo, F. Zhao, W. Lv, J. Zhang, Y. Peng, Y. Tang, Y. Wang, *Carbon N. Y.* **2016**, *96*, 685.

§ 5.7 Supporting information

5.7.1 Results

PI and PI:C5-BTBT thin film characterization

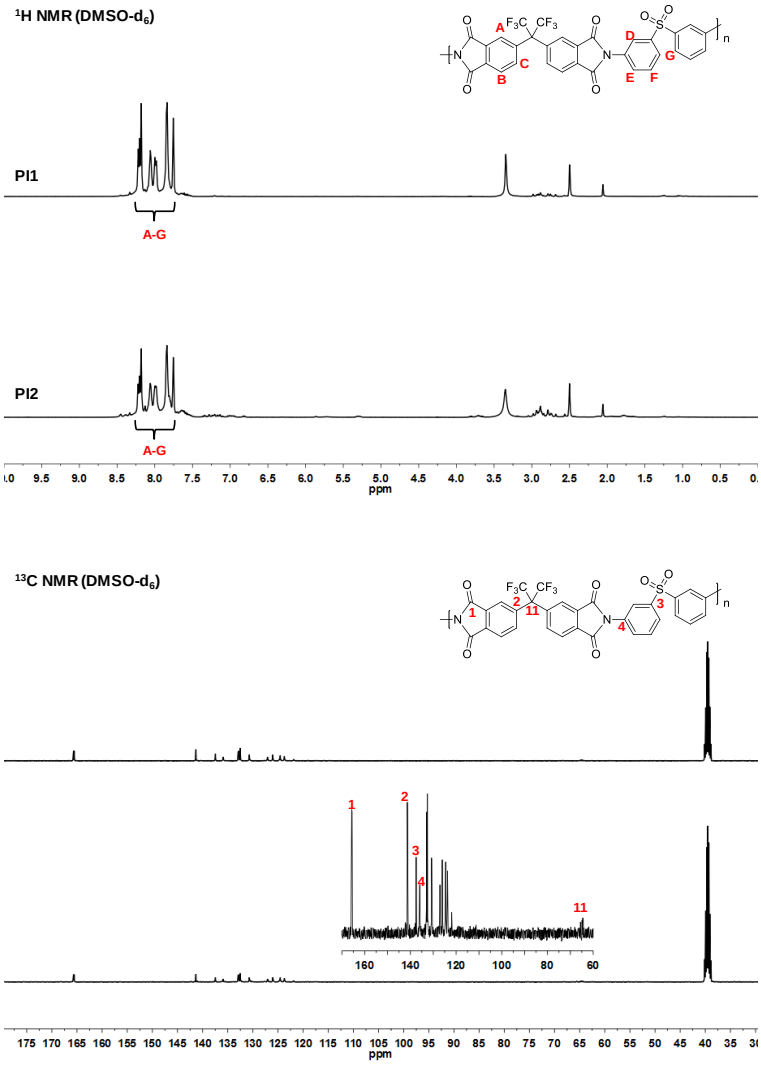

Fig. S5.1. NMR spectra of two MW PI (upper) ^{1}H and (lower) ^{13}C NMR (Bruker Avance 400 MHz in DMSO-d6).

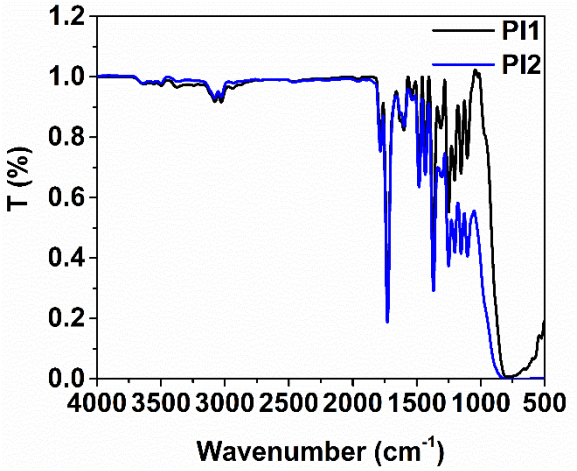

Fig. S5.2. FT-IR spectra of PI having two MWs in transmittance mode (thin films were drop-cast on KBr disc from chloroform).

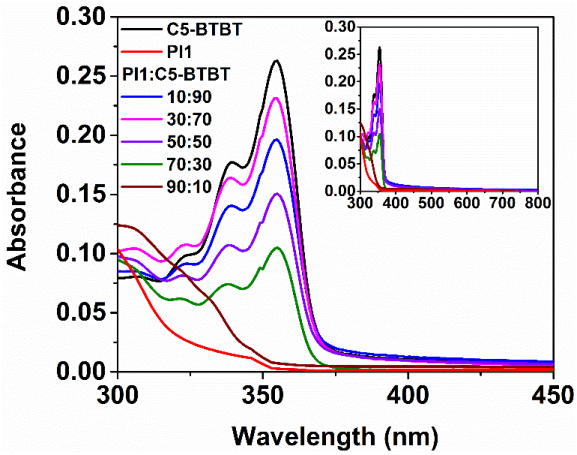

Fig. S5.3. UV-vis spectra of C5-BTBT, PI1, and PI1:C5-BTBT thin films on glass slides spin-coated under the same conditions as those on Si-wafers (inset represents a full wavelength region of the measurements.

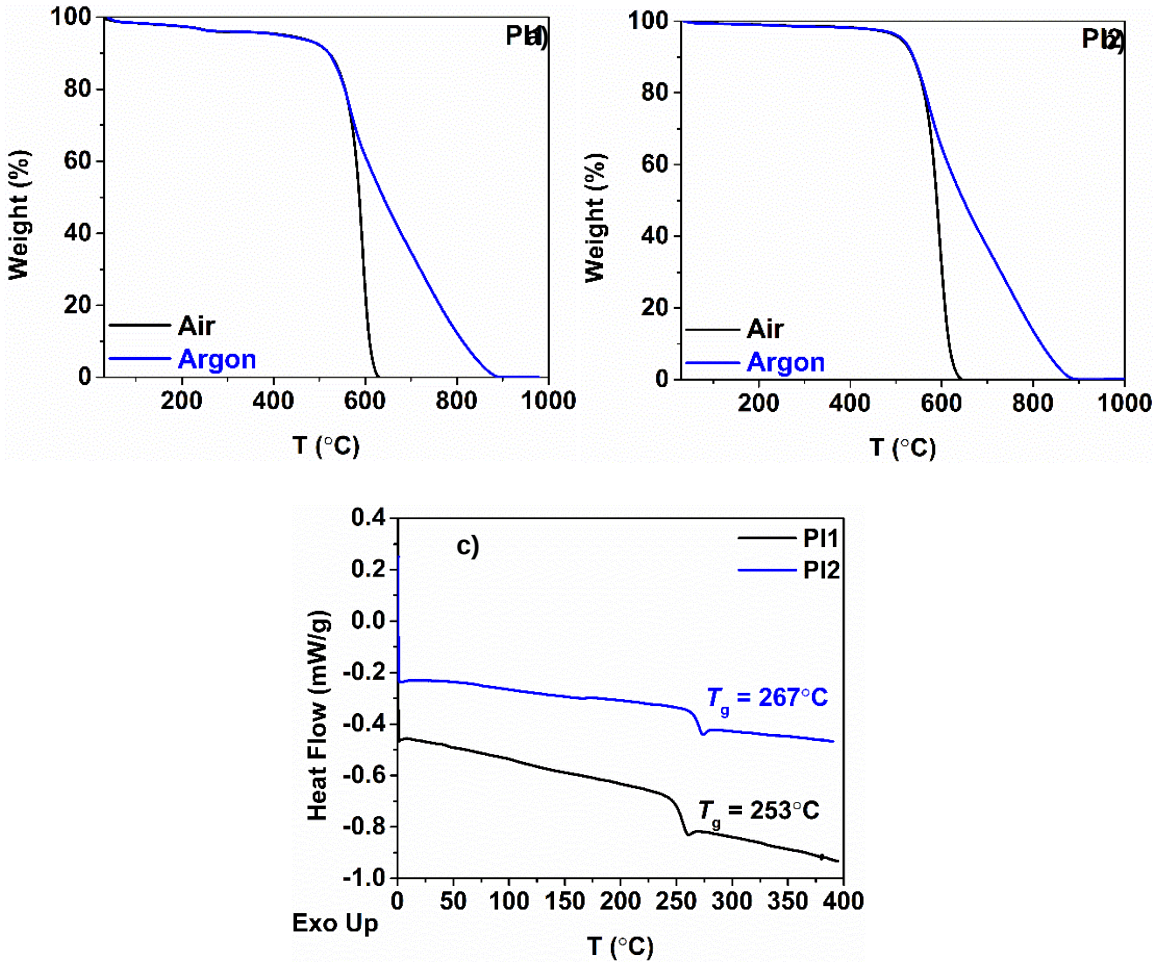

Fig. S5.4. Traces of (a-b) TGA of PI (two MWs) in air and nitrogen (inert) and (c) DSC of PI1 (black line) PI2 (blue line) with reported T_g.

Thin-film morphology and structure

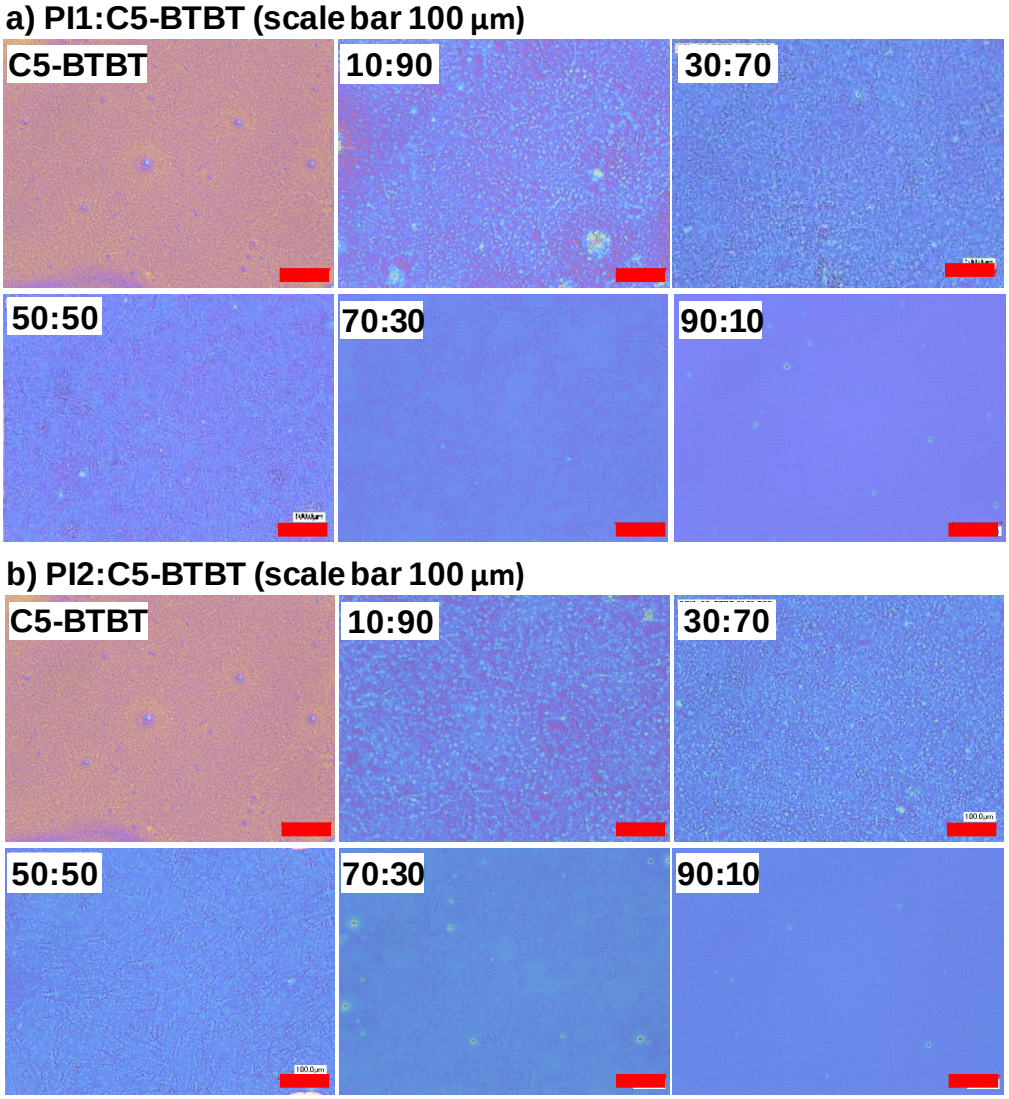

Fig. S5.5. Optical microscope images of (a) PI1:C5-BTBT and (b) PI2:C5-BTBT thin film blends deposited on HMDS modified Si-wafer under the same conditions as thin films used for photoelectrical properties measurements; the same image of a thin film based on C5-BTBT is given in the lower row of both PI:C5-BTBT series.

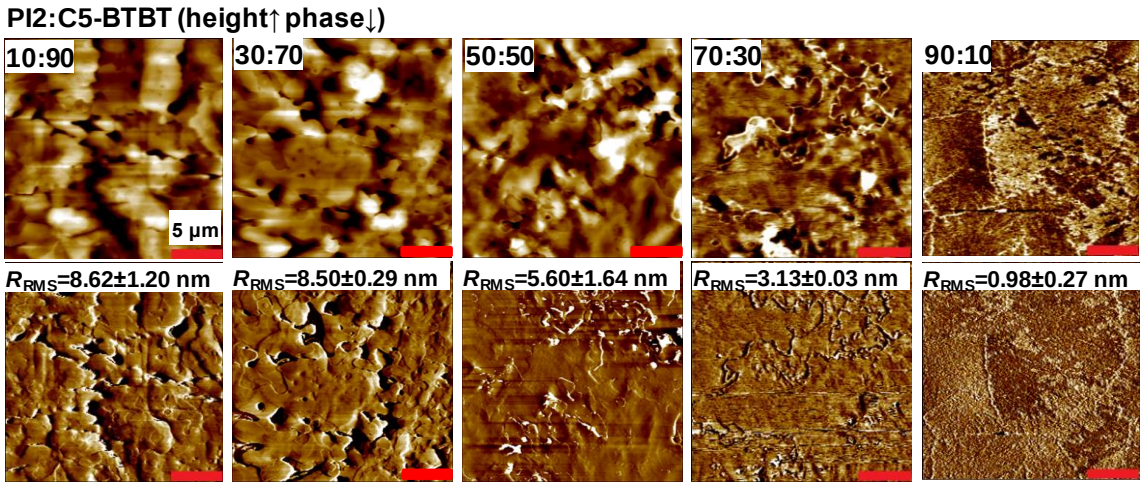

Fig. S5.6. AFM height (upper row) and phase images (lower row) of PI2:C5-BTBT thin films on HMDS modified Si-wafer with reported R_{RMS} values estimated from the 20x20 μm height images.

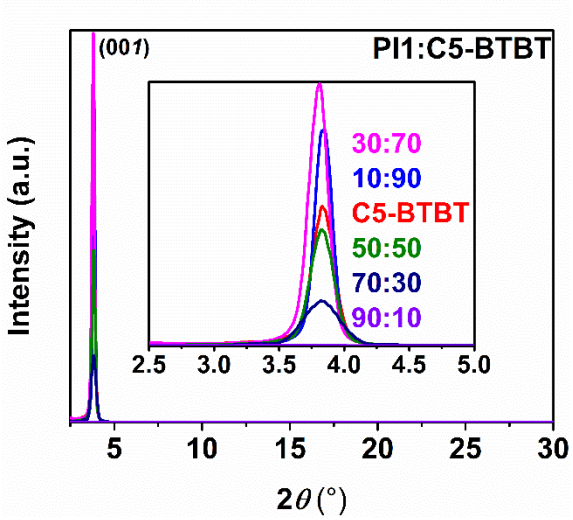

Fig. S5.7. Out-of-plane XRD[2] of PI1:C5-BTBT thin films on HMDS modified Si-wafer; inset plots show a zoom-in of 2θ=2.5-5.0°; 001-designates a preferred molecular orientation in C5-BTBT crystal structure and blended with amorphous PI (2θ=3.8° corresponds to *d*-spacing of 2.3 nm).

Table S5.1 Electrical parameters for C5-BTBT and PI:C5-BTBT PT estimated from the transfer characteristics in the dark

Parameter / OPT	C5-BTBT	PI1:C5-BTBT			
		10:90	30:70	50:50	70:30
Thickness (nm) ±10	210	210	220	220	320
$\mu_{FE,\ DARK}$ ($cm^2\ V^{-1}\ s^{-1}$)	0.28±0.09	0.07±0.01	0.08±0.03	0.12±0.04	1.00±0.17
On/*Off, dark*	10^6	10^5	10^6	10^6	10^6
$V_{Th,\ DARK}$ (V)	-31±5	-29±3	-37±3	-37±5	-33±4
V_{SO} (V)	-19±7	-16±5	-28±3	-24±6	-16±5
$N_{trap,\ dark}$ (cm^{-2})x10^{12}	2.86	2.68	3.50	3.45	3.12
SS (V/dec)	2.5	3.3	2.1	2.9	3.4
D_{it} ($cm^{-2}\ V^{-1}$)x10^{12}	4.0	5.3	3.4	4.7	5.6
			PI2:C5-BTBT		
Thickness (nm) ±10		230	260	210	300
$\mu_{FE,\ DARK}$ ($cm^2\ V^{-1}\ s^{-1}$)		0.19±0.05	0.07±0.02	0.07±0.02	0.92±0.16
On/*Off, dark*		10^5	10^6	10^5	10^6
$V_{Th,\ DARK}$ (V)		-31±6	-28±4	-29±2	-31±4
V_{SO} (V)		-19±7	-16±5	-16±3	-14±5
$N_{trap,\ dark}$ (cm^{-2})x10^{12}		2.9	2.6	2.7	2.9
SS (V/dec)		2.8	2.5	3.3	3.2
D_{it} ($cm^{-2}\ V^{-1}$)x10^{12}		4.5	4.1	5.4	5.2

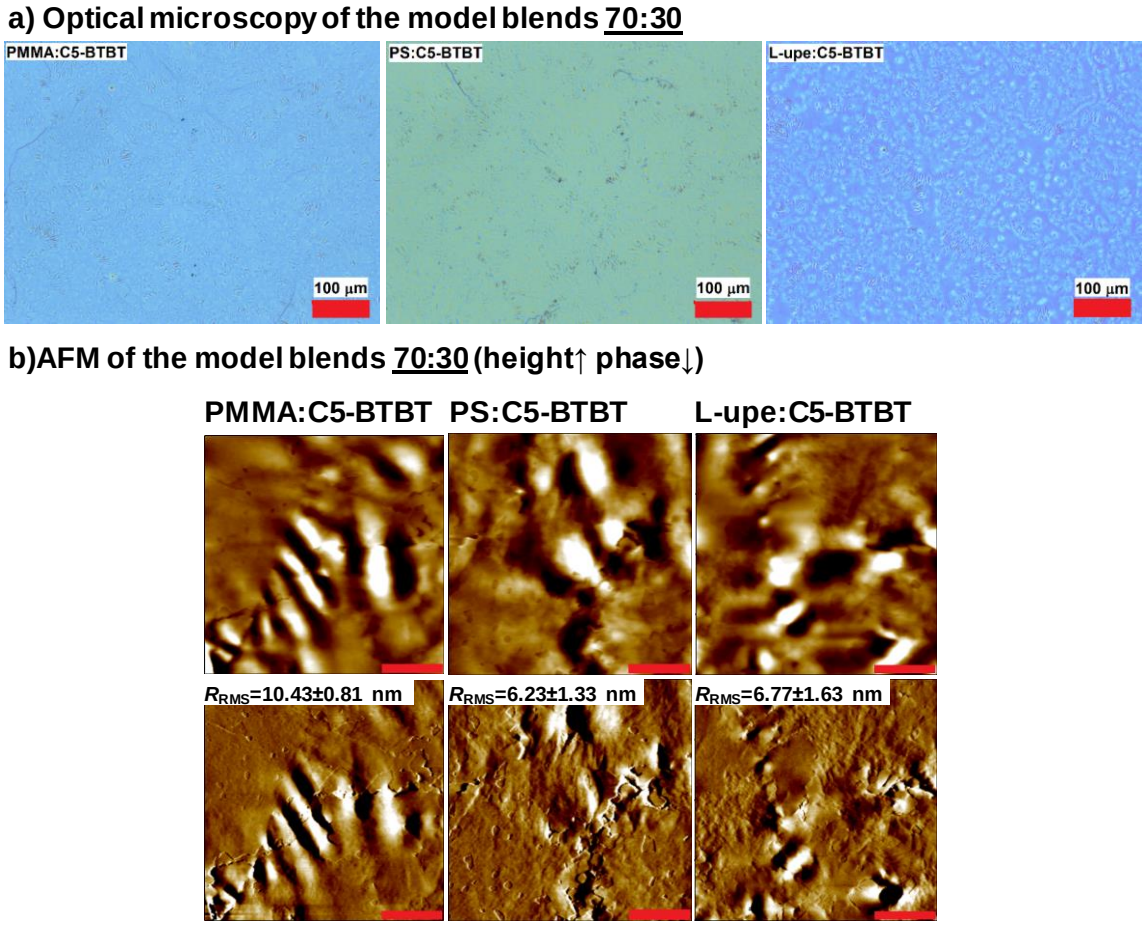

Fig. S5.8. (a) Optical microscopy images of 70:30 model blend thin film blends deposited on HMDS modified Si-wafer under the same conditions as thin films of 70:30 PI:C5-BTBT blends and (b) AFM height and phase images of 70:30 model blend thin films on HMDS modified Si-wafer (a 5 µm scale bar of 20x20 µm height and phase images with R_{RMS} values included).

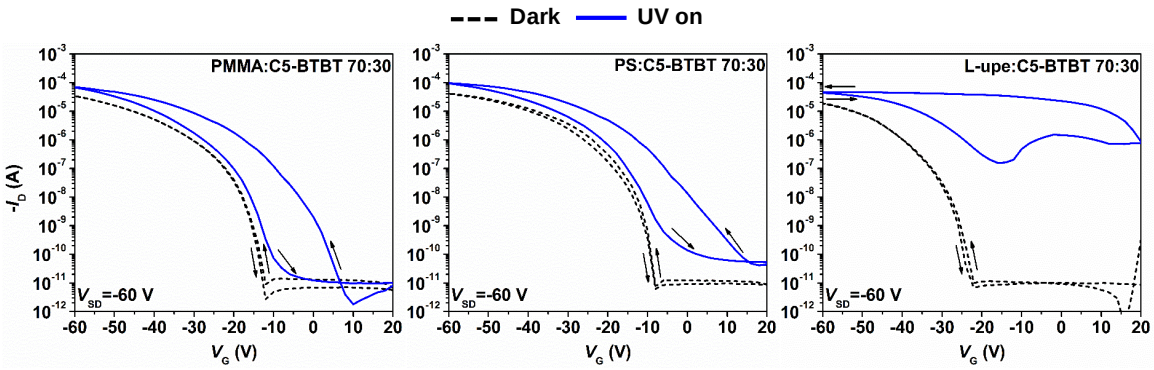

Fig. S5.9. Transfer characteristics of OPTs fabricated with the model polymer:C5-BTBT blends (blending ratio 70:30).

Table S5.2. Estimated parameters of PTs fabricated with the polymer:C5-BTBT blends (70:30 blending ratio) to investigate the mobility increase.

	PMMA:C5-BTBT 70:30	PS:C5-BTBT 70:30	L-upe:C5-BTBT 70:30
$\mu_{FE,\ DARK}$ ($cm^2\ V^{-1}\ s^{-1}$)	0.417±0.004	0.353±0.05	0.355±0.05
On/Off dark	10^6	10^6	10^6
$V_{Th,\ DARK}$ (V)	-26±3	-19±1	-36±1
V_{SO} (V)	-9±3	-6±1	-22±1
$N_{trap,\ dark}$ (cm^{-2})x10^{-12}	2.43	1.75	3.35
SS (V/dec)	3.5	2.7	3.1
D_{it} ($cm^{-2}\ V^{-1}$)x10^{-12}	5.7	4.4	5.1

Table S5.3 Photoelectrical parameters of PI1:C5-BTBT OPTs given as average values determined from at least five devices

OPT	I_{phc}/I_D @ V_G=20 V (x10^6)	I_{phc}/I_D @ V_G=0 V (x10^6)	R (AW^{-1}) @ V_G=0 V	τ_{r1} (s)*	τ_{r2} (s)*	τ_{d1} (s)*	τ_{d2} (s)*
C5-BTBT	0.077	2.1	10.6±2.5	16.17±7.96	-	4.6±0.9	76.4±21.5
				PI1:C5-BTBT			
10:90	1.8	1.2	5.5±1.1	0.95±0.24	20.3±6.5	3.2±0.6	131.9±23.4
30:70	0.94	32	4.6±0.8	0.74±0.11	16.7±6.3	2.2±0.2	99.6±12.8
50:50	0.37	4.7	6.4±0.8	1.2±0.2	13.0±10.6	2.8±0.4	121.1±10.9
70:30	2.2	6.6	30.6±2.6	2.43±0.72	19.4±17.7	5.4±0.4	149.3±9.5

*Coefficient of determination R^2 resulted from the bi-exponential fitting of the experimental results are: 0.98-1 for the response times and 0.99-1 for the decay times.

Table S5.4 Photoelectrical parameters estimated from the transfer curves generated under P_{UV} of 3 $mWcm^{-2}$ and 0.12 $mWcm^{-2}$ to probe the UV light sensitivity of PI:C5-BTBT OPTs (results represent maximum values of one OPT subjected to illumination of the low and high UV light intensity).

Parameter	I_D/I_{phc} (10^6)				R (AW^{-1})	
	@ V_G=20 V	@ V_G=0 V	@ V_G=20 V	@ V_G=0 V	@ V_G=0 V	
OPT / P_{UV} ($mWcm^{-2}$)	3		0.12		3	0.12
C5-BTBT	0.11	1.5	0.0089	0.25	13	209
PI1:C5-BTBT						
10:90	1.7	2.0	0.66	1.4	5.5	104
30:70	1.0	3.3	0.57	2.6	6.1	116
50:50	0.53	0.94	0.26	0.62	5.7	93.2
70:30	0.041	0.19	0.011	0.85	30	429

Table S5.3 Electrical parameters for C5-BTBT and PI:C5-BTBT OPTs estimated from the transfer characteristics generated in the dark under 50 cycles of forward/reverse V_G sweep (results represent maximum values of one OPT subjected to 50 cycles).

Parameter / OPT	Cycle	C5-BTBT	PI1:C5-BTBT			
			10:90	30:70	50:50	70:30
$\mu_{FE, DARK}$ ($cm^2 V^{-1} s^{-1}$)	1st	0.22	0.091	0.13	0.10	0.83
	50th	0.29	0.12	0.17	0.17	1.2
On/*Off, dark*	1st	10^6	10^5	10^6	10^6	10^6
	50th	10^5	10^5	10^8	10^7	10^6
$V_{Th, DARK}$ (V)	1st	-27	-23	-37	-30	-36
	50th	-39	-31	-41	-41	-43
V_{SO} (V)	1st	-18	-10	-26	-20	-18
	50th	-30	-18	-30	-28	-26

Equations

The threshold voltage, V_{Th}, was estimated from the slope of $I_D^{½}$ vs. V_G curves. The turn-on voltage (V_{SO}), was determined from the slope of the logI_D-V_G transfer curves while the field-effect hole mobility in saturation regime (μ_{FE}), was estimated from using equation [1]:

$$\mu_{FE} = \frac{2L}{W} \cdot \frac{I_D}{C_{ox}(V_G - V_{Th})^2} \qquad \text{(Eqn. S5.1)}$$

where L and W are channel length and width in cm, respectively; C_{ox} is the capacitance per unit area of the SiO_2 dielectric layer (15 $nFcm^{-2}$). The charge trap density at the SiO_2/channel interface in the dark ($N_{trap,dark}$) was determined by [2]:

$$N_{trap,\ dark} = \frac{|V_{Th}|C_{ox}}{q} \qquad \text{(Eqn. S5.2)}$$

where q is an elementary charge.

The slope of the linear part of the logI_D-V_G curves at V_G<V_{Th} was used for estimation of the inverse subthreshold slope (*SS*) [3]:

$$SS = \left(\frac{dlogI_D}{dV_G}\right)^{-1} \qquad \text{(Eqn. S5.3)}$$

The density of deeper traps at the interface (D_{it}) was computed using [2][4]:

$$D_{it} = \left[\frac{qSSlog(e)}{k_bT} - 1\right]\frac{C_{ox}}{q^2} \qquad \text{(Eqn. S5.4)}$$

where T and k_B are absolute temperature and the Boltzmann constant, respectively.

Photosensitivity, I_{phc}/I_D ratio, was calculated using [5]:

$$Ratio = \frac{I_{phc}-I_D}{I_D} \qquad \text{(Eqn. S5.7)}$$

Photoresponsivity, R, of OPTs, was estimated using [5]:

$$R = \frac{I_{phc} - I_D}{P_{UV} \cdot A} \qquad \text{(Eqn. S5.8)}$$

where P_{UV} is the intensity of the incident UV light and A (LxW) is the effective area illuminated by UV light.

5.7.2 References

[1] C. D. Dimitrakopoulos, P. R. L. Malenfant, *Adv. Mater.* **2002**, *14*, 99.

[2] J. Smith, R. Hamilton, Y. Qi, A. Kahn, D. D. C. Bradley, M. Heeney, I. McCulloch, T. D. Anthopoulos, *Adv. Funct. Mater.* **2010**, *20*, 2330.

[3] A. Takshi, J. D. Madden, *J. Comput. Electron.* **2010**, *10*, 154.

[4] X. Liu, G. Dong, L. Duan, L. Wang, Y. Qiu, *J. Mater. Chem.* **2012**, *22*, 11836.

[5] K.-J. Baeg, M. Binda, D. Natali, M. Caironi, Y.-Y. Noh, *Adv. Mater.* **2013**, *25*, 4267.

6 EFFECTS OF GATE DIELECTRIC SURFACE MODIFICATION ON PHOTOTRANSISTORS WITH POLYMER-BLENDED 2,7-DIPENTYL [1]BENZOTHIENO[3,2-B][1]BENZOTHIOPHENE SEMICONDUCTOR THIN FILMS

In this chapter, the effects of the gate dielectric surface modification using organosilanes on photoelectrical and dynamic characteristics of a solution-processed UV responsive organic phototransistors using polyester polymer/2,7-dipentyl[1]benzothieno[3,2-b][1]benzothiophene blend as the active channel

material is presented. This chapter is based on the paper published in the peer-reviewed journal, as follows: “D. Ljubic, V. Jarvis, C.S. Smithson, Y. Wu, S. Zhu, Effects of gate dielectric surface modification on phototransistors with polymer-blended benzothieno[2,3-b]benzothiophene semiconductor thin films, *Organic Electronics*., **2017**, 44, 253-262 (DOI: 10.1016/j.orgel.2017.02.027). Reprinted with permission from *Organic Electronics*, **2017**, 44, 253-262. Copyright © 2017, Elsevier.

Author contributions

Darko Ljubic designed and conducted the experiments, and wrote the first draft of the manuscript under the guidance of Dr. Shiping and Dr. Yiliang Wu. Victoria Jarvis performed the 2D XRD analysis and provided a knowledge base for the understanding of XRD results. Dr. Chad S. Smithson provided the first revision of the manuscript. Dr. Nan-Xing Hu provided valuable advices in understanding the chemistry of surface modification and revised the manuscript. The final revision was provided by Dr. Wu and Dr. Zhu.

§ 6.1 Abstract

In the present work, we investigated effects of the dielectric/semiconductor interface modification on the photoelectrical properties of phototransistors comprising a UV responsive semiconductor blend 2,7-dipentyl[1]benzothieno[2,3-

b][1]benzothiophene (C5-BTBT) and a linear unsaturated polyester (L-upe). Using various self-assembly monolayers with different end groups at the dielectric/semiconductor interface we modulated the drain photocurrent and response times under the UV light illumination of phototransistors. Treatment of the SiO_2 dielectric surface with organosilanes lead to the variation of the max mobility in the dark 0.10-0.18 $cm^2 V^{-1} s^{-1}$ and under UV light 0.08-0.50 $cm^2 V^{-1} s^{-1}$. Interestingly, detailed crystal structure analysis using 2D X-ray diffraction and photoelectrical characterization revealed that mobility in the dark predominantly depends on the alignment of C5-BTBT crystallites at the interface. Under UV light, the mobility increased with the electron withdrawing/donating nature of the SAM end-functional group. Additionally, chemical modification of the SiO_2 dielectric surface increased photocurrent relaxation/decay times upon UV light removal while retaining fast response times when exposed to UV light, which enhanced memory properties of fabricated phototransistors (fast UV response=writing and long relaxation=long data storage).

§ 6.2 Introduction

The organic thin film transistor (OTFT) is an important building block of modern consumer electronics. Dynamic development of OTFTs over the past two and a half decades is justified by a variety of organic materials and their tunable properties for the fabrication of large-area electronics via printing, solution deposition, and melt processing [1]. OTFTs are applied as backplanes for OLED

displays, flexible e-paper, sensors, re-writable memory devices and radio frequency identification tags [2–4]. Furthermore, OTFTs are a great platform for phototransistors (PTs) that utilize the unique structure of field-effect transistors (FETs), thus, broadening their functionalities [5][6].

When quantifying the performance of OTFTs, field-effect charge carrier mobility (μ_{FE}) is one of the most important properties and it has been constantly improved through molecular design and device engineering [7][8]. The mobility for small molecule-based OTFTs reported to date is as high as 17.2 $cm^2V^{-1}s^{-1}$ for vacuum deposited tridecyl substituted [1]benzothieno[3,2-b][1]benzothiophene (asymmetric, C13-BTBT) [9], and 43 $cm^2V^{-1}s^{-1}$ [10] for solution processed OTFTs based on C8-BTBT. Recently Kim et al [11] reported a thienoisoindigo-naphthalene polymer based OTFT with an ultra-high mobility of 14.4 $cm^2V^{-1}s^{-1}$ utilizing a high-k polymer dielectric. FETs based on a-Si:H semiconductor have a mobility of ~ 1 $cm^2V^{-1}s^{-1}$, thus, OTFTs can largely exceed the performance of the Si-based FETs [12]. Constant improvements in performance and design of OTFT and PTs are critical to reaching higher-mobility, increased photosensitivity, and better environmental/operation stability [13–15].

Many research groups have reported different approaches for mobility enhancement via i) semiconductor molecular design [16] and use of additives [17], or ii) control of molecular ordering in a crystal lattice and thin film morphology by altering processing conditions [18][19]. Furthermore, interface engineering using organosilanes, photochromic molecules, polymeric buffer layers and metal oxides is sought as an effective way to improve mobility while avoiding lengthy

optimizations of fabrication conditions and complex chemical synthetic routes [20–23]. Active channel/dielectric interface is one of the most important interfaces in OTFTs that determines mobility. This is particularly true since OTFTs operate in accumulation mode, i.e. injected charge carriers are accumulated at the dielectric/channel interface when a bias voltage is applied, forming a conductive channel. Molecular ordering of the first few layers of semiconductor, at the active channel interface, determines overall mobility in the channel. It is demonstrated that mobility has a strong dependence on the presence of a self-assembled monolayer (SAM) and resulting surface energy of the dielectric [24][25]. The surface energy of the dielectric layer controls semiconductor crystal growth. It can be easily tuned by the SAM with different end groups that can enhance molecular ordering at the interface and, thus, increase the mobility [26][27]. Additionally, the density of accumulated charge carriers at the interface has been demonstrated to be controlled by dipole moments of the end functional groups present in the SAM, which, in turn, improved OTFTs performance [28]. Dipole moments of the end functional groups in the SAM can also enhance mobility via built-in electric field affecting the threshold and the turn-on voltage of the OTFT [29].

The most studied effect of SAM on mobility and overall performance of OTFTs was reported for pentacene and P3HT based OTFTs in the dark [30]. To the best of our knowledge, little or no effort was made to investigate the effect of dielectric surface modification using organosilanes on the performance of solution processed PTs. There is a lack of knowledge about the influence of the dielectric surface treatment on charge carrier generation/separation, drain photocurrent,

subthreshold characteristics, field-effect mobility, and response times of PTs under the light illumination. This is very important for the design, development, and operation optimization of PTs used as sensors and optically writable memory devices.

Herein, we report on the effects of the dielectric surface treatment with eight different SAMs on the photoelectrical characteristics of field-effect hole mobility and PT performance under UV light (λ=365 nm and 3 mW cm^{-2}) and in the dark. The semiconductor system was a previously reported blend of linear unsaturated polyester (L-upe) and 2,7-dipentylbenzo[b]benzo[4,5]thieno[2,3]thiophene semiconductor (C5-BTBT) (Fig. 6.1a) [31]. We employed a variety of organosilanes with different end groups to form SAM covalently bonded to the SiO_2 dielectric surface via a silanization reaction (Fig. 6.1b). Additionally, PTs with a bare SiO_2 dielectric (referred as OH groups) were fabricated and characterized as well. Based on findings in the work reported previously [31], that electron withdrawing (EW)/electron donating (ED) functional groups present in the channel significantly affect photoelectrical characteristics of UV responsive PTs, we purposely selected organosilanes with functional groups having strong EW/ED properties. Moreover, we compared the performance of those PTs to that of devices having a bare SiO_2 or an electroneutral SAM.

§ 6.3 Experimental

6.3.1 Materials

Surface modifying agents (organosilanes): hexamethyldisilazane (CH_3), trichloro(phenethyl)silane (R'-Ph), (3-Chloropropyl)trimethoxysilane (R''-Cl), (3-aminopropyl)trimethoxysilane (R''-NH_2), (3-mercaptopropyl)trimethoxysilane (R''-SH), trichloro(phenyl)silane (Ph), and 4-(chloromethyl)phenyl trichlorosilane (Ph-CH_2-Cl) were purchased from Sigma Aldrich (Canada), except for 2-(4-chlorosulfonylphenyl)ethyl trichlorosilane (R'-Ph-SO_2Cl), which was purchased from Gelest (Morrisville, PA, US). Acetone, chloroform, and isopropanol were purchased from Caledon (Canada) while anhydrous toluene and 1,1,2,2-tetrachloroethane (TCE) were obtained from Sigma Aldrich (Canada). All organosilanes and solvents were used as received. Analytical grade small molecule semiconductor 2,7-dipentylbenzo[b]benzo[4,5]thieno[2,3]thiophene (C5-BTBT) was synthesized following the reported procedures [32][33]. Linear unsaturated polyester (L-upe, MW=50000), comprised of propoxylated bisphenol A and fumaric acid monomer units, was kindly supplied by the Xerox Research Center of Canada. Chemical structures of the active channel materials and organosilanes are displayed in Fig. 6.1a. Highly n-doped silicon wafers (Ø4 inch) with 200-nm thermally grown SiO_2 as a dielectric layer were purchased from Silicon Quest International (San Jose, CA, USA).

6.3.2 Preparation of L-upe+C5-BTBT blend

The L-upe+C5-BTBT blend (1:1) was prepared according to our previously reported procedure [31] summarized in Supp. Info. We purposely used a 1:1 blend ratio since our previous studies showed that this ratio gave the best quality thin films formed by spin-coating onto HMDS modified Si wafers [33].

6.3.3 Modification of SiO_2 dielectric surface and phototransistors fabrication

Substrates (1x1 inch) were thoroughly cleaned in cold acetone and isopropanol, followed by a 5 min sonication in a sonication bath, successively in hot acetone, isopropanol then chloroform. The final cleaning step of substrates was the treatment with plasma/UV for 2 min in plasma cleaner PDC-32G (Harrick Plasma, USA). Thereafter, the substrates were soaked in DI water for 10 min to saturate active sites on the surface of SiO_2, forming hydroxyl end groups. Air dried substrates (two for each type of organosilanes) were immersed in a freshly prepared organosilane solution in toluene (0.12 mol L^{-1}). Silanization reaction was optimized to carry out for 30 min at 60°C. Upon completion, the substrates were rinsed with fresh toluene, sonicated (sonication bath) also in fresh toluene for 2 min to remove any excessive layers of organosilane on the surface of SiO_2, rinsed again with toluene and air dried. The result was a SAM covalently bonded to the substrate(s) via strong Si_s-O-Si bonds (Fig. 6.1b). Substrates were then dried in a vacuum oven for 20 min at 70°C to remove any residual toluene.

The top-contact bottom-gate architecture was used for all PTs, fabricated in ambient conditions (Fig. 6.1c). L-upe+C5-BTBT blend-based solution in TCE was spin-coated (SCS P-6700 spin-coater, Sitek Process Solutions, Inc., CA, USA) onto SAM-modified substrates under the following conditions: 120 sec solution wetting of the substrate, total spinning time 120 s at 2000 rpm, ramp time 2 s. Two substrates treated only with plasma/UV and DI water (no organosilane treatment) were used to fabricate the control PTs. The thickness of the L-upe+C5-BTBT thin-films on all substrates was 250±10 nm. The semiconductor layer was dried in a vacuum oven for 30 min at room temperature to remove any residual solvent. Source-drain Au electrodes of 60 nm were deposited on top of the L-upe+C5-BTBT thin films through a shadow mask using electron beam evaporation system (Kurt J. Lesker, USA), yielding 930±10 μm and 85±5 μm active channel width and length, respectively.

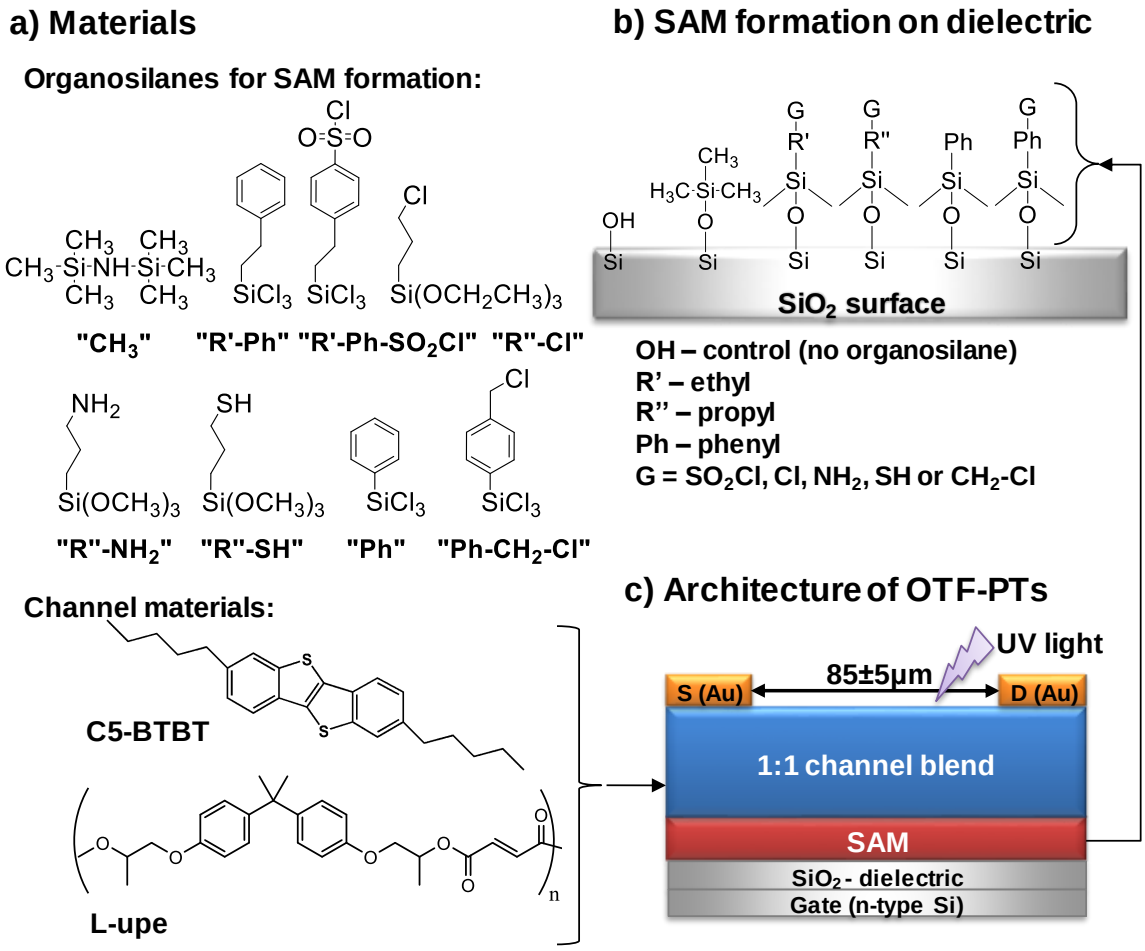

Fig. 6.1. Schematic depiction of (a) chemical structures of active channel materials and organosilanes used in this work (abbreviations for SAMs used in the further text are given under quotation marks), (b) a covalently bonded SAM molecule to SiO_2 surface (general representation), and (c) a staggered top-contact-bottom-gate OTF-PT structure (S and D represent source and drain electrodes, respectively).

PTs devices with different SAMs at the dielectric/active channel interface but the same active channel material is denoted as OH (control), CH_3, R'-Ph, R'-Ph-

SO_2Cl, R''-Cl, R''-NH_2, R''-SH, Ph, and Ph-CH_2-Cl (Fig. 6.1a), corresponding to the end group perpendicularly oriented toward the active channel and substrate (for R', R'' and Ph refer to Fig. 6.1b). In this work, we assumed that SAM formed on the SiO_2 surface has predominately an ideal structure depicted in Fig. 6.1b, even though there are other possible structures formed over the course of the silanization reaction, as reported in the reference [34].

6.3.4 Characterization

Complete physical and photoelectrical characterization of PTs was performed using previously reported techniques [31][33] and is summarized in Sup. Info. Contact angles of water and diiodomethane on all SAM-modified dielectric surfaces were measured on a Krüss Drop Shape Analysis System DSA10 instrument by the pendant drop method at room temperature. Contact angles of water and diiodomethane droplets (~8 µL) of at least five spots on each of the two substrates were measured. To calculate the surface energy using water and diiodomethane contact angles, the instrument software DSA10 (version 1.80.0.2) programmed with the Owens-Wendt-Rabel-Kaelble method was used. Common values for polar and dispersive components of water (Gebhardt) and diiodomethane (Owens) used for the mathematical model were found in the database of the software. Contact angles for the control and organosilane treated dielectric surfaces are given in Table S6.1, reflecting successful surface modification of the SiO_2 surface. Additionally, surface energies (γ_S) of organosilane treated SiO_2 surfaces are in the

range of 38-49 mJ/m^2 while the control surface has an expectedly higher surface energy of 66 mJ/m^2. The γ_S values for the modified substrates are given in Table S6.1, which are consistent with the values reported in the literature [25][29].

Crystal structure data of L-upe+C5-BTBT and pure C5-BTBT thin films spin-coated on SAM-modified SiO_2 surfaces were collected in a two-dimensional X-ray diffractometer (XRD^2) equipped with a Bruker Smart6000 CCD area detector, Bruker 3-circle D8 goniometer, Rigaku RU200 Cu K$\bar{\alpha}$ rotating anode, and Göebel cross-coupled parallel focusing mirrors. Experimental conditions were as follows: scan type Omega sweep (from 0.5°-13°), frame Exposure: 300s, 2θ = 2.5° - 35°, at the detector distance of 11.86 cm and power setting 90 mA and 50 kV.

§ 6.4 Results and discussion

6.4.1 Photoelectrical characteristics of PTs

To investigate the effect SAM have on the performance of UV responsive L-upe+C5-BTBT blend-based PTs, we evaluated their photoelectrical characteristics in the dark and under UV light illumination (λ=365 nm, 3 mW cm^{-2}). Fig. 6.2 is an overlay of output characteristics of all the PTs in the dark and under UV light, at the gate voltage V_G= - 60 V, while a source-drain voltage (V_{SD}) was swept from 20 to -60 V. I_D – V_{SD} curves for each PT are given in Fig. S6.1, showing typical output characteristics for p-type PTs at V_G 20 – -60 V (10 V steps) and a V_{SD} 20 – -60 V sweep span. All output curves generated in the dark (solid curves) and under UV

light (dotted lines) are characterized by linear (ohmic contact) and saturation regimes. Some deviation from linearity (s-shape curves) was observed for all the devices. This can be attributed to contact resistance induced by the insulating L-upe polymer at the contact region. Cut-off bias voltage for PTs in the dark and under UV light was -40 V and 20 V, respectively.

Output characteristics for all the PTs showed that I_D significantly increased under UV light at all V_G, because of the photo charge carriers generated in the channel and resulting photovoltaic effect, which is consistent with our previous report [31]. More interestingly, the level of I_D generated in the channel, in the dark, and under UV light, was strongly dependent on the type of SAM at the interface. Maximum I_D (dark) achieved at V_G= -60 V, was more than five orders of magnitude higher, when R''-SH SAM was used, compared to the control PT (Fig. 6.2a). Under UV light illumination, the maximum I_D in PTs with R'-Ph-SO_2Cl and R''-Cl SAMs was more than three orders of magnitude higher than the control device (Fig. 6.2b). PTs with OH groups at the interface had lowest I_D due to strong charge trapping effects of hydroxyl groups.

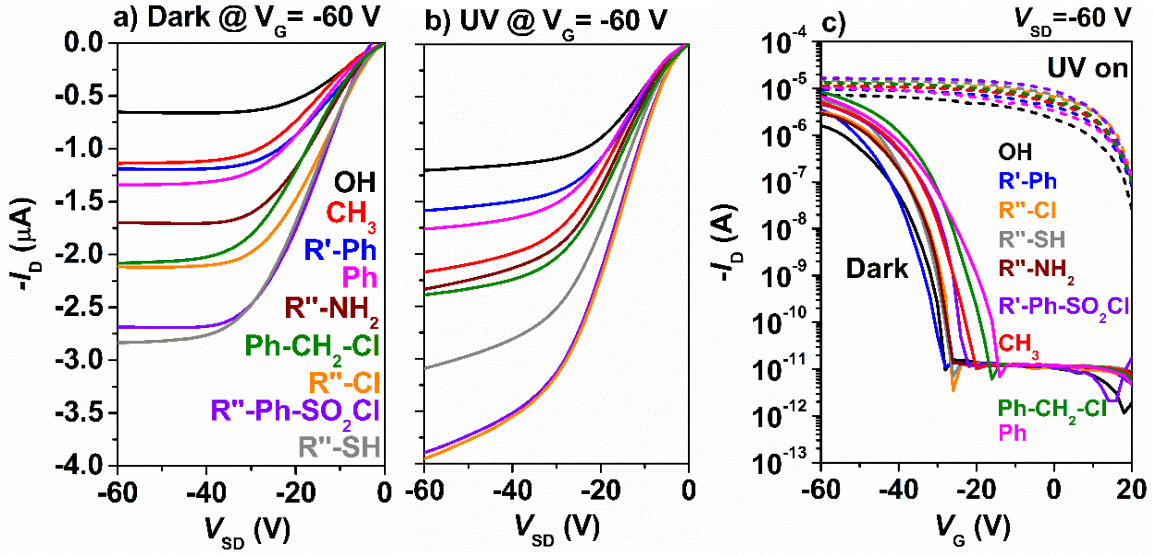

Fig. 6.2. Overlay of the output curves at V_G= -60 V (a) in the dark and (b) under UV light (λ=365 nm and 3 mW cm^{-2}), (c) transfer curves (in dark-solid line and under UV light-dashed line, at V_{SD}= -60 V) for L-upe+C5-BTBT PTs with different SAMs at the dielectric/active channel interface; scan rate was 6 Vs^{-1} (*L*/*W*=85/930 μm).

Investigation of the transfer characteristics offers deeper insights into the effect of different dielectric surface treatment on the photoelectrical properties of PTs. Fig. 6.2c displays typical I_D vs V_G curves at V_{SD}= -60 V in the dark (solid lines) and under UV light (dashed lines). The applied source-drain voltage of -60 V (L/W=85/930) yielded an electric field of 6.7 x10^3-7.5x10^3 V cm^{-1} that is in line with electric fields reported in the literature for SAM treated dielectric/channel interfaces of OTFTs: 3.3x10^3-1.7x10^4 Vcm^{-1} [29] and 6.0x10^3-1.0x10^4 Vcm^{-1} [35]. Transfer curves for each PT, including hysteresis investigation, are given in Fig. S6.2a-i. In this work and in our previous report, L-upe+C5-BTBT PTs with HMDS treated

dielectric surface (CH_3 in this work) were hysteresis free in the dark but showed large lower-back hysteresis under UV light. Therefore, the dielectric surface treatment did not change forward/reverse characteristics of I_D during V_G sweep in the dark, at a scan rate of 6 V s^{-1}.

Transfer characteristics of all the PTs were used to estimated μ_{FE} in the saturation regime, On/Off ratio, threshold voltage (V_{Th}), turn-on voltage (V_{SO}), the inverse subthreshold slope (*SS)*, charge trap density ($N_{trap,dark}$) and density of deeper traps at the interface (D_{it}). These values are summarized in Table 6.1. Commonly used equations are shown in Supp. Info (Eqns. S6.1-S6.4). It should be noted that the estimated mobility for the devices under the light illumination should be considered as an apparent mobility since the output and transfer curves exhibited non-ideal field-effect transistor behavior. Using the same equation to calculate the apparent mobility is easier for us to compare the effects of different surface treatments on the performance of PTs.

Table 6.1 Mean values for the photo-electrical properties of L-upe+C5-BTBT based PTs with different SAMs at the dielectric/active channel interface extracted from the transfer curves of at least five devices (each device was subjected to 10 sweeping cycles of the gate voltage).

SAM	Parameter									
	μ_{FE} (cm^2 V^{-1} s^{-1}) (max)		On/Off (dark)	V_{Th} (V)		V_{SO} (V)		SS (V/dec)	D_{it} (cm^2V^{-1}) x10^{12}	$N_{trap,dark}$ (cm^{-2}) x10^{12}
	Dark	UV on		Dark	UV on	Dark	UV on			
OH	0.05±0.02 (0.07)	0.08±0.01 (0.10)	10^5	-35±1	23±1	-24±2	>20	2.7	4.5	3.2
CH_3	0.06±0.01 (0.08)	0.11±0.04 (0.15)	10^5	-32±3	21±1	-21±2	>20	3.3	5.3	3.0
R'-Ph	0.10±0.01 (0.12)	0.13±0.01 (0.16)	10^5	-35±1	23±1	-26±1	>20	2.2	3.6	3.2
R'-Ph-SO_2Cl	0.07±0.01 (0.08)	0.34±0.01 (0.50)	10^5	-28±3	23±1	-21±1	>20	1.7	2.8	2.6
R''-Cl	0.08±0.01 (0.09)	0.29±0.10 (0.44)	10^5	-32±1	24±1	-23±1	>20	2.3	3.8	3.0
R''-NH_2	0.06±0.01 (0.08)	0.19±0.01 (0.21)	10^5	-31±1	24±1	-24±1	>20	1.9	3.1	2.9
R''-SH	0.13±0.03 (0.18)	0.29±0.04 (0.35)	10^5	-31±2	23±1	-24±1	>20	2.0	3.2	3.0
Ph	0.09±0.01 (0.11)	0.06±0.01 (0.08)	10^5	-31±3	22±1	-12±1	>20	5.1	8.2	2.9
Ph-CH_2-Cl	0.10±0.01 (0.12)	0.18±0.05 (0.23)	10^5	-26±1	23±1	-14±1	>20	3.4	5.4	2.4

From Table 6.1, one can see that mobility in the dark was slightly dependent on the type of the surface treatment while under the UV light this dependence was more evident. Fig. 6.3a displays an overlay of the average mobility of PTs, in the dark and under UV light. Average and max mobility in the dark were highest when the R''-SH SAM was used, while under UV light average mobility was highest when R'-Ph-SO_2Cl was used (max 0.50 cm^2 V^{-1} s^{-1}). All PTs have a larger V_{Th} that originates from the C5-BTBT semiconductor and the V_{Th} slightly shifted toward

positive values by blending with L-upe. V_{Th} of C5-BTBT OTFT fabricated using HMDS organosilane (CH_3 SAM) is -31±5 V (our work, See Supp. Info, Fig. S6.2j) and -21 V in the literature [32]. In the dark, Ph and Ph-CH_2-Cl SAMs shifted V_{Th} and V_{SO} the most toward more positive values, especially Ph, even though it is a neutral SAM. Most likely, the better formation of the SAM resulted in the lower interface trap density, which is indicated by low $N_{trap,dark}$ values for these two SAMs. V_{Th} and V_{SO} under UV light were not significantly affected by SAMs, indicating a predominant influence of the bulk of the channel on these parameters. Additionally, densities of the photogenerated charge carriers (ΔN_{trap}) in Table 6.2 were also not affected by SAM, since ΔN_{trap} is related to the type of the semiconductor, its concentration in the blend, and intensity of the light.

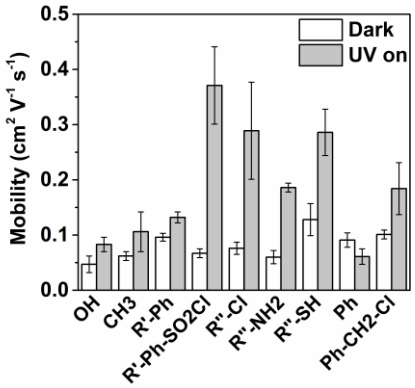

Fig. 6.3. Average field-effect hole mobility for L-upe+C5-BTBT PTs as a function of SAM present at the dielectric/active channel interface; mobility is extracted from the transfer curves in saturation regime in the dark (empty columns) and under UV light (grey columns); error bars represent sample standard deviations calculated from transfer characteristics data L/*W*=85/930 μm.

Moreover, the photoresponsivity (R, AW^{-1}) and photosensitivity (I_{phc}/I_D) both at V_G= 0 V, as well as the density of charge carriers generated by UV light (ΔN_{trap}) indicate that, among these parameters, chemical modification of the dielectric surface affected the only R of PTs (Table 6.2). This is an indication of the built-in electric field from the SAM dipole that contributes to the photo field effect in addition to the gate voltage [36] responsible for exciton dissociation. Equation S6.6 used to compute R is given in Supp. Info.

Table 6.2 Photoelectrical parameters of PTs with different SAMs based on at least five devices from each substrate (for clarity only standard deviations for response times are reported)

SAM	Parameter				
	ΔN_{trap} x10^{12} (cm^{-2})	$I_{phc}/I_{D,}$ x10^5 (max)	R (AW^{-1}) (max)	Rise times, fast/slow, (τ_{r1}/τ_{r2})* (s)	Decay times, fast/slow, (τ_{d1}/τ_{d2})* (s)
		V_G = 0 V			
OH	5.4	10^5 (10^6)	1.3 (1.7)	2.1±0.5/16.3±0.2	7.0±0.2/48.7±1.6
CH_3	5.0	10^5 (10^6)	1.4 (2.2)	2.8±1.8/11.7±0.9	6.4±2.1/44.8±6.1
R'-Ph	5.4	10^5 (10^6)	1.7 (2.0)	2.1±1.4/12.5±3.6	6.3±0.9/44.7±2.2
R'-Ph-SO_2Cl	4.8	10^5 (10^6)	4.3 (4.9)	2.4±0.6/38.5±1.3	5.1±1.8/45.5±3.1
R''-Cl	5.3	10^6 (10^6)	3.1 (4.7)	3.8±1.7/42.1±2.1	5.8±0.2/46.0±0.8
R''-NH_2	5.1	10^5 (10^6)	2.2 (2.6)	5.0±1.0/60.0±3.6	11.2±0.4/117.9±7.8
R''-SH	5.1	10^5 (10^5)	3.1 (3.7)	4.8±0.3/67.6±2.1	12.3±0.7/146.1±9.8
Ph	5.0	10^5 (10^5)	1.0 (1.5)	5.2±0.6/11.4±0.6	14.0±1.6/165.9±16.7
Ph-CH_2-Cl	4.6	10^5 (10^6)	2.5 (3.3)	2.0±0.3/7.8±0.8	11.4±0.1/142.2±3.1

*The coefficients of determination for the fit (R^2) for the rise and decay times are in the range 0.9678-0.9997 and 0.9966-0.9999, respectively.

Likewise, output and transfer characteristics, different SAMs affected the evolution of the time-dependent drain photocurrent (I_{phc}) at bias V_G= 0 V and V_{SD}=

-60 V (Fig. 6.4a). We further investigated effects of different SAMs on switching properties of PTs under two cycles as displayed in Fig. 6.4b (i.e. I_D – time at V_G= 0 V and V_{SD}= -60 V). First cycling sequence, which was identically repeated for the second time, was *Dark@0s ≫ UV on@20 s ≫ UV off@~100 s – Reset@200 s*. From I_D – time curves in Fig. 6.4b (a representative device with R''-SH SAM), and for all other devices displayed in Fig. S6.3 a-h, the presence of different SAMs did not affect behavior under the cycling conditions, demonstrating reproducibility of the I_{phc} rise in a similar time frame. All the curves are characterized by a fast/slow rise (UV on) and a fast/slow decay (UV off). Interestingly, fitting of the experimental data using bi-exponential equations for rising and decay times (Supp. Info., Eqns. S6.4 and S6.5), revealed that SAM has an influence on the I_{phc} time response (Table 6.2), which will be discussed in the section below.

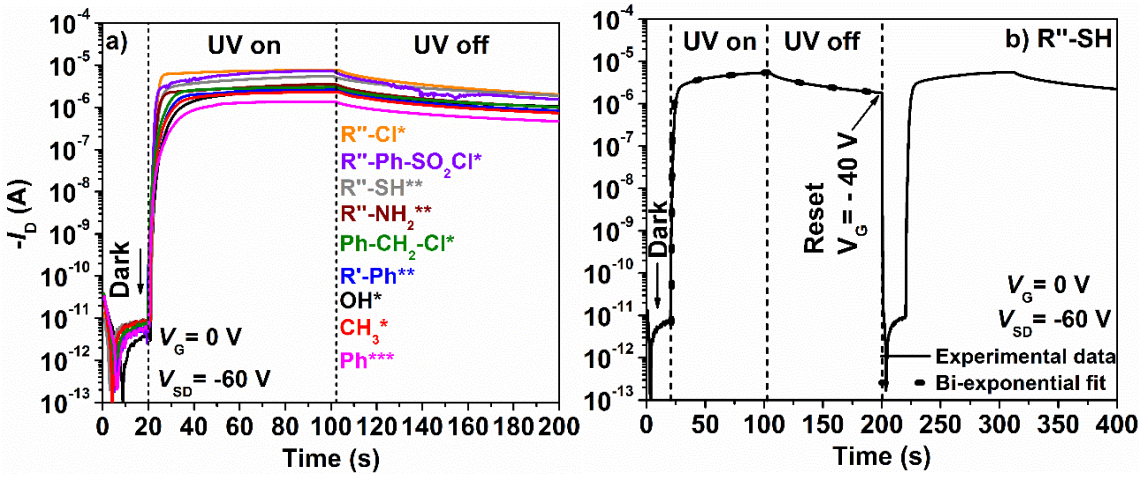

Fig. 6.4. Overlay of (a) I_D vs time curves for L-upe+C5-BTBT PTs with different SAMs at dielectric/channel interface (stars at the sample notation represent reset gate voltage applied to return the device in the OFF state; * = -60 V,** = -40 V, and ***= -80 V), and b) I_D vs time curves of the representative PT with R''-SH SAM demonstrating switchable properties (cycling characteristics–solid line) of the device and bi-exponential data fitting (dotted line) to calculate response times given in Table 6.2 for PTs; L/W=85/930 μm; UV light: λ=365 nm and 3 mW cm^{-2}.

Furthermore, chemical modification of the gate dielectric lowered the reset bias gate voltage by 20 V in PTs containing R'-Ph, R''-NH_2 and R''-SH SAMs (**notation in Fig. 6.4a). All other PTs required a reset voltage of -60 V (*notation in Fig. 6.4a), except for the Ph device that unexpectedly required even higher reset voltage of -80 V to return to the OFF state (***notation, Fig. 6.4a). It becomes clear that certain SAMs lowered the overall power consumption while maintaining excellent properties of PTs. However, the reason for the difference in reset voltage is not fully understood and its mechanism involved is yet to be elucidated.

6.4.2 Effects of morphology and microstructure of the thin films

To further correlate the effects of a SAM on the photoelectrical properties of PTs, we investigated the surface morphology of the semiconductor thin films. Fig. 6.5 represents height (upper row) and amplitude (lower row) AFM images in tapping mode of selected thin films with optical micrographs as insets (optical micrographs of the other thin films are displayed in Fig. S6.4). Based on the photoelectrical performance of PTs (mobility and type of functional group), we choose four representative PTs for microstructural and morphological characterization. All the thin films showed similar surface morphologies regardless of the dielectric/channel interface, reducing any effect the thin film morphology could have on the system. However, it should be noted that AFM does not necessarily give information about the interface morphology, i.e. the first few layers or nanometers of the active channel at the dielectric surface, where conductivity occurs. It is observed that root mean square surface roughness (R_{rms}) of the SH thin film is half of the other thin films analyzed by AFM (Fig. 6.5a-d), which is important for the effective charge carrier injection from the source electrode into the channel. In the case of SH PTs, this may be also one of the factors contributing to the highest mobility estimated for these devices in the dark.

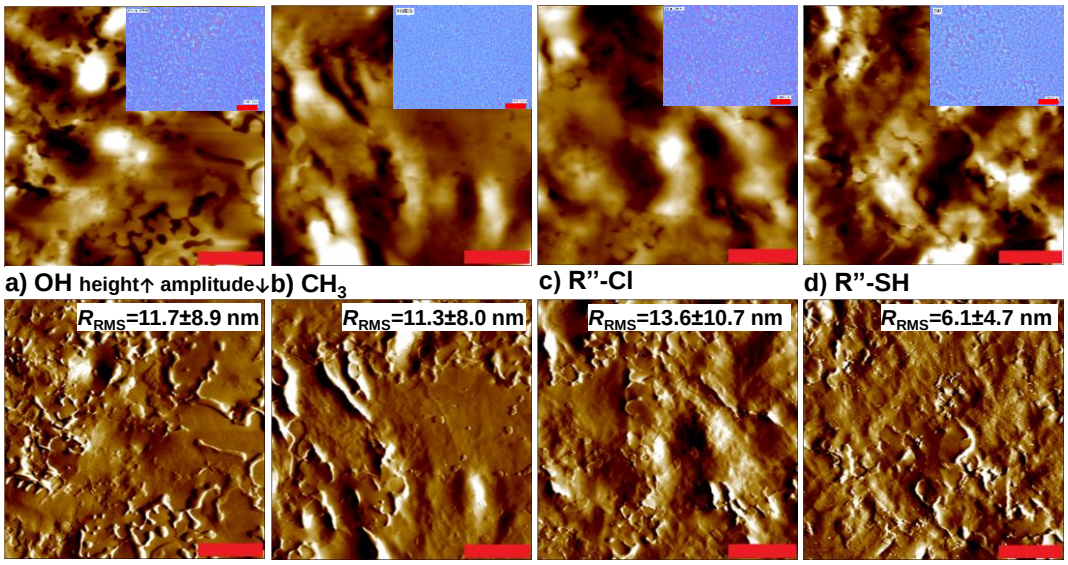

Fig. 6.5. AFM surface morphology of selected L-upe+C5-BTBT blend based thin films formed on different SAM-modified SiO_2 surfaces of a Si-wafer (a-d); 20x20 μm height (upper raw) and amplitude (lower raw) images were acquired in a tapping mode (scale bar 5 μm, root means square roughness, R_{RMS}, is estimated from the 20x20 μm height images) while inset images (scale bar 100 μm) represent digital optical micrographs of the same thin films selected for AFM analyses.

X-ray diffraction (XRD) is a powerful tool to characterize the microstructure of a thin film made of a semiconductor or its blend with polymers. To support our rationale discussed above for the effect of a SAM on mobility in the dark, we employed 2D XRD analysis (XRD^2). Out-of-plane XRD patterns of the structure of representative thin films are displayed in Fig. 6.6. From the frame images of XRD^2 measurements (Fig. 6.6a), we generated intensity vs. 2θ patterns of blend based thin films spin-coated on SAM-modified dielectric surfaces as well as the reference

C5-BTBT thin film (no polymer component). Thin films of a pure semiconductor were fabricated under the same conditions (1 wt% C5-BTBT solution in TCE) as those made of a blend. Parameters, such as characteristic peak positions (2θ), *d*-spacing, full width at half-maximum (FWHM), and crystallite size (Eqn. S9) were determined and reported in Table S2 for all the thin films. The pseudo-Voigt method was used to determine FWHM by fitting XRD peaks in Fig. 6.6b. The same fitting method was applied to estimate FWHM from the intensity vs. γ peaks reported in Fig. 6.6c, to investigate the texture in thin film microstructure.

As seen in Fig. 6.6b, surface modification did not change the crystal structure of C5-BTBT in a polymer blend compared to the pure C5-BTBT thin films. Five characteristics (00*l*) peaks in the XRD pattern of the blend-based and pure C5-BTBT thin films were identified and found to be identical in position and shape. All the thin films gave similar crystallite sizes (34-40 nm) estimated from the 2θ peak at 3.8° and undisturbed (by polymer or fabrication conditions) crystal structure (*d*-spacing ~23 Å) (Table S2). Slightly higher values for crystallite size in the blend-based thin films were most likely originated from the different dynamics of the C5-BTBT crystal growth due to present polymer phase. Almost identical XRD patterns of both types of thin films (polymer blend based and pure C5-BTBT thin films) suggested that generated similar surface energies dominated over the formation of the similar thin film structures that also exhibited similar morphologies. Thus, similar photoelectrical properties were expected but not completely achieved.

Factors affecting hole mobility in the studied PTs lay in the nature of the functional groups at the interface and their interaction with the active channel materials.

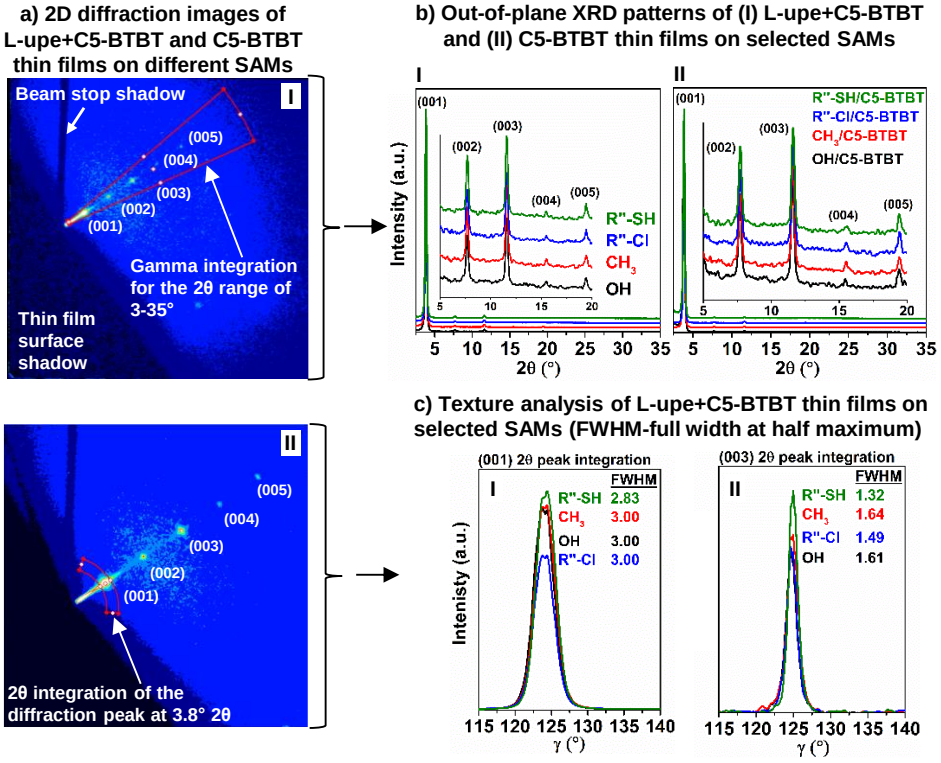

Fig. 6.6. XRD[2] microstructure analyses: a) 2D diffraction images of (I) L-upe+C5-BTBT and (II) C5-BTBT thin films obtained using an area detector; 2D images were integrated to generate (I) intensity vs. 2θ plots in (b), and (II) intensity vs. azimuth angle (γ) plots in (c) only for L-upe+C5-BTBT thin film XRD peaks (red wire frames in an(I-II) represent the integration area); b) Out-of-plane XRD patterns of (I) L-upe+C5-BTBT and (II) C5-BTBT thin films on selected SAMs (inset plot is zoom-in of 5-20 2θ, and c) intensity vs γ plots generated for (I) (001) and (II) (003) 2θ peaks in (b-I), used to determine FWHM (reported in the plot) for texture analysis of L-upe +C5-BTBT thin films on selected SAMs.

Many research groups reported strong effect caused by the dipole of a SAM on mobility in the dark, the threshold voltage and the turn-on voltage of OTFTs [21]. The built-in electric field at the interface induced by SAM dipole, weak charge transfer from SAM to the channel, and microstructure of the semiconductor were the arguments explaining effects of various SAMs on electrical properties of OTFTs in the dark. Our argument is that the literature reported effects were different from those in L-upe+C5-BTBT blend-based PTs. Keeping in mind that we had a dielectric polymer component present in the active channel that also determined photoelectrical properties of PTs studied here and previously reported by our group [31][33]. The fact that the SAM/mobility relationship in the dark could not be simply projected to the same relationship under UV light suggested that different SAMs interacted with the channel materials in a more complex manner. Therefore, characteristics of the SAM (chemical structure and molecular electronic nature) and its interaction with the first few layers of the active channel materials via intermolecular forces determined how certain SAM affected the properties of PTs.

For instance, R”-SH SAM that increased mobility the most in the dark is chemically different from R’-Ph-SO_2Cl SAM which increased mobility the most under UV light. Although these two SAMs introduced similar surface energies, mobilities in the dark and under UV light were somewhat different (Table 6.1). If we apply the argument that SAM dipoles play an important role in enhancing the dark mobility via a built-in electric field, it is then expected that R’-Ph-SO_2Cl SAM has the highest mobility since it has the strongest electron withdrawing group [29]. This rationale is valid but only under UV light where the mobility was increased the most

due to strong electron withdrawing properties of -SO_2Cl group. Lastly, dark mobility of PTs with neutral CH_3, R'-Ph and Ph SAMs were similar or higher than those with functional groups -Cl, NH_2 and -CH_2-Cl, which also demonstrated that SAM dipole and built-in electric field were not dominant factors affecting mobility in the dark. However, these factors dominated mobility enhancement under UV light.

XRD^2 crystallite alignment analysis was employed to explain the increased mobility of the R"-SH SAM PTs, in the dark. 2θ integration in the azimuthal direction (gamma angle), as represented by red wire cursor in the Fig. 6.6a-l enabled estimation of the FWHM from the intensity vs. γ curves for (001) and (003) 2θ peaks (Fig. 6.6c). FWHM is related to the distribution of crystallite alignment or to the volume fraction of the group of crystallites that are similarly aligned toward preferred orientation [37][38]. Lower values for FWHM indicate better alignment. The X-ray measurements of the C5-BTBT single crystal indicated a lamella structure and the out of plane XRD experiment on the thin films showed preferred orientation along *c*-axis, (001) 2θ peak, where molecules are perpendicular to the substrate (Fig. S6.5). The figure of merits for the C5-BTBT single crystal is given in Table S6.3. Within one layer, C5-BTBT molecules are arranged in a characteristic herringbone structure necessary for the efficient 2D charge carrier transport. This means that for the analyzed (001) and (003) 2θ peaks in L-upe+C5-BTBT thin films, crystallites or C5-BTBT layers are more aligned since the FWHM values are smaller compared to the other analyzed samples. In this manner charge carriers are less trapped and scattered [39] within and/or between aligned crystallites while

drifting through the channel results in the highest mobility when R”-SH SAM is at the interface.

Better alignment of C5-BTBT crystallites on R”-SH SAM may also be addressed to the intermolecular interactions between similar features in the SAM and C5-BTBT molecules, i.e. dispersion forces and interdigitation of the alkyl chains in SAM and C5-BTBT molecule. Additionally, dispersion forces may have also contributed to the lower surface roughness observed by AFM analyses. Most likely, a polymer phase is spatially more vertically segregated toward the gas phase (air). The lone pairs interactions between sulfurs in R”-SH SAM and the core of C5-BTBT molecule may pull C5-BTBT crystals to segregate toward the dielectric. In this scenario, more C5-BTBT crystals are in contact with the interface, which governs their better alignment, resulting in a higher hole mobility in the dark as compared to the other PTs.

6.4.3 Effects of SAM electrostatic nature on PT properties under UV light

In contrast to the dark, the SAM dipole/polarity and resulting built-in electric field dominated mobility dramatic variation under UV light by affecting exciton dissociation kinetics and thus a number of free charge carriers. This resulted in different levels of I_{phc} for the subthreshold region. Unlike mobility in the dark, mobility under the UV light was strongly dependent on the electrostatic nature of SAM, i.e. EW/ED nature. According to Table 6.1 and Fig. 6.3 SAMs with EW/ED

nature (R'-Ph-SO_2-Cl, R''-Cl, R''-SH, Ph-CH_2-Cl, and R''-NH_2) significantly increased mobility under UV light compared to the neutral SAMs (CH_3, R'-Ph, and Ph) that did not significantly affect the mobility under UV light illumination. The highest maximum mobilities under UV light occurred for the R'-Ph-SO_2-Cl (0.50 $cm^2\ V^{-1}\ s^{-1}$) and R''-Cl (0.44 $cm^2\ V^{-1}\ s^{-1}$) SAMs followed by R''-SH (0.35 $cm^2\ V^{-1}\ s^{-1}$), Ph-CH_2-Cl (0.23 $cm^2\ V^{-1}\ s^{-1}$), and R''-NH_2 (0.21 $cm^2\ V^{-1}\ s^{-1}$). The Ph SAM that is directly attached to the surface (no alkyl chain) have an unexpectedly negative effect on mobility by decreasing it to the level of a control PT (Fig. 6.3). At this point, we cannot offer any rational explanation for such effect and it is the subject of further investigation. OH groups at the interface are strong charge carrier traps and devices without organosilane treatment are known to have poor performance.

Not only mobility under UV light but photoresponsivity (*R*, AW^{-1}) of PTs was also affected by electrostatic characteristics of used SAMs (Table 6.2). Under UV light, charge carriers are generated in bulk of the channel where electrons are accumulated at the dielectric/channel interface. Accumulation of electrons (i.e. photo-exciton dissociation is governed by the gate voltage) is accelerated by built-in electric field due to SAM dipolar or electron donating/withdrawing capabilities of the end functional group present in the SAM. The stronger the electron withdrawing group, the higher the output drain photocurrent per power of UV light and the higher the *R*.

The SAM has a distinct impact on PT response time of the time-dependent I_{phc} (Table 6.2 and Fig. 6.4a). All response times were determined at V_G=0 V, which eliminates the field-effect contribution to the charge carrier generation and takes

into account only photo-generated charge carriers. Response times can be explained by the following processes at the dielectric/channel interface and in the bulk of the channel: charge carrier generation by UV light, carrier trapping/detrapping, carrier diffusion and carrier recombination [40]. Fast and slow rise times (τ_{r1} and τ_{r2}) of the I_{phc} refer to the photo-generation of the charge carriers and trapping of photoelectrons at the interface, in the dielectric and bulk of the channel. Reversing the process (recombination) at this stage is possible and creates an upper limit for the I_{phc} indicated by rising times. Rise times were observed to be shorter for neutral SAMs and those with EW groups, including OH, due to stronger trapping (withdrawing) of photoelectrons at the interface (EWG SAM and OH) and in the dielectric/bulk (neutral SAM). On the other hand, rise times were longer for SAMs with ED groups, indicating that a larger amount of recombination occurred during the I_{phc} rise stage due to the electron donating nature of these SAMs.

Fast and slow decay times (τ_{d1} and τ_{d2}) correspond to the detrapping of the photoelectrons trapped in the bulk and at the interface, spontaneously recombining with the free holes. The strongest influence by SAM on the response times is observed for the fast and slow decay times, which is important for the optically writable non-volatile organic memory. Longer decay times (slower I_{phc} relaxation) after UV removal translates to a longer retention of stored data for use as optical memory. Detrapping/recombination of photoelectrons is also associated with the defects in the material, the trap density at the interface and in the bulk (energy barriers), and diffusion rates of the photo-charge carriers [41]. All these effects are

included in the I_{phc} decay behavior characterized by fast decay (fast recombination of detrapped photoelectrons in proximity of the free photo holes) and slow persistent decay (slow recombination of the distant photoelectrons and delocalized photo holes) that reached a metastable state with very long times to decay to the initial low current state (~10^{-12} - 10^{-13} A).

Longer τ_{r2} are observed in R"-NH_2, R"-SH, Ph, and Ph-CH_2-Cl containing SAMs. For the first two SAMs, this can be explained by the ED nature that most likely repels photoelectrons in the bulk which, in turn, requires more time for photoelectrons to find photo holes and recombine. Additionally, dissipated photoelectrons were trapped in the bulk, not at the interface like in the case of EW SAMs where decay times are faster. Neutral SAMs (CH_3 and R'-Ph have similar times with EW SAM due to detrapping from the dielectric which most likely has fewer defects and density of states, thus a lower number of traps. Longer decay times in the case of Ph and Ph-CH_2-Cl SAMs at this point can be only addressed to defects at the interface and density of interface traps at the deeper energy levels (D_{it}). D_{it} that is highest for these two SAMs compared with other interfaces (Table 6.1), especially in the case of Ph SAM (8.2x10^{12} cm^2 V^{-1}). Very high D_{it} for Ph can also be responsible for the unexpected decreased in mobility caused by trapping both electron and holes under UV light as previously discussed.

Referring to Section 6.4.1, ED/EW groups present in SAM affected the reset voltage used to accelerate recombination of the spatially separated charge carriers that reached metastable I_{phc} level preventing the PT to return into off state without

an external stimulus (Fig. 6.4). R"-SH, R"-NH_2, and R'-Ph needed a reset gate voltage pulse of -40 V (3-4 s) to go back into initial low current state (~10^{-12} A) compared to the other PTs and reset voltage of -60 V. Ph SAM required a reset pulse of -80 V to return to their initial state. EW groups are deficient in electrons and a higher number of electrons is needed to recombine with the excess of photo holes in the bulk, as well as to detrap the existing ones. Therefore, a large negative bias voltage (-60 V) was needed to accelerate recombination via accumulation regime and erase the photocurrent. In contrast, EDGs are rich in electrons that via a built-in voltage due to excessive electrons lowers the negative reset voltage by 20 V and enables easy recombination with photo holes. Surprisingly, the Ph SAM required a larger reset voltage of -80 V which can be again associated with the existence of traps at the deeper energy levels that trapped the electrons. The same reason may explain the unusual mobility decrease under UV light when Ph is introduced as a SAM.

§ 6.5 Conclusions

In conclusion, we have demonstrated an effective way to modulate photoelectrical properties of L-upe+C5-BTBT blend-based phototransistors via simple chemical modification of the gate dielectric (SiO_2) using organosilanes, i.e. modification of the dielectric/channel interface. We utilized eight common and commercially available organosilanes that introduced dielectric surfaces of similar energies and thin film morphologies. Formed SAMs have different effects on the

UV responsive dielectric polymer/small molecule semiconductor blend-based phototransistors from those reported in the literature based only on a semiconductor. It is observed that mobility, under UV light, is affected the most by different SAM at the dielectric/channel interface. Detailed structure analysis by 2D X-ray diffraction and photoelectrical characteristics revealed that slight variation of mobility in the dark predominantly depended on the alignment of C5-BTBT crystallites at the dielectric/channel interface. In contrast, mobility under UV light strongly depended on the EW/ED nature of the SAM due to the existence of functional groups at the end of the individual SAM molecules that are perpendicularly oriented toward the channel. This is also confirmed by estimation of photoresponsivity (AW^{-1}) and response times of the drain photocurrent, indicating that ED/EW nature of SAM affects charge carrier photogeneration and recombination. In terms of application, organosilane surface modification represents a simple method to control and increase relaxation times of the drain photocurrent upon UV light removal, which is required for the optically writable organic memory to store data for a long period of time.

§ 6.6 References

[1] B. Kumar, B. K. Kaushik, Y. S. Negi, *Polym. Rev.* **2014**, *54*, 33.

[2] H. Sirringhaus, *Adv. Mater.* **2014**, *26*, 1319.

[3] P. S. K. Amegadze, Y.-Y. Noh, *J. Inf. Disp.* **2014**, *15*, 213.

[4] D. Elkington, N. Cooling, W. Belcher, P. Dastoor, X. Zhou, *Electronics* **2014**,

3, 234.

[5] Y. Guo, G. Yu, Y. Liu, Functional organic field-effect transistors. *Adv. Mater.* **2010**, *22*, 4427–4447.

[6] Y. Y. Noh, D. Y. Kim, K. Yase, *J. Appl. Phys.* **2005**, *98*, 7450.

[7] D. Braga, G. Horowitz, *Adv. Mater.* **2009**, *21*, 1473.

[8] C. Di, G. Yu, Y. Liu, D. Zhu, *J. Phys. Chem. B* **2007**, *111*, 14083.

[9] A. Y. Amin, A. Khassanov, K. Reuter, T. Meyer-Friedrichsen, M. Halik, *J. Am. Chem. Soc.* **2012**, *134*, 16548.

[10] Y. Yuan, G. Giri, A. L. Ayzner, A. P. Zoombelt, S. C. B. Mannsfeld, J. Chen, D. Nordlund, M. F. Toney, J. Huang, Z. Bao, *Nat. Commun.* **2014**, *5*, 3005.

[11] G. Kim, S. J. Kang, G. K. Dutta, Y. K. Han, T. J. Shin, Y. Y. Noh, C. Yang, *J. Am. Chem. Soc.* **2014**, *136*, 9477.

[12] H. Klauk, *Chem. Soc. Rev.* **2010**, *39*, 2643.

[13] B. Kumar, B. K. Kaushik, Y. S. Negi, *J. Mater. Sci. Mater. Electron.* **2014**, *25*, 1.

[14] G. Wu, C. Chen, S. Liu, C. Fan, H. Li, H. Chen, *Adv. Electron. Mater.* **2015**, *1*, 1500136.

[15] W. H. Lee, H. H. Choi, D. H. Kim, K. Cho, *Adv. Mater.* **2014**, *26*, 1660.

[16] J. Mei, Y. Diao, A. L. Appleton, L. Fang, Z. Bao, *J. Am. Chem. Soc.* **2013**, *135*, 6724.

[17] H. Luo, C. Yu, Z. Liu, G. Zhang, H. Geng, Y. Yi, K. Broch, Y. Hu, A. Sadhanala, L. Jiang, P. Qi, Z. Cai, **2016**, 1.

[18] G. Giri, E. Verploegen, S. C. B. Mannsfeld, S. Atahan-Evrenk, D. H. Kim, S.

Y. Lee, H. A. Becerril, A. Aspuru-Guzik, M. F. Toney, Z. Bao, *Nature* **2011**, *480*, 504.

[19] Y. Yuan, G. Giri, A. L. Ayzner, A. P. Zoombelt, S. C. B. Mannsfeld, J. Chen, D. Nordlund, M. F. Toney, J. Huang, Z. Bao, *Nat. Commun.* **2014**, *5*, 3005.

[20] Y.-Y. Lin, D. J. Gundlach, S. F. Nelson, T. N. Jackson, *IEEE Electron Device Lett.* **1997**, *44*, 1325.

[21] H. Zhang, X. Guo, J. Hui, S. Hu, W. Xu, D. Zhu, *Nano Lett.* **2011**, *11*, 4939.

[22] Y. Wu, P. Liu, B. S. Ong, *Appl. Phys. Lett.* **2006**, *89*, 13505.

[23] X. Liu, G. Dong, L. Duan, L. Wang, Y. Qiu, *J. Mater. Chem.* **2012**, *22*, 11836.

[24] D. H. Kim, Y. D. Park, Y. Jang, H. Yang, Y. H. Kim, J. I. Han, D. G. Moon, S. Park, T. Chang, C. Chang, M. Joo, C. Y. Ryu, K. Cho, *Adv. Funct. Mater.* **2005**, *15*, 77.

[25] Y. Jang, J. H. Cho, D. H. Kim, Y. D. Park, M. Hwang, K. Cho, *Appl. Phys. Lett.* **2007**, *90*, 111.

[26] S.-Y. Kwak, C. G. Choi, B.-S. Bae, *Electrochem. Solid-State Lett.* **2009**, *12*, G37.

[27] J. H. Fendler, *Chem. Mater.* **2001**, *13*, 3196.

[28] S. Kobayashi, T. Nishikawa, T. Takenobu, S. Mori, T. Shimoda, T. Mitani, H. Shimotani, N. Yoshimoto, S. Ogawa, Y. Iwasa, *Nat. Mater.* **2004**, *3*, 317.

[29] K. P. Pernstich, S. Haas, D. Oberhoff, C. Goldmann, D. J. Gundlach, B. Batlogg, A. N. Rashid, G. Schitter, *J. Appl. Phys.* **2004**, *96*, 6431.

[30] H. Dong, L. Jiang, W. Hu, *Phys. Chem. Chem. Phys.* **2012**, *14*, 14165.

[31] D. Ljubic, C. S. Smithson, Y. Wu, S. Zhu, *Adv. Electron. Mater.* **2015**, *1*,

1500119.

[32] H. Ebata, T. Izawa, E. Miyazaki, K. Takimiya, M. Ikeda, H. Kuwabara, T. Yui, *J. Am. Chem. Soc.* **2007**, *129*, 15732.

[33] D. Ljubic, C. S. Smithson, Y. Wu, S. Zhu, *ACS Appl. Mater. Interfaces* **2016**, *8*, 3744.

[34] A. Y. Fadeev, T. J. McCarthy, *Langmuir* **2000**, *16*, 7268.

[35] F. Yakuphanoglu, B. Gunduz, *Synth. Met.* **2012**, *162*, 1210.

[36] H.-W. Zan, K.-H. Yen, *Electrochem. Solid-State Lett.* **2008**, *11*, H222.

[37] A. Rodriguez-Navarro, W. Otañno-Rivera, J. Garcia-Ruiz, R. Messier, L. Pilione, *J. Mater. Res.* **1997**, *12*, 1689.

[38] Bruker AXS GmbH, **2013**, 1.

[39] M. Birkholz, B. Selle, F. Fenske, W. Fuhs, *Phys. Rev. B* **2003**, *68*, 205414.

[40] S. Dutta, K. S. Narayan, *Adv. Mater.* **2004**, *16*, 2151.

[41] M. Y. Cho, S. J. Kim, Y. D. Han, D. H. Park, K. H. Kim, D. H. Choi, J. Joo, *Adv. Funct. Mater.* **2008**, *18*, 2905.

§ 6.7 Supporting information

6.7.1 Experimental

Preparation of the thin film blend. Linear unsaturated polyester (L-upe) was dissolved in toluene and precipitated in methanol to remove any small molecular weight compounds. L-upe was dried in a vacuum oven at 80°C for 48 h

prior to solution preparation. Equal amounts of L-upe and C5-BTBT semiconductor were dissolved in TCE at 60°C for 6 h. The total amount of solids in the solution was 2 wt%. The solution was filtered through a syringe filter (acrodisc PTFE, Milipore 0.20 µm) prior to spin-coating onto the modified dielectric surface of a Si wafer.

Characterization. Digital optical micrographs of the thin-film surfaces on Si-wafers were recorded using a Keyence VHX-2000 (Keyence, Canada) while detailed thin film surface morphology was analyzed using an MFP-3D atomic force microscope (Asylum Research and Oxford Instrument Company, Santa Barbara, CA, USA) in tapping mode under ambient conditions. A silicone tip FMR-20 (Nano World, Switzerland) with force constant 2.8 N/m, and a frequency of 75 Hz was used. AFM data was acquired and processed using the Asylum Research AFM software build on Igor Pro (Wavemetrics, Portland, OR, USA). The L-pe+C5-BTBT blend thin film thicknesses were determined on the DektakXT (Bruker, USA) surface profiler. All thin films were spin-coated on 1x1 inch glass plates under the same conditions as the Si-wafers. Photoelectrical characteristics of all devices were determined under ambient conditions (humidity 30% RH and 23°C, yellow light) on a 4200-SCS Parameter Analyzer (Keithley Instruments, USA). For illumination of phototransistors, a UV lamp (Black-Ray, UVP B 100 AP, long wave UV lamp, 100 W, λ=365 nm, Entela, USA, UV-A light intensity of 3 $mWcm^{-2}$ at ~25 cm distance from the surface) was used, illuminating the entire surface of a phototransistor.

6.7.1 Results

Contact angle and surface energy (γ_S). Completeness of the SiO_2 dielectric surface modification was evaluated by contact angle measurements and calculations of the surface energy (γ_S) for each substrate. Water and diiodomethane (CH_2I_2) contact angles and corresponding γ_S (mJ/m^2) are given in Table S6.1. Surface energies are in the range of 38-49 mJ/m^2 for organosilane treated surfaces. Generally, chemically similar SAMs generated similar surface energies.

Table S6.1 Water and diiodomethane contact angles for SAM-modified SiO_2 dielectric and corresponding surface energies (γ_S) (average values based on at least five spots on each of the two substrates with standard deviation).

SAM	Contact angle (°)		γ_S (mJ/m^2)
	H_2O	CH_2I_2	
OH	26±1	50±3	66±1.0
CH_3	72±1	50±1	38± 0.3
R'-Ph	76±1	38±1	42±0.3
R'-Ph-SO_2Cl	76±3	39±1	41±0.3
R''-Cl	55±2	41±1	49±0.5
R''-NH_2	63±1	39±1	46±0.4
R''-SH	66±1	41±2	44±0.7
Ph	76±1	32±1	44±0.3
Ph-CH_2-Cl	78±1	31±2	44±0.6

Output and transfer characteristic of all PTs

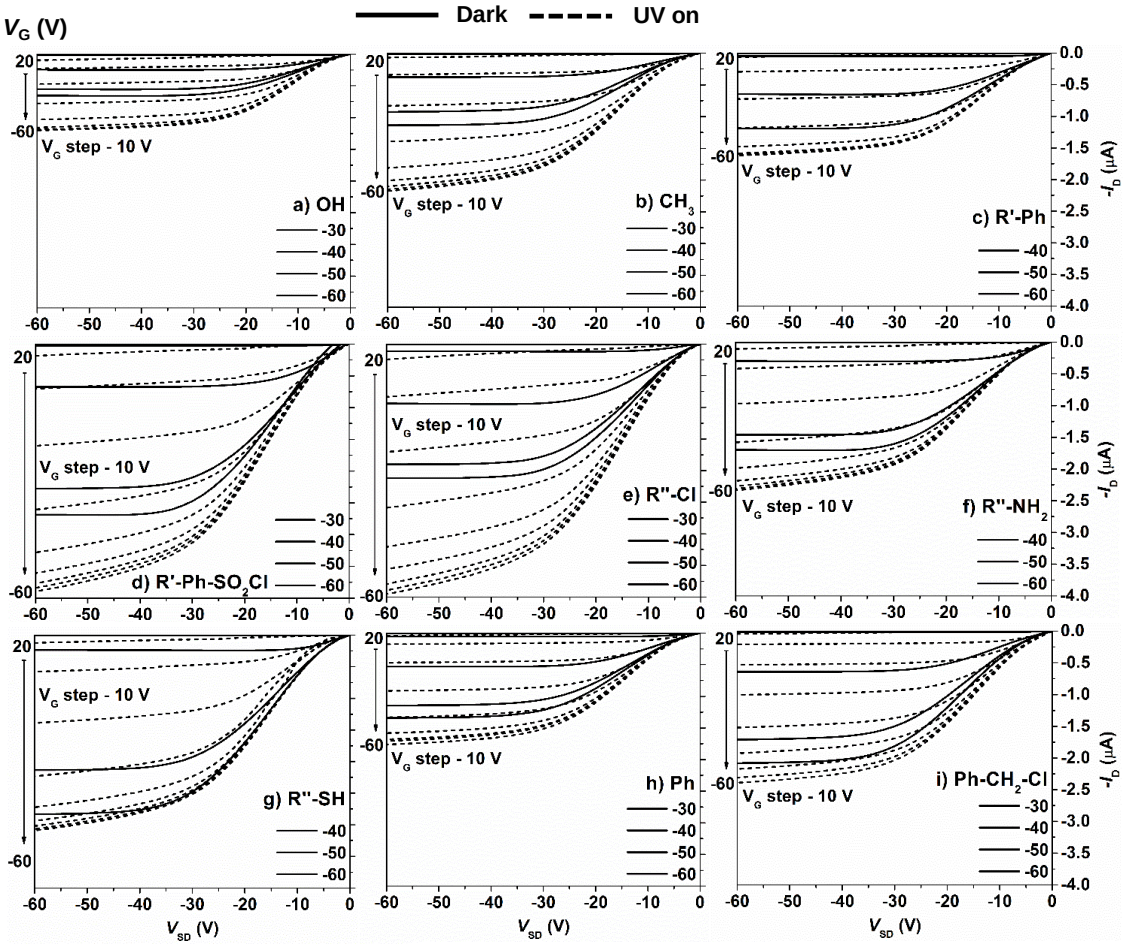

Fig. S6.1. Output characteristics of L-upe+C5-BTBT PTs with (a-k) different SAMs at the dielectric/channel interface obtained in the dark (solid curves) and under the UV light (dotted curves; λ=356 nm, 3 mW cm^{-2}); scan rate 6 V s^{-1} and V_G sweep 20 – -60 V (steps of -10 V; *L*/*W*=85/930 μm) were applied.

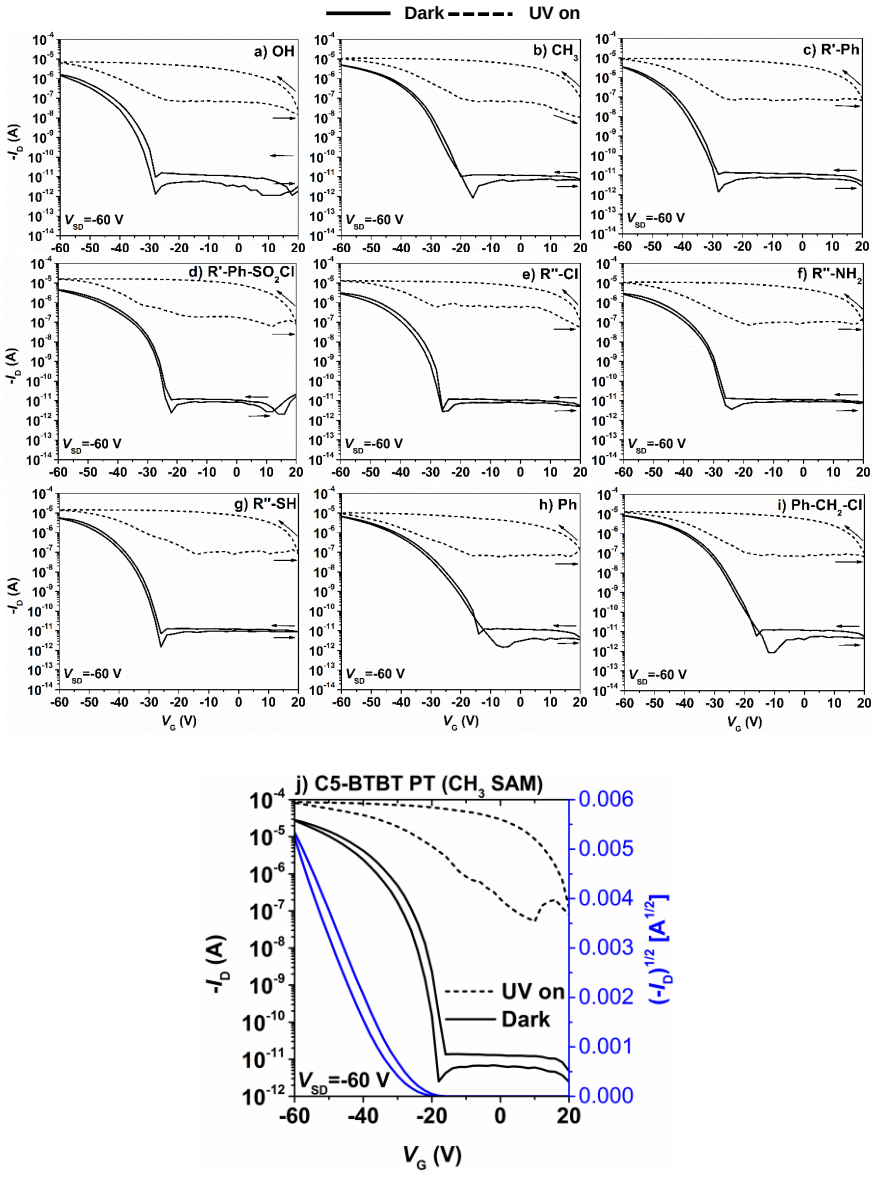

Fig. S6.2. Transfer characteristics in the dark (solid curves) and under the UV light (dotted curves; λ=356 nm, 3 mW cm^{-2}) of (a-i) L-upe+C5 BTBT PTs with different SAMs at the dielectric/channel interface and (j) C5-BTBT PT fabricated and characterize under the same conditions as L-upe+C5-BTBT PTs using HMDS (or CH_3) organosilane to modify the SiO_2 surface; (V_{SD}= -60 V, L/W=85/930 μm, and scan rate 6 V s^{-1}).

Equations

From transfer characteristics, threshold voltage, V_{Th} (slope of $I_D^{½}$ vs. V_G curves), turn ON voltage (V_{SO}), field-effect hole mobility in the saturation regime (μ_{FE}), and On/Off ratio in the dark for all PTs were determined. μ_{FE} in the saturation regime [1]:

$$\mu_{FE} = \frac{2L}{W} \cdot \frac{I_D}{C_{ox}(V_G - V_{Th})^2} \qquad \text{(S6.1)}$$

where L (cm) and W (cm) are active channel length and width, respectively; C_{ox} is the capacitance per unit area of the SiO_2 as a dielectric layer without silane treatment (15 nFcm^{-2}). Equation S1 can be re-written as: $I_D = (WC_{ox}/2L)\ \mu_{FE}\ (V_G - V_{Th})^2$. When plotting out the square root of $|I_D|$ as a function of V_G, the maximum slope of the plot will be $(\mu_{FE}WC_{ox}/2L)^{1/2}$ which can be used to calculate the μ_{FE} in the saturation regime.

The charge trap density ($N_{trap,dark}$) [2] was calculated using:

$$N_{trap,\ dark} = \frac{|V_{Th}|C_{ox}}{q} \qquad \text{(S6.2)}$$

where q is an elementary charge.

The inverse subthreshold slope (*SS*, the slope of the linear part of logI_D-V_G curves at V_G<V_{Th}) [3] and the density of deeper traps at the interface (D_{it}) [2][4] are estimated upon equations:

$$SS = \left(\frac{dlogI_D}{dV_G}\right)^{-1} \quad \text{(S3)} \qquad \text{and} \qquad D_{it} = \left[\frac{qSSlog(e)}{k_bT} - 1\right]\frac{C_{ox}}{q^2} \quad \text{(S6.3)}$$

where T and k_B are absolute temperature and the Boltzmann constant, respectively.

All the I_D vs. time data were fitted using bi-exponential equations below to calculate rise and decay times [5]. For the fast (τ_{r1}) and slow rise times (τ_{r2}) (i.e. response times under UV light) we used:

$$I_{phc}(t) = I_{D,0} + \mathrm{A}\left[1 - \exp\left(-\frac{t}{\tau_{r1}}\right)\right] + \mathrm{B}\left[1 - \exp\left(-\frac{t}{\tau_{r2}}\right)\right] \quad \text{(S6.4)}$$

while for the fast (τ_{d1}) and slow decay (τ_{d2}) (i.e. response time after UV was turned off) we used:

$$I_D(t) = I_{D,0} + \mathrm{C}\left[1 - \exp\left(-\frac{t}{\tau_{d1}}\right)\right] + \mathrm{D}\left[1 - \exp\left(-\frac{t}{\tau_{d2}}\right)\right] \quad \text{(S6.5)}$$

where I_{phc}, $I_{D,}$ and $I_{D,0}$ are photocurrent at time *t*, drain current (UV turned off) and dark drain current at t=0 of the measurements, respectively; A, B, C, and D are positive constants. All the experimental data fit both models well.

Photoresponsivity of PTs at V_G = 0 V (no electrical contribution to the charge carrier generation) was calculated using [6]:

$$R = \frac{I_{phc} - I_D}{P \cdot S} \qquad \text{(S6.6)}$$

where *P* is the power of the incident UV light (3 mWcm^{-2}) and *S* (*L*x*W*) is the effective area illuminated by UV light. The charge carrier density induced in the channel by UV illumination is characterized by the trap density (ΔN_{trap}) using [4] and it is proportional to the charge carrier density generated in the channel by UV light:

$$\Delta N_{trap} = \frac{\Delta V_{Th} C_{ox}}{q} \qquad \text{(S6.7)}$$

where ΔV_{Th} is a threshold voltage shift generated by UV light.

Switching characteristics

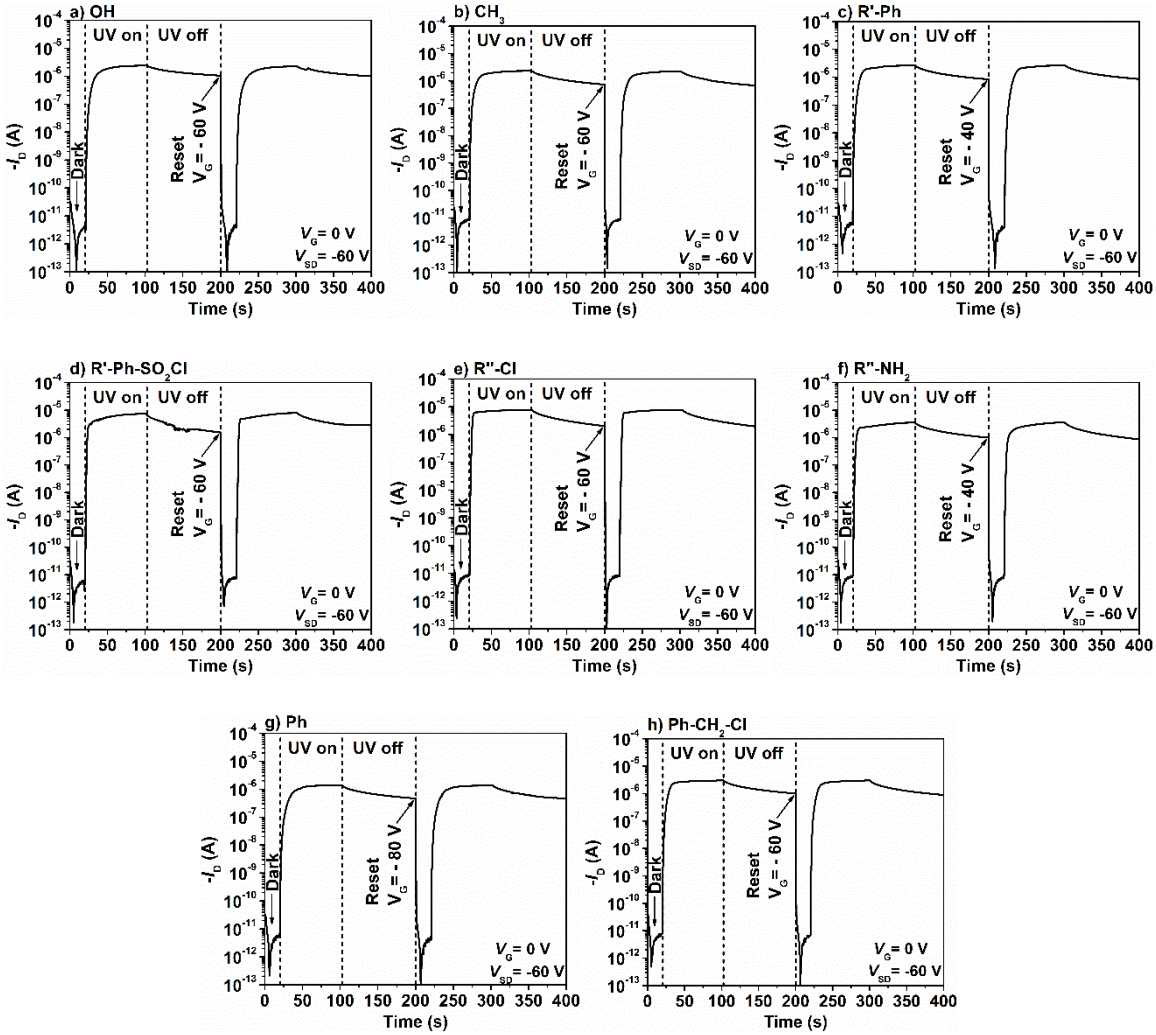

Fig. S6.3. I_D vs time curves of PTs with different SAMs demonstrating switchable properties of L-upe+C5-BTBT PTs with different SAMs at dielectric/channel interface (L/*W*=85/930 μm; UV light: λ=365 nm and 3 mW cm^{-2}).

Morphology and XRD of thin films

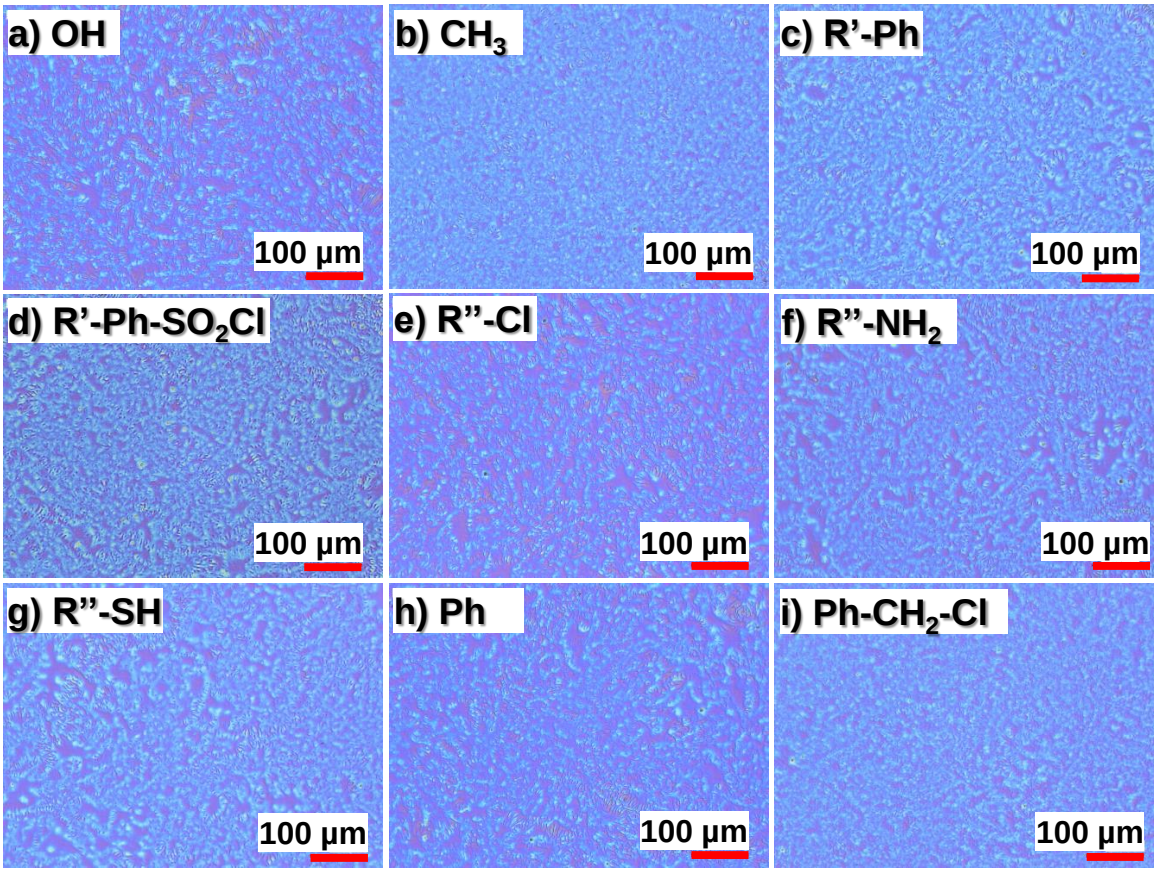

Fig. S6.4. Optical micrographs of L-upe+C5-BTBT thin films spun-coated on SiO_2 dielectric surface modified with different SAMs (scale bar 100 µm).

Crystallite size (*xs*, nm) was determined from the Scherrer equation [7]:

$$xs = \frac{C\lambda}{\mathrm{FWHM}\cdot\cos\theta} \qquad \text{(S6.8)}$$

where *C*, λ, FWHM and θ are a shape factor (typically 0.94), wavelength of the X-ray radiation (Cu source, λ =0.154 nm), the full width at a half maximum

(instrumental broadening subtracted) of the peak obtained by pseudo-Voigt fitting method (degrees), and θ is the Bragg angle (degrees), respectively.

Table S6.2 Crystal structure parameters estimated for L-upe+C5-BTBT and C5-BTBT thin films spin-coated on organosilane treated SiO_2 dielectric surface of Si-wafers (data for the estimation were collected using XRD[2]).

Sample	L-upe+C5-BTBT thin films			
	2θ (°)	*d*-spacing (nm)	FWHM (°)	xs (nm)
OH	3.82	2.31	0.219	37.9
CH_3	3.83		0.205	40.6
R"-Cl	3.83		0.212	39.2
R"-SH	3.83		0.206	40.4
	C5-BTBT thin films			
OH/C5-BTBT	3.83	2.31	0.225	36.9
CH_3/C5-BTBT	3.84	2.30	0.220	37.7
R"-Cl/C5-BTBT	3.81	2.32	0.243	34.2
R"-SH/C5-BTBT	3.83	2.31	0.238	34.9

C5-BTBT single crystal sample for XRD analysis was obtained from the controlled recrystallization in hexanes. Single crystal data were collected on a Bruker Smart Apex2 diffractometer (Mo$K\alpha$ radiation source, λ=0.71073 Å, 2θ= 2.5°–50.0°, resolution 0.1 Å) at ambient temperature (~23°C). A series of omega scans were collected with the area detector at a swing angle of 10.85° and a sample to detector distance of 4.95 cm. Only low angle diffraction spots were observed. The data were processed with Apex2 software, the structure solved using intrinsic phasing, and the refinement was done in Olex2 [8][9].

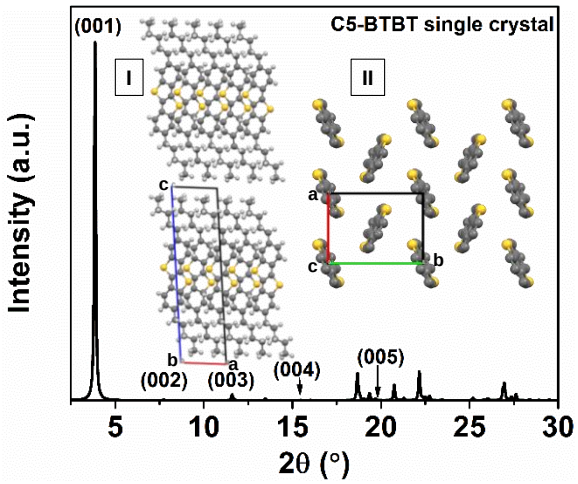

Fig. S6.5. Calculated powder XRD pattern obtained from the C5-BTBT crystal information file with labeled characteristic/planes orientation; inset images represent I) lamellar crystal structure of C5-BTBT in b-axis projection and II) molecular arrangements within one C5-BTBT layer in c-axis projection (two pentyl alkyl chains were omitted for clarity).

Table S6.3 Crystal structure parameters estimated for the C5-BTBT single crystal (data were collected using powder XRD).

Parameter	Value
Appearance	Clear colorless plate
Size	
MW ($C_{24}H_{28}S_2$)	380.58
2θ of the 001 peak(°)	3.86
d-spacing of the 001 plane (Å)	22.9
FWHM (°)	0.094
xs (nm)	88.1
Crystal system	Monoclinic
Space group	P 1 2_1/a 1
a (Å)	5.929(10)
b (Å)	8.0115(14)
c (Å)	23.05(4)
α (°)	90.00
β (°)	95.05(6)
γ (°)	90.0
Volume ($Å^{-3}$)	1091.11
Z	2
P (g cm^{-3})	1.158
Temperature (K)	296.15

6.7.2 References

[1] C. D. Dimitrakopoulos, P. R. L. Malenfant, *Adv. Mater.* **2002**, *14*, 99.

[2] J. Smith, R. Hamilton, Y. Qi, A. Kahn, D. D. C. Bradley, M. Heeney, I. McCulloch, T. D. Anthopoulos, *Adv. Funct. Mater.* **2010**, *20*, 2330.

[3] A. Takshi, J. D. Madden, *J. Comput. Electron.* **2010**, *10*, 154.

[4] X. Liu, G. Dong, L. Duan, L. Wang, Y. Qiu, *J. Mater. Chem.* **2012**, *22*, 11836.

[5] D. Gedamu, I. Paulowicz, S. Kaps, O. Lupan, S. Wille, G. Haidarschin, Y. K. Mishra, R. Adelung, *Adv. Mater.* **2014**, *26*, 1541.

[6] K.-J. Baeg, M. Binda, D. Natali, M. Caironi, Y.-Y. Noh, *Adv. Mater.* **2013**, *25*, 4267.

[7] B. B. B. He, J. H. H. Reibenspies, N. Bhuvanesh, *Two-dimensional X-ray Diffraction*; 2010; Vol. 25.

[8] O. V. Dolomanov, L. J. Bourhis, R. J. Gildea, J. A. K. Howard, H. Puschmann, *J. Appl. Crystallogr.* **2009**, *42*, 339.

[9] G. M. Sheldrick, *Acta Crystallogr. Sect. A Found. Crystallogr.* **2008**, *64*, 112.

7 COMPOSITION AND GATE DIELECTRIC DRIVEN PERFORMANCE OF 2,7-DIPENTYL[1]BENZOTHIENO[3,2-B][1]BENZOTHIOPHENE/POLYIMIDE BLEND-BASED ORGANIC PHOTOTRANSISTORS

In this chapter, the effects of the double gate dielectric layer and composition of the 2,7-dipentyl[1]benzothieno[3,2-b][1]benzothiophene/polyimide blends as channel materials on characteristics of UV responsive OPTs is presented. This chapter is based on the newly prepared manuscript entitled “Composition and gate dielectric driven performance of 2,7-dipentyl[1]benzothieno[3,2-

b][1]benzothiophene/polyimide blend-based organic phototransistors", D. Ljubic, W. Liu, N-X. Hu., Y. Wu, S. Zhu, to be submitted to Organic Electronics journal.

Author contributions

Darko Ljubic designed and conducted the experiments on organic phototransistors, synthesized the polyimide, and wrote the first draft of the manuscript under the guidance of Dr. Shiping and Dr. Yiliang Wu. Dr. Weifeng Liu designed the polyimide and assisted the synthesis, provided valuable inputs for the manuscript, and the first revision of the manuscript, Dr. Nan-Xing Hu provided valuable advises while writing the manuscript and revised the manuscript. The final revision was provided by Dr. Wu and Dr. Zhu.

§ 7.1 Abstract

Herein, we report on composition and the gate dielectric modification effects on organic phototransistors (OPTs) characteristics based on 2,7-dipentyl[1]benzothieno[3,2-b][1]benzothiophene (C5-BTBT)/polyimide (PI) blends as channel materials. We fabricated OPTs with double gate dielectric composed of PVP/pMSSQ (top) and SiO_2 (bottom) dielectrics (bottom) while the content of C5-BTBT in a blend was varied from 90-10 wt.%. It was found that the highest-performance of OPTs was achieved with the lowest content of C5-BTBT in the blend (20 wt.%). Blends with only 10 wt.% of C5-BTBT were nonconductive. The hole mobility and on/off ratio of 1.37 $cm^{-2}V^{-1}s^{-1}$ and 10^7, respectively, were calculated for the 20:80 C5-BTBT:PI OPTs. Under UV light intensity of 3 $mWcm^{-2}$,

20:80 C5-BTBT:PI OPTs also exhibited the highest photosensitivity (10^7) and photoresponsivity (67 AW^{-1}) with negligible hysteresis. This is attributed to the strong trapping of photoexcited electrons at the C5-BTBT/PI interface due to strong electron accepting nature of the PI. The introduction of the second dielectric layer enabled shifting of the threshold voltage with the increasing content of PI toward more positive values and eliminated hysteresis in the dark. Moreover, the double gate dielectric approach facilitated the stable and reliable performance of 20:80 C5-BTBT:PI OPTs at very low V_{DS} of -0.1 V . Investigation of the photoresponsivity versus light intensity revealed that OPTs maintained the high photosensitivity of 10^7 even under weak UV light intensity of 0.11 $mWcm^{-2}$. The dynamic characteristics of OPTs were also affected by the content of PI and were explained using DFT calculations. The decay times of the persistent photocurrent were increasing with the increasing content of PI while maintaining the fast response when the light was on. The OPTs have potential application as photo memory elements.

§ 7.2 Introduction

Organic phototransistors (OPTs) are of the immense importance for commercialization of optoelectronics. OPTs represent unique devices due to their structure as organic field-effect transistors (OFETs) and the light as the fourth “electrode” to control and modulate the output current. This enabled OPTs application as an on/off switch, light detectors, and signal amplifiers at the same

time. Compared to photodiodes, OPTs have a high signal to noise ratio making them promising devices for fabrication of the large area optoelectronics. In the recent years, OPTs attracted a significant research interest due to their low-cost and ease of fabrication. A variety of organic materials can be used to tune OPTs response to the light with different wavelengths.[1] Moreover, compatibility of the organic materials with plastic substrates enabled fabrication of the flexible and printable high-performance devices for sensing and detection.[2] Recently, Zhao et al. reported a photoresponsivity and photosensitivity of ~10^4 AW^{-1} and 10^5, respectively, for the new benzo[1,2-b:4,5- b′]dithiophene dimers at UV light intensity of 37 μWcm^{-2}.[3] Wu et al. reported OPTs based on solution processed 2,7-dioctyl[1]benzothieno[3,2-b][1]benzothiophene (C8-BTBT) single crystal ribbons with remarkable photoresponsivity of 1.2x10^4 AW^{-1} and photosensitivity of 10^4.[4] Very recently, Yu et al [5] developed flexible and low-voltage OPTs based on dinaphtho[2,3-b:2',3'-f]thieno[3,2-b]thiophene (DNTT) semiconductor on a PET substrate. OPTs operated stably at -5 V with photoresponsivity and photosensitivity of 50 $AW^{-1}$and 5, respectively, at the blue light intensity of 5 μWcm^{-2}. Clearly, OPTs have the potential for optoelectronic devices since their performance largely exceeded that of the Si-based PTs (300 AW^{-1}). [6]

The three main directions of fundamental development of OPTs are 1) to develop active new channel materials to receive or emit the light, 2) gate dielectric engineering and development, and 3) the interface engineering. So far, the focus was on the synthesis of new light responsive organic semiconductors (OSCs)[7–11] and the interface engineering using photochromic molecules [12–14]. As a relatively

new approach, the blending of existing OSCs and the dielectric polymers became an attractive method for the high-performance OPTs with large potential in applications for flexible and printed devices.[15–18] Using a blending approach, our group pioneered OPTs which high photocurrent response was achieved by solution blending of a UV responsive C5-BTBT and the dielectric polyesters.[15] The high photocurrent in the subthreshold region was addressed to the strong interface trapping due to electron accepting groups in the polyester. Chu et al and Huang et al went a step further and developed the flexible and printed 2D arrays and a sensor utilizing the OPT structure, respectively. The channel materials were dinaphtho[2,3-b:2',3'-f]-thieno[3,2-b] thiophene (DNTT)/PLA [19] and C8-BTBT/PLA [18] with photosensitivity of 10^4 and 10^5, respectively, owing to the large interface and trapping.

Often, improving only the channel materials is not sufficient to fabricate an OPT with reliable properties. Therefore, engineering of the gate dielectric is a good strategy to enhance the performance of the active channel in an OPT. The gate dielectric plays very important role for the device performance since it governs the electric-field, controls the leakage currents, and determines the interface characteristics at the channel. Commonly used SiO_2 dielectric layer on Si-gate often contains interface traps due to an affinity for oxygen and moisture. Polymer dielectrics are widely used for solution processed flexible OPTs [20–22]. Still, the issue with polymeric gate dielectric can be their pin-holes, thus high leakage currents. [23] On the other hand, use of the double gate dielectrics, for example, polymeric/SiO_2, for rigid photo memory elements is the feasible method to fabricate

reliable, stable and the high-performance OPTs [24–26]. The SiO_2 dielectric gives the low leakage current, while polymer dielectric, especially if hydrophobic, eliminates the traps via electronically neutral and very smooth surface. Usually, the double gate approach also enables lowering the operation voltage and control of the threshold voltage [27][28][29][30] which is important for real applications of OPTs.

In this paper, we report on solution processed, reliable, and high-performance, OPTs with double gate dielectric composed of SiO_2 and PVP/pMSSQ dielectrics. The PVP/pMSSQ dielectric (commercially available from Xerox as XD dielectric)) is hydrophobic, electroneutral, crosslinked and with the moderately high capacitance of 7-8 $nFcm^{-2}$.[31] XD used as the gate dielectric layer, facilitates a hysteresis-free and the low-threshold voltage OFETs which was reported in the previous works [32–34]. OPTs based on OSC/polymer blends generally exhibit lower mobility, higher operating voltage, hysteretic behavior under light illumination, and lower photoresponsivity. Furthermore, in our previous work (Chapter 5) we demonstrated that using a strong electron accepting polyimide (PI) in a blend with C5-BTBT, the photoelectrical and dynamic characteristics could be highly modulated and enhanced. Yet, hysteresis under light illumination was somewhat high at higher PI content while the threshold voltage in dark was unaffected. To completely suppress hysteresis, increase the mobility, lower the operating voltage, control the threshold voltage, and modulate the dynamic characteristics of OPTs, we utilized the XD dielectric deposited on the top of SiO_2 and C5-BTBT:PI blends as channel materials. Thus, effects of the blend composition and second dielectric layer were investigated. The performance of OPTs was evaluated by means of

photoelectrical characteristic and compared to those without an XD layer. Surprisingly, OPTs exhibited highly enhanced photoelectrical characteristics at a low content of C5-BTBT in a blend. The second dielectric layer, enabled modulation of the threshold and turn-on voltage, and eliminated hysteresis (dark) or suppressed it under the light. OPTs had a relatively fast response to the light and improved photo memory properties, i.e. longer retention of the persistent photocurrents (PPC). The mechanism of the longer decay times of the PPC was discussed by means of DFT calculations and energy levels diagram.

§ 7.3 Experimental

7.3.1 Materials

C5-BTBT was synthesized following procedures in the literature[35][36]. The synthesis procedure for PI was previously reported by our group (Chapter 5, Section 5.3.2). XD polymer dielectric was kindly supplied by Xerox Research Centre of Canada (Mississauga, ON) and it commercially available as XDI-DCS. Hexamethyldisilazane (HMDS) and 1,1,2,2-tetrachloroethane (TCE) were purchased from Sigma-Aldrich (Canada). Highly n-doped Si wafers with 200 nm thermally growth SiO_2 were supplied by Silicon Quest International (San Jose, CA, USA).

7.3.2 Preparation of C5-BTBT:PI blends and OPTs fabrication

C5-BTBT and PI were blended in 20:80 using TCE as a solvent. The total content of a solute was kept 2 wt.%. Calculated amounts of both components were weighted and dissolved in TCE for 4 h at 70°C. Upon dissolution, solutions were filtered twice through an acrodisc PTFE syringe filter (Millipore 0.20 μm). A solution of C5-BTBT in TCE (2 wt.%) was prepared under the same conditions. Fabrication of all OPTs was carried as follows. Si-wafers as substrates were cut into 1x1 inch square, successively cleaned in hot acetone, chloroform, and isopropanol in a sonication bath, air-dried, and treated with UV/plasma for 2 min (PDC-32G, Harrick Plasma, USA). After UV/plasma treatment, substrates were immersed in DI water for 10 min, rinsed with isopropanol, air dried, treated with 0.12 M HMDS/toluene solution for 30 min at 60°C. Lastly, they were rinsed with fresh toluene and dried *in vacuo* at 70°C for 20 min. The second dielectric layer of XD polymer was deposited on the top of HMDS modified SiO_2 dielectric according to a standard procedure of the manufacturer. Filtered dielectric solution was spin-coated at 2000 rpm, ramp 2s, for 60 s, dried at 80°C for 10 min, followed by curing at 140°C for 30 min. All substrates were again treated with HMDS under the same conditions as bare Si wafers. The active channel was formed upon spin-coating of the blend solution under the same spinning conditions as the second dielectric layer, followed by drying in vacuo at room temperature for 20 min. Source and drain gold electrodes (60 nm) (length/width: 80/930 μm) were deposited through a shadow mask using electron beam evaporator (Nano 36, FTM-2400, Kurt J. Lesker, UK). All the blend-

based OPTs were labeled in respect to the ratio of the C5-BTBT and PI wt.% content in the blend as, for example, 20:80 C5-BTBT:PI OPT. The control C5-BTBT OPTs (no PI) were fabricated under the same conditions as blend-based OPTs from the 2 wt.% solution in TCE.

7.3.3 Characterization

Basic properties of PI were previously determined (Chapter 5) and were summarized in Table S7.1. UV-vis spectra of thin films on glass slides were recorded using Nicolete UV-Vis-NIR (Cary 5000, Varian, USA) surface. DektakXT (Bruker, USA) surface profiler was used for determination of thin film thicknesses while for the thin film morphology a Keyence VHX-2000 (Keyence, Canada) digital optical microscope and MFP-3D atomic force microscope (Asylum Research and Oxford Instrument Company, Santa Barbara, CA, USA) in tapping mode (silicone tip FMR-20, Nano World, Switzerland, force constant 2.8 N/m, and a frequency of 75 Hz) were employed under ambient conditions. Photoelectrical measurements were carried out on a 4200-SCS (Keithley Instruments, USA) under yellow and UV light (Black-Ray, UVP B 100 AP, long wave UV lamp, 100 W, P_{UV}=3 mWcm^{-2} and 0.11 mWcm^{-2}, λ=365 nm, Entela, USA) on at least five OPTs from two different substrates and statistical data were given where applicable.

§ 7.4 Results

7.4.1 Thin-film characterization

Morphologies of 20:80 C5-BTBT:PI and C5-BTBT thin films on XD-HMDS were investigated by optical and atomic force microscopy (AFM). The optical micrographs of a 20:80 C5-BTBT:PI thin film showed the better quality with fewer defects and better smoothness (Fig. S7.1). The thin film morphology of a 20:80 C5-BTBT:PI blend compared to that of C5-BTBT is represented by AFM topology images in Fig. 7.1. AFM images show that the C5-BTBT phase (large flake-like grains) could not be identified in the 20:80 thin film because of its immersion into PI phase. The surface roughness R_{RMS} (R_{RMS}-root mean square, estimated from the 50x50 μm AFM height images) of 20:80 thin film was 10 times lower compared to that of C5-BTBT due to a PI phase. The R_{RMS} of the pristine PI thin film is ~1 nm (Fig. S7.1b). This suggests that the blend may be vertically phase separated into C5-BTBT rich phase being at the dielectric/channel interface, a blended phase (C5-BTBT is dispersed into PI), and a PI rich phase being on the top (gold electrodes/channel interface). This is not hard to understand since PI is more polar than C5-BTBT, and C5-BTBT (hydrophobic, contact angle 105°) is more compatible with hydrophobic XD-HMDS surface. Bare XD surface is highly hydrophobic[34] and its hydrophobicity was adjusted to enable adhesion of the channel material during spin-coating. Without the HMDS treatment, during the spin-coating, we experienced spinning-off of the solution without a thin film

formation due to the highly energetically incompatible surface of XD and the solution. When the solution of C5-BTBT was spin-coated a thin film was formed but with the inferior performance of the OPT. The origin of the XD hydrophobicity comes from its composition. The XD represents a mixture of poly(vinyl phenol) (PVP, κ=4.0) and pMSSQ that is a low surface tension component.[31] According to manufacturer specification, the XD polymer forms a 400-700 nm dielectric layer (surface roughness 10 nm. Upon spin-coating, PVP and pMSSQ form separate phases where pMSSQ migrates to the top of the layer inducing the water contact angle between 80-100°.[34]

The XRD patterns showed that the intact crystal structure of C5-BTBT (a 00*l*-characteristic peak at 2θ = 3.8°, *d*-spacing of 2.3 nm) was not affected by PI nor XD at the channel/dielectric interface. XRD patterns of 10:90 C5-BTBT:PI thin films showed the absence of the C5-BTBT crystal structure at this ratio. The UV-vis measurements confirmed the XRD patterns where no C5-BTBT characteristic peak at 355 nm was identified (Fig. 7.1d). The UV-vis spectra of pristine components and their blends showed that blends were UV light responsive and visible light blind. Based on this finding, 10:90 C5-BTBT:PI was not used for the OPT fabrication since it is assumed that they will be nonconductive which coincides with our previous findings for these systems (Chapter 5, Section 5.4.2).

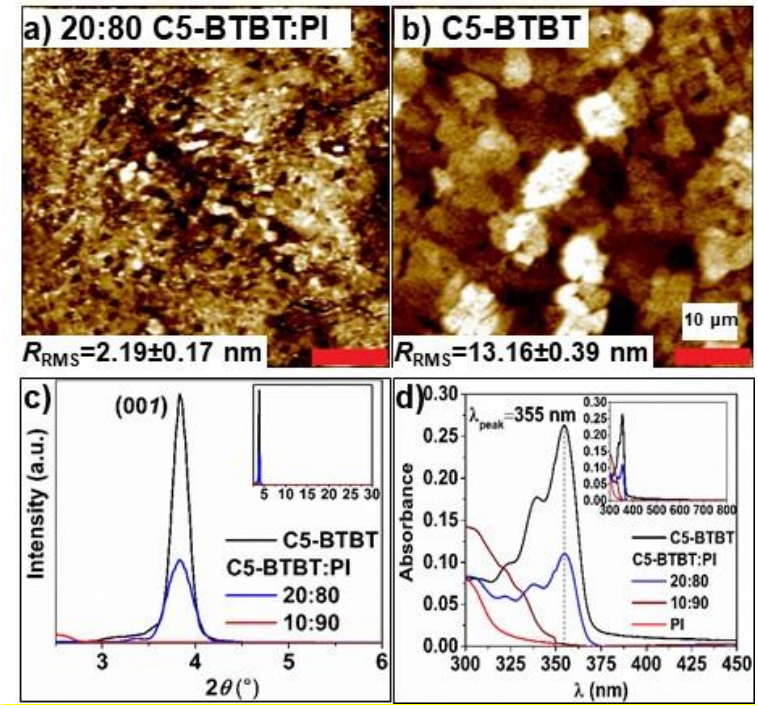

Fig. 7.1. AFM height and phase images of a) C5-BTBT:PI, b) C5-BTBT thin films on XD-HMDS dielectric; c) XRD diffractograms of pristine C5-BTBT, PI, and their blends, and d) UV-vis spectra of C5-BTBT, PI, and C5-BTBT:PI thin films on glass slides spin-coated under the same conditions as those on Si-wafers (inset represents a full wavelength region of the measurements.

7.4.2 Photoelectrical characteristics of OPTs

The output and transfer characteristics of top-contact, bottom-gate OPTs (Fig. 7.2a) with the 20:80 C5-BTBT:PI blend (the best performing blend) and a control C5-BTBT OPT are shown in Fig. 7.2(b-e). The OPTs with 10:90 C5-BTBT:PI blend was nonconductive and will be omitted in this report. This was expected since no C5-BTBT crystal phase and UV absorption was identified in Fig. 7.1 c and d,

respectfully. The output characteristic of 20:80 C5-BTBT:PI OPTs (Fig. 7.2b and c) showed typical p-type operation regime with the ohmic contact, in the dark and under UV light illumination. Under UV light intensity (P_{UV}) of 3 $mWcm^{-2}$, no saturation regime was observed compared to the I_D-V_{DS} curves in the dark of the same OPT. The dark I_D was significantly higher compared to C5-BTBT OPTs. The I_D under the UV light, i.e. drain photocurrent, I_{phc}, was ~3 times higher than I_D of the same OPT. Moreover, the blend-based OPTs were highly sensitive to the UV light being in the on-state already at V_G = 60 V indicating the strong influence of PI on I_D-V_{DS} characteristics. Surprisingly, the introduction of the XD layer had detrimental effects on pristine C5-BTBT OPTs as seen in Fig. 7.2c and e, most likely due to incompatibility of the solvent and the dielectric surface leading to a poor formation of the channel upon spin-coating. Therefore, we didn't subject the C5-BTBT OPTs to further analyses.

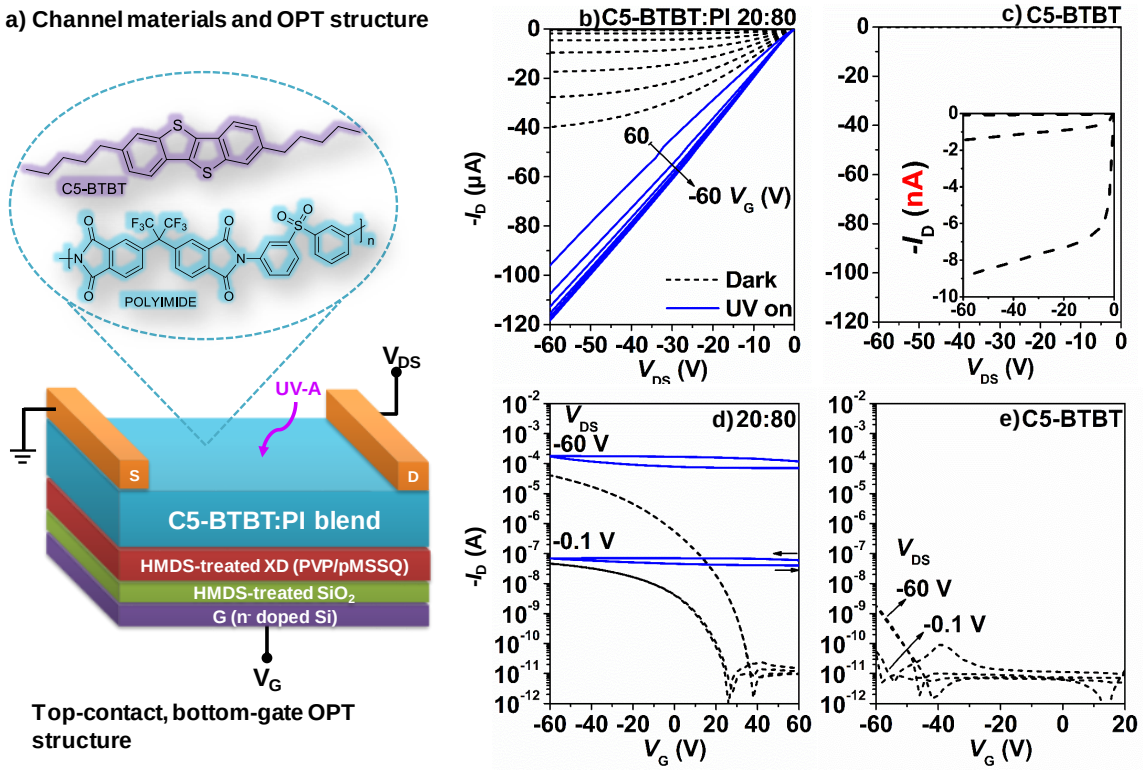

Fig. 7.2. (a) Chemical structures of the channel materials and schematic of the top-contact, bottom-gate configuration of OPTs, (b-c) output characteristics (V_G steps of -10 V; inset in (c) is the zoom-in of I_D in dark from 0 – -10 nA), and (d-e) transfer characteristics (V_{DS} of -60 V and -0.1 V; scan rate 6 Vs^{-1}) of 20:80 C5-BTBT:PI and a reference C5-BTBT OPTs, respectively, in the dark (dashed line) and under UV light (solid line, P_{UV}=3 $mWcm^{-2}$); *L*/*D*=80/930 μm.

The transfer characteristic of 20:80 C5-BTBT:PI OPTs were evaluated in the dark and under UV light illumination (P_{UV}=3 $mWcm^{-2}$), at two distinct V_{DS} of -60 V and -0.1 V (Fig. 7.2d). The V_{DS} of -0.1 V was determined as the lowest possible V_{DS} at which the blend-based OPT operated stably indicating the low-voltage

operation capabilities of our OPTs. Similarly, to the output characteristics, the blend-based OPTs operated in the p-type regime, in the dark, and under UV light illumination. The presence of PI significantly improved the performance of OPTs since stable I_D in the dark was generated even at the low V_{DS} of -0.1 V. Leakage currents (I_G-V_G) of OPTs were low in the dark and under UV light at both V_{DS} (Fig. S7.2). A 20:80 blend-based OPTs showed hysteresis-free operation in the dark while negligible hysteresis was observed under UV light (Fig. 7.2d). Typically, C5-BTBT OPTs without double dielectric layer (HMDS modified SiO_2 dielectric) have a small hysteresis in the dark and a large hysteresis under the UV light at V_{DS}=-60 V (Fig. S7.3b). It is important to emphasize, that many OTFTs reported in the literature exhibited hysteresis at some extent in the dark. We have suppressed it by simply using XD as the second gate dielectric.

Under the UV light, a large I_{phc} was generated in the subthreshold region of 20:80 C5-BTBT:PI OPTs where they were normally in the off-state in the dark. OPTs were in the on-state immediately upon UV light was turned on. The max I_{phc} was instantaneously reached being independent on the further variation of the V_G. This is attributed to the electron trapping at the C5-BTBT/PI interface due to the strong EW nature of PI. A large amount of photo charge carriers were generated upon accelerated dissociation of the excitons affected by PI EW nature, giving a rise to the I_{phc} in the subthreshold region. [16]

7.4.3 Effects of the blend composition and XD layer on OPTs in dark

To investigate the effects of PI content on OPTs characteristics, we fabricated 90:10 and 30:70 C5-BTBT:PI OPTs under the same conditions as those of 20:80 C5-BTBT:PI OPTs. From the corresponding transfer curves generated under the electric field of $7.5x10^3$ Vcm^{-1} (V_{DS}=-60 V), we estimated the field-effect hole mobility (μ_{FE}), the threshold (V_{Th}) and turn-on (V_{SO}) voltages. All the parameters were summarized in Table S7.2. The common equations employed to estimate all the parameters as an average of at least five OPTs at each blend ratio were described in Supp. Info, Section 7.7. The μ_{FE}, On/Off, V_{th} and V_{SO} as a function of the PI content and the fixed V_{DS} are displayed in Fig. 7.3. Fig. 7.3a shows that saturation hole mobility of OPTs was strongly dependent on the PI content at the certain V_{DS} applied.

The max mobility (1.37 $cm^{-2}Vs^{-1}$) at V_{DS}= -60 V was achieved with the lowest content of C5-BTBT in the blend (20 wt.%). Blends with 10 wt.% of C5-BTBT in the blend were nonconductive. When PI was a minor component (10 wt.%), the maximum mobility was 0.055 $cm^{-2}Vs^{-1}$ which is ~25 times lower than that of 20:80 C5-BTBT:PI OPTs. Moreover, the highest On/Off ratio was also achieved with the lowest content of C5-BTBT (20 wt.%) (Fig. 7.3b). Surprisingly, these results demonstrate that 20:80 OPTs had the best performance despite the low content of C5-BTBT. The same phenomenon was observed by Lei et al [37] for the 40:60 diketopyrrolopyrrole-dithienylthieno[3,2-b]thiophene: polyacrylonitrile blends used as channel materials in OTFTs. OTFT showed the highest mobility and the on/off

ratio. As investigated by the TEM-EDX, conjugated polymer was phase separated, self-assembled and crystallized into polyacrylonitrile matrix at the SiO_2/channel interface. This process was called “polymer-matrix-mediated molecular self-assembling”. We believe that similar process occurred in our 20:80 and 30:70 blends also assisted with the differences in polarity of C5-BTBT and PI. Additionally, AFM images and estimated surface roughness showed that thin films were vertically phase separated as previously explained (Fig. 7.1).

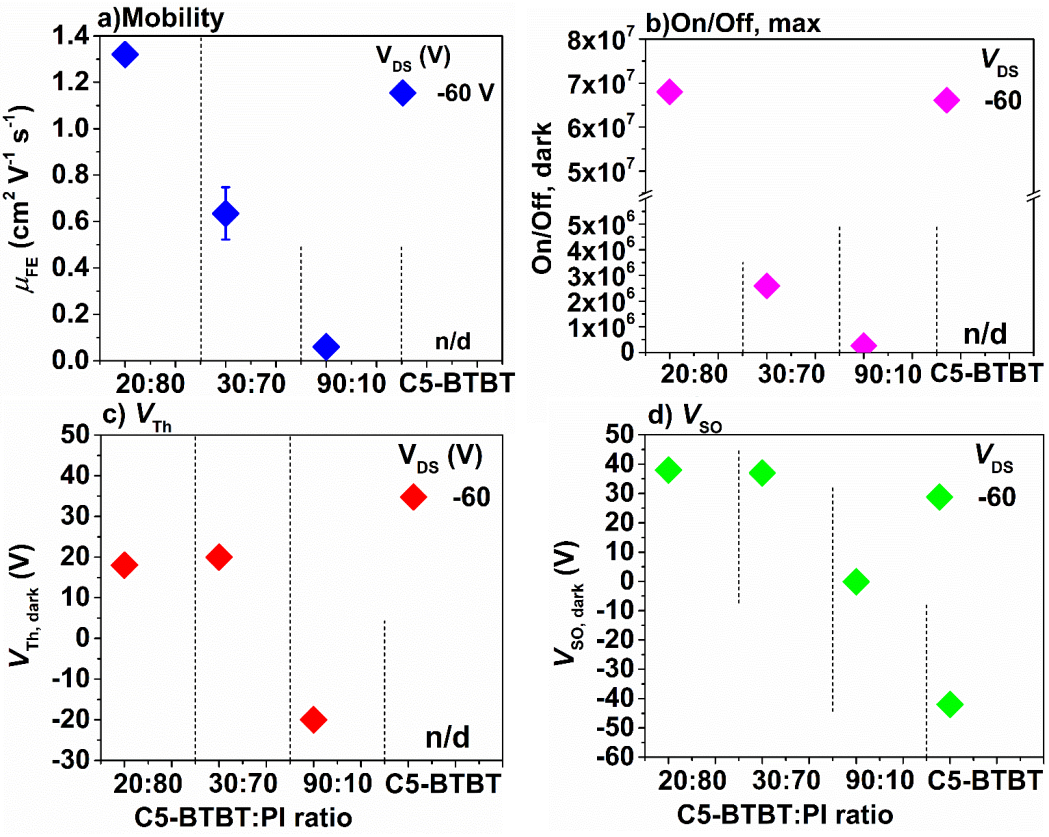

Fig. 7.3. (a) Saturation hole mobility, (b) maximum on/off ratio, (c) threshold voltage and (d) turn-on voltage as a function of PI content of C5-BTBT:PI OPTs including a reference C5-BTBT OPT.

Fig. 7.3c and d, show that when PI is a major phase in the blend, the V_{Th} and V_{SO} were shifted toward highly positive V_G at V_{DS} of -60 V. At the low PI content in the blend (10 wt.%), V_{Th} and V_{SO} were slightly shifted toward more positive values of the gate voltage but were still in the negative range relative to C5-BTBT OPTs. Shifting of the V_{Th} and V_{SO} was 1) due to deep traps introduced by the strong electron accepting PI and 2) XD since it eliminated traps at the SiO_2/channel interface. To demonstrated this, we compared V_{Th} and V_{SO} of 20:80 C5-BTBT:PI OPTs with and without the XD layer (Fig. 7.4). From Fig. 7.3a, it is clear that XD enabled the stronger effect of PI on V_{SO} in dark compared to an OPT without an XD layer. Both V_{SO} and V_{Th} were highly shifted to a positive range of V_G while the voltage shift in OPTs without an XD layer was much lower relative to C5-BTBT OPT (no XD, Table 7.1). Additionally, V_{SO} of -0.11 V of a 90:10 C5-BTBT:PI OPT with XD is still lower than that of 20:80 C5-BTBT:PI OPT without the XD clearly demonstrating the effect of XD on photoelectrical characteristics of OPT in synergy with PI. XD as a PVP/pMSSQ blend generated a highly hydrophobic and electronically neutral surface upon curing at 140°C. Therefore, electronically neutral XD surface with the crosslinked structure generated a surface with fewer trapping sites enabling together with the PI shifting of the V_{Th} and V_{SO} in the blend-based OPTs.

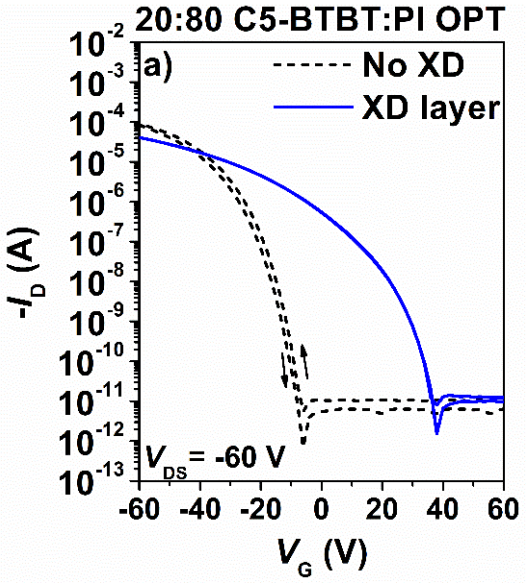

Fig. 7.4. Comparison of I_D-V_G characteristics of 20:80 C5-BTBT:PI OPTs fabricated with (solid line) and without (dashed line) a second dielectric layer XD on SiO_2/Si-substrates.

Table 7.1 Comparison of electrical parameters of 20:80 C5-BTBT OPTs with and without an XD dielectric layer in dark.

Parameter	20:80 C5-BTBT:PI OPTs		C5-BTBT OPTs
	XD	No XD	No XD
$\mu_{FE, DARK}$ (cm^2 V^{-1} s^{-1})	1.32±0.03	0.92±0.16	0.28±0.091
On/Off, dark	10^7	10^6	10^6
$V_{Th, DARK}$ (V)	18±0.9	-26±1	-31±5
V_{SO} (V)	38±0.7	-8±1.6	-19±7

7.4.4 Effects of the blend composition and XD layer on OPTs under UV light

Effects of PI content and XD under the UV light illumination intensity (P_{UV}) of 3 $mWcm^{-2}$ were investigated. Furthermore, characteristics of 20:80 C5-BTBT:PI OPTs with XD were evaluated by the photosensitivity (I_{phc}/I_D) and photoresponsivity (R, AW^{-1}) as a function of V_G at two V_{DS} and compared with 30:70 and 90:10, C5-BTBT:PI OPTs with XD. As seen in Fig. 7.5a, with decreasing content of PI in the blend, the level of I_{phc} in the subthreshold was decreasing. The same effect was observed at V_{DS}=-0.1 (Fig. S7.3a). It is noteworthy that only 10 wt.% of PI in a blend significantly increased I_{phc} of more than 6 orders of magnitude in the subthreshold region compared with I_D in dark. I_{phc}/I_D and R values at V_{DS}= -60 V were the highest with the lowest content of C5-BTBT in the blend (20 wt.%). At the point where these two parameters were overlapping, the values of I_{phc}/I_D and R were ~$1.9x10^7$ and 65 AW^{-1}. I_{phc}/I_D and R at V_{DS}= -0.1 and under the same UV light intensity were $7x10^4$ and ~33 mAW^{-1} (Fig. S3b). These results indicate a high I_{phc} in the subthreshold region even under very low V_{DS} and the high-performance OPTs with 20:80 C5-BTBT:PI ratio. Our I_{phc}/I_D and R values are comparable to those reported for C8-BTBT/PLA blend-based OPTs (10^2 and 56 AW^{-1}) [18] and OPTs based on DPP-DTT/$PC_{61}BM$ bulk heterojunctions (10^4 and 103 AW^{-1}). [38]

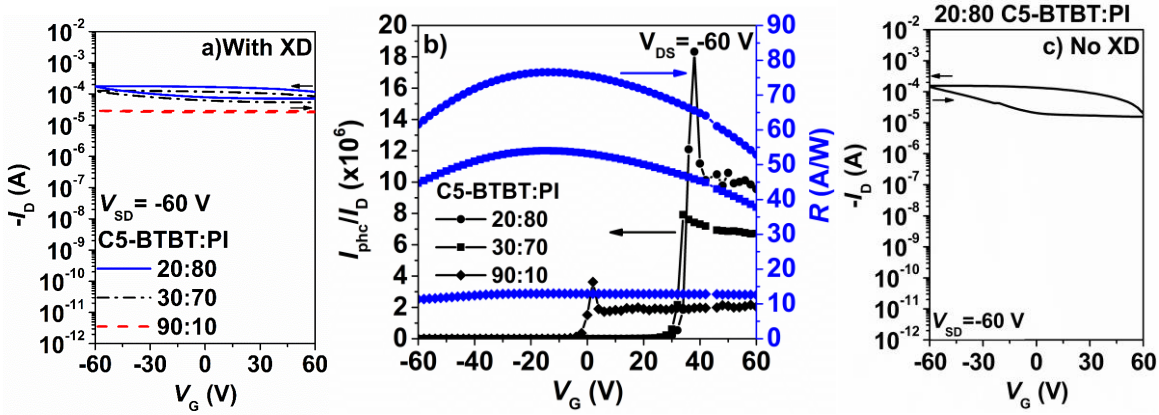

Fig. 7.5. (a) Transfer characteristics under UV light illumination as a function of the PI content, (b) I_{phc}/I_D and R as a function of the PI content in the blend and V_G of OPTs, and (c) transfer characteristics under UV light illumination of 20:80 OPT without an XD layer (at V_{DS}= -60 V, P_{UV}=3 mWcm^{-2}).

The advantage of using a double gate dielectric was clearly visible from the elimination or nearly complete suppression of the hysteresis under the UV light in transfer characteristics of the blend-based OPTs. In our previous work (Chapter 5), we demonstrated that the low- or equal content of PI in C5-BTBT:PI blend-based OPTs could eliminate hysteresis under light illumination. On the other hand, when PI was a major component (70 wt.%) hysteresis started to appear again but at much lower extent compared to pristine C5-BTBT OPT on HMDS modified SiO_2 dielectric. Here, we attempted to completely eliminate hysteresis under light illumination using both PI and XD layer. XD served to eliminate charge traps at the dielectric/channel interface. When we compare hysteresis under UV light illumination of 20:80 C5-BTBT:PI OPTs with and without XD showed in Fig. 7.5a

and c, it is clearly visible that hysteresis of 20:80 OPT with XD layer was significantly smaller than that of 20:80 OPTs without XD. Trapping of the charge carriers in the gate dielectric is known to induce a lower back current hysteresis in OTFTs. Our approach of using a second layer of the polymeric dielectric to isolate the gate electrode in addition to the strong electron accepting PI appeared to be a good method to eliminate/lower the hysteresis under the UV light and, thus, make reliable, high-performance OPTs.

7.4.5 Transient and photo memory characteristics of 20:80 C5-BTBT:PI OPTs

The transient characteristics of 20:80 C5-BTBT:PI OPTs were investigated as a function of V_{DS} and the UV light intensity. Those characteristics were compared with 90:10 C5-BTBT:PI OPTs since we could not fabricate C5-BTBT OPTs with the double gate dielectric. Fig. 6a displays the I_{phc} vs. *time* curves generated under P_{UV}=3 mWcm^{-2} at V_{DS} of -60 V and -0.1 V. We subjected OPTs to a two-cycle measurement with the *Dark* (0 s) - *UV on* (10 s) - *UV off* (50 s) - *Reset -80 V* (100 s) sequence to investigate reproducibility of the response. The I_{phc} vs. *time* curves of 20:80 OPTs exhibited a large I_{phc} evolution of more than 7 orders of magnitude at V_{DS}= -60 V and ~4 orders of magnitude at V_{DS}= -0.1 V. From the same curves, we estimated the characteristic response times of OPTs. The response times of at least five OPTs were estimated by fitting of the experimental data into the bi-exponential equations $I_{phc}(t) = I_0 + A_1\left(1 -\right.$

$e^{-t/\tau_{rf}}\right) + A_2\left(1 - e^{-t/\tau_{rs}}\right)$ and $I_{phc}(t) = I_D + B_1 e^{-t/t_{df}} + B_2 e^{-t/t_{ds}}$ for rise and decay times, respectively.[39] In the equations $A_{1,2}$ and $B_{1,2}$ are the constants, while τ_{rf}, τ_{rs} and τ_{df}, τ_{ds} are times of the fast/slow I_{phc} rise, and the fast/slow I_{phc} decay, respectively. Representation of the bi-exponential fit is displayed in Fig. 7.6b. At both V_{DS}, response or rise of the I_D of 20:80 OPTs under the UV light was fast, followed by fast saturation and then the slow decay of the persistent drain photocurrent when light was off. At V_{DS}= -60 V, the estimated fast/slow rise times of I_D were 1.4±0.3/11.6±1.5 for τ_{rf} / τ_{rs} and 9.4±0.4/205.3±29.3 for τ_{df} / τ_{ds}. The average response times of 90:10 C5-BTBT OPTs were 0.85±0.14/12.2±3.7 and 4.6±0.3/81.9±24.0 for τ_{rf} / τ_{rs} and τ_{df} / τ_{ds}, respectively. It is obvious that 20:80 C5-BTBT:PI OPTs had three times longer decay than 90:10 OPTs which means that PI enhanced the photomemory properties of 20:80 OPTs. The τ_{ds} was highly dependent on V_{DS}, which was 408.6±66.1 s at V_{DS}= -0.1 V being two-fold longer than at V_{DS}= -60 V. All the times were slightly dependent on the content of PI in the blend as showed in Table S7.2.

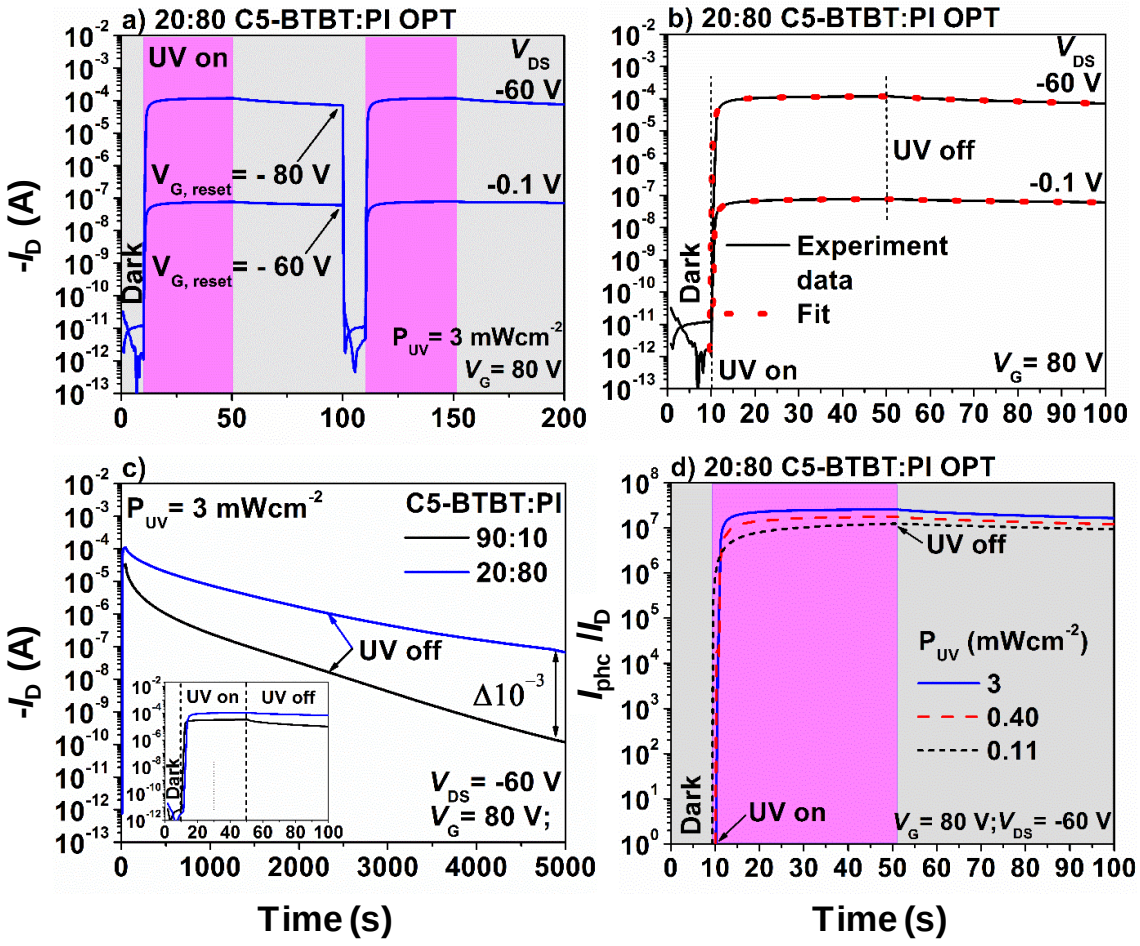

Fig. 7.6. (a) Transient characteristics at different V_{DS} and P_{UV}=3mWcm^{-2}, (b) bi-exponential fit of the experimental data, (c) photosensitivity as a function of time and the UV light intensity, and (d) long time decay (photo memory characteristics) of 20:80 C5-BTBT:PI OPTs compared with C5-BTBT OPTs as a reference.

The 20:80 blend-based OPTs appeared to be a feasible channel material for optically writable/electrically erasable organic memory. This is supported by investigation of how long 20:80 OPTs stored the information written by UV light before they returned to the initial state (dark current level) without a reset voltage

applied. Fig. 7.6c shows comparison of the 20:80 C5-BTBT:PI OPT with the 90:10 C5-BTBT:PI OPTs. It is clearly observed that PI significantly slowed down the decay of the I_{phc}. The optically written information was held up to ~1.35 h (end of the measurement). The I_{phc} drop upon UV light was turned off was only 3 decades while in OPT with 10 wt.% of PI more than 5 decades relative to their maximum reached I_D. Therefore, the recombination rate of the charge carrier generated by light was significantly slowed down by PI electron accepting nature. We used DTF molecular calculations performed using Gaussian 09 software under conditions reported in Supporting Info., Section 7.7. It was found that LUMO to LUMO+3 levels of PI is lower than LUMO of C5-BTBT and higher than HOMO of C5-BTBT as displayed in energy level diagram, in Fig. S7.4. The photogenerated electrons excited to the LUMO of C5-BTBT when falling toward HOMO level are seeking recombination with the photo holes that are moving through HOMO levels of C5-BTBT. On the way down, photoelectrons need to transit through LUMO+3→LUMO (PI) and finally recombine with holes on HOMO of C5-BTBT. At each LUMO of PI photoelectrons reside some time, thus, slowing down the recombination process, and therefore extending the decay times of PI-containing OPTs in the channel.

Lastly, we investigated photosensitivity of the 20:80 OPTs compared to C5-BTBT OPTs or I_{phc} dependence on the intensity of the UV light. The applied intensities of the UV light were 3, 0.40, and 0.11 mWcm^{-2} as Fig. 7.6d shows. I_{phc}/I_D as a function of time at fixed V_{DS}=-60 V showed a somewhat decreasing trend with the decreasing P_{UV}. Still, the I_{phc}/I_D ratio as high as 10^7 was achieved with the lowest P_{UV} of 0.11 mWcm^{-2}. Furthermore, the estimated response times as a

function of P_{UV} showed no significant change (Table 7.2). In contrary, the decay times were slightly increased meaning that at the lower P_{UV} an optically written information was retained longer before OPT resets to the off current.

Table 7.2 Response times as a function of the UV light intensity at fixed V_{DS}=-60 V of 20:80 C5-BTBT:PI OPTs.

P_{UV} (mW cm^{-2})	V_{DS} (V)	Response times (s)			
		τ_{rf}	τ_{rs}	τ_{df}	τ_{ds}
3	-60	1.7±0.3	11.6±1.5	9.4±0.4	205.3±29.3
0.40		1.3±0.2	11.0±1.3	10.5±0.4	164.0±29.9
0.11		2.8±0.4	14.4±0.6	16.1±1.1	239.3±24.2

§ 7.5 Conclusions

In summary, we demonstrated solution processed UV responsive OPTs with double (polymeric/inorganic) gate dielectric that exhibited the high-performance at a low content (20 wt.%) of the small molecule organic semiconductor. The effects of the blends content of the strong electron accepting polyimide and the second dielectric layer composed of a PVP/pMSSQ blend on OPTs performance were investigated. 20:80 C5-BTBT OPTs showed the best performance indicated by very high photosensitivity of <10^7, photoresponsivity of 67 AW^{-1} at P_{UV}=3 mWcm^{-2}, and the high mobility of 1.37 cm^{2}V^{-1}s^{-1} at V_{DS}=-60 V. The same devices were reliable, with hysteresis-free in the dark, and with negligible hysteresis under UV light at both high (V_{DS} =-60V) and low (V_{DS} =-0.1 V) drain voltage. Developed OPTs

were extremely sensitive to the UV light with a weak intensity of 0.11 $mWcm^{-2}$ as indicated by the maintained photosensitivity of 10^7. Results presented in this report showed that combination of C5-BTBT/polyimide blends and the double dielectric were beneficial for modulation of the response times, especially those of the decay of the persistent photocurrent when UV light was off. Therefore, our approach enabled fabrication of OPT for potential application in photo memory elements.

§ 7.6 References

[1] H. Dong, H. Zhu, Q. Meng, X. Gong, W. Hu, *Chem. Soc. Rev.* **2012**, *41*, 1754.

[2] M. Kim, H. J. Ha, H. J. Yun, I. K. You, K. J. Baeg, Y. H. Kim, B. K. Ju, *Org. Electron. physics, Mater. Appl.* **2014**, *15*, 2677.

[3] G. Zhao, J. Liu, Q. Meng, D. Ji, X. Zhang, Y. Zou, Y. Zhen, H. Dong, W. Hu, *Adv. Electron. Mater.* **2015**, *1*, 1500071.

[4] G. Wu, C. Chen, S. Liu, C. Fan, H. Li, H. Chen, *Adv. Electron. Mater.* **2015**, *1*, 1500136.

[5] F. Yu, S. Wu, X. Wang, G. Zhang, H. Lu, L. Qiu, *RSC Adv.* **2017**, *7*, 11572.

[6] K.-J. Baeg, M. Binda, D. Natali, M. Caironi, Y.-Y. Noh, *Adv. Mater.* **2013**, *25*, 4267.

[7] X. Liu, G. Dong, L. Duan, L. Wang, Y. Qiu, *J. Mater. Chem.* **2012**, *22*, 11836.

[8] B. Yao, W. Lv, D. Chen, G. Fan, M. Zhou, Y. Peng, *Appl. Phys. Lett.* **2012**, *101*, 163301.

[9] B. Gunduz, F. Yakuphanoglu, *Sensors Actuators, A Phys.* **2012**, *178*, 141.

[10] Z. Qi, J. Cao, H. Li, L. Ding, J. Wang, *Adv. Funct. Mater.* **2015**, *25*, 3138.

[11] P. Gu, Y. Yao, L. Feng, S. Niu, H. Dong, *Polym. Chem.* **2015**, *6*, 7933.

[12] Y. Wakayama, R. Hayakawa, H.-S. Seo, *Sci. Technol. Adv. Mater.* **2014**, *15*, 24202.

[13] E. Orgiu, P. Samorì, *Adv. Mater.* **2014**, *26*, 1827.

[14] Q. Shen, L. Wang, S. Liu, Y. Cao, L. Gan, X. Guo, M. L. Steigerwald, Z. Shuai, Z. Liu, C. Nuckolls, *Adv. Mater.* **2010**, *22*, 3282.

[15] D. Ljubic, C. S. Smithson, Y. Wu, S. Zhu, *Adv. Electron. Mater.* **2015**, *1*, 1500119.

[16] D. Ljubic, C. S. Smithson, Y. Wu, S. Zhu, *ACS Appl. Mater. Interfaces* **2016**, *8*, 3744.

[17] C. S. Smithson, Y. Wu, T. Wigglesworth, S. Zhu, *Adv. Mater.* **2015**, *27*, 228.

[18] J. Huang, J. Du, Z. Cevher, Y. Ren, X. Wu, Y. Chu, *Adv. Funct. Mater.* **2017**, *27*, 1604163.

[19] Y. Chu, X. Wu, J. Lu, D. Liu, J. Du, G. Zhang, J. Huang, *Adv. Sci.* **2016**, *3*, 1.

[20] S. Bisoyi, U. Zschieschang, M. J. Kang, K. Takimiya, H. Klauk, S. P. Tiwari, *Org. Electron. physics, Mater. Appl.* **2014**, *15*, 3173.

[21] T. Leydecker, M. Herder, E. Pavlica, G. Bratina, S. Hecht, E. Orgiu, P. Samorì, *Nat. Nanotechnol.* **2016**, *11*, 769.

[22] A. Facchetti, M.-H. Yoon, T. J. Marks, *Adv. Mater.* **2005**, *17*, 1705.

[23] X. Liu, Y. Guo, Y. Ma, H. Chen, Z. Mao, H. Wang, G. Yu, Y. Liu, *Adv. Mater.*

2014, *26*, 3631.

[24] D. Khim, E. Y. Shin, Y. Xu, W. T. Park, S. H. Jin, Y. Y. Noh, *ACS Appl. Mater. Interfaces* **2016**, *8*, 17416.

[25] C. Liu, Y. Li, T. Minari, K. Takimiya, K. Tsukagoshi, *Org. Electron. physics, Mater. Appl.* **2012**, *13*, 1146.

[26] A. Kalita, A. Dey, P. K. Iyer, *Phys. Chem. Chem. Phys.* **2016**, *18*, 12163.

[27] D. K. Hwang, C. S. Kim, J. M. Choi, K. Lee, J. H. Park, E. Kim, H. K. Baik, J. H. Kim, S. Im, *Adv. Mater.* **2006**, *18*, 2299.

[28] K. Choi, D. K. Hwang, K. Lee, J. H. Kim, S. Im, *Electrochem. Solid-State Lett.* **2007**, *10*, H114.

[29] J. H. Noh, C. S. Kim, S. Y. Ryu, S. J. Jo, *Jpn. J. Appl. Phys.* **2007**, *46*, 4096.

[30] D. Tsamados, N. V. Cvetkovic, K. Sidler, J. Bhandari, V. Savu, J. Brugger, A. M. Ionescu, *Solid. State. Electron.* **2010**, *54*, 1003.

[31] Y. Wu, H. K. Mahabadi, B. S. Ong, P. F. Smith, Phase-separated dielectric structure fabrication process **2010**.

[32] C. Cao, J. B. Andrews, A. D. Franklin, *Adv. Electron. Mater.* **2017**, *1700057*, 1.

[33] L. Burgi, M. Turbiez, R. Pfeiffer, F. Bienewald, H. J. Kirner, C. Winnewisser, *Adv. Mater.* **2008**, *20*, 2217.

[34] J. Lefebvre, J. Ding, Z. Li, F. Cheng, N. Du, P. R. L. Malenfant, *Appl. Phys. Lett.* **2015**, *107*, 243301.

[35] H. Ebata, T. Izawa, E. Miyazaki, K. Takimiya, M. Ikeda, H. Kuwabara, T. Yui, *J. Am. Chem. Soc.* **2007**, *129*, 15732.

[36] M. Saito, I. Osaka, E. Miyazaki, K. Takimiya, H. Kuwabara, M. Ikeda, *Tetrahedron Lett.* **2011**, *52*, 285.

[37] Y. Lei, P. Deng, M. Lin, X. Zheng, F. Zhu, B. S. Ong, *Adv. Mater.* **2016**, *28*, 6687.

[38] M. Yasin, T. Tauqeer, K. S. Karimov, S. E. San, A. Kösemen, Y. Yerli, A. V. Tunc, *Microelectron. Eng.* **2014**, *130*, 13.

[39] D. Gedamu, I. Paulowicz, S. Kaps, O. Lupan, S. Wille, G. Haidarschin, Y. K. Mishra, R. Adelung, *Adv. Mater.* **2014**, *26*, 1541.

§ 7.7 Supporting information

7.7.1 Experimental

Characterization

Crystal structure data of C5-BTBT:PI thin films and a C5-BTBT control, on double gate dielectric layer Si-wafers, were acquired in a two-dimensional X-ray diffractometer (XRD^2) equipped with a Bruker Smart6000 CCD area detector, Bruker 3-circle D8 goniometer, Rigaku RU200 Cu K$\bar{\alpha}$ rotating anode, and Göebel cross-coupled parallel focusing mirrors. Acquisition conditions were as follows: scan type Omega sweep (from 0.5°-13°), frame exposure: 300 s, 2θ = 2.5° - 35°, at the detector distance of 11.86 cm and power setting 90 mA and 50 kV.

Theoretical calculations of the polyimide repeating unit were performed using Gaussian 09 program. We optimized the basic unit by means of the density

functional theory (DFT), using the hybrid functional B3LYP (Becke, three-parameter Lee-Yang-Parr) [1][2][3] and the Pople double-zeta polarized basis set 6-31G(d).[4][5] The isosurfaces of the molecular orbitals were constructed with the VMD[6] visualization software using a value of 0.02 Bohr.

7.7.2 Results

Basic properties of polyimide

Table S7.1 Basic properties of PI

Property	Observation
Appearance	White powder
Solubility at room temperature (60 mg ml^{-1})	THF, 1,1,2,2-tetrachloroethane, DMSO, DMF
MW (GPC)	14800
T_g (°C) (DSC)	267
T_m (°C) (DSC)	Not observed
T_{onset} (°C) (TGA)	~550

Thin-film morphology

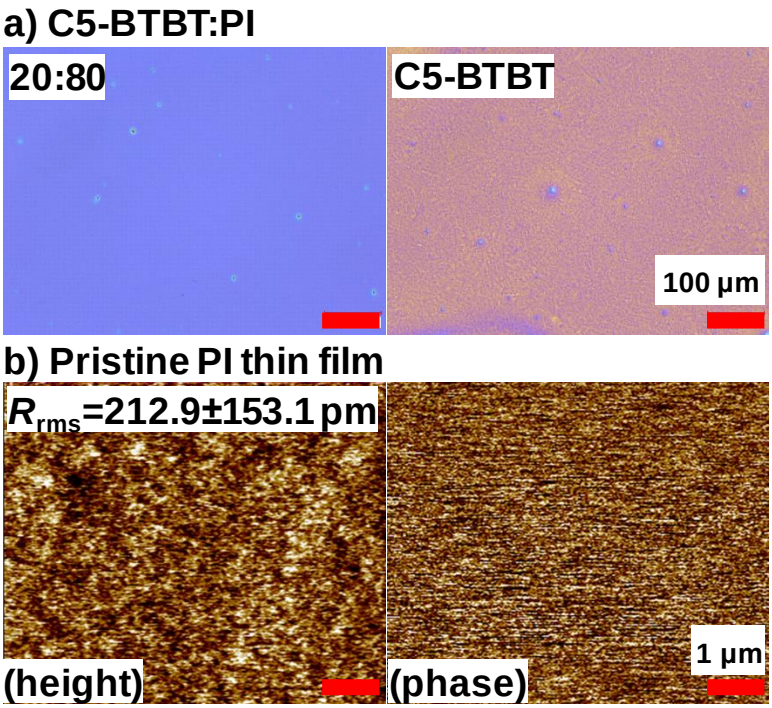

Fig. S7.1. (a) Optical microscope images of C5-BTBT:PI and pristine C5-BTBT thin films and (b) AFM height and phase images of pristine PI deposited on XD-HMDS under the same conditions as thin films used for photoelectrical properties measurements.

Photoelectrical characteristics of OPTs

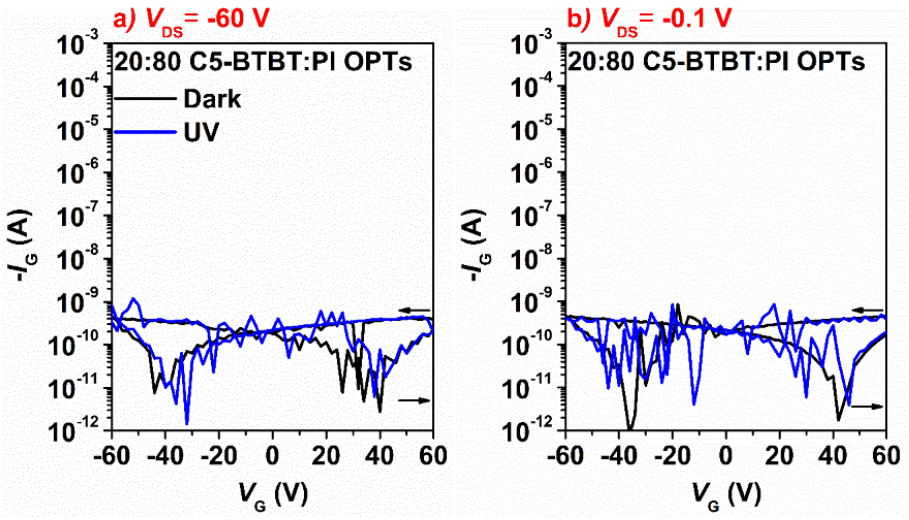

Fig. S7.2. Leakage currents of 20:80 C5-BTBT:PI OPTs in dark and under UV light at two different V_{DS}.

Table S7.2 Electrical parameters of C5-BTBT:PI and C5-BTBT OPTs estimated from transfer characteristics in the dark at V_{DS} of -60 V.

OPT / Parameter	C5-BTBT:PI 20:80	C5-BTBT:PI 30:70	C5-BTBT:PI 90:10	C5-BTBT
Thickness (nm) ±10	320	310	220	150
$\mu_{FE,\ DARK}$ ($cm^2\ V^{-1}\ s^{-1}$)	1.32±0.03	6.35±1.13 ($x10^{-1}$)	6.04±1.26 ($x10^{-2}$)	n/d
On/Off, dark	10^7	10^6	10^5	n/d
$V_{Th,\ DARK}$ (V)	18±0.9	20±0.4	-20±2.1	n/d
V_{SO} (V)	38±0.7	37±0.9	-0.11±1.64	-42

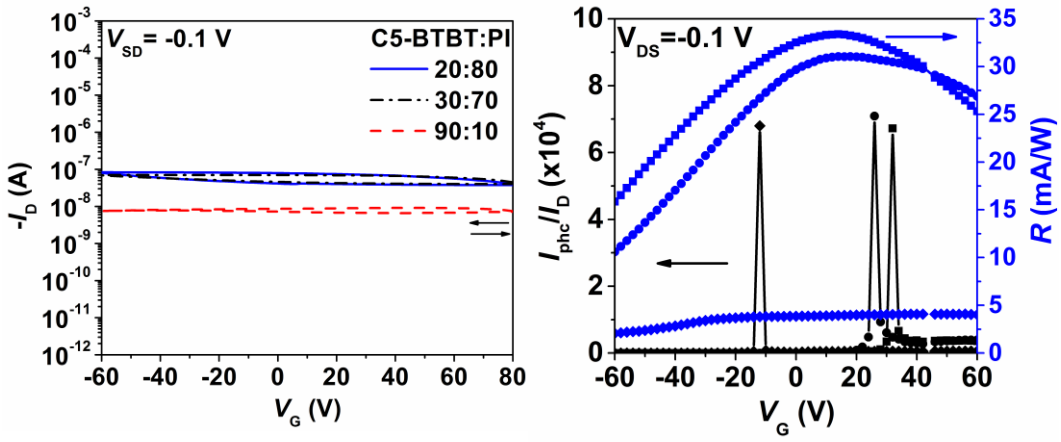

Fig. S7.3. Transfer characteristics under UV light illumination (P_{UV}=3 mWcm^{-2}) as a function of the PI content in the blend compared to a reference C5-BTBT OPTs and (b) I_{phc}/I_D and R as a function of the PI content in the blend and V_G of OPTs at V_{DS}= -0.1 V.

Table S7.3 Response times of C5-BTBT and C5-BTBT:PI OPTs as a function of a blend composition and V_{DS} at constant P_{UV}=3 mWcm^{-2} (V_G=80 V).

Parameter / OPT	V_{DS} (V)	Response times (s)			
		τ_{rf}	τ_{rs}	τ_{df}	τ_{ds}
C5-BTBT	-0.1	n/d			
	-60				
C5-BTBT:PI					
90:10	-0.1	0.52±0.11	6.9±1.9	5.3±1.8	131.9±31.7
	-60	0.85±0.14	12.2±3.7	4.6±0.3	81.9±24.0
30:70	-0.1	1.1±0.4	10.2±2.1	8.9±1.7	239.6±12.7
	-60	1.7±0.3	10.2±1.9	6.0±0.2	109.6±12.0
20:80	-0.1	1.3±0.2	9.3±0.8	11.9±2.0	408.6±66.1
	-60	1.7±0.3	11.6±1.5	9.4±0.4	205.3±29.3

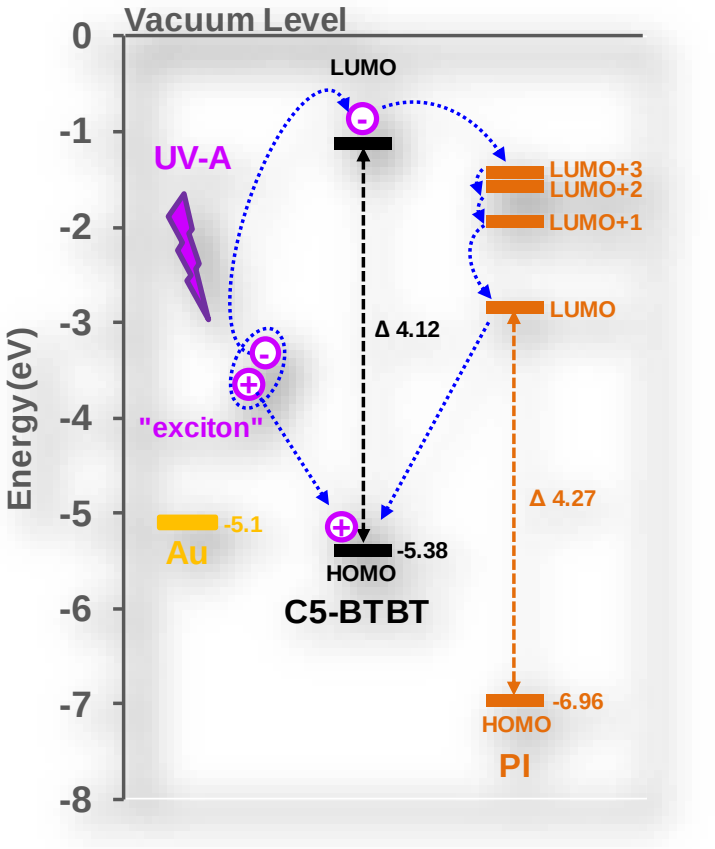

Fig. S7.4. Schematic of the mechanism proposed for the charge carrier generation/recombination when UV light is on/off, respectively, of PI:C5-BTBT OPTs.

Equations

The threshold voltage, V_{Th}, was estimated from the slope of $I_D^{½}$ vs. V_G curves. The turn-on voltage (V_{SO}), was determined from the slope of the logI_D-V_G transfer curves while the field-effect hole mobility in saturation regime (μ_{FE}), was estimated from using equation: [7]

$$\mu_{FE} = \frac{2L}{W} \cdot \frac{I_D}{C_{ox}(V_G - V_{Th})^2} \qquad \text{(Eqn. S7.1)}$$

where L and W are channel length and width in cm, respectively; C_{ox} is the capacitance per unit area of the SiO_2 dielectric layer (15 nFcm^{-2}). The charge trap density at the SiO_2/channel interface in the dark ($N_{trap,dark}$) was determined by: [8]

$$N_{trap,\ dark} = \frac{|V_{Th}|C_{ox}}{q} \qquad \text{(Eqn. S7.2)}$$

where q is an elementary charge.

The slope of the linear part of the logI_D-V_G curves at V_G<V_{Th} was used for estimation of the inverse subthreshold slope (SS):[9]

$$SS = \left(\frac{d\log I_D}{dV_G}\right)^{-1} \qquad \text{(Eqn. S7.3)}$$

The density of deeper traps at the interface (D_{it}) was computed using [8][10]:

$$D_{it} = \left[\frac{qSSlog(e)}{k_bT} - 1\right]\frac{C_{ox}}{q^2} \qquad \text{(Eqn. S7.4)}$$

where T and k_B are absolute temperature and the Boltzmann constant, respectively.

Photosensitivity, I_{phc}/I_D ratio, was calculated using: [11]

$$Ratio = \frac{I_{phc} - I_D}{I_D} \qquad \text{(Eqn. S7.7)}$$

Photoresponsivity, *R*, of OPTs was estimated using: [11]

$$R = \frac{I_{phc} - I_D}{P_{UV} \cdot A} \qquad \text{(Eqn. S7.8)}$$

where P_{UV} is the intensity of the incident UV light and *A* (*L*x*W*) is the effective area illuminated by UV light.

7.7.3 References

[1] C. Lee, W. Yang, R. G. Parr, *Phys. Rev. B* **1988**, *37*, 785.

[2] A. D. Becke, *J. Chem. Phys.* **1993**, *98*, 5648.

[3] J. P. Perdew, K. Burke, M. Ernzerhof, *Phys. Rev. Lett.* **1996**, *77*, 3865.

[4] W. J. Hehre, R. Ditchfield, J. A. Pople, *J. Chem. Phys.* **1972**, *56*, 2257.

[5] M. M. Francl, W. J. Pietro, W. J. Hehre, J. S. Binkley, M. S. Gordon, D. J. DeFrees, J. A. Pople, *J. Chem. Phys.* **1982**, *77*, 3654.

[6] W. Humphrey, A. Dalke, K. Schulten, *J. Mol. Graph.* **1996**, *14*, 33.

[7] C. D. Dimitrakopoulos, P. R. L. Malenfant, *Adv. Mater.* **2002**, *14*, 99.

[8] J. Smith, R. Hamilton, Y. Qi, A. Kahn, D. D. C. Bradley, M. Heeney, I. McCulloch, T. D. Anthopoulos, *Adv. Funct. Mater.* **2010**, *20*, 2330.

[9] A. Takshi, J. D. Madden, *J. Comput. Electron.* **2010**, *10*, 154.

[10] X. Liu, G. Dong, L. Duan, L. Wang, Y. Qiu, *J. Mater. Chem.* **2012**, *22*, 11836.

[11] K.-J. Baeg, M. Binda, D. Natali, M. Caironi, Y.-Y. Noh, *Adv. Mater.* **2013**, *25*, 4267.

8 CONTRIBUTIONS AND RECOMMENDATIONS

In this chapter, the major contributions from this thesis work are summarized first, followed by recommendations on potential future directions in the field of organic phototransistors.

§ 8.1 Contributions

The major contributions in this thesis work are on engineering of the organic phototransistors, highlighted as follows:

- The new strategy in the field based on blending of a small molecule semiconductor and dielectric polymer to enhance photoelectrical characteristics of UV-A responsive OPTs via interface trapping phenomena has been demonstrated. It is shown that the interface trapping phenomena

can be utilized to enhance the performance of OPT under light illumination, despite the general theories predicting negatively affects of interface trapping on OTFTs performance.

- A novel polyimide has been designed and synthetized, which is highly soluble in common organic solvents and with strong electron withdrawing nature. The polyimide is integrated into an active channel of OPTs as a binary blend with small molecule semiconductor. The OPTs exhibited high-performance in dark and remarkable stability, photoresponsivity, and photosensitivity under UV light illumination. The OPTs have potential for photo sensing and photomemory elements.
- Fundamental understanding of OPTs performance evolution based on the channel/gate dielectric interface phenomena has been offered. With simple surface modification by organosilanes containing electron donating/withdrawing groups, this study enabled fundamental understanding of the operation mechanisms and performance evolution in OPTs. Mobility in dark is governed by the crystal structure of semiconductor, while under light illumination, it is by the ability of interface to donate or withdraw electrons.
- An engineered photoelectrical and photo memory performance of UV responsive OPT using double gate dielectric and optimized composition of a small molecule semiconductor/polyimide blend has been achieved. This

approach enabled development of the high-performance, low-voltage, and highly photosensitive OPTs with application as photo memory.

8.1.1 Recommendations for the future work

As stated in the summary and outlook section of Chapter 2, organic phototransistors have a bright future. In the recent years, the field has simply bloomed due to the design of new materials, smart molecular engineering, and devices engineering. The field of solution processed OPTs is of the great importance due to the possibility to print, solution-cast over a large area flexible substrate. Besides, the performance of OPTs based organic semiconductors has largely exceeded the performance of Si-based PTs.

The blending of organic semiconductors of various molecular weights becomes very attractive in the development of OPTs for sensing the broad range of spectrum wavelengths including those in the NIR range. Recently, blending of small molecule semiconductors and dielectric polymers is sought as a promising strategy for high-performance OPTs for printed and flexible devices. Meanwhile, the following directions should be emphasized in the future research for the real applications of OPTs:

- Achieving reliable, stable and robust OPTs via materials design, molecular engineering, optimization of the existing active channel materials and engineering of the device structures.

- Designing and synthesizing materials having highly ordered structures to achieve high field-effect mobility, On/Off ratio, photoresponsivity, and photosensitivity.
- Developing theoretical models for blends to estimate the above parameters under the UV light.
- Printing OPTs on flexible substrates using the blends established in this thesis.